ORNL/TM-13661

Potential Damage to Gas-Cooled Graphite Reactors Due to Severe Accidents

R.P. Wichner
S.J. Ball

Los Alamos
NATIONAL LABORATORY
Los Alamos, New Mexico 87545

ornl
Oak Ridge National Laboratory
Oak Ridge, Tennessee 37831

ORNL/TM-13661

Potential Damage to Gas-Cooled Graphite Reactors Due to Severe Accidents

R. P. Wichner*
S. J. Ball†

Contributors
B. A. Worley†
J. M. Davidson‡
T. D. Burchell†

*Lockheed Martin Energy Systems, Inc.
†Oak Ridge National Laboratory.
‡Los Alamos National Laboratory.

April 1999

Prepared by
OAK RIDGE NATIONAL LABORATORY
Oak Ridge, Tennessee 37831
managed by
LOCKHEED MARTIN ENERGY RESEARCH CORPORATION
for the
U.S. DEPARTMENT OF ENERGY
under contract DE-AC05-96OR22464

~~OFFICIAL USE ONLY~~

CONTENTS

APPENDIXES

LIST OF FIGURES

LIST OF TABLES

ABBREVIATIONS

AGR	Advanced Gas-Cooled Reactor
APF	axial peaking factor
ATWS	anticipated transient without scram
BEPO	British Experimental Pile Zero (or British Experimental Pile Operation)
CEGB	Central Electricity Generating Board
EDF	Electricite de France
GCR	gas-cooled reactor
GLEEP	Graphite Low-Energy Experimental Pile
GRSAC	Graphite Reactor Severe Accident Code
HASCAL	Hazard Assessment System for Consequence Analysis
HPAC	Hazard Prediction and Assessment Capability
HTGR	High-Temperature Gas-Cooled Reactor
LOFC	loss of forced convection
MORECA	Modular ORNL RECA (code)
NRC	U.S. Nuclear Regulatory Commission
ORGR	Oak Ridge Graphite Reactor
RPF	radial peaking factor
SCIPUFF	Second-Order Closure Integrated PUFF
UKAEA	United Kingdom Atomic Energy Authority

ABSTRACT

A comprehensive computer code for predicting severe accident progression and consequences in gas-cooled, graphite-moderated reactors is described and documented. This work applies primarily to the older gas-cooled-reactor (GCR) types that use metallic fuels rather than to those with ceramic fuels (e.g., the modern high-temperature gas-cooled reactors) or oxide fuels (e.g., the British advanced gas-cooled reactors). The Graphite Reactor Severe Accident Code (GRSAC) models the combined effects of graphite, cladding (magnesium or aluminum), and metallic fuel (uranium) oxidation; the release of Wigner (stored) energy from the graphite; nuclear (fission and decay) heating; and fission product release in a three-dimensional representation of the reactor core thermal hydraulics. The report highlights the modeling used to represent oxidation, stored energy release, and fission product release. A detailed analysis of the Windscale reactor accident in 1957 was done to support model validation. The analyses presented here emphasize extreme-case, very-low-probability air-ingress accidents. Hence the results should not infer inadequate safety performance of reactors of this class, which have historically been extremely safe and reliable. An overview of the GCR's historical development, along with discussions of GCR safety and physical characteristics, is also presented.

1. INTRODUCTION

1.1 OBJECTIVE

Early studies of postulated severe accidents in graphite-moderated reactors span the time period from the late 1940s through the early 1960s in support of the U.S. Manhattan Project and the gas-cooled reactor (GCR) programs of Britain and France. Later, from the 1970s through the 1990s, interest in the High-Temperature Gas-Cooled Reactor (HTGR) in the United States, Europe, and Japan promoted most of the existing literature in this field. Much of the early work was done in response to the Windscale accident in England in 1957 and the French G1 reactor accident in 1956. These early studies dealt almost exclusively with graphite oxidation and, because of computational limitations, did not treat the combined effects of oxidation of the cladding (magnesium or aluminum) and uranium metal fuel, as well as the release of Wigner (stored) energy from the annealing of irradiated graphite. These combined effects would all be very much interrelated in the course of severe accidents for this type of reactor. As a result, the core-wide release of radioactivity from fuel elements, which depends on the summation of the local damaging effects of elevated local temperatures and oxygen availability, could not be estimated accurately. Realistic analyses also need to account for the spatial dependencies of temperatures, power distributions, and coolant flow distributions in the large cores. Simplified oxidation calculations often discounted the limiting effect of oxygen starvation on the succession of events. In such analyses it is important to consider the compounding effects of the many mechanisms involved to determine, for example, under what circumstances a self-sustaining or runaway accident could ensue.

The objective of the work presented here is threefold: (1) to document the development of a comprehensive computational code system for analyzing the progression of a severe accident in a GCR using an integrated approach that accounts for all the major interrelated physical phenomena; (2) to utilize the core damage, thermal conditions, and degree of oxidation to determine the quantity of radioactivity released from the fuel elements; and (3) to perform analyses using the code system as a means of defining the range of damage to graphite-moderated, gas-cooled reactors from postulated severe accidents that involve core overheating, emphasizing events with air ingress. The study is limited to the older gas-cooled-reactor types using metal fuels as opposed to the ceramic fuels used in the modern HTGR and the oxide fuels used in the British Advanced Gas-Cooled Reactor (AGR) designs. The starting point for the analyses is that a severe accident progression has been initiated, with no assumptions made relative to the cause or likelihood of the accident. Thus this study should not be used to infer an inadequate safety performance of the existing group of GCRs, because historically they have been one of the safest classes of reactors in operation.

1.2 SCOPE OF REPORT

Graphite-moderated, gas-cooled reactors played a major role in nuclear development, both for nuclear weapons material production and commercial energy production. As a matter of nomenclature, within the nuclear industry and in this report, the term GCR is synonymous with graphite-moderated, gas-cooled reactors. This report deals with a particular type of GCR characterized by metallic natural uranium fuel enclosed in a magnesium alloy or aluminum cladding. Another reactor type using graphite as the moderator—graphite-moderated, water-cooled reactors—also played a significant role in nuclear weapons material production in the United States and the former Soviet Union but were developed into commercial power plants only in the former Soviet Union as the RBMK reactor type, including the now-familiar four Chernobyl reactors. Except to note the differences between RBMKs and GCRs, the RBMK is not discussed in this report. Finally, this report addresses potential damage

to GCRs using natural uranium metallic fuel and not the more modern designs using enriched uranium oxide or carbide fuels, such as the AGRs and HTGRs.

In this chapter a brief overview of the historical development of GCRs is presented, along with designs typifying those of interest in this work. The safety characteristics, physical phenomena, and accident progressions of these GCRs are summarized in Chapter 2, along with the issues related to modeling such accident progressions. The development and integration of models into a computer code is described in Chapter 3, and code validation studies are presented in Chapter 4. The application of this code to accident progression scenarios selected to address the potential damage to GCRs is discussed in Chapter 5. Chapter 6 summarizes the major conclusions from our work. The basis for choosing the computational models and model details are presented in the Appendixes along with detailed descriptions of validation and accident analysis studies, and the reactor designs that characterize the spectrum of metal-fuel GCRs highlighted in this study.

1.3 GAS-COOLED REACTORS—HISTORICAL OVERVIEW

The first controlled nuclear fission took place in a large graphite "pile" on December 2, 1942, in a squash court under the West Stands of University of Chicago's Stagg Field. Graphite was chosen because, of all materials that could effectively slow down neutrons with proper moderating properties, graphite was the only one which could be obtained in sufficient quantity with the desired degree of purity necessary for achieving criticality with natural uranium. Impurities were an important consideration, for while pure graphite readily scatters neutrons, absorption reactions are rare. Neutron absorption in commercially available graphite is strongly influenced by the presence of such naturally occurring impurities, such as boron and vanadium. Another important requirement was that the fuel be of high density in order to maximize the amount of uranium that could be used within the pile. The designers of the Chicago pile, referred to as CP-1, had difficulty in obtaining uranium fuel in the high-density metallic form, thus the pile was initially fueled with uranium oxide pellets because metallic uranium of the desired purity did not exist at that time. Even though several manufacturers were attempting to produce the uranium metal, it was not until November 1942 that several tons of the highly purified metal was delivered and placed in the pile as close to the center as possible.

After self-sustainable fission was demonstrated in CP-1 (Fig. 1), the first operating reactor was built in 1943 at what is now Oak Ridge National Laboratory in Tennessee for the purpose of prototyping the production of plutonium and its extraction from the spent fuel prior to the operation of the major plutonium production plants built at Hanford, Washington. The Oak Ridge Graphite Reactor produced about 3.5 megawatts of thermal power [MW(t)], was air-cooled, and used metallic uranium fuel clad in aluminum. Soon thereafter, the Hanford reactors were built with a major design change from the Oak Ridge Graphite Reactor in that water was used as the coolant. Water was a much more effective coolant, and the requirement to remove the high heat loads at the production plants outweighed the loss of neutrons by absorption in the water coolant. In any event, natural uranium fuel was used in the early Hanford designs.

After the end of World War II, one more U.S. graphite-moderated, gas-cooled reactor was built at Brookhaven National Laboratory for general research related to the effects of irradiation, neutron science, and isotope production. Construction of the Brookhaven Graphite Research Reactor began in the fall of 1947, and the reactor reached initial criticality in August 1950. Full-power operation with natural uranium was achieved April 1951, and the reactor was later converted to use enriched fuel in January 1957.

The construction and operation of the Chicago piles, the Oak Ridge Graphite Reactor, and the Brookhaven Research Reactor were the extent of the U.S. experience with GCR metal-fueled reactors. Soon thereafter, the commercial development of GCRs in the United States shifted to the use of enriched uranium oxide and carbide fuels encased in silicon carbide spheres within graphite pellets, and these plants took on the nomenclature of HTGRs because of the high operating temperatures

afforded by the use of helium coolant and ceramic fuels. Two commercial HTGRs were operated in the United States: Peach Bottom was a 40-MW(e) power plant in Pennsylvania that operated from 1967 through 1974, and Fort St. Vrain was a 330-MW(e) power plant in Colorado that operated from 1981 through 1989. Both reactor systems were developed by General Atomics. During the late 1960s and 1970s, General Atomics received orders for ten large HTGRs from U.S. utilities. However, a combination of institutional issues, oversupply of electrical generating capacity, and technical design problems at Fort St. Vrain eventually led to the cancellation of all ten reactors. General Atomics and the U.S. Advanced Reactors Program have developed numerous designs for a variety of applications ever since, but in 1994 the U.S. government decided to phase out the HTGR program following a decision not to pursue advanced reactor research and development. General Atomics has continued to market advanced HTGR concepts abroad, most recently in Russia. Nonetheless, the HTGR advanced reactor program has provided a long-term base of technology development that is directly applicable to the subject of the current study.

Outside the United States, the post war development of GCRs was aggressively pursued in the United Kingdom (UK) and France. Britain exported one each of its power reactors to Italy (Latina) and Japan (Tokai-Mura); France exported one to Spain (Vandellos). Much later, Germany and Japan developed graphite reactor programs for commercial power and process heat based on designs that fall into the category of the U.S. HTGR design concepts. The early designs pursued by the United Kingdom and France are of particular significance for this study because a large number of the reactors use natural uranium metal fuel.

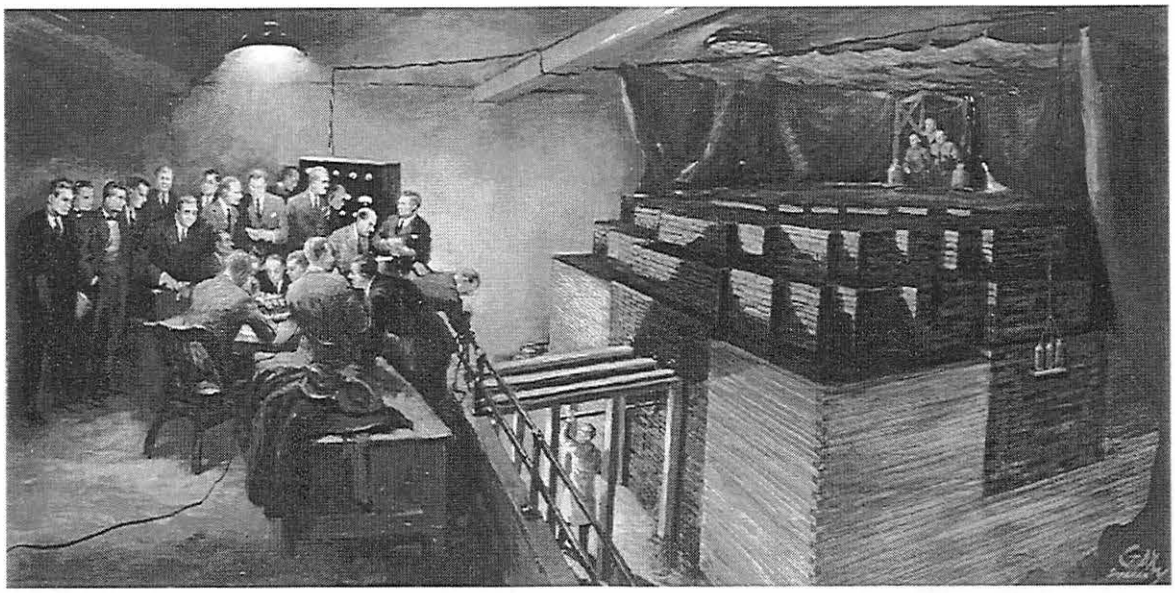

Fig. 1. Photograph of the painting "Birth of the Atomic Age" by Gary Sheahan depicting the events at CP-1. Reprinted with permission from the Chicago Historical Society.

1.3.1 British GCR Development

The first British reactor, the graphite low-energy experimental pile (GLEEP) began operation on August 15, 1947, and became the first controlled nuclear chain reaction in Western Europe. Like CP-1, this reactor used natural uranium metallic and oxide fuel because of the shortage of uranium metal at the time. The fuel cladding was aluminum, and the reactor was air-cooled. GLEEP operated at a design power of 100 kW(t) and was shut down in 1990 after 43 years of operation. GLEEP was

followed by the higher power 36-MW(t) BEPO (British Experimental Pile Zero or British Experimental Pile Operation) at Harwell in 1948. GLEEP and BEPO were both used to develop the technology and experience base needed to build and operate the air-cooled, twin plutonium production reactors commissioned on the Windscale site at Sellafield, England in 1950. The Windscale reactors consisted of a graphite moderator with 20-cm square lattices of natural uranium metal fuel rods clad in aluminum and utilized horizontal air coolant flow and fuel loading. In many respects, these reactors are essentially thermally enhanced versions of the Oak Ridge Graphite Reactor, since they had the same fuel and cladding material and removed heat by means of air flow along horizontal channels. One of the major advances at Windscale was the application of heat transfer enhancers on the cladding, which enabled a significant increase in the power density of the core. The Windscale reactors had a design power of about 160 MW(t) and were operated until 1957 when the fire in Unit 1 led to the shutdown of both units.

From 1951 to 1953, a study was performed at the UK's Atomic Energy Research Establishment at Harwell that addressed the feasibility and prospects for developing a nuclear power generation system for the United Kingdom. This research culminated in a decision to build a set of closed-circuit, CO_2-cooled reactors to be located at Windscale and used for the production of both power and plutonium (hence, the acronym, PIPPA). A four-reactor site, designated Calder Hall, was selected and construction initiated in 1953, with power being switched into the national grid on October 17, 1956. The last of the four units was brought on line in 1959, and all four units continue to produce approximately 200 MW(e) total output which varies somewhat because the steam produced is used for other processes besides electricity production. The four units were initially commissioned at 240 MW(e) but have a reduced rating to minimize CO_2 corrosion problems recognized in the late 1960s. Besides being referred to as PIPPA or Calder Hall–type reactors, the first set was also referred to by the British as the Magnox reactors. The Calder Hall units were replicated in the four Chapelcross units, which became part of the South of Scotland Electricity Board (SSEB) grid in 1959. The Magnox designation refers to the fuel cladding material fabricated from the Magnox series of magnesium alloys containing small quantities of aluminum and beryllium. The French subsequently built GCRs similar in overall concept to the Calder Hall reactors, also using natural uranium metal fuel and a cladding alloy of predominantly magnesium but with the minor constituent being zirconium instead of aluminum and beryllium. As a result, the French reactors of this type are often referred to as French Magnox reactors.

In September 1955, the Central Electricity Authority [later the Central Electricity Generating Board (CEGB)] undertook, in cooperation with the United Kingdom Atomic Energy Authority (UKAEA) and the SSEB, the development of GCRs with half the capital costs of the Calder Hall–type stations but retaining the preferred lower fuel costs and performance of the natural uranium cycle. This effort led to a second generation of nine twin reactor Magnox stations built in the United Kingdom, plus two single reactor foreign sales.

The Magnox experience is also varied because of the proliferation of design differences and customization among the plants. All the plants utilize a square lattice core except Tokai-Mura, for which a triangular core lattice was developed for improved earthquake resistance. Because of concerns about Wigner energy buildup near the core inlet regions where there is a combination of cooler gas temperature and high flux, some of the later Magnox designs utilized graphite sleeves around the coolant channels. This insulated the surrounding graphite, allowing it to run at higher temperatures, causing less stored energy, and constrained radiation damage mainly to the graphite sleeves. Channel sleeving also presumably allowed for re-sleeving should it ever be deemed necessary. Most graphite radiation damage occurs in the first radial inch of the graphite surrounding the fuel, hence the idea of sleeving accomplished two purposes, not just one. Except for Calder Hall and Chapelcross, the Magnox stations also have on-line refueling with spent fuel storage in water pits, except at Wylfa, where dry storage is used. In most Magnox reactors, the backup shutdown system consists of an independent set of shutdown rods; however, Tokai-Mura uses poisoned steel balls, which can be

dropped into the core, similar to the boronated graphite balls in the reserve shutdown system at Fort St. Vrain.

Following the development of the Magnox line of reactor, the United Kingdom initiated the AGR design program. The AGRs use slightly enriched oxide fuel with stainless steel cladding and, for more efficiency, operate at a higher gas temperature of approximately 650°C vs 400°C for the Magnox reactors. The first prototype AGR was built at the Windscale sight and started operation in 1962. The first power station AGR was Dungeness B, followed closely by Hinkley Point B, Hunterston B, Heysham I, and Hartlepool. The Hinkley Point B/Hunterston B design evolved into the fourth and final AGR design, constructed at Heysham II and Torness. These stations, which were ordered in 1978 and commissioned in 1988 and 1989, hold the record for the "fastest work-up to full power" of any commercial reactor in the world.

The third phase of the UK GCR development program was the British HTGR design, similar to the U.S. HTGR design, using enriched uranium and thorium in graphite cladding, cooled by pressurized helium at a maximum temperature of 750°C, a concept similar to the Peach Bottom plant in the United States. The Dragon HTGR reactor was built as a prototype in 1964 and operated until 1974. The British did not pursue the development of the HTGRs, however, and instead planned on developing the pressurized-water-reactor (PWR) concept.

1.3.2 French GCR Development

In France, the government's air-cooled G1 reactor at Marcoule was operated from 1956 to 1968 for both plutonium production and small electricity production, gross power 1.7 MW(e), maximum air temperature of 284°F. Like Windscale, the G1 reactor utilized horizontal coolant flow and fuel loading and widely spaced square lattices of natural uranium metal fuel rods. But unlike Windscale, the fuel was clad in magnesium cans.

It was soon recognized that higher power density cores and enhanced safety could not be achieved with air-cooled reactors. The logical next step in the evolution was the adoption of a sealed pressurized circuit to produce better conditions for heat transfer needed for temperatures useful for steam production for large-scale electricity generation and, in some instances, cogeneration. However, like Britain, a secondary consideration for France in this next, but first generation, of closed-circuit GCRs continued to be plutonium production as well as power generation. The first closed-circuit, CO_2-cooled, or UNGG, reactors built by the French were the government's G2 and G3 plants built at Marcoule and commissioned in 1959 and 1960, respectively. These reactors were utilized for the production of both electricity at 40 MW(e) and plutonium.

Commercial GCR development by Electricitie de France (EDF) began in 1957 with the initiation of construction of Chinon A1 (EDF1), which was a 70-MW(e) demonstration plant. Chinon A1 was operated from 1963 to 1972, and then decommissioned because operating costs were projected to be too high at the time. Chinon A1 used a square lattice, tubular-fueled vertical flow core in a cylindrical steel pressure vessel. The vessel and primary circuit are contained within a building. Chinon A2 (EDF2) and Chinon A3 (EDF3) followed as early prototypes of hexagonal lattice, upflow cores. EDF used a spherical steel vessel, and EDF3 used a cylindrical concrete vessel. Unit 1 at St. Laurent, however, became the basic design configuration followed in the remaining French GCRs. St. Laurent 1 utilized a hexagonal lattice, downflow core arranged in a cylindrical PCRV, with the core located above the steam generators and circulators. The configuration is similar in many respects to that used at Fort St. Vrain, except that the St. Laurent circulators are mounted horizontally through the sides of the PCRV. St. Laurent 2, Vandellos (Spain), and Bugey 1 incorporated the construction features of St. Laurent 1. Bugey 1, the last of the French GCRs, utilized tubular fuel elements with center hole cooling. The Bugey fuel element used herringbone fins on both the inner- and outer-clad surfaces of the tubular fuel element.

The French GCR development program ended in 1972 with the completion of Bugey 1. Although there was some subsequent work on the HTGR as a process heat source, most of this effort ended in the middle 1970s. The French reactor program is currently based primarily on the PWR.

1.3.3 Summary of the Historical Development of GCRs

One striking characteristic that becomes apparent in reviewing the development of GCR designs is the wide range of design configurations that are possible in building a graphite-moderated, gas-cooled reactor using natural uranium metallic fuel. A list of such reactors that have operated with power levels in excess of 100 kW(t) is given in Table 1. The impact of these various design possibilities is that the computational code being developed for this work must have the flexibility to model all the reasonable combinations. However, to give the reader a more complete understanding of GCR design details that are necessary in carrying out accident progression analysis, five specific reactors of particular significance in our work are presented in the following section.

Table 1. Graphite-moderated gas-cooled reactors using uranium metal fuel

Name	MW(t)	Coolant	Clad	Flow	Vessel	Refueling	Status[a]
			UNITED STATES				
Oak Ridge GR	3.5	Air	Al	Horizontal	None	Online	1943–1963 (D)
Brookhaven GRR	20	Air	Al	Horizontal	None	Online	1951–? (D)
			UNITED KINGDOM				
GLEEP	0.1	Air	Al	Horizontal	None	Online	1947–1990 (S)
BEPO	6.5	Air	Al	Horizontal	None	Online	1948–1957 (S)
Windscale 1	160	Air	Al	Horizontal	None	Online	1950–1957 (S)
Windscale 2	160	Air	Al	Horizontal	None	Online	1951–1957 (S)
Calder Hall 1	270	CO_2	Mg alloy	Up	Steel	Batch	1956–present
Calder Hall 2	270	CO_2	Mg alloy	Up	Steel	Batch	1957–present
Calder Hall 3	270	CO_2	Mg alloy	Up	Steel	Batch	1959–present
Calder Hall 4	270	CO_2	Mg alloy	Up	Steel	Batch	1959–present
Chapelcross 1	260	CO_2	Mg alloy	Up	Steel	Batch	1959–present
Chapelcross 2	260	CO_2	Mg alloy	Up	Steel	Batch	1959–present
Chapelcross 3	260	CO_2	Mg alloy	Up	Steel	Batch	1959–present
Chapelcross 4	260	CO_2	Mg alloy	Up	Steel	Batch	1960–present
Berkeley 1	585	CO_2	Mg alloy	Up	Steel	Online	1962–1988 (S)
Berkeley 2	585	CO_2	Mg alloy	Up	Steel	Online	1962–1988 (S)
Bradwell 1	500	CO_2	Mg alloy	Up	Steel	Online	1962–present
Bradwell 2	500	CO_2	Mg alloy	Up	Steel	Online	1962–present
Hunterston A1	545	CO_2	Mg alloy	Up	Steel	Online	1964–? (S)
Hunterston A2	545	CO_2	Mg alloy	Up	Steel	Online	1964–? (S)
Dungeness A1	780	CO_2	Mg alloy	Up	Steel	Online	1965–present
Dungeness A2	780	CO_2	Mg alloy	Up	Steel	Online	1965–present
Hinkley Point A1	947	CO_2	Mg alloy	Up	Steel	Online	1965–present

Table 1 (continued)

Name	MW(t)	Coolant	Clad	Flow	Vessel	Refueling	Status[a]
Hinkley Point A2	947	CO_2	Mg alloy	Up	Steel	Online	1965–present
Sizewell A1	800	CO_2	Mg alloy	Up	Steel	Online	1966–present
Sizewell A2	800	CO_2	Mg alloy	Up	Steel	Online	1966–present
Oldbury 1	893	CO_2	Mg alloy	Up	PCRV	Online	1967–present
Oldbury 2	893	CO_2	Mg alloy	Up	PCRV	Online	1968–present
Trawsfynydd 1	860	CO_2	Mg alloy	Up	Steel	Online	1965–? (S)
Trawsfynydd 2	860	CO_2	Mg alloy	Up	Steel	Online	1980–? (S)
Wylfa A1	1760	CO_2	Mg alloy	Up	PCRV	Online	1971–present
Wylfa A2	1730	CO_2	Mg alloy	Up	PCRV	Online	1972–present
FRANCE							
Marcoule G1	38	Air	Mg	Horizontal	None	Online	1956–1968 (D)
Marcoule G2	255	CO_2	Mg alloy	Horizontal	Concrete	Online	1958–1980 (D)
Marcoule G3	255	CO_2	Mg alloy	Horizontal	Concrete	Online	1959–1984 (D)
Bugey 1	2000	CO_2	Mg alloy	Up	Concrete	Online	1972–1994 (S)
Chinon A1 (EDF-1)	300	CO_2	Mg alloy	Up	Steel	Batch	1962–1973 (S)
Chinon A2 (EDF-2)	800	CO_2	Mg alloy	Up	Steel	Batch	1965–1986 (S)
Chinon A3	1300	CO_2	Mg alloy	Up	None	Batch	1965–1986 (S)
St. Laurent A1	1570	CO_2	Mg alloy	Down	PCRV	Online	1969–? (S)
St. Laurent A2	1690	CO_2	Mg alloy	Down	PCRV	Online	1971–? (S)
BELGIUM							
BR-1	4	Air	Al	Horizontal	None	Online	1956–?
ITALY							
Latina	650	CO_2	Mg alloy	Up	Steel	Online	1963–? (S)
JAPAN							
Tokai-mura	515	CO_2	Mg alloy	Up	Steel	Batch	1965–1998 (S)
PEOPLES DEMOCRATIC REPUBLIC OF KOREA							
Yongbyon-1	~20	CO_2	Mg alloy	Up	Steel	Batch	1986?
Yongbyon-2	~200	CO_2	Mg alloy	Horizontal	None	Online	1985?
Taechon	~800	CO_2	Mg alloy	Horizontal	None	Online	1985?
SPAIN							
Vandellos 1	1670	CO_2	Mg alloy	Down	None	Online	1972–? (S)

[a] S = shut down; D = decommissioned.

1.4 GAS-COOLED-REACTOR DESIGNS OF INTEREST

The range of design variation for GCRs that have used metal fuels can best be exemplified by examination of specific reactors. For this purpose, the Oak Ridge, Windscale, Calder Hall, G1, and G2/G3 reactor designs are summarized in the following sections, in which major design differences between them are discussed. Tables of key parameters and layouts for Windscale, G1, G2/G3, and Calder Hall are given in Appendix H.

1.4.1 Oak Ridge Graphite Reactor

The Oak Ridge Graphite Reactor (ORGR) (Fig. 2) consisted of a cube of graphite moderator, 24 ft on each side, fueled by aluminum-clad natural uranium cylinders fed and discharged through 1,239 horizontal cylindrical holes. A charging machine inserted fresh slugs through the front face of the reactor and pushed spent slugs out through the rear, where they fell into a water-filled channel. Workers transferred buckets of these irradiated slugs to the neighboring separation plant using an underwater monorail. Exhaust fans pulled cooling air through the pile, keeping it under a slight vacuum to prevent an escape of contamination. Air cooling was selected for its simplicity, even though engineers had abandoned gas cooling in favor of water cooling for the full-scale Hanford reactors in February 1943. Seven feet of concrete shielding protected reactor operators from radiation. Controls included four horizontal "shim" rods, two horizontal regulating rods, six vertical safety rods, and a backup system using boron steel shot suspended over the reactor core. Designers provided various openings in the reactor to facilitate the insertion and removal of experimental samples. Initially, the reactor had a power output of 1,000 kW; this output was soon quadrupled.

The ORGR reactor became operational on November 4, 1943, and focused on the production of small amounts of plutonium for Manhattan District studies, research on shielding, and the biological effects of radiation. By February 1944, ORGR was producing several grams of plutonium per month. The high neutron background from this material greatly influenced the design of the plutonium bomb being developed at Los Alamos. Later, ORGR produced radioactive lanthanum, for use as a tracer in high-explosives experiments, and irradiated bismuth targets to produce polonium-210 for weapon initiators. After the war, Oak Ridge scientists continued to use the reactor for reactor research nuclear physics, and isotope production for medical, industrial and agricultural applications. Oak Ridge produced radioactive lanthanum ("Rala") until 1956.

1.4.2 Windscale Reactor

Work on the first of two Windscale reactors (Fig. 3) began in 1947, about four years after the Manhattan Project's ORGR. Even though the first water-cooled reactor at Hanford was already in operation, the British decided on a simpler gas-cooled concept, primarily for siting problems, safety concerns (loss-of-cooling accidents), and secondarily for lack of materials availability. Windscale had many features in common with the ORGR, including once-through air cooling, horizontal flow, aluminum cladding, and metallic uranium fuel. A major improvement was the use of extended surfaces as an integral part of the fuel element cladding, enabling improved heat transfer and higher power density.

Cooling air was forced into a plenum at the charge face, passed horizontally through 7 m of core in the fuel channels, into an exit plenum at the discharge face, through a duct containing fission product monitors and into the base of a 400-ft stack capped by a set of fission product traps. One blower house was located on each side of the main building, each containing four main blowers and two shutdown fans. When essentially zero cooling was desired, as during a Wigner energy anneal, flow dampers at the outlet of each fan were shut and a hatch at the base of the chimney was opened, thereby breaking the vacuum created by the stack. Shutdown rods entered vertically from the top of the core. Control rods entered horizontally, perpendicular to both the shutdown rods and the fuel channels.

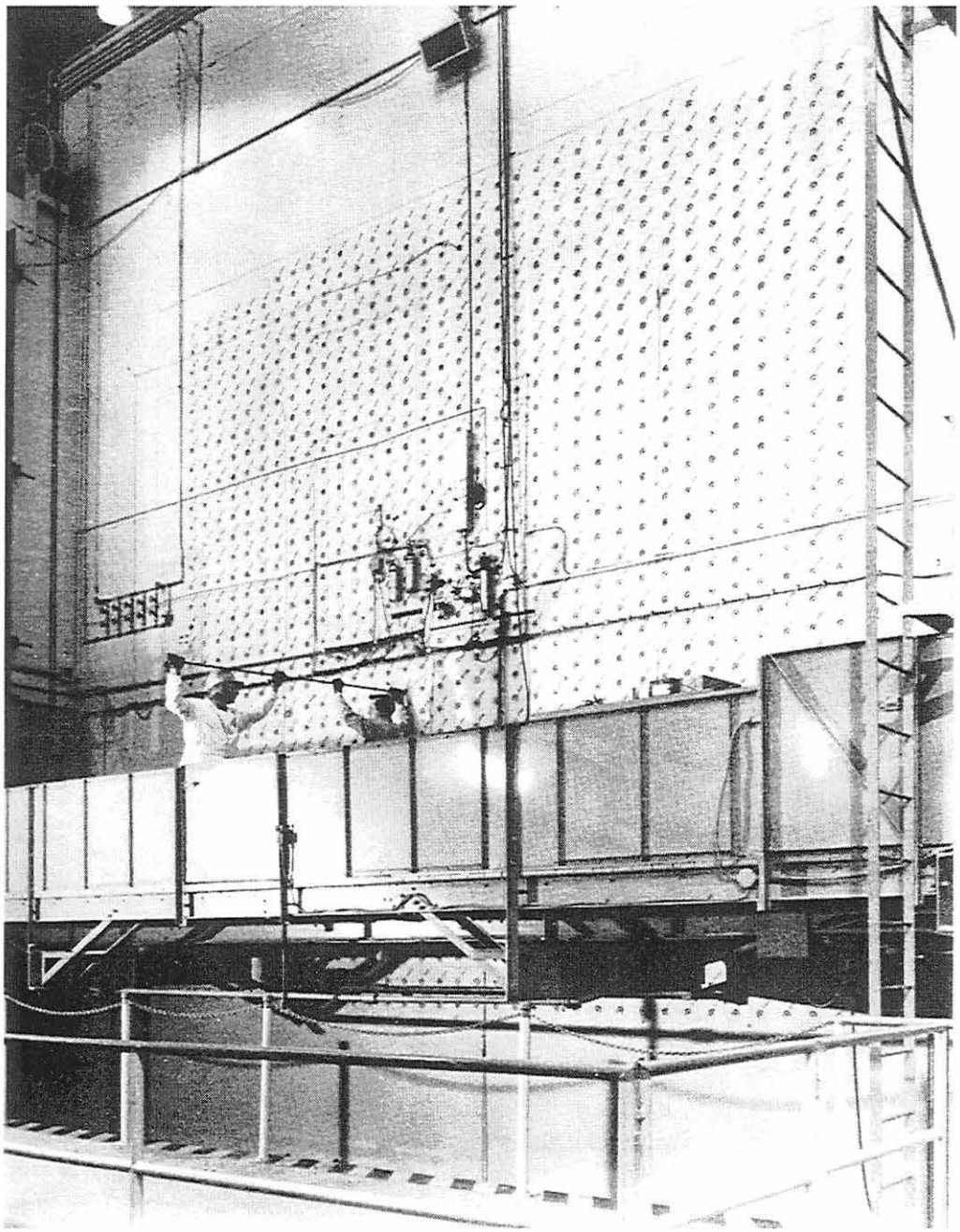

Fig. 2. Oak Ridge Graphite Reactor. Code-named "X-10," the reactor produced the world's first gram quantities of plutonium. It was the pilot plant for Hanford's full-size plutonium production reactors. X-10's core is a graphite block. A charging machine inserted fresh uranium metal slugs through holes in the reactor's front face, pushing irradiated slugs out the back. Fans pulled cooling air over the fuel slugs. Oak Ridge scientists used X-10 for research and isotope production until it was decommissioned in 1963. Source: *AEC Handbook on Oak Ridge,* U.S. Atomic Energy Commission, June 1958.

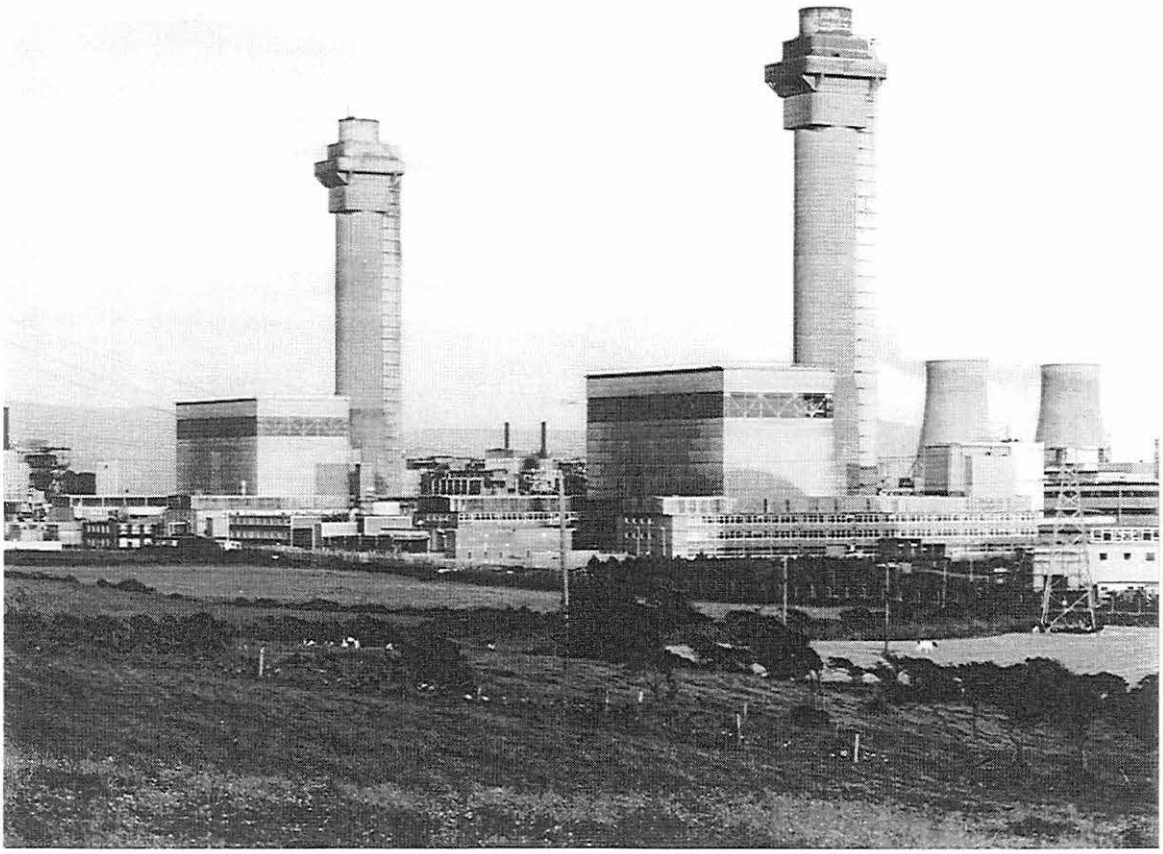

Fig. 3. The Windscale piles. These graphite-moderated, air-cooled production reactors went critical in 1950–1951. Reprinted with permission from British Nuclear Fuels plc.

1.4.3 G1 Reactor

In 1956, six years after Windscale 1, the French G1 reactor (Fig. 4) first reached criticality. Like Windscale, the G1 reactor was a natural uranium–fueled, graphite-moderated, air-cooled reactor. One major design difference of the reactor was the unique cooling flow arrangement that had air entering a vertical plenum located at the midplane of the core. Air passed in both directions from this central plenum into horizontal fuel channels, exiting the core from both the fuel feed and discharge faces. The core was contained in two steel plates supported on a concrete structure contained in a prestressed concrete vessel. A distinctive feature of the fuel element was the extended surface, an integral part of the magnesium cladding, with 16 longitudinal fins.

1.4.4 G2 Reactor

The G2 reactor (Fig. 5), built in Marcoule, France, near Avignon, was the second French plutonium-producing reactor and was designed to use natural uranium fuel and cooled with pressurized CO_2 following the lead of the British Calder Hall units. The G2 reactor became

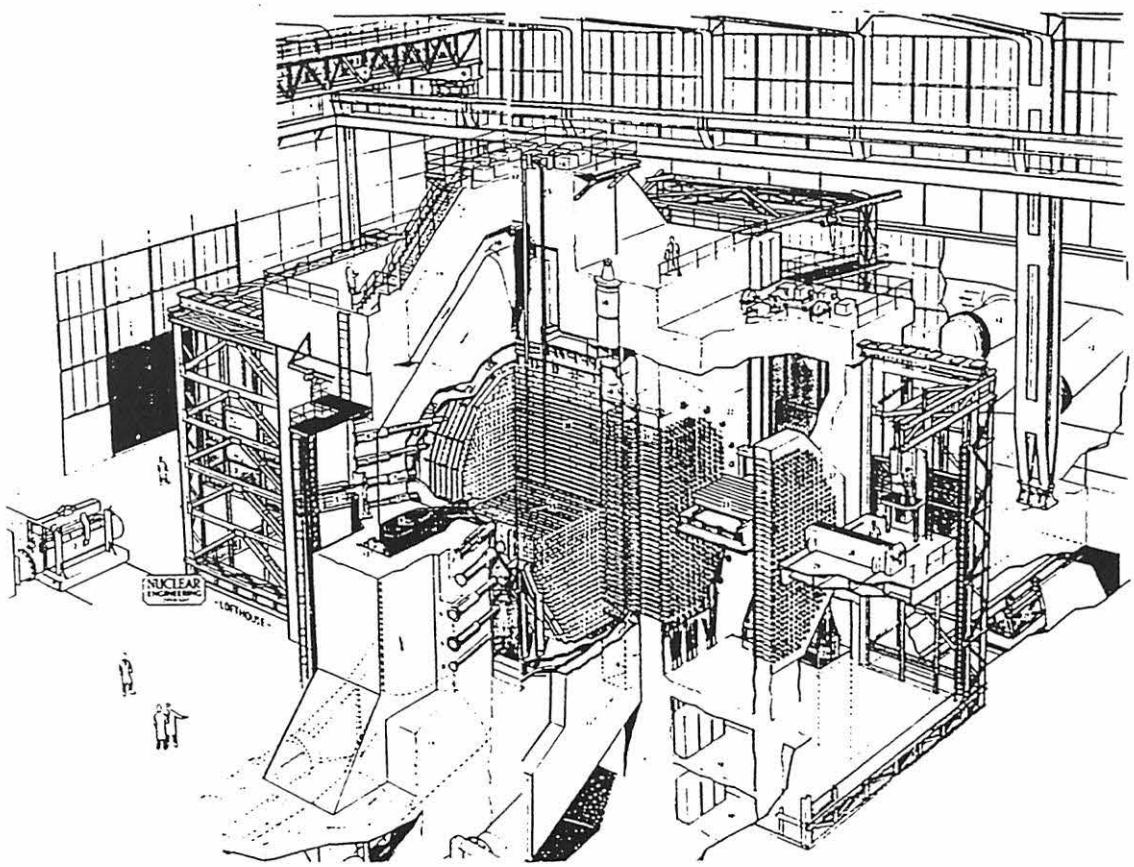

Fig. 4. The French G1 reactor. Source: *Nuclear Engineering International,* June 1958.

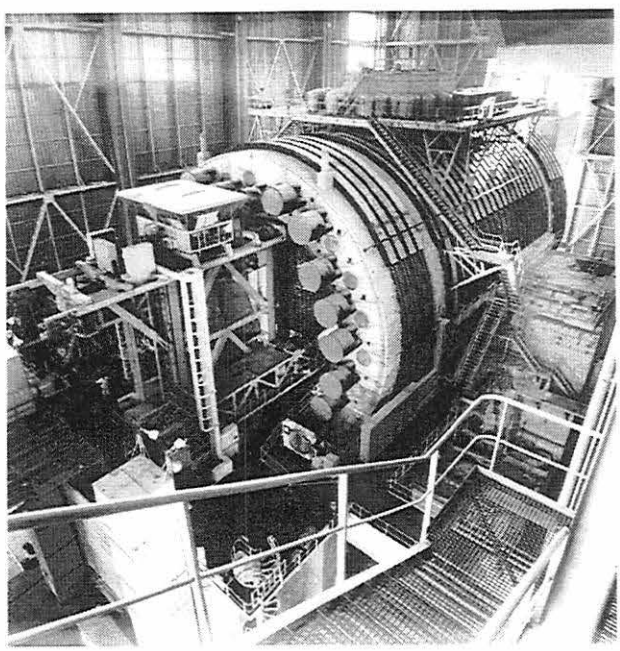

Fig. 5. The G2 reactor at Marcoule. The 40-MW(e) reactor, which first generated power in 1959, introduced the concepts of on-load refueling and the prestressed concrete pressure vessel, although it only enclosed the core. Reprinted with permission from CEA/JAHAN.

operational in 1958. The first big design difference between the Calder Hall units and the G2 design was the choice of prestressed concrete for the G2 reactor vessel, in preference to a steel vessel. This successful innovation was subsequently widely adopted. The second significant difference was the core orientation, in which the fuel rods were loaded horizontally in G2 instead of vertically as in the Calder Hall designs. The coolant flows horizontally through the reactor from front to back and returns around the reactor sides to the front. An identical sister plant, referred to as G3, became operational in 1959. The G2 and G3 reactors used metal-clad (magnesium-zirconium alloy) metallic natural uranium fuel in a square lattice, horizontal coolant flow configuration. The fuel claddings, initially provided with longitudinal cooling fins, were later manufactured with herringbone fins. The G2 and G3 reactors have concrete outer vessels with two cooling circuits, one for the reactor and another to cool the vessel.

1.4.5 Calder Hall Reactor

The Calder Hall I reactor (1956) (Fig. 6) was the first to use the newly developed magnesium alloy for the metal fuel cladding that would permit higher operating temperatures than possible with the aluminum cladding used in the Windscale reactors. In addition, the coolant was pressurized CO_2 instead of air and was circulated in a closed path, as opposed to the once-through forced-air cooling in Windscale. Thus, any contamination would be held up in the primary circuit rather than pass directly to the atmosphere. Calder Hall was the first of the "Magnox" reactors, so named because of the magnesium alloy cladding.

The Calder Hall I and its later sister plants, Calder Hall II, III, and IV, used a succession of improved fuel-element fin designs, allowing successively higher power ratings. Units II, III, and IV became operational in 1957, 1958, and 1959, respectively.

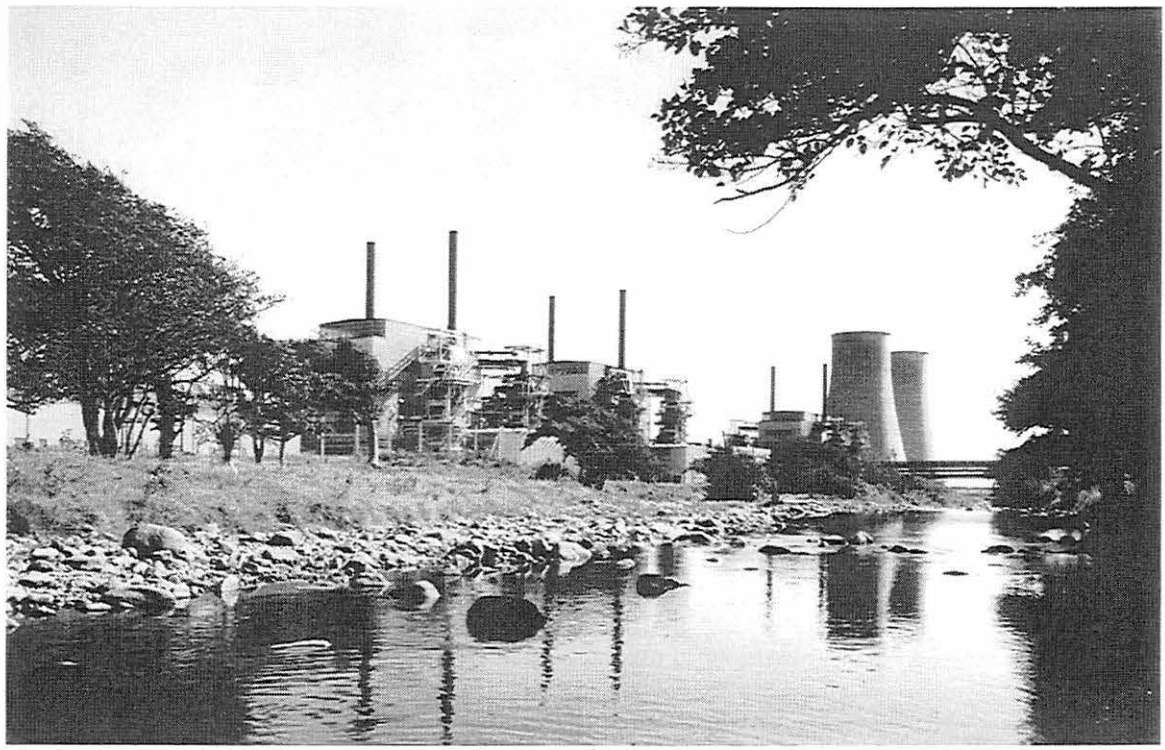

Fig. 6. Calder Hall Unit I. The first nuclear generating station in the West, this reactor was opened on October 17, 1956. Reprinted with permission from AEA Technology-Harwell.

2. GAS-COOLED REACTOR SAFETY CHARACTERISTICS AND ACCIDENT PROGRESSIONS

2.1 INTRODUCTION

Many studies have been carried out that address the safety and postulated accidents of metal-fueled gas-cooled reactors.[1-5] These reports collectively discuss phenomena important to GCR accident progressions, such as graphite behavior, fuel behavior, Wigner energy, and oxidation during air ingress. The purpose of this work is to build upon the prior knowledge base, in an effort to address the possible outcome of an accident progression that has been initiated, without estimating or judging the risk or likelihood that such an accident progression could occur in existing or postulated metal-fueled GCRs. The approach is to develop computational models that attempt to incorporate, to the extent possible, all the important physical phenomena that come into play during accident progression in the metal-fueled GCR designs, including those summarized in the previous chapter.

Because a wealth of literature exists on each of these separate phenomena, in this chapter we review the basic phenomena involved in GCR accident progression to the level of detail necessary to understand their significance in modeling accident progression, including the well-reviewed accidents that occurred at Windscale in 1957 and Marcoule in 1956. But before summarizing the accident issues, it is important to first review the unique safety characteristics of GCRs relative to other reactor types to give an accurate perspective on the safety of GCRs in general.

2.2 SAFETY CHARACTERISTICS OF GAS-COOLED REACTORS

2.2.1 Inherent Characteristics of GCRs

The early GCR designs had a number of attractive inherent safety features, some of which they shared with the water-cooled reactors, but some of which were unique.[6] Later versions, such as the AGRs and HTGRs, capitalized on these advantages and introduced other safety-related design features, such as high-temperature ceramic fuel, that led to the modular, inherently safe designs (MHTGRs). These later designs are predicted to be able to rely solely on passive heat removal to cool the core sufficiently and thus to avoid fuel damage and fission product release.

The three primary signature safety characteristics of Magnox reactors, AGRs, and HTGRs are (1) the high core heat capacity; (2) the high thermal conductivity of the core graphite; and (3) for later designs, the high temperature capability. The first two of these features, coupled with a relatively low power density, make most GCR temperatures slow to respond as compared to LWRs. The third characteristic provides "headroom" for the over-power or under-cooling excursions before damage occurs. The low core power density and high heat capacity combination leads to long times (minutes to hours) available for control and/or safety systems or operators to take corrective or mitigating actions. The heatup rates for GCRs are especially slow for the long-term accidents (with afterheat as the heat source), because of the large graphite moderator and reflector heat capacities.

In addition, there is a safety advantage in the use of a relatively inert coolant such as CO_2 compared with water, which may in severe accidents contribute to the hazard by chemical reaction with cladding and fuel. The presence (or absence) of the coolant has essentially no effect on reactivity. There is a distinct safety advantage in having a gaseous coolant. The use of gas eliminates uncertainties in accident scenarios that could lead to chugging, DNB (departure from nucleate boiling), etc., which are a concern with liquid coolants. Of lesser importance is the typical loose coupling that exists between the various plant systems. In gas-cooled systems, a fault (accident) in one system is less likely to have as significant (or damaging) an effect on other systems.

An inherent negative power coefficient of reactivity is another safety feature of the Magnox and AGR designs. However, in the AGRs and in certain parts of the Magnox core fuel cycle, there is a positive moderator temperature coefficient with a magnitude greater than that of the negative fuel coefficient. Those designs rely on redundant and reliable shutdown cooling systems to ensure that for long-term heatup accidents, a (slow) moderator heatup does not occur. In the case of the HTGRs, most designs have negative temperature coefficients for both the fuel and the graphite moderator over the entire fuel cycle.

The low power density of the GCR core and hence also of decay heat may also be counted as inherent safety features of GCRs. For example, in the event of total failure of the gas circulators (complete loss of forced coolant flow), natural convection in the vertical core is normally sufficient to remove decay heat at operating pressures if secondary cooling is provided. All designs are such that in the event of a complete loss of coolant gas, the decay heat can be removed by means of a safety-grade emergency cooling system, maintaining adequate gas circulation even at atmospheric pressure. In the case of depressurization with subsequent air ingress, there is an additional concern about possible oxidation of the graphite moderator, the clad, and eventually—if exposed—the fuel.

2.2.2 Differences Between GCRs and the Chernobyl (RBMK) Reactor

A common feature of the GCR and the RBMK is the use of a graphite moderator. The very significant differences from the RBMKs are the use of boiling water as the coolant in zirconium alloy pressure tubes and the use of zirconium cladding for the fuel. Under the extreme malfunctioning conditions that existed at the time of the Chernobyl accident, the reactor had a positive void coefficient of reactivity. With such characteristics, core reactivity increased with increasing power, producing still higher power levels and steam generation rates. This autocatalytic effect from the strong positive reactivity feedbacks, along with erroneous operator actions and a positive reactivity effect from insertion of the scram rods, led to a very severe power spike that caused extremely high fuel and cladding temperatures that resulted in dispersion of fuel into the coolant. The subsequent steam explosion ruptured the pressure tubes, and water/steam contacted the hot graphite moderator. The pressure buildup due to the fuel-clad coolant reactions and to water/steam contacting hot graphite was much greater than the low-pressure calandria vessel surrounding the reactor core could contain. This pressure buildup resulted in the rupture of the reactor containment and destruction of the upper-reactor structure. Because of the major differences in fuel, coolant, nuclear, and structural designs, this type of accident is not possible in Magnox reactors, AGRs, or HTGRs.

A GCR, when compared to an RBMK reactor, is stable and easy to control due to the many important differences in design. First, the physical phenomena involved in the GCR single-phase coolant system are relatively simple. Second, the addition of steam to the core (which could occur if there were a failure of steam generator tubes) does not lead to a reactivity increase for Magnox cores. If the coolant flow of a typical Magnox GCR core were deliberately stopped and the power level (somehow) maintained constant, the fuel would heat up about 30°C per second and the graphite, 0.2°C per second. (In an actual event of this type, the fuel negative temperature coefficient would dominate reactivity changes and quickly shut down the reactor.) In the case of a sudden loss of forced flow with no control or safety rods inserted, some melting of fuel cladding may occur, but the fission products would be retained within the primary system. Insertion of the control rod is assured on the basis of engineered or "active" systems and can be accomplished by either primary or secondary shutdown systems (which also are redundant); under these circumstances, there would be no fuel melting.

The safety challenges that are of most concern to GCRs do not involve positive reactivity coefficients but instead are the very low-probability, heat-up accidents associated with the steady buildup of decay heat without adequate heat removal. Such faults could eventually melt the cladding and lead to fission product escape from the fuel into the coolant system. The probability of these scenarios is very low, because mitigating actions are typically not required for very long times. In such

cases where fuel element damage occurs permitting release of radioactivity from the fuel, the fraction escaping to the atmosphere depends on numerous factors, including the degree of damage to the reactor vessel and building, and the presence or absence of a functioning filtration system in the building. In addition, the fractional release to air would also vary the chemical nature of the particular fission product (i.e., noble gases would be expected to be completely released to air, whereas iodine would be retained to some degree in the vessel and the building).

2.3 GCR PHYSICAL PROPERTIES AND PHENOMENA IMPORTANT TO ACCIDENT PROGRESSIONS

2.3.1 Graphite Properties

Graphite has been used widely as a moderator in nuclear reactors, not only because of its good neutron moderating properties, but also because of its small neutron capture cross section. Equally important are its excellent structural properties and its ability to withstand radiation damage. Moderation of fast neutrons to the thermal energy range is necessary to maintain a chain reaction in a thermal reactor. Neutron moderation occurs by energy transfer from the fast neutron (born in fission) to the carbon atoms through elastic and inelastic collisions. Carbon has the highest atomic number of any material that can in practice serve this purpose in a natural uranium–fueled reactor. The collision rate is proportional to the number of carbon nuclei per unit volume of graphite. Therefore, the density of the graphite must be reasonably high if the volume of the reactor core is to be minimized. In general, densities of at least 1.5 g/cm^3 are required for nuclear-grade graphite, and densities of about 1.7 g/cm^3 are routinely fabricated into large moderator blocks.

Maximum impurity concentrations are also specified for nuclear-grade graphite in order to limit parasitic absorptions of thermal neutrons (i.e., absorptions that do not contribute to the chain reaction). This is an important feature due to the inherently high absorption cross section of graphite (for a neutron moderator) and low excess reactivity of reactors fueled with natural uranium. Impurity concentrations less than the equivalent of the absorptive effect of 5 ppm of natural boron are required for nuclear-grade graphite. At this concentration, approximately half of the parasitic absorptions in the moderator are due to carbon and the balance to the impurities. With enriched fuel, this concern still exists but is not nearly as important because of the excess reactivity gained by enrichment.

Several comprehensive reviews of the properties of nuclear graphites exist.[7-9] Nuclear graphites, in addition to meeting the criteria above, must possess adequate strength to meet the structural requirements of the reactor core, adequate thermal conductivity to facilitate heat removal from the energy deposited in the graphite during operation (~6%), and low thermal expansion to minimize core distortion and thermal stresses during heatup and cooldown.

Many physical properties of nuclear graphite have important effects on the course and consequences of accident scenarios. Two of them, stored energy and oxidation, are discussed in more detail below. Another important property is thermal conductivity, which can vary considerably with manufacturing (quality) and orientation, as well as with temperature and irradiation/annealing histories. At higher temperatures, the effective conductivity for a core assembly often includes the lumped-in effects of thermal radiation within coolant holes and between blocks. Core conductivity is important in long-term loss of forced convection (LOFC) accidents in which a major component of the heat transfer is conduction from the core to the vessel and cavity/shield cooling system.

The specific heat of the core graphite is another extremely important property, as it directly governs the bulk core heatup rate in an LOFC. It has a positive temperature dependence, and its variation with irradiation is small. Temperature and irradiation also affect both moderator and reflector graphite nuclear feedback properties over the life of the core, and its variations can have significant effects on the outcome of anticipated transient without scram (ATWS) cases.

2.3.2 Stored (Wigner) Energy

Energy is stored in graphite during irradiation, and the physical changes induced in graphite properties such as stored energy, dimensional distortion, and reduced thermal conductivity are all collectively termed Wigner disease. Stored energy generation and estimates of its release characteristics are important considerations because they are relevant to estimating consequences of serious overheating accidents.

Graphite is normally a highly crystalline structure of carbon atoms. Energy storage in graphite occurs from displaced "knock on" carbon atoms being ejected from their normal graphite lattice position by fast neutrons (or by other secondary collisions and electronic excitation) into interstitial positions between the layer planes and/or migrating to edges of the crystallites. The interstitial carbon atoms can combine with other carbon atoms in a number of ways, usually in clusters, and at higher temperatures, the vacancies may coalesce to form loops. Stored energy release is the consequence of recombination of carbon atoms and vacancies, breakup of C_2 or C_n complexes, and reduction of crystallite lattice strain. At very high exposures, irradiation damage in graphite can become even more complex by extensive crystallite breakup and formation of a larger variety of carbon atom complexes. In such cases, the "classic" representation of a sharp stored energy peak in the vicinity of 200°C will no longer be the dominate feature of stored energy. Stored energy generated in graphite may reflect the specific type and formulation of the graphite, but observed stored energy release characteristics are not significantly altered for different nuclear graphites under similar conditions of irradiation. However, carbons and less than fully graphitized graphites will exhibit a distributed stored energy annealing spectra because they lack fully developed crystallite order.

Thermal annealing of graphite releases stored energy, partially repairs other damage effects, and returns the graphite lattice to some degree, but not completely, to the preirradiated condition. Annealing of stored energy is accomplished by heating the graphite through a range of temperatures higher than the temperature of irradiation. Stored energy annealing can also result from a spontaneous stored energy release, further heating the graphite to a temperature equal to the specific heat deficit. The mechanism of annealing is independent of the specific cause of the radiation damage but depends instead on the "nature" of the existing damage, namely, the extent of atomic dislocations, type of dislocations, interstitial complex aggregations, and the maximum temperature reached during annealing. The temperature reached in annealing determines whether only the simple interstitials, such as single atoms or C_2 complexes, are healed or a more thorough reorganization of the lattice damage is effected.

Different release characteristics of stored energy depending on temperature of irradiation are important for engineering application and assessment. At low irradiation temperatures (30–100°C) and high exposures, a large amount of stored energy can be generated in graphite, sometimes over 600 cal/g. Much of the stored energy for such exposure conditions is releasable by thermal annealing, which usually takes place in a release peak around 200–250°C. For such spectra, the release can greatly exceed the specific heat of graphite at those temperatures and, when initiated, can result in a spontaneous temperature rise up to several hundred degrees centigrade. For very high exposures, stored energy resides in higher-temperature annealing regions and, while its release generally does not exceed the specific heat of graphite at each annealing temperature, the stored energy serves to effectively reduce the specific heat of the graphite. This region has been coined the "tails" of the 200°C peak. In a closed-loop GCR with higher moderator temperatures, stored energy is still accumulated in the graphite, but usually not as much. The annealing distribution for these conditions extends over a large temperature range and does not show the 200°C peak. Also, because of the smaller quantity accumulated and absence of discrete peaking, the bulk of the stored energy in a GCR generally would not be expected to exceed the specific heat of graphite at any temperature. At even higher temperatures of irradiation (>500°C), only a very small amount of stored energy (a

few calories per gram) is stored in graphite. Such conditions are found in HTGRs and water-cooled reactors whose design affords very high temperature operation of the moderators.

The first unexpected release of stored energy occurred in Windscale Pile 2 in May 1952, but the cause of a sudden jump in moderator temperature was unrecognized at the time. The next unplanned release occurred in Windscale Pile 1 on September 30, 1952, after the reactor had been operating 2 years. Once stored energy was generally understood to be a potential safety and operational problem, it was deliberately annealed in a number of air-cooled, graphite-moderated reactors. Windscale Piles 1 and 2, BEPO, Belgian BR-2, BNL graphite reactor, Oak Ridge Graphite Reactor, and French G1 all were subject to significant amounts of stored energy accumulation because of the low operational temperature of their graphite moderator. They all were annealed to prevent unplanned releases.

Water-cooled, pressure-tubed, graphite-moderated reactors at Hanford incurred significant radiation damage to the graphite, causing serious dimensional changes in the graphite stack and very large quantities of stored energy to be generated. Most of this damage occurred during WW-II when the graphite moderator temperatures were deliberately (erroneously) restricted well below 200°C to avoid potential oxidation. Periodic annealing of stored energy was not deemed necessary because the water-cooled pressure tubes provided adequate heat removal capacity to handle any stored energy release if the reactor were to be shut down quickly. Nevertheless, stored energy remained a concern. Eventually, thermal annealing and radiation annealing were used to dispose of stored energy and other manifestations of graphite damage, including serious distortions of the moderator stack.

Stored energy in graphite can be thermally annealed to low residual values over a wide range up to the highest annealing temperature. Re-irradiation will restore some or most of its former characteristics in the range of annealing with relatively short additional exposure. This may dictate a need for re-annealing at planned intervals. To effect thermal annealing of a reactor, the graphite moderator is brought up in temperature somewhat quickly (over a matter of hours) to a higher temperature than that normal for operations, initiating a release of stored energy. This heat input can be obtained from nuclear heating or by the use of electrically heated hot air. Also, the operating temperatures of the graphite moderator can be gradually increased such that no overt stored energy release is encountered but will still cause annealing. Most of the annealing during this slow rise in temperature occurs by thermal annealing and the remainder through a process of "radiation" annealing.

The Windscale reactors were annealed deliberately many times after the first unexpected release of stored energy. Such annealing became standard over the next several years and was uneventful. However, during a routine annealing operation of Windscale Pile 1 in October 1957, the reactor suffered a runaway disabling accident. All the annealing operations before the last one were uneventful, although it was reported that stored energy anneals were more difficult to accomplish as the reactors accumulated more exposure. This annealing difficulty was probably due to the graphite becoming ever more damaged at increasingly higher exposures and the relatively low final temperatures reached during the deliberate annealing operations. Additionally, the planned Windscale annealing operations only relieved that stored energy in the 200°C annealing peak. It should be noted that these repeated reactor-annealing operations did not accomplish any reduction of the stored energy residing above the highest annealing temperatures. This unannealed stored energy played a significant part in the Windscale accident as new high temperatures were reached during the accident.

2.3.3 Graphite Oxidation

Oxidation of the graphite moderator due to air ingress in a long-term LOFC accident has the potential to be a significant heat input affecting the course of the accident. Our studies have shown that there can be many critical factors affecting an accident's outcome. In particular, if forced cooling is restored after a certain point in the heatup accident, it may either be successful in cooling down the core or it can "fan the flames," depending on the temperature the hottest region of the core attains just before the attempted "cooldown."

The subject of graphite oxidation or "burning" is a very controversial one because of the accounts of the Chernobyl and Windscale accidents, which affected the public's perception of safety for graphite core gas-cooled reactors in general. Hence it is important to carefully define the terms used:

- "Oxidation" applies to the general chemical reaction in all its forms, from slow (as in corrosion) to rapid.
- "Burning" is reserved for robust, self-sustaining oxidation in the gas phase involving vaporized material mixing with oxygen, and usually produces a visible flame.
- "Combustion" is synonymous with "burning."

The physical processes governing graphite oxidation are more complex than those of metals because graphite is a relatively porous material. Characterizing graphite oxidation from experimental data obtained from small-specimen testing may not be appropriate for large-core blocks because they do not oxidize uniformly. The variation in oxidation rates for given temperatures and other operational conditions can also be extremely variable with different graphites, being a function of composition, quality (with impurities acquired both during manufacture and operation), irradiation damage, and even the formation of carbon deposits.

Thus graphite oxidation may broadly be placed into two categories, heterogeneous oxidation, in which oxygen in air is transported to a graphite surface where it chemisorbs, reacts, and desorbs as CO or CO_2, or true burning (or combustion), in which temperatures are sufficiently high to vaporize graphite to permit oxidation in the gas phase. Because of its very low vapor pressure, graphite is extremely difficult to burn. No graphite oxidation experiment has ever "burned" graphite, according to this definition, as it would not be expected below 3500°C.

Heterogeneous oxidation may be subdivided into two zones, Regimes I and III. Regime I (or Zone I) occurs at relatively low temperatures or in small laboratory specimens. The chief characteristic is uniform oxidation rate throughout the volume of the specimen. Regime I oxidation is independent of the oxygen delivery rate to the surface and depends solely on the intrinsic chemical reaction rate of the graphite and its internal pore surface area.

Regime III (or Zone III) represents the other extreme in which heterogeneous oxidation occurs primarily within a thin surface skin of the graphite. This would occur at high temperatures where the inherent chemical oxidation rate of graphite exceeds the oxygen transport rate to its surface, or in very large specimens where the thickness of active oxidation zone is small relative to the overall size of the specimen. Here, the surface mass transfer rate controls the overall rate; the inherent chemical rate of graphite becomes inconsequential. It should be noted that this regime may occur with either laminar or turbulent flow adjacent to the surface. If the flow is laminar, the rate will vary with temperature due to its effect on the diffusivity of O_2 in air; the rate will be essentially independent of temperature for turbulent flow.

In CO_2-cooled reactors, carbon deposits form in the pores of the graphite near the cooled channel surface. Since deposits are considerably more reactive than the moderator graphite and since deposit buildup may accumulate to a significant level (2–3%), its oxidation during postulated air-ingress accidents is considered.

An important feature of oxidation modeling is the capability for predicting oxygen starvation effects. The rate of graphite oxidation in the chemical control regime is observed to depend on the

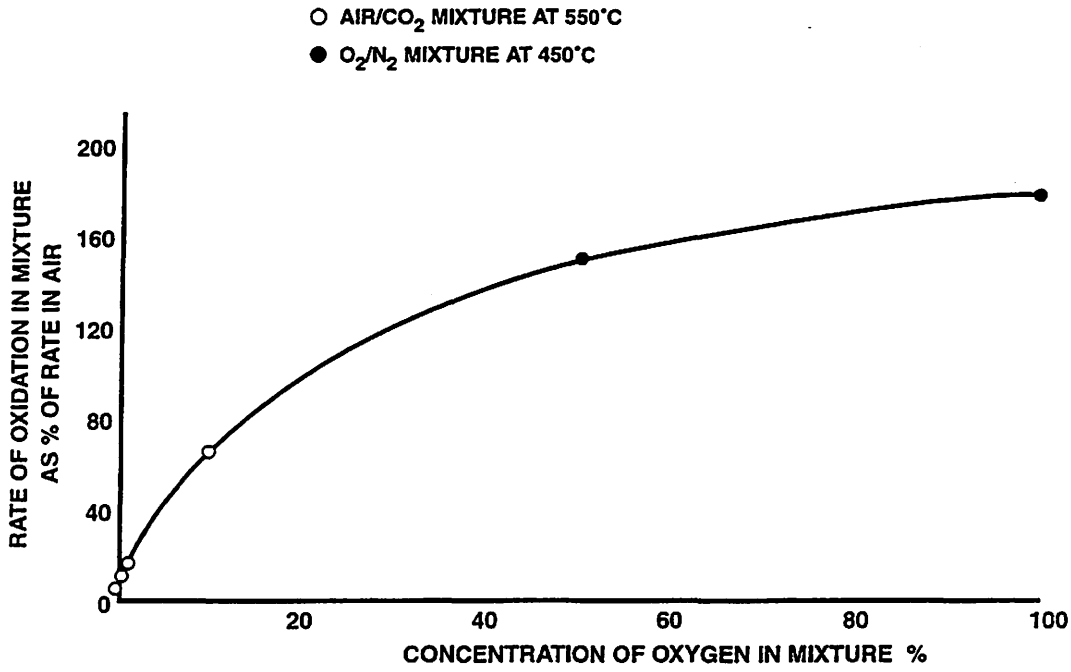

Fig. 7. Graphite oxidation as a function of oxygen concentration for Windscale graphite. *Source*: Nairn and Wilkinson (Ref. 4).

local oxygen pressure, $P(O_2)$, raised to a power, n, between 0.6 and 0.9. For example, Fig. 7 shows the dependence of rate on oxygen pressure for Windscale graphite at 450°C and 550°C as reported by Nairn and Wilkinson.[4] According to this curve, n has a value of about 0.65 at air compositions. Oxygen starvation may also occur in the mass transfer since reduction of oxygen concentration in the free stream reduces the driving force for mass transfer to the surface. Given all these complexities in the characterization of graphite oxidation and noting its potential importance in postulated air ingress heatup accident scenarios, it is clear that careful and detailed modeling and validation are necessary.

2.3.4 Cladding and Metal Fuel Oxidation

Magnox cores contain metallic cladding (aluminum or magnesium alloy), uranium in metal form, and graphite, all of which can theoretically undergo true, gas-phase burning—provided sufficiently high temperatures are generated and air is available. Most vulnerable is the cladding, especially the magnesium alloy, because of its relatively high vapor pressure. At lower temperatures or unfavorable oxygen concentration conditions, surface oxidation occurs instead of gas-phase burning for cladding, uranium (if exposed), and graphite. Whereas true burning depends mainly on vapor pressure, heterogeneous oxidation depends either on the intrinsic chemical oxidation rate of the material, when oxygen supply is adequate, or upon the mass transfer rate of oxygen to the surface at high temperatures when the intrinsic rate is high and the surface reaction is limited by oxygen availability. As a consequence, modeling metal oxidation requires correlations for heterogeneous oxidation, both in the chemical reaction and mass transport limiting phase, and for true gas-phase burning, as well as criteria for selection of the oxidation mode under the local conditions.

The criteria for selection of oxidation regime is illustrated in Fig. 8, which shows the variation of heterogeneous and burning oxidation rates as a function of surface temperature, assuming constant air velocity. The oxidation regime in each temperature zone is depicted by the dashed line. The

chemically controlled, heterogeneous oxidation regime exists at temperatures less than T_1 (Regime I). Here there is ample oxygen supply to the surface, the rate being limited by the slow kinetics of the surface reaction. Above T_1 but less than T_2 is the heterogeneous oxidation regime controlled by mass transfer, termed Regime III. As seen in the figure, the oxidation rate to a first approximation is independent of temperature (assuming turbulent flow in the free stream) in this regime. Above T_2 is the burning regime, where vaporization from the surface and transfer to the free stream begin to dominate over oxygen transfer to the surface.

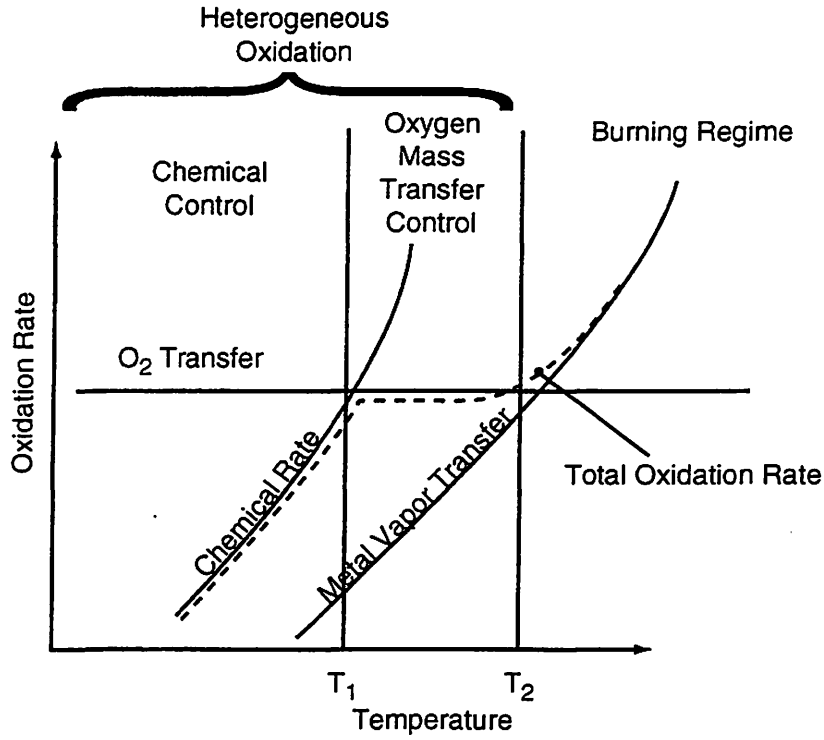

Fig. 8. Metal oxidation regimes (fixed cooling flow rate).

Correlations are needed for all three oxidation modes for the cladding only—aluminum and magnesium alloy. Only the heterogeneous oxidation models are needed for uranium and graphite. Thus far, accident cases have not achieved the high temperatures required for uranium or graphite burning, which would occur, respectively, at about 3000 and 3800°C.

Accidents that do not result in a breach of the reactor vessel, permitting air leakage to the core, may still result in releases of fission products from fuel due to oxidation of metallic uranium by CO_2. It has been shown that chemically controlled oxidation rates of metallic uranium, while lower than rates in air, become comparable at high temperature, that is, above about 1200°C (see Appendix B, Sect. B.17).

Therefore, GRSAC has provisions for estimating oxidation and subsequent radiation release for the fuel in a CO_2 environment. The methodology is identical to that used for release and oxidation by air, with the difference that chemically controlled uranium oxidation rates are set lower than the air rates. The release rate correlations themselves remain the same since, as in the case of air, the release is due to oxidation of uranium.

2.3.5 Fission Product Release

Fission products may be released from the fuel when the cladding has been breached and temperatures are elevated enough to cause a sufficiently high vapor pressure at the fuel surface. As a result, noble gases, krypton and xenon, exhibit high release rates, both because of their high vapor pressures and the lack of chemical interactions (such as solubility) which could diminish the effective vapor pressure.

Most fission product elements do have chemical interactions with uranium metal which tend to retain them within the fuel. As a result, release rates depend heavily on the degree of uranium oxidation, which tends to elevate the effective vapor pressure of many fission product elements. In addition to the degree of oxidation and temperature, tests show that fuel burnup also contributes to an elevation of the release rate from fuel, probably because of the degradation of the fuel at high burnup.

Predicting the release of fission products from magnesium-alloy-clad uranium metal fuel elements relies on a relatively small body of experimental data. Correlations used for modeling releases have large uncertainties due both to the traditionally high scatter experienced by fission product release experiments and to an incomplete understanding of the release mechanisms. Most existing data on fuel element fission product release were obtained to support zirconium-clad oxide fuel elements in LWRs.

The data applicable to this study show that releases typically depend heavily on the degree of uranium metal oxidation. Hence the fission product release rates are dependent (as a function of time during the course of the accident) on the uranium metal oxidation. For the many fission products actually involved in typical releases, this study makes use of the same simplified chemical grouping scheme adopted by the U.S. Nuclear Regulatory Commission (NRC) for LWR severe accidents.[10,11] A listing and a discussion of the eight representative groups are given in Appendix C. The basic information used in this and other similar studies depends primarily on the experiments of George Parker et al.,[12] R. K. Hilliard,[13] and Hilliard and Ried.[14] Fission product releases in GCR heatup accidents vary significantly in the different parts of the core. Since the release rates to the primary cooling system are zero until there is cladding failure and since much of the release thereafter depends on air availability to oxidize the uranium metal fuel, it is evident that the spatial as well as temporal considerations are important. Experimental data indicate that the release of each of the fission product groups is typically a function of burnup, temperature, and uranium oxidation. Noble gases, however, have been shown to be released even in the absence of uranium oxidation.

The phenomena considered in detail in this report are restricted to predictions of fission product releases from the fuel elements. The larger issue of release to the atmosphere involves many other complex phenomena, including identification of release pathways and the prediction of leakage flows as a function of time. Radioactivity trapping mechanisms on reactor vessel and building surfaces include condensation or chemisorption of vaporized fission products and, for lower vapor pressure materials, deposition of fission product aerosols. In some cases, leakage to the atmosphere may occur through control equipment such as filters, the efficiency of which would have to be accounted for in estimation of releases to air.

2.4 ACCIDENT PROGRESSIONS IN GAS-COOLED REACTORS

2.4.1 Historical Accident Occurrences in GCRs

Before discussing GCR accident progressions in general, and for the purpose of relating those discussions to actual events, the only two significant actual occurrences of GCR accidents are summarized below. These accidents occurred in the Windscale 1 reactor in 1957 and the G1 reactor at Marcoule in 1956.

2.4.2 The Windscale Accident

In October 1957, the Windscale 1 plutonium production plant was shut down, and the ninth annealing of the core was to be carried out. The annealing process, as pointed out above, was necessary to release the stored Wigner energy in the graphite to prevent spontaneous uncontrolled energy release. Two nuclear heatings were carried out during this annealing, and a primary cause of the ensuing accident was the second nuclear heating on October 8. This second nuclear heating was applied too soon and too rapidly when some graphite temperatures were seen to be falling but when others were still showing steady increases. This led to the fire through a complex sequence of events. Besides the nuclear heating and Wigner energy releases, other factors that contributed to the excessive heatup were oxidation of graphite and lithium-magnesium cartridge elements, which began to fail at temperatures above ~430°C. Later in the accident sequence, when blowers were turned on in an attempt to cool the core, cladding failure and subsequent metal fuel exposure led to much more extensive rapid oxidation of graphite and uranium in the central portion of the core, while the bulk of the core was cooled quickly.

An important point to be made is that the Windscale reactors were of an open-cycle, air-cooled design. Subsequent reactors built in Great Britain, the Magnox reactors, were modified significantly in several key respects which rendered them far less susceptible to the type of accident that occurred at Windscale in 1957. First of all, graphite moderator temperatures were generally higher throughout the core, resulting principally from the use of a circulating coolant loop rather than once-through ambient air cooling. Higher graphite temperatures reduced the level of Wigner energy in the graphite by increasing the rate of self-annealing during normal operation. As a result, the initiating event for the Windscale fire is not applicable to Magnox reactors. Second, the air cooling that permitted rapid oxidation of overheated graphite and metallic parts of the Windscale core has been eliminated in CO_2-cooled Magnox reactors, unless there is a severe accident which breaches the reactor vessel and exposes the core to air. In addition, use of recirculating coolant and enclosing the core in a reactor vessel avoid the potentially hazardous discharge of coolant from the reactor core directly into the atmosphere.

2.4.3 The G1 Reactor Accident

The G1 reactor accident, also referred to as the G1 channel fire, occurred on October 26, 1956. The reactor was brought to full power of 40 MW(t). During this time, abnormally high temperatures were observed, and soon after reaching full power, the radioactive monitoring systems activated an alert. Observation of the core through optical devices indicated that a large portion of a fuel canister's magnesium cladding had burned and the uranium fuel was resting on a bed of magnesia. Later studies indicated that cladding temperatures must have exceeded 630°C and that a fire had started in a normally hot region, possibly intensified by a reduced flow rate. The cause of the accident was speculated to be either (1) a fuel canister leak during the temperature rise, (2) reduced coolant flow by protrusion of the cartridge into the central slot, or (3) partial obstruction of the channel by a foreign body.

2.4.4 Accident Progression Scenarios

Accident progression scenarios of most concern for the earliest gas-cooled-reactor designs—those with relatively low power densities and once-through air cooling—were primarily blocked flow channel incidents and the potential problems resulting from stuck control or scram rods. Following the discovery of the Wigner stored energy effect, and especially after the Windscale fire accident that resulted from an attempt to anneal the core, the dangers and uncertainties in dealing with the Wigner effect became apparent and led to the shutdown of the second Windscale unit as well.

Long-term loss-of-coolant accidents (LOCAs) for the lower power density cores, such as the French G1, Brookhaven, and Oak Ridge Graphite reactors, were not of particular concern, as long as control rods (or backup boron balls) could be inserted, since the afterheat was small for these massive cores with very high heat capacities. The potential for stuck control or scram rods was greater in the early cores due to radiation-induced warping of the graphite core blocks, which tended to distort the entry paths for the rods. There were also reliability problems with boron balls backup systems (the test of the ORGR system following the reactor's final shutdown found the balls rusted together in a clump; i.e., they did not fall).

With the later higher power density Magnox designs, postaccident long-term shutdown cooling did become a concern because it would be required, along with a scram, to prevent overheating of the fuel. For the case where the fuel was taken to higher burnup levels, the moderator temperature-reactivity coefficient could become positive, and in some cases could in the long term override the negative coefficient effect of the fuel. (The AGR cores have this characteristic overall core-positive coefficient, and elaborate redundant means are provided to ensure the availability of long-term core cooling.)

Because the Magnox cores operate at higher temperatures than did their predecessors (so the specific energy storage does not reach a critical value as it could when the graphite is irradiated at the lower temperatures), and because they have closed-cycle CO_2 cooling, there is not as much concern about Wigner energy release (even though the total amount of energy stored in the older Magnox cores is estimated to be many times the amount stored in the Windscale cores).

For Magnox reactors, long-term-heatup accidents that involve air ingress are also of concern because of the potential for graphite, cladding, and metal fuel oxidation. For air ingress scenarios where significant oxidation could occur, there would need to be breaks in the primary system that would allow access for inlet air as well as another break for the exit air. If this were such that a chimney effect occurred, then a substantial oxidizing air flow could occur. Another scenario would be for a single break to occur at the circulator(s) inlet, with air access to that break, and then for the circulator to continue operation. Hence while these are possible scenarios, they would clearly be considered low-probability accidents.

The Windscale accident was also caused by "air ingress," in a sense, in that the air cooling system was used in a final attempt to cool the overheated core, and resulted instead in causing rapid oxidation of a significant portion of the central core's fuel elements (both the aluminum cladding and uranium metal fuel) and a substantial portion of the surrounding graphite.

The AGRs use of stainless steel cladding material and oxide fuel eliminated the concern for fuel element oxidation in air ingress accidents, although the possibility of graphite oxidation for prolonged air ingress would persist, but to a much lesser extent without the exacerbating effects of fuel element oxidation.

In the newer ceramic fuel core designs, with either pebble or prismatic elements and high-pressure helium coolant, the HTGRs are much more resistant to all of the above postulated accident scenarios. In the modular designs (MHTGR), the core design is such that for all loss of helium coolant and forced convection, a safe cooldown (without fuel damage) can be achieved with only conduction and radiation heat transfer out from the center of the core to a passive heat reject system (vessel cavity cooler).

In the steam cycle HTGRs, a positive reactivity may be induced by steam/water ingress due to steam generator tube breaks. The extent of the concern depends on the nuclear design and the speed and magnitude of the potential reactivity insertion. Prior simulations of beyond-design-basis accidents of this type for the U.S. design indicated that core damage would be minimal. For the gas turbine cycle designs, the chances of a water ingress accident are much reduced, since the water-cooled heat exchangers in the primary cooling system have low-pressure water-cooling systems.

2.5 MODELING ISSUES

The modeling capabilities found to be crucial in studies of GCR accident scenarios included a very wide spectrum of interacting effects, with one of the key features being the complex interactions among all of the effects modeled. First, models of the heat transport (conduction, convection, and radiation) within the core, primary system, and heat rejection systems are basic to the problem. Second, the heat generation (fission and afterheat) also needs to account for the spatial distributions. The modeling of heat produced from oxidation (graphite, cladding, and metal fuel) is especially dependent on local oxygen availability as well as the local temperatures of the materials of combustion. In the older air-cooled and even in the later Magnox designs, modeling of the distributed Wigner stored energy releases can be crucial to the accident outcome. To complicate matters even more, the modeling of oxidation and Wigner energy release is dependent upon graphite properties and prior annealings and can be very spatially dependent. For example, in the Windscale accident, only a portion of the core was involved in the accident while the average core temperature remained quite low.

In this work, we extended state-of-the-art models that have been developed for modern HTGR accident simulations to include models for the important physical phenomena, and accident progressions, for the metal-fueled GCRs that are the subject of this report. In the next chapter, we describe the development of the Graphite Reactor Severe Accident Code (GRSAC) for simulating the accident progressions of interest. The prediction of accident consequences also includes determination of the extent of fuel failure and the fission product release from the fuel.

3. GRSAC—A GRAPHITE REACTOR SEVERE ACCIDENT CODE

3.1 GENERAL DESCRIPTION

GRSAC (Graphite Reactor Severe Accident Code) is a general-purpose program based on the ORNL MORECA code[15] for simulating accident scenarios for selected types of gas-cooled reactors. MORECA was originally developed at Oak Ridge National Laboratory (ORNL), beginning in 1974 under sponsorship of the U.S. Nuclear Regulatory Commission (NRC), to perform confirmatory licensing-related studies of the Fort St. Vrain HTGR and later the 350-MW(t) steam cycle modular HTGR (MHTGR). MORECA was later developed under sponsorship of the U.S. Department of Energy (DOE) to simulate the MHTGR design for the direct-cycle gas turbine HTGR. MORECA is known as a "hard-wired" code (i.e., the Fortran simulation program with C-language programs for the user interface is set up for a particular reactor configuration). For the many versions of MORECA, coding changes are needed to alter the models for the core and component configurations.

The conversion of MORECA to GRSAC involved the addition of a front-end graphical user interface that can generate the connectivities needed to assemble, check out, and run simulations for a wide variety of graphite-moderated, gas-cooled reactor designs. The basic designs that the user may modify currently include the British and French Magnox reactors, including Calder Hall, G1, G2/G3, and Windscale. Special provisions have been made in the code to simulate Bugey-1 (France), and the HTTR (Japan). Most importantly, to extend the MORECA capabilities to analyze the early metal-fueled GCRs, graphite, cladding, and fuel oxidation models have been incorporated which predict oxidation rates and heat generation from the oxidation in each core node.

3.2 NUCLEAR SIMULATION

The three-dimensional (3-D), hexagonal geometry core model in GRSAC uses one node each for the 163 fuel and 42 reflector elements in each of 14 axial regions. The core representation (205 × 14 = 2870 nodes) thus allows for detailed investigations of azimuthal temperature asymmetries in addition to axial and radial profiles. Variable core thermal properties are computed as functions of temperature and are dependent on orientation and radiation damage. An annealing model for graphite accounts for the increase in thermal conductivity that occurs during heatup accidents.

Using the anticipated transient without scram (ATWS) option, the expected scram would not occur at the time of an LOFC accident but instead could occur at an arbitrary later time or not at all. Slow rod withdrawal accidents can also be simulated if they are in conjunction with an LOFC accident. The point kinetics approximation for the neutronics is a prompt jump, single precursor group model that compares favorably, for transients of the appropriate rate and magnitude, with calculations using a "full" point model with prompt neutron generation time and six delayed neutron precursor groups included. Temperature-reactivity feedback from the 3-D modeling of fuel, moderator, and reflectors utilizes nuclear importance weighting. Models for xenon and samarium poisoning are included.

Selection and modification of the radial and axial peaking factors can be done via special graphical interfaces, automated "curve generation," and automatic consistency checking. Azimuthal perturbations (for hot channel studies) can also be implemented.

3.3 THERMAL HYDRAULIC SIMULATION

The primary coolant flow models cover the full ranges expected in both normal operation and accidents, including pressurized and depressurized accidents (and in between), for forced and natural circulation; for upward and downward flow; and for turbulent, laminar, and transition flow regimes. For the primary system gas (CO_2, helium, or air), loop pressure calculations consider variable inventory (due to depressurization actions) and loop temperature changes. An option allows for air ingress following depressurization.

The selection of fuel element designs is made via a special graphical interface. Currently, the Windscale, Calder Hall, G1, and G2/G3 reference design elements are included, with parameters tied to performance data found in the literature. The programmed input option allows for preprogrammed operational changes in lieu of entering the changes via the interactive accident screens while the simulation is in progress. The user can preprogram a delayed scram; depressurization (start time, duration, and an option to change the primary coolant from carbon dioxide to air following the depressurization); operation of the shutdown and shield/cavity coolers; speedup/slowdown of the blower coastdown on LOFC, flow, and power vs time; and an increase/decrease in unison of the initial power and primary flow. A model for Wigner energy release from the annealing of irradiated graphite and a model for failure and oxidation of isotope target cartridges and aluminum cladding are available. More details on models of particular importance to the current study are given in the Appendixes.

3.4 OXIDATION MODELING

Oxidation models are included in GRSAC for the graphite moderator, magnesium and aluminum cladding, and uranium metal fuel in each of the 1630 active core nodes. They are activated when the appropriate oxidation flags are set (user input selections) during accident runs when air is in the coolant circuit (for air-cooled reactors or for CO_2- or helium-cooled reactors for which a depressurization and air- ingress accident has occurred). The application of the oxidation models in GRSAC is described in this section. The models are fully described in Appendix A for graphite and in Appendix B for metallic components.

At the start of an oxidation transient, inlet gas flow to the core is assumed to be 100% air, which mixes with any oxygen-depleted reverse flows there may be from the core. It is assumed that only CO_2 is produced from graphite oxidation and that the heat of reaction is deposited in solid material in the node. Oxygen and CO_2 concentration changes in the direction of flow are assumed not to affect air transport properties used for flow and heat/mass transfer correlations.

The oxidation rate of each material depends on the oxidation regime, which must be determined for the current conditions in each node in order to select the appropriate rate equations. Two regimes of heterogeneous oxidation (HO) are assumed possible for each material: chemically controlled or mass transfer controlled. With the notable exception of magnesium, one or the other type of HO is the expected oxidation regime for all Magnox core materials under even fairly severe accident conditions. HO is a relatively slow form of oxidation, intuitively visualized as a lump of glowing graphite or metal. A third oxidation regime assumed in GRSAC may be termed "true burning," defined as a vigorous, self-sustaining, gas-phase oxidation. True burning occurs at high temperatures when vaporization of the base material begins to dominate over the diffusion rate of oxygen to the surface (and there is sufficient availability of oxygen). Accordingly, true burning occurs for bulk uranium and graphite only at temperatures exceeding about 3300°C and 3800°C, respectively, but is known to occur for magnesium in the 600 to 900°C temperature range. The current version of GRSAC contains a true burn model only for magnesium. Carbon deposit oxidation is also modeled for CO_2-cooled reactors.

A key factor in the progression of oxidation through the core is the availability of oxygen. Oxidation rates in both chemically controlled and mass transfer controlled HO regimes depend directly

on the oxygen concentration. The oxygen concentration therefore must be tracked by means of oxygen and CO_2 mass balances along each flow path. When oxidation rates are sufficiently high to consume all oxygen within a time step, a method is applied which terminates the oxidation at the appropriate time during the time step, apportioning the oxygen between materials according to the calculated initial rates. Necessity for this procedure was demonstrated during GRSAC trials of the French G1 accident mockup when rapid magnesium oxidation rates were observed.

Cladding and fuel oxidation models are activated via a user input flag, separate from the one used to activate graphite oxidation. In the default case, the cladding is assumed to prevent fuel oxidation in each node until its melting temperature is reached or until 90% of the cladding becomes oxidized. An alternative selection (user input) inhibits fuel oxidation until the cladding is oxidized. In the case of aluminum cladding, oxidation is inhibited due to a protective oxide film until the aluminum melting temperature is reached.

3.5 STORED (WIGNER) ENERGY RELEASE MODEL

Graphite irradiated at relatively low temperatures will accumulate significant amounts of stored energy that may be released either under controlled annealing conditions or uncontrolled accident conditions. For a reactor with major low-temperature regions, such as the air-cooled Windscale reactor, inadvertent or excessive releases of stored energy may be important factors in the progression of an accident. Stored energy release is less important for Magnox reactors, which operate with higher graphite temperatures. In addition, some early commercial Magnox reactors have insulating sleeves in the coolant channels which are designed to further elevate graphite temperatures.

General features of stored energy release are described in Chapter 2. The stored energy model in GRSAC incorporates most of the features shown in Fig. 9; a "trigger" or initiation temperature begins at roughly 50°C above the irradiation temperature, and a peak release rate at about 200°C followed by a decline to a steady level extending to higher temperatures. GRSAC approximates this behavior by means of a triangular function, where the peak and constant levels are dependent on both irradiation temperature and exposure. In Windscale, the 200°C peak is prominent near the cooler (inlet) part of the core and diminishes, as shown, in the hotter (outlet) region. For Magnox reactors, most of the core graphite is irradiated at higher temperatures, for which the 200°C peak has all but disappeared. The total amount of stored energy (calories per gram) available for release is also a function of the irradiation temperature and exposure, and this function is built into the model as well. Only a fraction of the total stored energy is typically released upon annealing. This fraction is not well established due to difficulties in making high-temperature energy release measurements, as well as in determining flux-irradiation temperature distributions and the effectiveness of prior annealings.

3.6 FISSION PRODUCT RELEASE MODELS

Models for the release of radioactivity from damaged uranium metal fuel elements are presented in Appendix C, together with a description of the available data base. An important simplification is grouping the many fission products into chemically similar categories and applying a release model to all isotopes in the category. The following categories are recommended for use in reactor safety studies[10] and are programmed in GRSAC: noble gases; halogens, mainly the iodine isotopes, but also some short-lived bromines; alkali metals, principally several cesium isotopes; the "tellurium" group; alkaline earths, strontium, and barium; noble metals; lanthanides; and the cerium group. The elements within each group are given in Appendix C. Accident evaluations generally place highest importance on groups 2, 3, and 4. Many nuclides in these groups have the highest combination of volatility, dose factor, and potential for biological concentration. This judgement may need to be reevaluated for

extremely energetic events that can release low-volatility material from groups 5 to 8. Many nuclides in these latter four groups have high inhalation dose factors.

Once the cladding is breached, fission products may be released from the uranium metal fuel body due to (1) uranium oxidation, (2) elevation of temperature, (3) melting, and (4) damage due to burnup. Section C.3 describes the effects of these release mechanisms on each fission product group. Application of release models from fuel in GRSAC requires accounting for the degree of uranium oxidation and the fuel temperature at each node. The fuel burnup, also required in the model, is provided as an input parameter. The release model is activated when GRSAC determines that cladding failure has occurred, defined as when either the cladding temperature in the node exceeds the melting point, or when GRSAC determines that 90% of the cladding has oxidized. Traditionally, large error bands are associated with fission product release correlations due mainly to the difficulty of the experiment. Error band percentages are largest for the less-volatile materials with the smallest release factors.

3.7 OTHER GRSAC FEATURES

User-Friendly Features. Considerable effort was applied to the task of making GRSAC user friendly. For example, units conversion options are available on all data input screens and on the "Initial Conditions," "Accident," and "Plot" screens. On-line help is provided on each screen via a help button. The pop-up screen that is displayed is designed to give the user help in understanding the options available on that screen. On-line documentation and "Help" screens are updated with each new release of GRSAC.

Input Validation. A "run with validation" selection runs a verification check on the user input values for the simulation. A text window displays what problems, if any, exist with the data. The user

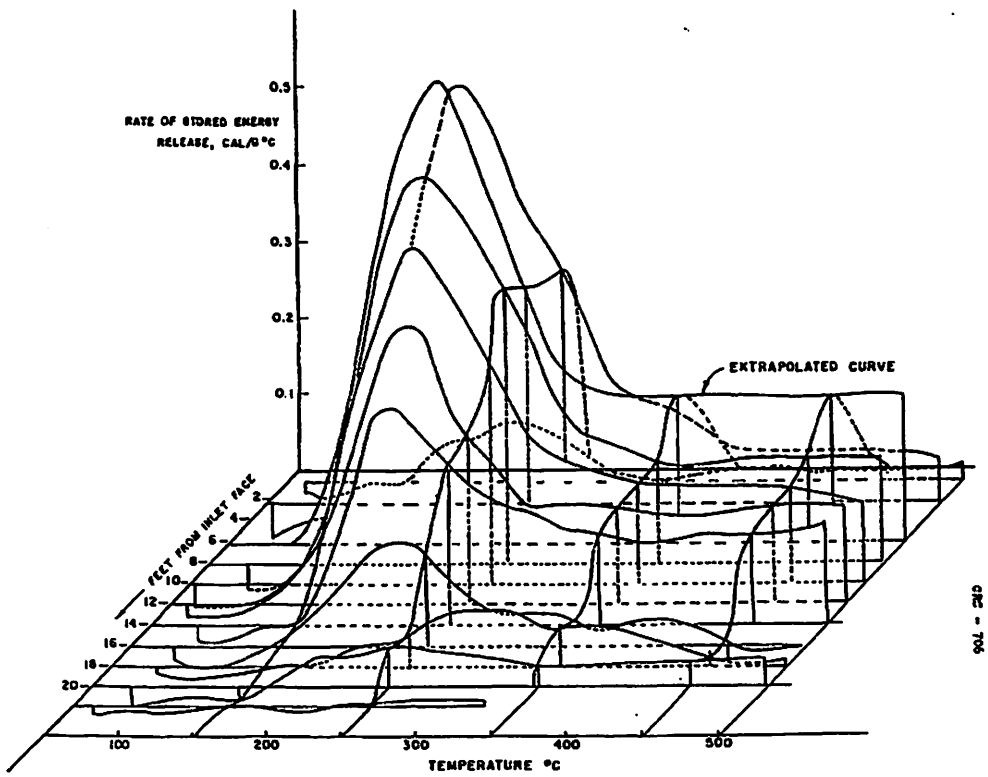

Fig. 9. Stored energy release spectra spatial distribution in Windscale 1. *Source:* Attree et al. (Ref. 16).

is not prevented from running the simulation if some invalid input exists, but there is no guarantee on how the simulation will run given bad input.

Sensitivity Study Option. A sensitivity study option helps to quantify the accuracy limitations of the simulation, as well as to determine the relative importance of various parameters to the outcome of the accident. The rationale is to seek out a set of parameters within specified uncertainty bands that results in the worst-case (or best-case) accident consequences. Sets of 15 model (design) parameters and 13 operational/run parameters are currently available for automatic variation (from run to run) and allow the user to select up to 10 from this set for any given study. To study the effects of a single parameter variation in more detail, a single-parameter option can be used. A report generator, the results of which are available after the runs are completed, lists detailed results of the study.

Plotting. The dynamic plot options for both initial condition and accident runs feature plotting of selected variables vs time and/or other sets of variables vs "length"—that is, profiles vs axial position in the core. Some radial profiles are also available for initial condition plots. The user can toggle between the accident (or initial condition) and plot screens, and may print or change plot specs during runs. Both on-line and post-run plotting are available.

Fast Run Times. Timing runs were done with various features implemented. For non-ATWS runs with graphite, fuel, and clad oxidation and with Wigner energy, GRSAC ran 1250 times faster than real time on a single ™CPU SUN SPARCstation 20. Not including oxidation or Wigner, GRSAC ran 1700 times real time. Using a dual CPU SUN SPARCstation 20, GRSAC ran 2100 times real time with oxidation and Wigner included and 2600 times real time without them. Using a DEC Alpha 500/500, GRSAC ran at 11,300 times real time, which means that a one-week accident could be simulated in about one minute. On-line plotting appears to have a negligible effect on timing.

4. GRSAC CODE VALIDATION

Two instances of "fires" in air-cooled, graphite-moderated, uranium metal–fueled cores were used to validate the thermal hydraulic and damage estimate features of the GRSAC code. The first is that of a fire at the Windscale reactor located at Sellafield, England, which was started by events occurring on October 8, 1957. The second case is a channel fire in the French G1 reactor on October 26, 1956. An extensive description of benchmarking the Windscale fire is given in Appendix E, and the French channel fire experiments, in Appendix F.

4.1 COMPARISON WITH THE WINDSCALE PILE FIRE

4.1.1 Important Windscale Design Features

In Windscale, cooling air was forced into a plenum at the charge face, passed horizontally through the core in the fuel channels and into an exit plenum at the discharge face, through a duct containing fission product detectors, and into the base of a 400-ft stack. The significance of once-through cooling with ambient air is both the introduction of oxygen into the core and creation of large regions of cool graphite, ideal for storing radiation-induced energy. Lithium-magnesium alloy "AM" cartridges inserted in a number of the isotope channels were used as target material for the production of tritium. Ignition of this alloy was an important link in the chain of events leading to the fire. The cladding was aluminum; although oxidizable and flammable under aggressive conditions, the oxidation resistance of aluminum is superior to that of magnesium used in Magnox reactors.

4.1.2 Description of the Pile Fire

The five-day accident, from the first anneal through the termination of the fire, has been described in detail in various publications, most recently in Chapter 4 of the extensive historical account *Windscale 1957* (Ref. 17). Because of the sensitivity of the results to the precise details of the sequence, an effort was made to verify sequence details provided in summary reports with information given in testimony of the Court of Inquiry, other written statements, and control room log data. A fairly complete record of occurrences is given in Sect. E.7 of Appendix E, abstracted from the following sources: the Windscale Pile 1 control room log,[18] Summary Table for the Event,[19] and the Testimony at the Court of Enquiry.[1]

Figure 10 shows critical events in a time line covering the full 5-day period. (The time line shown in Fig. E.3b of Appendix E focuses on the last 40 h.) The accident occurred during a procedure for annealing the Wigner stored energy from graphite. Following the first heating, from Monday evening to early Tuesday, opinion was that a second heating was required as indicated by some core temperatures declining more rapidly than expected for a successful anneal. The critical second nuclear heating was conducted from late Tuesday morning into the evening. It is highly likely that the accident was initiated by an event, or events, which occurred during this second heating. A sharp rise in uranium temperature, from 80°C to 380°C, occurred within 15 min after the start of the second heating, as indicated by a thermocouple reading.

Factors involved in the overheating of the core were the intentional shift in fission power peaking (to concentrate the heat in the cooler inlet portion of the core most in need of annealing) and the manual control scheme used to adjust the power level. Power was controlled to limit fuel temperature rise rate. However, since there were no thermocouples monitoring fuel temperatures in the core inlet region, the operators relied on fuel temperature rise rates in the center of the core where the power peaking factors were low. This led to an underestimation of the extent of the heating occurring near the inlet.

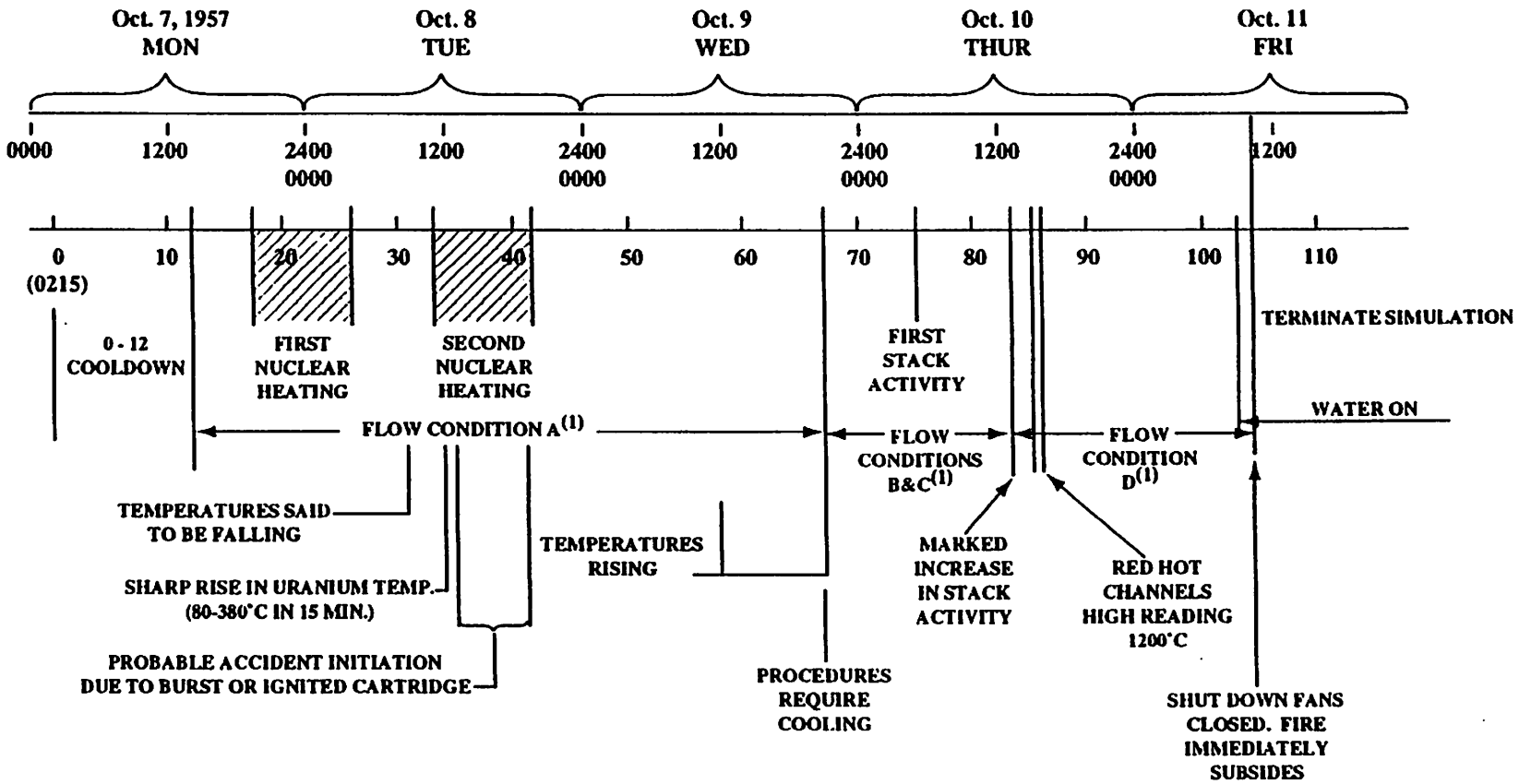

(1)FLOW CONDITIONS

A	0.01-0.05	kg/s	[Dampers Closed, Hatch Open]
B	0.3	kg/s	[Dampers Closed, Hatch Closed]
C	7.5	kg/s	[Dampers Open, Hatch Closed]
D	~120	kg/s	[Shutdown fans on]

Fig. 10. Five-day overview of Windscale accident events.

Air flow through the core was maintained at its lowest possible level. Some thermocouples indicated a gradual rise in temperature during the latter half of this period, in retrospect probably caused by local oxidation of leaking AM cartridges damaged during the second nuclear heating in addition to continued Wigner energy release. In such cases of observed temperatures in excess of set values, procedures called for increased air flow to produce a cooling effect. Therefore, late Wednesday an increased flow was generated by sealing the hatch at the base of the chimney, assumed in this analysis to be about 0.3 kg/s (flow condition B in the time line).

In Sect. E.5 of Appendix E, the effects of increased air flow on an overheated core are discussed. A cooling effect is achieved provided temperatures are below some specific value. Above this critical temperature, which depends on the particular geometry and materials, increased air flow no longer provides a net cooling effect but has the opposite effect of generating even more heat from oxidation.

In retrospect, the following period, from 2200 Wednesday to 1000 Friday, is just such a time of exacerbated oxidation in the central core region, resulting from repeated increases in air flow. This period is shown with more detail in Fig. E.3b of Appendix E. From this time (2200 Wednesday), air flow was never reduced back to condition A (see Fig. 10). Instead, the chimney hatches were kept shut and the dampers were repeatedly opened (flow condition C), causing increased air flows assumed to be about 7.5 kg/s.

The increases in air flow did not succeed in lowering central core temperatures. A marked increase in stack activity was observed following the third damper opening. A fourth damper opening at about noon Thursday was similarly followed by high activity reading, this time at the meteorological station on the roof of the reactor. Finally, at 1330 Thursday, the shutdown fans were turned on (flow condition D), increasing air flow to about 120 kg/s. The shutdown fans remained on until the end, at 1000 Friday. It was hoped the fans would cool the pile, which momentarily seemed to be the case. However, there were soon reports of high activity readings at the roof station, and the highest recorded uranium temperature began to rise rapidly, reaching 460°C. The previous concerns regarding pile behavior gelled at this point into the realization that a serious event was in progress.

From the time that the shutdown fans were turned on (1330 Thursday), the core condition steadily deteriorated. Glowing fuel and graphite were observed at 1700 Friday involving 100 to 144 channels, and progressively higher temperature flames were seen emanating from the exit face of the core. In addition, there were indications that the involved zone was spreading radially. With a calculated risk, water from a fire truck was introduced into the core at 0900 Friday. Flames continued emanating from the rear of the core. According to the Penney Inquiry,[1] the fire immediately subsided upon shutting off the shutdown fans at 1000 Friday. This action cut off oxygen and suffocated the fire. Water flow continued, finally cooling the core.

4.1.3 Reported Damage Summary

A detailed description of the damage suffered by the Windscale core has not been published. What appears clear is that relatively few fuel channels were involved, although there were indications of gradual radial spreading towards the end. According to the Penney Inquiry, 150 fuel channels of the 3440 total were observed glowing red (at 1630 on Thursday), signifying temperatures of about 700°C, beginning about 2 m from the inlet face. This indicates that 3.1% of the fuel was involved in the fire. The fire involved a fairly slim axial column of material in the core. And, according to a later reminiscence by Sir John Cockroft, a member of the Penney Inquiry, some 10 tons of uranium were melted during the accident, amounting to about 6% of the total amount of uranium. The degree of aluminum damage is not known. Testimony by a core designer stated the expectation that aluminum was not flammable. Aluminum does oxidize and burn, although much less readily than magnesium. The Windscale-specific GRSAC setup includes a model for aluminum oxidation.

A memorandum written for the Penney Inquiry states that probably most of the AM cartridges in the observed area of red hot uranium were burned away, which at the time the plugs were first removed (1400 Thursday) extended over an area of 3 m by 2.5 m. Smith et al.[20] tried to estimate the

scale of core damage from iodine concentrations monitored at air stations downwind. The method is a bit uncertain and possibly may be improved using modern software. Table 2 presents damage estimates based on three assumptions.

Since iodine release depends primarily on the degree of oxidation and only secondarily on melting or excess temperature, the term *fuel melted* should possibly be *fuel oxidized* (see fission product release from fuel discussion, Appendix C). But the estimate is consistent in terms of total damage with both Cockcroft's recollection and the observed involvement of about 150 channels reported by the Penney Inquiry.

Table 2. Windscale damage estimate based on noble gas release

Assumption	Quantity of fuel melted	Number of channels
1. No iodine retention on filters	8.9 tonnes	156
2. Filters retain 50% of iodine	9.3 tonnes	164
3. No iodine released	11.0 tonnes	193

Source: Smith et al., Ref. 20.

From an account in Arnold (Ref. 17, p. 74) inspection of the core revealed that both fuel and graphite appeared undamaged for a distance of about 2 m from the charge face. Further on, damaged graphite and blocked channels with "mangled and melted fuel" were visible. "Of 180 tonnes of uranium in the core, about 22 tonnes were not recovered; it was estimated that 5 tonnes had been burned and that 17 tonnes remained in the core." In terms of percentages, these estimates are equivalent to about 3% of the uranium oxidized and an additional 10% melted. No mention is made of the degree of graphite or aluminum damage. A concurring estimate is that 20 tonnes of uranium could not be removed from the core and remain in place to date.

4.1.4 Fission Product Release

Several studies have been made where iodine, cesium, and tritium (in one case) concentrations in air were traced back, by means of atmospheric transport assumptions, to yield estimates of release from the core. A summary is given in Appendix IX of the Arnold Reference.[17] Results are summarized in Table 3.

Table 3. Estimated volatile fission product releases to the atmosphere (curies)

	Command 1225[21]	Beattie[22]	Clarke[2]	Chamberlain[23]
Iodine-131	20,000	20,000	16,200	27,000
Cesium-137	600	600	1,230	---
Tritium	---	---	---	100,000(?)

Source: Arnold, Ref. 17.

4.1.5 Windscale-Specific Core Damage Models

Section E.4 of Appendix E describes the specific damage models necessitated by the unique materials in the Windscale core. A study cited in Appendix E indicates that the Windscale graphite, having been subjected to air and sea spray contaminants, oxidized at a significantly higher rate than one would find in a closed-loop, pressurized, gas-cooled graphite reactor. In addition, the active oxidation depth, a parameter vitally important to a graphite oxidation assessment, also appears to have been greater than expected, based on comments made in postaccident testimony. A Windscale-specific graphite oxidation rate expression was derived, applicable to the chemically controlled, heterogeneous oxidation regime. The model for oxygen-transport-controlled, heterogeneous oxidation is not affected.

Aluminum was used as a cladding material in Windscale. Literature searches failed to locate any oxidation rate data in the chemically controlled, heterogeneous oxidation regime. An additional problem is noted with the adherent oxide film that protects against oxidation under some conditions. After due consideration the following approach was selected: It was assumed that an adherent oxide layer would provide oxidation protection up to 640°C (20°C below the melting temperature). Above 640°C, the chemically controlled, heterogeneous rate equation for magnesium was used for aluminum. The rationale for this selection is that under aggressive conditions, the adherent film would not be protective when the base metal becomes molten. No change is required in the oxygen transport rate expression.

Also unique to Windscale were the aluminum-clad, isotope production targets containing a lithium-magnesium alloy. These so-called AM cartridges were used for the production of tritium. The oxidation model for these targets was based completely on their reported behavior when heated in air. Table E.4 in Appendix E shows that AM cartridges begin to fail at 440°C and may ignite at 450 to 550°C. The empirical model takes into account the reported time-at-temperature behavior. The stored energy release model used for Windscale is based on the data shown in Fig. 9 for Windscale irradiated moderator graphite removed between the eighth and ninth anneal. (The accident occurred during the ninth anneal.) The numerical procedure for approximating stored energy release is described in Appendix E.

4.1.6 GRSAC Simulation of Windscale

The GRSAC modeling for the Windscale fire is described in Sects. E.6.1 and E.6.2 of Appendix E. The major features are the following:

1. cooling by air in horizontal passages,
2. replication of the unique power peaking factors used at Windscale for inducing Wigner energy release,
3. programmed core power history for the accident sequence,
4. programmed coolant flow history,
5. model for simulating the failure and subsequent oxidation of the AM cartridges,
6. models for oxidation of aluminum (not used in Magnox reactors) and the more reactive Windscale graphite, and
7. model for graphite thermal conductivity modification due to annealing.

4.1.7 GRSAC Simulation Results

Final damage state

Comparison of reference case GRSAC predictions for the reactor end state with reported estimates are given in Table 4. Observed damage state estimates for Windscale are sketchy, and values listed in the table are in some cases interpretations from qualitative reports. (See Sect. E.6.8 of

Appendix E for sources of the values listed under "reported observation.") As the table shows, benchmark damage results for Windscale give a reasonable approximation of the reactor end state, given the uncertainty of the observations.

A "damaged" fuel element is defined for Table 4 as one in which the uranium is exposed. The GRSAC estimate of 15% is based on the calculated amount of cladding subjected to temperatures above the melting point (a portion of which may have later oxidized). On the other hand, the "observed" 3.1% is based on the volume of the core obviously involved in the fire. On this basis, the observed damage is expected to be lower than the GRSAC estimate since there certainly was fuel damage outside of the fire zone.

Table 4. Windscale final damage comparison

	GRSAC result	Reported observation
Damaged fuel elements (%)	15	3.1
Maximum fuel temperature (°C)	1740	NA[a]
Uranium oxidized (tonnes)	36.5	~5–11
Uranium melted (tonnes)	27.3[b]	~17–20
Aluminum oxidized (tonnes)	2.2	NA[a]
Aluminum melted (tonnes)	2.7[b]	NA[a]
Graphite oxidized (tonnes)	71	NA[a]

[a]No estimate found.
[b]GRSAC reports material above original melting temperature.

The amounts of uranium oxidized and molten as estimated by GRSAC agree fairly well with the reported Windscale estimates. The reported 5- to 11-tonne oxidation range, based on the iodine release study cited earlier, is lower than the GRSAC 36.5-tonne estimate. Also, the reported range of 17 to 20 tonnes molten, from largely anecdotal sources, is in fair agreement with the 27.3-tonne GRSAC estimate. As should be expected, GRSAC damage estimates are higher than the reported values. The reasons are that during the accident, much fuel was removed from regions surrounding the central damage zone in an attempt to control the spread of the fire, and channel blockages occurred due to debris formation, thus reducing the flow of oxygen. These features were not modeled and hence should lead to higher GRSAC damage estimates. No reports were found describing cladding damage or degree of graphite oxidation. The GRSAC estimates are given in Table 4.

Replication of the accident sequence

Perhaps the most significant feature of the GRSAC simulation is demonstrating the validity of the authoritative observation of Hill[24] that in the early stages of the accident the Windscale core was delicately balanced between capability for cooldown and progression to fire. The GRSAC simulation clearly demonstrated this behavior. Slight modifications of the reference case decreasing the tendency for fire (e.g., reduction in Wigner energy release, graphite reactivity, air flow rate, or other chemical reactivity of other materials) usually led to a prediction of cooldown when higher air flows were implemented.

Another important feature of the sequence demonstrated by GRSAC is the manner in which the accident was terminated. The simulation shows that cutting off the shutdown fans at 1000 on Friday, when the fire was at its most intense level and spreading, effectively suffocated the fire. According to the account in Arnold,[17] this was the way the fire was extinguished. Some accounts attribute termination of the fire to dousing of the core by water pumped in from fire trucks beginning at about 0900 Friday. The account by Arnold indicates that water had no visible effect on the flames emanating from the rear of the core.

In addition, the complex chain of events starting with the Wigner energy anneal and ultimately leading to an aggressive fire, as pieced together from historic accounts, was successfully modeled by the GRSAC simulation. The progression of linking events includes (1) ignition of lithium-magnesium cartridges in the affected zone during the second nuclear heating, (2) initiation of a smoldering situation in overheated graphite, which called for (3) increased air flow, mistakenly, to cool the core, leading to (4) increased oxidation rate, now involving the cladding and, finally, to (5) uranium in a fire reaching 1750°C in a zone encompassing about 150 fuel elements. Based on the extensive GRSAC modeling done to date, the testimony of the Windscale operating and analysis teams, and other observations, replication of this complex situation has led to a heightened confidence in the capability of the code.

4.1.8 Windscale Simulation Conclusions

The GRSAC analysis of the October 1957 Windscale 1 reactor accident provided an opportunity to incorporate detailed models of the essential features of the accident and the means to study the interactions and relative importance of these various effects. Some characteristics and operational maneuvers were obviously different from the many similar annealing operations that had taken place without incident on both Windscale 1 and 2. Because there are so many variables involved, each with its own accompanying uncertainty band, it is not feasible to predict precisely the extent to which each of the factors contributed to the accident. However, based on the testimony of the Windscale operating and analysis teams and other observations, some conclusions can be drawn:

1. The two fission heating periods, concentrating power in a selected core region, and the resulting release of Wigner stored energy in the inlet region were the two major factors in raising the temperature of the "lower central inlet" portion of the core to a higher-than-usual level.

2. Once this portion of the core was at the higher temperature level, the relatively uncooled core temperatures were high enough to cause the further release of energy from additional annealing (Wigner energy), failure and oxidation of AM cartridges (which were known to begin failing at temperatures in excess of ~440°C), and graphite oxidation. In this portion of the accident sequence, the heating process was "oxygen limited"—that is, small increases in air coolant flow would raise the temperatures in this hot region rather than provide a net cooling effect as was intended.

3. At this early point in the sequence, there was in fact a very delicate balance between an ultimate safe shutdown and the ultimate accident. Sensitivity studies described in Appendix E show how very minor changes in the models and/or the scenario could make the difference between the two extreme outcomes.

4. In the reference case GRSAC sequence (Appendix E), the increased flow (due to closure of the chimney hatch and the successive damper openings) caused the initial cladding failure to occur just following the fourth damper opening. The release of fission gases and the uranium metal fuel oxidation that occurs at this point correspond to the initial observation of chimney stack activity caused by fission products noted in the testimony.

5. The relative timing of GRSAC predictions for the release of tritium (earlier in the sequence, due to AM cartridge failure) and later of fission products due to clad failure, which began during the last part of the damper opening sequence, corresponds to the observations made in Germany, where the tritium fallout was detected about a day earlier than the fission product fallout.[23]

6. The vast majority of the damage to the fuel, cladding, and graphite occurred following the restart of the shutdown fans, which was a last-ditch attempt to cool the core. Even though the fans succeeded in cooling most of the core, the hot section of the core was at a high enough temperature that the heat generated from oxidation of the clad, fuel, and graphite far exceeded the cooling effects. Most of the heat generated in this period was from graphite oxidation, although heat from fuel and clad oxidation, Wigner energy release, and AM cartridge oxidation also contributed to the problem as the high-temperature front was pushed through the core by the air flow. The abrupt cessation of flaming when the fans were turned off (in GRSAC) also corresponds to observations.

7. The GRSAC reference case damage estimates for oxidation of clad, fuel, and graphite are predictably high compared with those in reports available to date. Certain limitations of the GRSAC analysis would tend to make its damage estimates higher than actual: removal of fuel, blockage of channels due to rubble from damaged elements (which would tend to protect channel components from oxidation), and water cooling effects which were not modeled.

4.2 COMPARISON WITH FRENCH CHANNEL FIRE TESTS

4.2.1 Test Description

On October 26, 1956, the French G1 reactor experienced a fire in one of its 1337 fuel channels. The G1 reactor has several basic similarities to Windscale: both were graphite moderated, once-through air cooled, and fueled with natural uranium metal. A major difference was the cladding alloy: Windscale used aluminum; the G1 used a Magnox alloy consisting of >99% magnesium with the balance, zirconium. No mention is made in the literature regarding the Wigner energy release situation or the possible presence of lithium, both prominent features at Windscale. The cause of the channel fire was never clearly identified, but the most likely cause was a mispositioned fuel element that restricted air flow.

Out-of-pile tests were conducted by Martin to simulate the channel fire.[25] These tests are described, and the benchmarking calculations based on these tests are discussed more fully in Appendix F. The test apparatus consisted of a 30- and 60-cm-long prototypic G1 fuel element contained in graphite cooling channels. Nuclear heating was simulated by electric resistance heaters set along the axis of the hollowed-out uranium cylinder. A series of air flows were tested: zero, 3%, 15%, and 66% of full flow. Observations were made photographically and by means of pretest and posttest examinations.

4.2.2 Test Results

Results of the out-of-pile French channel fire tests are summarized in Table 5. The most significant feature of these tests is the ignition- and vapor-phase burning of the magnesium cladding. Ignition was observed to occur at localized hot spots at magnesium bulk temperatures between 620 and 645°C at all air-flow rates. Following ignition, the burning zone moved in the flow direction at 2 cm/min at low flow and up to 30 cm/min at high air flow.

Table 5. Summary of channel fire test observations

	Air flow (g/sec) (percent nominal)			
	0 (0%)	3–4 (3%)	15[c] (15%)	60–65 (66%)
Magnesium ignition (°C)	640–650	620–625	620–625	645
Magnesium max. temp. (°C)	700	1050	790	1200
Magnesium oxidized (%)		100	42[a]	100
Burning rate (cm/min)		2	2–3	30
Uranium max. temp. (°C)		800	800	NA[b]
Uranium oxidized (%)		0.33	0.26	NA[b]

[a]Probably would have been 100% had not ends been cool.
[b]Iron used instead of uranium.
[c]Flow applied "in brief pulses."

These observations emphasize the heightened probability for a magnesium fire in Magnox reactor accidents involving air ingress to the core. They also lead to the introduction of the "burning model" into the group of oxidation rate algorithms in GRSAC, at least for magnesium. Burning rates are much higher than heterogeneous oxidation rates because of the elimination of the mass-transfer resistance of oxygen transport to the surface. A burning model was necessary to approximate the magnesium fire in the French tests. Note that while magnesium burning was essentially complete at all air flows, the uranium was only slightly oxidized. Martin notes that uranium oxidation was limited to within 0.2 mm of the surface. It was also noted that graphite was affected only "quite superficially."

The magnesium burn model incorporated to simulate these tests results is described in Appendix F. A more general treatment with application to uranium and graphite is described in Appendix B.

4.2.3 GRSAC Simulation Results

The manner in which the GRSAC code, designed for multiple node, whole-core analysis, was adapted to single-channel simulation required for the channel fire experiments is described in Sect. F.5.1 of Appendix F. Comparisons of simulation results with the test data are summarized in Table 6. As noted, magnesium oxidation rates predicted by GRSAC significantly exceed the observed rates, especially for the intermediate air flow case. A factor contributing to the low oxidation rate at the intermediate flow rate was likely the unsteady air flow that was used for this case. The overestimates were quite likely caused by the fact that a burn front moved axially along the specimen. Hence, only a small portion of the specimen was burning at any particular time. In contrast, the GRSAC model assumed uniform burning in each of the five nodes modeling the specimen. Phenomena such as burn fronts, which represent a variation within a node, are difficult to model in a node-based code such as GRSAC. In addition, it is possible that the current form of the burn model is incomplete. Possibly a rate-limiting mechanism (e.g., gas-phase mixing rates) may be required.

Table 6. French channel fire benchmarking test results

	Flow		
	3%	15%[d]	60%
Observed magnesium oxidation rate (mol/min)[a]	0.87	1.09	13.1
Calculated magnesium oxidation rate (mol/min)	2–3	10	26
Observed peak temperature (°C)	1050	800	1200
Calculated peak temperature (°C)	1650	1650	1450
Observed uranium oxidized (g)	66	16	*c*
Calculated uranium oxidized (g)[b]	<5	<5	*c*

[a]Linearized rate from 20% to 100% magnesium oxidation.
[b]GRSAC runs terminated when 100% magnesium oxidation occurred.
[c]Test used steel rod instead of uranium.
[d]Flow (experimental) applied "in brief pulses."

Note that small amounts of uranium metal were burned in the low- and intermediate-flow cases; that is, only 66 g of uranium, representing about 1% of the uranium in the 60-cm specimen. (A steel rod was used in the high-flow-rate case.) Similar to the manner in which the tests were run, the GRSAC model was terminated when magnesium oxidation was complete, which is the point at which the model presumes uranium oxidation to start. The comparison shows that a small amount of uranium oxidation does in fact occur prior to complete oxidation of the magnesium cladding.

4.3 VALIDATION CONCLUSIONS

Although these two cases are not true benchmarking in the sense that quantitative results are accurately reproduced, they nevertheless proved to be invaluable code development exercises that led to confidence in GRSAC. Not many opportunities arise for benchmarking a severe accident code for a gas-cooled graphite reactor. The two chosen cases may be the only events that include the important oxidizable materials graphite, cladding, and metallic uranium. True validation would require engineering-scale, integral tests and a special protocol. Windscale involved a much more complex set of events than may be expected for a typical Magnox reactor severe accident. An odd thermal power distribution, large amounts of Wigner energy stored in graphite, an inventory of a volatile lithium-magnesium alloy, an uncertain oxidation behavior of the aluminum cladding, and an unusually high chemical reactivity of the graphite contributed to the complexity. Nevertheless, the simulation was able to replicate the chain of connected steps ultimately leading to the fire, as well as to demonstrate the termination mechanism.

The principal gain from the channel fire exercise was a clear demonstration of the need for a magnesium burn model (defined as aggressive, vapor-phase oxidation of vaporized material) for severe accident simulation of Magnox reactors. Initially, burn models were avoided because of a lack of clear direction from the available literature. The channel fire experiments showed that heterogeneous oxidation models cannot simulate the high oxidation rates of true burning. Although the burn model developed for this case approximately replicates observed magnesium oxidation rates, it must be considered as speculative in view of a lack of corroborative data in the literature.

5. SEVERE ACCIDENT SIMULATIONS

The GRSAC code was developed to allow the analyst to implement and study a wide variety of severe accident scenarios, including anticipated transient without scram (ATWS) accidents, rapid (or slow) loss of forced circulation (LOFC) accidents, and depressurization accidents. Following depressurization, there is the option of assuming air ingress, which can lead to oxidation of the graphite, the cladding, and, subsequently, the fuel. In this report, two variations of severe accident scenarios in large typical CO_2-cooled Magnox-type reactors are presented as examples and discussed in detail in Appendix G. In the first example, scenarios are investigated in which there is long-term clad and fuel failure from ATWS, LOFC, depressurization, and air ingress that results in considerable fuel element oxidation. The second example investigates factors that affect the chances of short-term clad failure in combined ATWS-LOFC scenarios. The GRSAC simulation assumptions for these cases are discussed in detail in Appendix G.

5.1 AIR INGRESS SIMULATION

The example runs presented in detail in Appendix G illustrate several significant aspects of core heatup air ingress accidents in which there is the potential for "fanning the flames" upon restart of the blowers. In the first case, there is a small but significant amount of fuel element cladding damage (~1.2%) that occurs in the initial (10-min) stage of the LOFC and ATWS, before the depressurization. This accident would result in significant circulating activity in the primary loop, mainly from the noble gases released, which would be driven out of the primary system by a subsequent depressurization. Hence any fuel element damage would be readily detectable.

Following the depressurization, a small amount of air ingress is assumed, which causes localized oxidation of the damaged fuel elements, and the heat released by oxidation heats up these elements and their environs much faster than the bulk core heatup rate. In the reference scenario, with the early fuel damage, restart of the blowers (at 10% of full-rated flow) within 10.8 h would result in a core cooldown; later restarts, however, would result in an accident with significant fuel oxidation. In a slight variation on the reference case in which no early clad damage occurs, the similar "point of no return" is not reached until 30.3 h into the accident, hence giving the operator much more leeway in mitigating the accident. As in the case of the Windscale reactor accident, most of the significant clad, fuel, and graphite oxidation is done with the blowers on; however, with only air available to cool the core internally, use of external (shield) cooling would be the only means of mitigating the accident consequences. Examples and details of these effects are described in Appendix G, and some results of a parameter sensitivity study are given in Table 7.

The second variation of the long-term LOFC air-ingress accident showed that there are delays of about a day before any fission product releases occur. Also, the more significant releases (from a dose standpoint) gradually increase over a several-day period, so that a one-shot release approximation would not accurately characterize the transient.

Table 7. Summary of damage estimates from example GRSAC severe accident analyses for a large Magnox reactor: long-term ATWS-LOFC accident with depressurization and air ingress

	Variation	Damage induced (at 40 h)		
		Blower restart (h)	% Clad > T-melt	% Fuel > T-melt
R	Reference case[a]	11.3	4.2	2.5
V1	Blower flow 8% (vs 10%)[b]	10.8	7.1	4.5
V2	Scram delay 15 min (vs 10 min)	11.3	38.8	22.2
V3	T-clad melt 625°C (vs 640°C)	11.3	11.7	1.8
V4	Depressurize at t = 30 min (vs 60 min)	11.3	7.8	6.1
V5	Core-specific heat (×0.9)	11.3	29.1	26.9
V6	Power density (×1.1)	11.3	31.4	22.9
V7	Afterheat (×1.1)	11.3	11.2	8.9
V8	Seal off core at t = 30 h	11.3	5.5	1.7
V9	No early clad damage[c]	30.8	13.2[d]	11.2[d]

[a]Earlier restarts result in cooldown with no additional fuel element damage.
[b]A flow of 10% at this restart time would have resulted in a cooldown.
[c]Restarts earlier than this restart time would have resulted in a cooldown.
[d]Damage after 60 h.

5.2 SHORT-TERM DAMAGE SIMULATION WITH NO AIR INGRESS

In the reference case short-term ATWS-LOFC, no clad damage is predicted (cladding exceeding the 640°C melting temperature). Numerous variations on the reference assumptions were studied. In this example, it was concluded that the "worst case" for a flow coastdown scenario would be the "very fast" coastdown case. Within reasonable uncertainty bounds, like a 25% reduction in the fuel temperature-reactivity feedback coefficient and a 75% reduction in moderator coefficient, along with a somewhat faster-than-reference-case coastdown, 2.9% of the cladding would exceed the 640°C melting temperature. At this point there would be no clad melting for any coastdown speed assumptions without these changes in feedback coefficients (see Fig. G.16 in Appendix G). In this case, a 25% reduction in the fuel coefficient may be considered within the uncertainty range, and the 75% reduction in the moderator coefficient is an expected change with core burnup for Magnox reactors. Other runs showed that depressurization made little difference in the potential for short-term clad damage. Results are summarized in Table 8.

Table 8. Summary of damage estimates from example GRSAC severe accident analyses of a large Magnox reactor: short-term ATWS-LOFC accident

	Maximum temperature (°C)		Percentage exceeding the melting temperature	
	Cladding	Fuel	Cladding	Fuel
1. Reference case	608	750	0	0
2. Flow coastdown faster (×5)	623	780	0	0
3. Flow coastdown faster (×10)	627	800	0	0
4. Flow coastdown slower (×3.33)	597	730	0	0
5. Flow coastdown slower (×10)	589	710	0	0
6. Faster coastdown (×5), fuel temperature-reactivity feedback reduced 50%	669	830	6.6	0
7. Faster coastdown (×5), fuel temperature-reactivity feedback reduced 25% and moderator feedback reduced 75%	641	800	2.9	0

5.3 SEVERE ACCIDENT PROGRESSION IN GRAPHITE-MODERATED, METAL-FUELED, GAS-COOLED REACTORS

Severe accidents in Magnox reactors may be broadly classed into those with or without air entry to the core. Accidents that do not result in air ingress may cause damage to core components due to excessive temperatures, but with no breach in the primary pressure boundary, any radioactivity release rates would be limited to the radioactivity that would escape with the normal leakage.

Accidents with air ingress cause oxidation of core components to a degree depending on the severity of the initiating event and the magnitude of the air exposure. Significant radioactivity releases from the primary vessel may occur through a breach in the pressure boundary. At the low-severity end are limited events, such as the channel fire in the French G1 reactor in 1956, which burned some magnesium cladding but oxidized uranium and graphite only slightly.[3] The oxidation zone remained localized probably due to a prompt reduction of reactor power and an absence of other heat sources, such as stored energy release.

By contrast, the accident in the Windscale reactor in 1957 demonstrates that when a set of critical conditions is surpassed, events could lead to a major fire. One such path to a major fire is illustrated by the most likely progression of events at Windscale:

1. ignition of a volatile material by three heat sources (the volatile material was the AM alloy target), namely, fission heating, afterheat, and Wigner stored energy release;
2. initiation of a persistent heterogeneous oxidation of graphite, sustained by heat addition from the four sources noted in (1);
3. gradual spread and increasing rate of AM cartridge and graphite heterogeneous oxidation and further release of stored energy, prompting measures to be taken to increase introduction of air in attempts to cool the core (damper openings); and leading to
4. much more rapid oxidation and a degenerating situation involving cladding and uranium metal oxidation after the fans were turned on.

At Windscale the critical conditions leading to the spreading fire were surpassed during step 2. Cutting off the air supply at the end possibly prevented more extensive damage involving more of the core. Following early attempts to define the critical conditions beyond which major fire occurs, it was recognized that when heat addition due to oxidation surpasses the rate of heat removal, a rapidly degenerating situation may ensue.[4] This instability, as it was called, develops when chemical reaction rates increase more rapidly with temperature than does the heat removal, at least by mechanisms of conduction and convection. Therefore, according to this simplified model, any increase in temperature beyond some critical point serves to progressively increase the disparity between heat addition and removal.

Many important factors and interrelationships contributing to the development of a major fire in a Magnox-type reactor cannot be taken into account without the use of modern computing capability. In the early models, heat loss assumptions were much simplified. Three-dimensional heat flows, radiant transfer, changes in convection regimes, and variation of thermal conductances were all necessarily neglected. Also, restriction of oxidation rates at high temperature due to oxygen diffusion from the free stream to the surface could not be taken into account. The simultaneous or sequential oxidation of cladding, graphite, and uranium could not be included in these earlier analytic treatments.

Also significant is the necessity for tracking oxygen availability along a flow channel. Oxidation rates depend on the oxygen concentration; therefore, mass balances for the determination of oxygen concentration are necessary for the determination of the oxidative heat sources. Therefore, it is essential to use a comprehensive model like GRSAC to define the critical conditions beyond which major damage by fire occurs and below which damage is restricted.

For the set of conditions peculiar to Windscale during the critical period when the operators were trying to decide how to lower some of the core temperatures, it appears that the critical turning point temperature was in the 520 to 540°C range. Above 540°C, turning on the fans would increase the temperatures, while below 520°C, it probably would have cooled the entire core. Several aspects of Windscale would make this critical temperature lower than in Magnox plants–namely, the graphite being more reactive, the existence of the ready-to-fail AM cartridges, and the considerable stored energy available for release at relatively low temperatures. In other studies of Magnox plants, the critical turning point temperature appeared to be 20 to 40°C higher. As noted, the presence of exposed uranium metal fuel (due to prior cladding failure) lowers this critical temperature significantly.

6. CONCLUSIONS

This work has addressed the potential damage to metal-fueled GCRs following the initiation of a severe accident. To perform the analysis, a state-of-the-art GCR accident code was used as a starting point and extended to include physical phenomena models important in modeling the early metal-fueled GCRs. The development of the models has been discussed in general in the text and in detail in the Appendixes. The development of the GRSAC model was discussed, and validation against the two historical GCR accidents was performed. Two classes of severe accidents were modeled and analyzed in order to characterize the potential damage to a metal-fueled GCR in general. Below are our major conclusions drawn from this effort.

Unique features in GCR accident modeling were included in GRSAC.

1. The GRSAC code, an established neutronics/thermal hydraulics code for gas-cooled graphite reactor accidents, augmented by damage models for material oxidation and fission product release models developed in this study, may be used for prediction of severe accident consequences with reasonable confidence. The confidence is based on benchmarking comparisons with two severe accident cases: the fire in the Windscale reactor in 1957 and the French tests duplicating a channel fire in the G1 reactor.

2. GRSAC presumes two general types of oxidation: heterogeneous (or surface) oxidation and true burning, currently included for magnesium only. Burning (or fire) is defined as vigorous oxidation in the gas phase of vaporized material. Burning is a much more rapid process than heterogeneous oxidation. Graphite reactors with Magnox cladding subjected to severe accidents that overheat the core and permit air ingress are very likely to experience a magnesium fire. A magnesium burn model was therefore developed and included in GRSAC.

3. No precedent has been established in the literature for development of a burn model for bulk metals or graphite. Hence, the current GRSAC burn model must be deemed speculative despite reasonable benchmarking results for magnesium. Estimation of burn rates needs additional investigation and analysis.

Validation exercises aided development and enhanced credibility.

1. The benchmarking exercises proved to be extremely valuable development tools. GRSAC successfully replicated the chain of events leading to the Windscale fire, a damage sequence more complex than expected for larger-scale reactors. In addition, the predicted degree of core damage agreed reasonably well with the sparse information available on the actual end state of the Windscale core. More data on actual core damage may be available following decommissioning.

2. The benchmarking exercise using the French channel fire experiment proved the need for a magnesium burn model. Heterogeneous oxidation rates were about a factor of 100 too low. In addition, this test series demonstrated an important oxidation feature: magnesium cladding was observed to protect uranium from oxidation until it was almost fully oxidized. Carrying this observation over to GRSAC yielded fairly good simulations. In contrast, a GRSAC side calculation assuming earlier uranium exposure to air and simultaneous oxidation of cladding and uranium led to a much more severe result. Therefore, the degree of protection given uranium by oxidizing (or melting) cladding is an important factor in damage assessment.

Some major uncertainties remain which result in wide error bands.

1. Despite many graphite oxidation studies conducted over the past 40 years, predictive methodology for severe accidents is still relatively uncertain. The principal uncertainty lies in estimation of the "active oxidation depth," which is required for translating small specimen data to large blocks. Only four data points exist for this key parameter.

2. Estimates of fission product release using the models developed in Appendix C that were added to GRSAC are especially important for the first three fission product groups: noble gases, halogens (mainly iodine), and alkali metals (mainly cesium). Iodine releases may be compared with Windscale release estimates obtained from air monitoring data when source-term estimates are factored into the GRSAC calculation. Appendix C includes a fairly complete summary of the available fission product release data from overheated uranium metal fuel. Only three experiments have been conducted in this area; uncertainties are fairly high, especially for the less-volatile fission products.

Accident severity predictions often depend heavily on small changes in design and operational factors.

1. A significant factor in the ultimate severity of Magnox ATWS-LOFC accidents with depressurization and subsequent air ingress is whether or not early clad failure occurs. The fission products released into the primary circuit could be driven out of the reactor building rapidly by subsequent depressurization.

2. Oxidation of fuel in elements damaged early in the accident sequence can also lead to localized heatup rates greater than that of the bulk core. Subsequent restart of the blowers must be earlier, therefore, to avoid "fanning the flames" than in the case where no early clad failure occurs. A criterion for determining a critical temperature for "fanning the flames" depends on a large number of design and operational parameters. In the Windscale accident, the critical temperature appeared to be in the 520 to 540°C range. It appeared to be 20 to 40°C higher for conventional Magnox plants.

3. Near-term effects of an ATWS-LOFC accident without air ingress for a large Magnox reactor resulted in much less damage compared with a similar case with air ingress. No cladding or fuel damage is predicted for the reference case.

4. Sensitivity study variations on the short-term ATWS-LOFC accident series included variations in the fuel and moderator temperature-reactivity feedback coefficients. In one case, a 50% reduction in the fuel coefficient from the reference case led to the melting of 6.6% of the cladding. In a second case, a 25% reduction in the fuel coefficient and a 75% decrease in the moderator coefficient (which typically occurs with high burnup in Magnox reactors) led to melting of 2.9% of the cladding.

7. REFERENCES

1. Penney Inquiry, *Report on the Accident at Windscale No. 1 Pile on the 10th October, 1957,* Court of Inquiry, Sir William Penney, Chairman (October 1957).

2. Clarke, R. H, "An Analysis of the Windscale Accident Using the WEERIE Code," *Ann. Nucl. Sci. Eng.* **1,** 73–82 (1974).

3. de Rouville, M., et al., "Partial Combustion of a Fuel Cartridge in Reactor G1," pp. 490–492, Session B-10 in *Proc. of the 2nd United Nations International Conference on Peaceful Uses of Atomic Energy*, P/1180 (1958).

4. Nairn, J. S., and V. J. Wilkinson, "The Prediction of Conditions for Self-Sustaining Graphite Combustion in Air," in *Proc. US/UK Meeting on Compatibility Problems of Gas-Cooled Reactors*, Oak Ridge, Feb. 24–26, 1960, TID-7597 (1961).

5. Schweitzer, D. G., "Oxidation and Heat Transfer Studies in Graphite Channels, IV. Combined Effects of Temperature, Flow Rate, Diameter, and Chemical Reactivity on the Length of Channel Cooled by Air," *Nucl. Sci. Eng.* **12,** 59–62. See also parts I, II, and III, *ibid.* pp. 39–45, 46–50, and 51–58, respectively (1962).

6. "Gas Cooled Reactor Design and Safety," IAEA Technical Report Series No. 312, IAEA, Vienna (1990).

7. Nightingale, R. E., *Nuclear Graphite*, Academic Press, New York (1962).

8. Simmons, J. H. W., *Radiation Damage in Graphite*, Pergamon Press, Oxford (1965).

9. Engle, G. B., and W. P. Eatherly, "Irradiation Behavior of Graphite at High Temperatures," *High Temperatures-High Pressures*, 119–158 (1972).

10. Soffer, L., et al., *Accident Source Terms for LWRs*, NUREG-1465 (1995).

11. McKenna, T. J., and J. G. Glitter, *Source Term Estimation for Severe Nuclear Power Accidents*, NUREG-1228 (1988).

12. Parker, G. W., et al., *Out of Pile Studies of Fission Product Release for Overheated Reactor Fuels at ORNL 1955–1965*, ORNL-3981 (1967).

13. Hilliard, R. K., *Fission Product Release from Uranium Heated in Air*, HW-60689 (1959).

14. Hilliard, R. K., and D. L. Ried, *Fission Product Release from Uranium—Effect of Irradiation Level*, HW-7231 (1962).

15. Ball, S. J., and D. J. Nypaver, *MORECA-2: Interactive Simulator for Modular High-Temperature Gas-Cooled Reactor Core Transients and Heatup Accidents with ATWS Options*, NUREG/CR-5945, ORNL/TM-12233 (1992).

16. Attree, R. W., R. L. Cushing, and J. Pieroni, *Stored Energy in Graphite Irradiated at Windscale and at Hanford,* CRC-706, Chalk River, Ontario (1957).

17. Arnold, L., *Windscale 1957, Anatomy of a Nuclear Accident,* St. Martin's Press (1992).

18. Unknown., "Production," history obtained from the British Ministry of Defense (1995).

19. Hand-marked journal, "Windscale Pile 1 Incident: Summary of Events," written for Mr. Touhy immediately after the accident (1957).

20. Smith, B. S., et al., *Some Estimates of the Scale of the Windscale Accident Based upon the Noble Gas Released,* AERE HP/M 133 (1958).

21. Command 1225, "Second Report to the Medical Research Council on the Hazards to Man of Nuclear and Allied Radiations," HMSO (1960).

22. Beattie, J. R., *An Assessment of Environmental Hazard from Fission Product Releases,* U.K. Atomic Energy Authority, Authority Health and Safety Branch Report (5) R64 (1963).

23. Chamberlain, A. C., *Emission of Fission Products and Other Activities During the Accident at Windscale Pile No. 1 in October 1957,* AERE-M 3194, Sect. 5.5 (July 1981).

24. Hill, J. M., "A More Detailed Assessment of the Early Stages of the Windscale Fire," memorandum to Sir Leonard Owen, January 17, 1958.

25. Martin, D., et al., " The Combustion in Air of Fuel Elements," *Proc. Symp. on Reactor Safety and Hazards Evaluation,* IAEA, Vienna (May 1962).

APPENDIXES

APPENDIX A. MODEL FOR AIR OXIDATION OF GRAPHITE

A.1 USE OF OXIDATION MODELS IN GRSAC

A.1.1 Potential Significance of Oxidation

All metal-fuel gas-cooled reactor core materials—cladding, fuel, and moderator—are oxidizable to some degree when an overheated core becomes exposed to air. An estimate of the relative importance of oxidation as a heat source in an accident situation is shown in Table A.1.

Table A.1. Windscale accident heat energy source distributions (%)[a]

	Up to time of blower restart[c]	Total accident duration[d]
Graphite oxidation	5.2	71.7
Cladding oxidation	0.8	1.1
Fuel oxidation	0.5	5.2
Stored energy release	32.5	6.8
Decay heat	39.6	8.8
Fission power[b]	16.7	2.6
AM cartridge oxidation	4.7	3.8

[a]Reference case calculation assumptions (Appendix E).
[b]Sum of two fission heating periods: 1.8 MW for 7 + 8.4 h.
[c]Total heat for 72-h period = 166 MWh.
[d]Total heat for 108-h period = 1052 MWh.

The Windscale accident scenario, described briefly in the main report and in much more detail in Appendix E, provides a vehicle for depicting the relative importance of oxidation energy contributions to "air ingress" accidents in one type of metal-fuel GCR. In this type of accident sequence, certain circumstances lead to the point where running the shutdown cooling blowers would result in fanning the flames rather than cooling down the troubled section of the core. For the Windscale accident, the major contributors in this period, according to the reference case GRSAC simulations (first column of Table A.1) were the decay heat and stored energy release, followed by the fission power heating that was done to initiate the annealing of the core. Graphite oxidation and (damaged) AM cartridge oxidation provided a crucial amount of incremental heat to push some of the clad temperatures to the failure point, thus exposing the fuel to the air. In a typical CO_2-cooled Magnox core, the stored energy contribution would probably be much less important, the AM cartridge contribution would be absent, and a fission power contribution would apply only if the accident were an ATWS.

For the total accident period (second column), graphite oxidation was dominant, as it persisted until the fans were shut down, long after the cladding and fuel in the affected parts of the core had

totally oxidized. The cladding and fuel oxidation contributions were critical here, however, in raising the hot-channel temperatures to the point where the graphite oxidation would be self sustaining with the fans on. In a typical CO_2-cooled Magnox reactor, the graphite would be less reactive than that in Windscale, while the magnesium alloy cladding would probably be more reactive than the Windscale aluminum clad. Hence the Magnox fuel and clad oxidation contributions would be larger relative to the Windscale case, and the graphite temperatures would have to be higher to get to the point where sustained oxidation would take place when the shutdown fans are turned on.

A.1.2 Role of Oxidation in Radiation Release

A related issue is the release of radioactivity. The review of data leading to the release models is summarized in Section 3.6 and described in detail in Appendix C. Fission product release rates from uranium metal fuel depend directly on the degree of oxidation, modified to some extent by temperature level. The reason for this behavior is the affinity of many fission product elements, most notably iodine, to either solid or liquid uranium. A much lower chemical affinity exists for the oxide. Hence, the uranium oxidation model is a prerequisite for determination of radioactivity release.

A.1.3 Type of Information Required for GRSAC Oxidation Models

GRSAC calculates local oxidation rates, in terms of mass per unit exposed area per unit time, for the temperature and oxygen level conditions existing at each node. Rates governed by chemical kinetics must be determined from correlations based on small specimen laboratory data (taken, hopefully, in the chemical control regime). Large scale experiments, such as those by Dahl,[1] Robinson and Taylor,[2] and Schweitzer,[3-6] may be used for code testing if sufficient descriptions are available, but are not the basic information source required for GRSAC.

The correlation for graphite oxidation is more involved than that for metals because of graphite porosity. Small specimen experiments usually report data under the assumption of uniform oxidation (i.e., in terms of g/g·time). Direct application to GRSAC is not valid because large moderator blocks do not oxidize uniformly. The method used for adapting small specimen data for graphite to large blocks is described in Section A.4.

A.1.4 Effect of Oxidation Behavior on Accident Progression

Experience at Windscale shows that oxidation may be locally limited and relatively slow but can expand to a major fire under certain conditions. An analysis based on a simplified situation (Section E.5) shows that a transition to sustained burning may occur when certain critical conditions are surpassed, namely, when sufficiently high local temperature develops under conditions of abundant air supply. Because actual conditions are complex, specification of these critical conditions are best determined by means of trial GRSAC runs.

A.1.5 Terminology

In this study, the term ***oxidation*** applies to the general chemical reaction in all its forms from slow (as in corrosion) to rapid.

Following the intuitive meaning, ***burning*** is reserved for robust, self-sustaining oxidation in the gas phase involving vaporized material mixing with oxygen. Burning is sustained by its own heat of combustion and usually produces a visible flame. The term ***combustion*** is synonymous. Because of its low vapor pressure, graphite is extremely difficult to burn, according to this definition. No graphite

oxidation experiment has ever burned graphite* according to this definition. True graphite burning probably did not occur at Windscale. The current version of GRSAC contains a true burn model only for magnesium, as necessitated by the benchmarking exercise using the French channel fire data (Appendix F). These tests show that burning of magnesium cladding in overheated Magnox cores exposed to air is a distinct possibility. Therefore, GRSAC definitely requires a magnesium burn model. Burn model development is described in Sect. B.7 of Appendix B, where it is shown that true burning of graphite should not be expected below about 3500°C.

Heterogeneous oxidation, as the name implies, occurs between oxygen in the gas phase and a solid or liquid phase. The following steps are required: (1) mass transport of oxygen to the surface, (2) chemisorption on the surface, (3) reaction, and (4) desorption and mass transport of oxidation products from the surface. Because of the mass transport resistances, heterogeneous oxidation is inherently slower than burning. Depending on conditions, the rate may be set either by the mass transfer rate (steps 1 or 4) or by the intrinsic chemical rate (steps 2 and 3), whichever is smaller.

Heterogeneous oxidation of a porous material like graphite has additional features resulting from diffusion along the internal porosity. As a result, interior surfaces may oxidize, especially at relatively low temperatures where the chemical rate is low. This phenomenon creates an "active oxidation zone" within a graphite block, the depth of which depends largely on the temperature—decreasing in scale with increasing temperature. Large blocks oxidize only within this zone, which moves progressively inward as the active zone becomes depleted. The total oxidation rate depends directly on the depth of the active oxidation zone. In addition, an accounting needs to be made for the change in internal pore surface area within this active zone as the oxidation proceeds. Initially, the pore surface increases as diameters are enlarged but decreases at later stages when pore volumes combine.

A.1.6 Approach

The heterogeneous oxidation model developed in this section involves estimating the rate two ways at each location and each time step—first, assuming chemical control of the oxidation rate and, second, assuming oxygen mass transport control. The lower of the two is selected as controlling the overall rate. Expressions are presented for both regimes. The oxidation rate under the chemical control of a large graphite block is assumed to occur within an active reaction zone, the thickness of which depends on temperature. The rate within this zone may be predicted using published correlations. A first-order variation with oxygen pressure is assumed. Allowance for rate variation with degree of burnoff is given. Standard correlations are assumed for oxidation under mass transfer control. It is assumed that CO_2 is the principal oxidation product and that all the oxidative heat is deposited in the graphite.

An oxidation model suitable for GRSAC needs to be relatively simple because it must be evaluated at each node and at each time step. Models based on solutions of differential equations would not be appropriate. In any case, no loss of accuracy results by use of a simpler algebraic model; oxidation mechanisms are complex and insufficiently understood to warrant elaborate mathematical modeling.

A.2 COMPOSITION AND STRUCTURE OF GRAPHITE

Graphite consists of several phases with differing degrees of chemical reactivity. The ***filler particles,*** often a calcined, ground, petroleum coke, are the least reactive phase. Calcining promotes growth of the characteristic planar crystal in the coke particles. The ***binder,*** a coal tar pitch, is mixed

---

* There are a few cases where CO, produced in a graphite oxidation test rig, was seen to burn at the exit of the apparatus. Precariously balanced conditions are required to produce this effect. It should not be considered true graphite burning in the sense of the above definition.

with the filler to permit extrusion into desired shapes. The binder forms a continuous phase surrounding the filler. Since the binder generally is less graphitic, it is somewhat more chemically reactive than the filler. Nuclear graphites also generally contain an ***impregnant*** which is forced into voids prior to final graphitization to increase density. The impregnant is the most chemical reactive portion of the graphite. Also, a broad range of impurities is present, some of which catalyze oxidation reactions under certain conditions. As a result of its complex nature, oxidation behavior is highly variable, even within the pure nuclear grades.

A.3 GENERAL FEATURES OF GRAPHITE OXIDATION

A.3.1 The Conventional Three Graphite Oxidation Regimes

Heterogeneous oxidation of graphite involves (1) mass transport of oxygen to and reaction products from the outer surface; (2) diffusion of gases into and from the graphite pores; and (3) chemisorption, chemical reaction, and desorption from internal surfaces. The slowest process for any given situation controls the overall rate.

Following traditional terminology, oxidation ***Zone I*** is controlled by the intrinsic chemical reactivity of graphite.[7] Mass transport rates are relatively rapid, and uniform oxidation occurs throughout the graphite mass. For small specimens used in experiments, (about 1 cm diameter) Zone I extends up to about 1000 K. For larger masses like moderator blocks, Zone I ends at a lower temperature due to high diffusion resistance to the interior of the block. The oxidation rate varies with temperature according to the Arrhenius relation, exp(–E/RT), where E is an activation energy; R, the gas constant; and T, the absolute temperature. According to Lewis,[8] E is about 60 kcal/mol for oxidation of pure graphites completely within Zone I.

Oxidation ***Zone II*** occurs at somewhat higher temperature where both chemical reactivity and in-pore diffusion affect the overall rate. The oxidation profile is not completely flat, and the overall rate shows a lower temperature dependency than for Zone I. According to Lewis,[8] an apparent activation energy less than 60 kcal/mol indicates that the experiment was not completely in Zone I or that catalytic effects marred the measurements.

Oxidation ***Zone III*** occurs at high temperature (>1300 K) where the mass transfer rate to the specimen surface controls the oxidation rate. To a first approximation, Zone III oxidation is not temperature dependent. Reaction depths are small, and oxidation proceeds by surface layer removal. The calculated mass transfer rate for Zone III depends first on the nature of the free stream flow—that is, laminar vs turbulent. If laminar, the mass transfer coefficient depends principally on the diffusion coefficient, which increases with temperature to the 1.5 power. The Reynolds analogy is used to determine the coefficient in turbulent flow (see Section A.6).

GRSAC computes graphite oxidation rates assuming both Zone I and Zone III oxidation at each node and each time step. The lower rate is selected as controlling. Further discussion of oxidation modes and criteria for selection is described in Sections B.7 and B.8. An important implication is that oxidation rates measured under Zone I conditions, which includes most experiments, cannot be directly used for other conditions. Zone I rates are properly expressed in terms of g/(g·time) because the oxidation profile is flat; Zone III rates must be expressed in terms of g/(cm^2·time) based on the outer surface area.

A.3.2 Observed Variability of Oxidation Rates

Intrinsic chemical reactivities vary widely between graphites because of differences in manufacture and concentrations of impurities, some of which may be catalytic. Dahl[1] reports a factor of six range of rates, from 0.0043 to 0.0252 g/(g·hr), for eight nuclear-grade graphites tested at 873 K

under Zone I conditions. The variability should become negligible under Zone III oxidation conditions.

A.3.3 Form of the Oxidation Equation in Zone I

The results of graphite oxidation tests are generally given in the form

$$R_I = A \exp(-E/RI \cdot T),$$

where units of R_I and A are g/(g·time), E is the activation energy in calories per mole, gas constant, *RI*, is 1.987 cal/(mol·K), and T is in Kelvin.

In addition to temperature, several other parameters affect the rate of graphite oxidation under Zone I conditions which must be accounted for in the equation. These factors include

- degree of oxidation,
- oxygen concentration,
- damage due to absorbed energy from neutron irradiation, and
- production and deposition of carbon.

Correlations accounting for these additional effects are described in the following sections. The completed correlation is summarized in Section A.6.

A.3.4 Effect of Degree of Oxidation

In Zone I conditions, oxygen permeates the graphite pores and reacts with the internal surface. As the reaction proceeds, the internal surface changes and, therefore, also the reaction rate. The total interior surface is termed the BET surface, after the method of measurement. Studies have shown that only a portion of the BET surface, termed the ASA surface (Active Surface Area) is chemically reactive. Despite some uncertainty, it is concluded that the easily measured BET area may be used as a measure of the ASA area; that is, ASA is proportional to BET.[9] An analysis by Bhatia and Perlmutter[10] relates the fraction of mass oxidized to the change in internal area, based on a "random pore" model.

Fuller et al.,[11] using Bhatia's expression, have shown that the Zone I reaction rate [R_I, g/(g·time)] varies with the fraction of mass oxidized (B) according to

$$f(B) = (1 - B)[1 - \psi \ln(1 - B)]^{0.5}, \qquad (A.2)$$

where ψ is an adjustable parameter evaluated to be 128 and 377 for two cases that were tested. (The average $\psi = 253$ will be used). For this value of ψ, f(B) rises rapidly to a value of about 6 at a burnoff of 10%, remains relatively steady up to about B = 80%, and then drops rapidly to zero. The significance of this observation is that the important experiments of Dahl[1] and possibly also of Bunnel[12] were conducted in this plateau region of elevated rates.

A.3.5 Effect of Oxygen Partial Pressure

Tests by Dahl[13] conducted on small annular specimens of nuclear-grade CSF graphite indicated a rate dependancy on oxygen pressure of $P(O_2)^{0.7}$, which was considered near first order. Dahl indicated that this agreed with other experiments conducted at atmospheric air pressure but not with low-pressure data (<100 μm Hg).

A.3.6 Effect of Neutron Irradiation

While Dahl[1] found little effect of neutron irradiation on graphite oxidation rate, the predominant opinion currently held is that damage to the crystal structure caused by energy absorbed from fast neutron bombardment causes a significant increase in rate. According to the method outlined in the operations manual[14] for the RHASD code* the fractional increase in oxidation rate is given by the relation,

$$g(t,r,z) = (1 + 0.0035\ D_f), \tag{A.3}$$

where

- $g(t,r,z)$ = fractional increase in oxidation rate due to neutron dose, a function of reactor age, t, and radial and axial location in the core,
- D_f = effective absorbed dose, in units MWd/At,†
- At = signifies adjacent metric ton of fuel.

According to the derivation provided in RHASD, the effective dose, D_f, may be estimated using the following expression:

$$D_f = DF \times 0.689 \times Af \times Br \times DOSE \times LF\ , \tag{A.4}$$

where

- DF = a damage factor which takes a value of 0.025 for most of the core,[15]
- Af = cross-sectional area of the fuel rod, in square inches,
- Br = a damage function which varies slightly with fuel element radius but not with axial distance,[15]
- DOSE = neutron dose absorbed by the graphite in terms of Mwd/AT,
- LF = the reactor load factor.

The IAEA reference[16] cites a typical fuel diameter for this sort of reactor to be about 1.15 in., which yields a value of 1.04 in.^{2} for Af. According to Hopkinson,[15] values of Br range from 1.43 near the surface of the fuel channel to 1.16 at the outermost radial node, these values being constant with axial diastance. We will assume a value for Br of 1.43. The value of DOSE is proportional to the age of the reactor, reaching a core-wide average of 25,250 at end-of-life.[15] In addition, DOSE depends on location in the core (i.e., the peaking factor at the location). Therefore, DOSE is calculated from

$$DOSE(t,location) = 25{,}250\ AGE(t)\ P(r,z)\ , \tag{A.5}$$

where

---

* The RHASD code is used in England for analysis of graphite behavior in graphite-moderated reactors under accident conditions.

† The unit At, signifying "adjacent ton," is often used in graphite irradiation effects studies. The concept is that the cumulative burnup in the fuel adjacent to the graphite provides a convenient measure of the neutron fluence or the dose. The measure requires correction for differences in core configuration and spectra between graphite reactors.

AGE(t) = an input parameter ranging from 0 to 1, describing the age of the core relative to age at end-of-life,
P(r,z) = power peaking factor, a function of radial and axial location in the core.

Incorporating the above values into Eq. (A.3) yields the fractional increase in graphite oxidation rate to neutron dose,

$$g(t,r,z) = [(1 + 1.37\ AGE(t)\ P(r,z)]\ . \qquad (A.6)$$

A.3.7 Effect of Carbon Deposit Accumulation on Graphite Oxidation Rate

Essentially pure, amorphous carbon deposits from gaseous carbon species are produced by oxidation of graphite by reactive, free radicals formed in carbon dioxide under photon irradiation.[17] Since the production rate of the generally short-lived free radicals is proportional to the photon intensity, radiolytic oxidation of graphite and subsequent deposition of carbon follows roughly the power profile within the core, wherever the carbon dioxide may diffuse.

According to information provided by Hopkinson,[15] carbon deposits occur predominantly on surfaces within the internal porosity of the graphite, the major part occurring within the first 6 mm from the coolant surface. As such, it serves to increase the volume reactivity of the graphite as the oxidation front proceeds inward from the surface.

The axial variation of the deposit is shown in Fig. A.1, which plots the radial average weight percent of deposits versus axial location for a reactor near end-of-life (i.e., experiencing a core average dose to the graphite of 25,250 MWd/At). As seen from the figure, the percent of carbon deposits in graphite reaches about 2.5% at the peak axial location in the core at end-of-life. A polynomial correlation based on the carbon production data provided by Hopkinson[15] yields the axial distribution at end-of-life shown in the figure. Assuming that production proceeds uniformly with age and is proportional to local power yields the following correlation for the percentage of carbon deposits in graphite:

$$\%\ deposit = AGE(t)\ P(r,z)\ (0.517x^4 + 3.247x^3 - 6.974x^2 + 4.921x + 1.465)\ , \qquad (A.7)$$

where

AGE(t) = an input parameter between 0 and 1 defining the age of the reactor,
P(r,z) = local to average power ratio in the core,
x = distance from the base of the core, in./100.

According to RHASD,[14] carbon deposit reactivity as a function of temperature and oxygen pressure may be described by

$$R_{cd} = 1.64 \times 10^6 \exp(-12{,}500/T)\ (P_{O2}/0.21)^{0.86}\ , \qquad (A.8)$$

where

R_{cd} = carbon deposit reactivity, g/g·min,
T = temperature, K,
P_{O2} = local oxygen pressure, atm.

Equation (A.8) yields a reactivity that is several thousand times higher than graphite at temperature below 1000°C, and several hundred times higher between 1000°C and 1400°C.

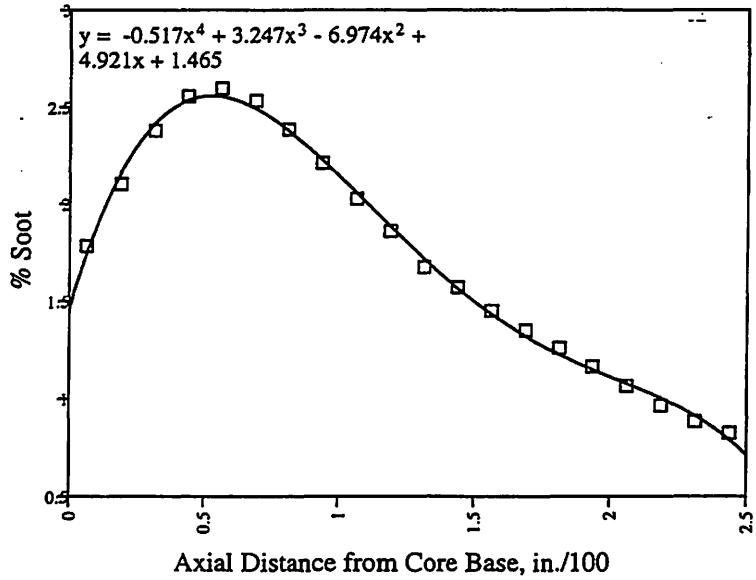

Fig. A.1. Percentage of carbon deposit vs axial location.

A.3.8 Effect of High Temperature

Several experimenters have observed that oxidation rates at high temperatures do not rise continuously with increasing temperature.[18] A peak appears to occur at about 1400 K followed by a decline up to about 2000 K, after which the oxidation rate again rises. The effect is possibly due to creep in the graphite which reduces the internal pore surface area. This effect is not understood.

A.3.9 Oxidation Products

Both CO and CO_2 are formed directly by the air–graphite reaction. For pure graphites, the CO portion rises with rising temperature and with diminishing oxygen partial pressure. At 844 K and 1 atm air pressure, the observed CO/CO_2 ratio is 0.5. Dropping the air pressure to 50 torr increases the ratio to 1.3. Other tests have shown the ratio to be independent of pressure for impure graphites.[19]

A.3.10 Secondary Burning of CO

CO will burn in the gas phase when O_2 and CO concentrations are within prescribed limits. According to Glassman,[20] CO will burn in air at concentrations above 12.5 and below 74 vol %. The relatively low temperature tests of Schwietzer et al.[3-6] and Robinson and Taylor[2] both occasionally showed a pale blue CO flame at the gas exit of the apparatus. At high temperatures, a blue flame has been seen surrounding a carbon particle.[21]

A.4 PREDICTING GRAPHITE OXIDATION RATES IN MODERATOR BLOCKS

Despite literally scores of oxidation experiments, prediction for moderator blocks under accident conditions is highly uncertain for several reasons. First, experiments that provide rate data were conducted on small specimens of about 1 cm diameter. Small specimen data cannot be used directly for large moderator blocks unless it is proven that both are either in the Zone I or Zone III oxidation

regime. Because of their large size, moderator blocks are not expected to be in Zone I, except at low temperatures.

Second, applying small specimen data to large blocks requires use of experimental burnoff profiles, which depend principally on temperature. Few such data exist. In general, the chemically reactive oxidation zone in a large specimen occurs within a thickness, Δh, that depends principally on the temperature. As the burnoff proceeds, the fraction oxidized within this zone increases. When depleted, this active zone moves inward from the surface. At full burnoff, a skeleton remains with about 10% of the original density. The few burnoff profile data sets that exist which permit estimation of the active oxidation zone thickness, Δh, are summarized in Table A.2.

Figure A.2 illustrates the dependence of Δh on temperature. An empirical fit with good accuracy is given by the following equation:

$$\Delta h = 9.368 \times 10^{-6} T^2 - 0.02859 T + 22.688 , \qquad \text{(A.9)}$$

where Δh is in millimeters and T is in Kelvin. Equation (A.9) is illustrated in Fig. A.2. The assumption in GRSAC is that when Δh is reduced to 0.1 mm, which occurs at about 1300°C, surface oxidation effectively occurs (Zone III) regardless of the mass transfer rate.

Table A.2. Active reaction zone measurements

Temperature (K)	Oxidant	Graphite	Δh (mm)	Reference
1413	H_2O	*a*	0.9	Helsby and Everett[22]
1303	H_2O	*a*	1.4	Helsby and Everett[22]
1223	H_2O	*a*	1.9	Helsby and Everett[22]
1000	air	TSX	3.2[b]	Bunnel[12]
873	air	CSF	5	Dahl[1]

[a] Gilsonite filler, triply pitch impregnated, isotropic graphite.
[b] Data at 800 K showed an anomaly and were not used.

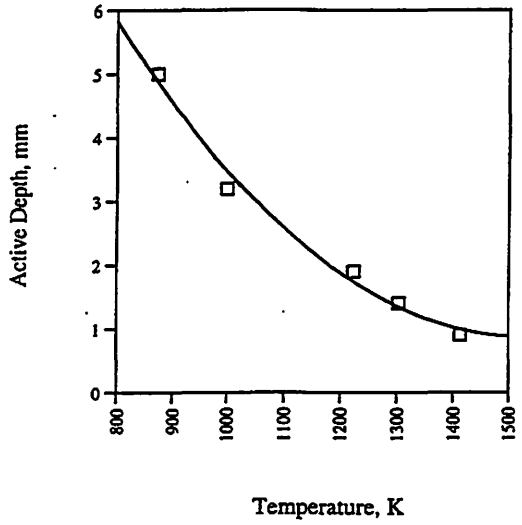

Fig. A.2. Active oxidation zone vs temperature.

As an illustration of the use of the "active oxidation depth" concept, consider a cylinder of arbitrary length and diameter oxidizing along the exterior. The specimen is assumed to be large; that is, the oxidation is not uniform throughout its volume. In such case, the oxidation rate must be reported in terms of its surface rather than its mass. The relationship between the surface oxidation rate, R_s, (moles/cm^2·min) and R_v, the rate reported as grams oxidized/minute per gram of total specimen, is

$$R_s = R_v \, (\Delta h \rho / MW) , \qquad (A.10)$$

where ρ is the graphite density and MW the molecular mass. The term in brackets accounts for the fact that oxidation occurs predominantly within the active depth, Δh.* GRSAC converts R_s mass units to moles for more convenient application of chemical mass balances.

The principal drawback in applying the "active oxidation depth" method is the paucity of data for determining Δh. Table A.2 lists only five determinations, three of which are for H_2O oxidant. However, some confidence in the method may be gained by comparing large block oxidation rates reported by Cowen et al.[23] with rates predicted by the active oxidation method, Eq. (A.10). Figures A.3 and A.4 show the data reported by Cowan as fraction oxidized per hour against specimen sizes ranging from 1/2-inch to 4-inch cubes. The test temperatures of 500°C and 550° C are a bit below the range for determining the active depth, requiring extrapolation of Eq. (A.9) to Δh values of 5.50 mm at 550°C and 6.19 mm at 500°C.

Figure A.3 shows the comparison of measured and predicted trends of oxidation rate with specimen size at 550°C. The square points represent the large block data normalized to its value for the largest block. [The irregularities in this curve are due to errors in reading values from the figure in Cowan et al.[23]] For the purpose of comparison, the cubic specimens are assumed to be spheres with radii equal to half the cube edge. The points shown as diamonds represent the predicted variation of the normalized rate with specimen size using the "active oxidation depth" method, computed as follows: according to the model, the reported large block oxidation rates R_{LB} (g/g·hr) are due to oxidation within a depth Δh, divided by the mass of the entire block. This leads to

$$R_{LB} = k \{1 - [1 - (\Delta h / a)^3]\} ,$$

where k is the graphite reactivity and the value "a" is the large block radius. Normalized values of R_{LB} are determined by setting the value of k to yield an R_{LB} of unity for the largest block size, radius a_1. If this value is called k(normalized), then

$$R_{LBi} \text{ (normalized)} = k \text{ (normalized)} \{1 - [1 - (\Delta h / a_i)^3]\} , \qquad (A.11)$$

where R_{LBi} is the normalized rate for block i. Equation (A.11) was used to determine the diamond points in Figs. A.3 and A.4, using the value of Δh from Eq. (A.9). The trend with block size appears to match the experimental trend fairly well for the entire range of sizes.

Figure A.4 shows the same comparison for the data taken at 500°C. Note here that the predicted trend using Eq. (A.11) matches the data well for the larger sizes, but departs from the data for the

---

* An alternative approach for determining large block oxidation rates from small specimen data is through solution of the diffusion equation for transport of oxygen in graphite. Interior oxidation rates are determined from oxygen concentrations computed as a function of location within the block. This method is not appropriate for GRSAC due to prohibitive run times and is also fraught with uncertainties in its own right, including the complexities of modeling counter diffusion in a variable composition gas mixture (of nitrogen, oxygen,and carbon dioxide), proper means for accounting for chemisorption along the transport path, and accounting for the variation of internal pore structure and chemisorption properties with degree of oxidation.

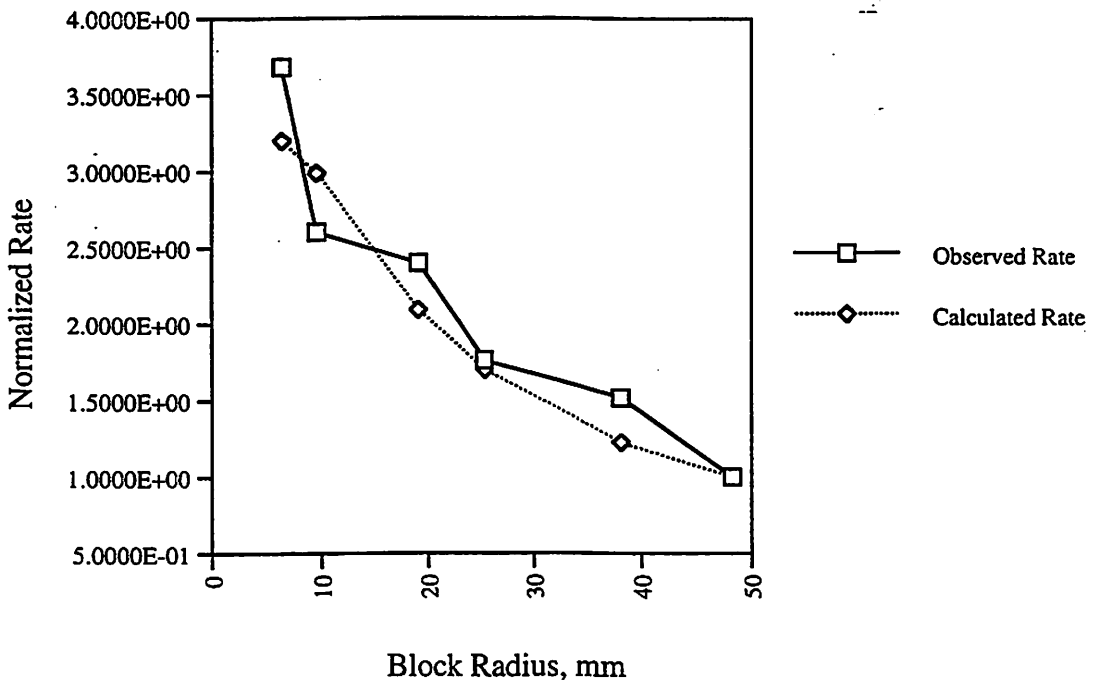

Fig. A.3. Observed and calculated large block oxidation rates at 550°C. *Source:* Cowen et al.[23]

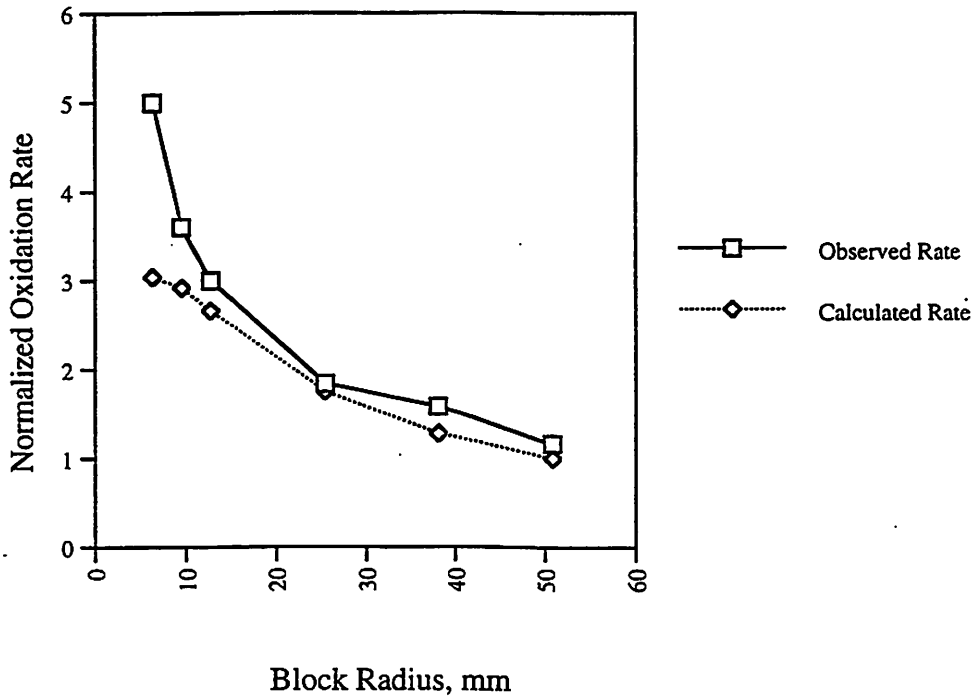

Fig. A.4. Observed and calculated large block oxidation rates at 500°C. *Source:* Cowen et al.[23]

smallest two blocks. This is undoubtedly due to an error in estimating Δh from the the empirical formula at this low temperature, 100°C lower than the lowest Δh determination.

The favorable comparison between large block oxidation rate data with predicted trends with size lends confidence to the "active oxidation depth" method used in GRSAC. Some further data on the value of Δh with temperature using air oxidant would improve confidence, especially at lower temperatures. It should be emphasized that this method is applied in GRSAC only to those situations shown to be in the chemical control regime. At high temperatures, oxidation tends to be a surface phenomenon controlled by the transport rate of oxygen to the surface.

A.5 PRINCIPAL LABORATORY-SCALE OXIDATION RATE EXPERIMENTS

A.5.1 Dahl[1]

Tests concentrated on CSF graphite projected for use in the Experimental Gas-Cooled Reactor. The specimens were annular, 2 in. long, and 0.426 in. OD × 0.25 in. ID. Temperatures ranged from 676 to 948 K. It is stated that the tests were conducted entirely under Zone I conditions. The technique used was to burn off a small amount (about 5%) to achieve a steady rate. The reported rate equation thus represents an elevated rate as predicted by the burnoff dependence given by Eq. (A.2). Dahl's rate equation for oxidation in air is reported as

$$R_I[g/(g\cdot hr)] = 9.22 \times 10^8 \exp[-45{,}200/(RI\cdot T)] \,. \qquad (A.12)$$

Tests with varying oxygen levels indicated that the rate was "near first order" in oxygen pressure. It is stated without details that the active oxidation depth at 873 K was 5 mm. [Eq. (A.9) predicts 4.1 mm at this temperature, which is a fair agreement.] The oxidation rates of eight nuclear graphites were compared at 873 K. A factor of 6 range was observed (0.0252 to 0.00429 hr^{-1}), which was clearly shown to depend mainly on purity.

A.5.2 O'Brien et al.[24]

Oxidation rates of two nuclear graphites considered for fusion components were studied in the range 1073 to 2073 K in order to assess safety in the event of an air ingress. The specimens were cylinders 2.7 cm in diameter and 1.27 cm in height. (Also included were a carbon composite and a pyrolytic graphite.) Above 1273 K, little or no oxidation penetration occurred [Eq. (A.9) predicts 1.5 mm at 1273 K], indicative of Zone III conditions. In this range the oxidation rate depends solely on the mass transfer properties of the apparatus. Below 1273 K, the rate depended on both chemical reactivity and mass transfer, indicative of Zone II conditions. The rate equations presented in this study are therefore of no general use.

An interesting feature of these tests was performance of an energy balance which attempted to locate where the oxidation heat was deposited. Above 1273 K, energy balances were consistent with (1) only CO formation at the graphite surface, and (2) all the graphite oxidative heat (i.e., oxidation to CO, about 30% of the total heat) deposited in the graphite. The balance was carried away as CO. At 2000 K, a CO flame became visible at the exit of the furnace.

A.5.3 A Review by Clark et al.[7]

This well-known review emphasizes reactions with CO_2. Air oxidation rates of Dahl (1961) are presented. A discussion of "burning" is presented.

A.5.4 A Review by Lewis[8]

This is a comprehensive review (60 pages) covering low- and high-temperature reactions, reactions with atomic gases, and physical factors affecting oxidation. Emphasis is on the basic science of gas-graphite reactions. It is stated that the rate of the C-O_2 reaction is less predictable than C-CO_2 or C-H_2O but is generally assumed to have the form

$$R_I = A \exp[-E/(RI \cdot T)] P(O_2)^n \quad (A.13)$$

where R_I is the Zone I rate in terms of g/(g·sec). This is identical to Dahl's expression [Eq. (A.12)] except that a value for n of 0.5 is proposed instead of unity. Lewis states that the value of E is clearly 60,000 cal/mol for pure graphite oxidizing under Zone I conditions. The value of A is not discussed.

Other topics covered in this review are discussed elsewhere in this memo—the CO:CO_2 ratio in the product gas, the reduction in oxidation rate from 1500 to 2000 K, and the BET surface area being a measure of the active surface area (ASA).

A.5.5 Bunnell et al.[12]

Bunnell measured the oxidation rate of TSX-grade nuclear graphite from 723 to 1473 K. At low temperatures corresponding to Zone I (723 to 900 K), a rate equation similar to Dahl's was obtained:

$$R_I[g/(g \cdot hr)] = 9.02 \times 10^8 \exp[-45{,}800/(RI \cdot T)] \, . \quad (A.14)$$

No information is presented on the data above 900 K. Some burnoff profile data are given, which are included in Table A.2 and used for developing the burnoff depth correlation, Eq. (A.9).

A.5.6 Fuller et al.[11]

This study dealt with nuclear graphite H-451, for use in the High Temperature Gas-Cooled Reactor. Test samples 0.333 in. in diameter and 0.75 in. long were used. Temperatures ranged from 667 to 1110 K. Most of the data appear to have been taken under Zone I conditions. An activation energy of 40,200 cal/mol was observed, possibly too low for Zone I. A reaction rate equation was not given.

A.5.7 Kuchta et al.[25]

This study covered a wide range of gas velocities (28 to 549 ft/sec) and temperatures from 1273 to 1473 K. The specimens were 0.3-cm-diam cylinders, 3 cm long. Spectrographic- grade carbon was used. The presented data could be useful for testing high-velocity oxidation correlations. It was shown that at high temperature, Zone III oxidation could revert to Zone I by increasing the air velocity.

A.6 GRSAC GRAPHITE OXIDATION MODEL

A.6.1 Zone I Oxidation Model

The Zone I oxidation model accounts for all the factors affecting graphite reactivity cited in Sections A.3 and A.4, namely,

1. variation with temperature (graphite and carbon deposit),
2. variation with oxygen pressure (graphite and carbon deposit),

3. variation of graphite reactivity with degree of oxidation,
4. increase of graphite reactivity with neutron dose,
5. accumulation of carbon within graphite pores,
6. oxidation of carbon deposits, and
7. non-uniform oxidation of large graphite blocks.

Collecting the information developed in Sections A.3 and A.4 leads to the following expression for the oxidation rate of graphite under Zone I (chemically controlled) conditions:

$$R = \{A_g [1 + 1.37\, AGE(t)\, P(r,z)] \exp(-E_g/RT)\, P_{O2}^{0.7}\ f(B) + A_{cd} \exp(-E_{cd}/RT) \times (P_{O2}/0.21)^{0.86}\, AGE(t)\, P(r,z)\, y(z)/100\}\, [\Delta h(T)\, \rho/MW]\,, \qquad (A.15)$$

where

R	=	Zone I graphite oxidation rate (moles/cm^2·min),
A_g	=	graphite reactivity factor, 2.04×10^7 (1/m),
AGE(t)	=	input parameter defining age of core, range 0 – 1,
P(r,z)	=	local to average core power factor,
E_g	=	activation energy for graphite oxidation, 45,000 cal/mole,
R	=	gas constant (cal/mole·K),
P_{O2}	=	local oxygen pressure (atm),
f(B)	=	factor accounting for graphite burnoff, Eq. (A.2),
A_{cd}	=	carbon deposit reactivity factor, 1.64×10^6 (1/m),
E_{cd}	=	activation energy for carbon deposit oxidation, 24,800 cal/mole,
y(x)	=	carbon deposit weight percent, a polynomial function of core height given in Fig. A.1 and Eq. (A.7),
x	=	core height (in./100),
$\Delta h(T)$	=	active oxidation depth (cm),
r	=	graphite density, about 1.8 (g/cm^3),
MW	=	molecular weight of graphite, 12 g/mole.

The first set of terms in the curly brackets refers to graphite; the second set, to carbon deposit. The factor (1+1.37 AGE P(r,z)) accounts for the increase in graphite reactivity with neutron dose, as developed in Section A.3.6. The exponential terms account for the variation of rate with temperature in the form expected for chemically controlled reactions. The factors $P_{O2}^{0.7}$ and $P_{O2}^{0.86}$ account for the effect of oxygen pressure reduction for graphite and carbon deposit, respectively. The factor $\Delta h(T)\ \rho/MW$ accounts for the non-uniform oxidation of large specimens of graphite, as developed in Section A.4. This term essentially limits an experimentally observed Zone I oxidation rate to volume within and active depth, Δh, which depends on the temperature. Also, it is implied that the deposit in the pores is restricted to graphite within 6 cm from the coolant surface. Data show that the major part of the deposit occurs within this depth.

A.6.2 General Method

1. Oxidation rates are determined for each lumped parameter location for each time step assuming both Zone I (chemical control) and Zone III (mass transport control) conditions. The lower rate is selected as controlling.

2. For Zone I conditions, the volume of the active oxidation volume in each block is determined from the active reaction zone thickness given by Eq. (A.9) and block dimensions. The reaction rate within this reactive volume depends on the temperature, the prior history as given by the

burnoff, B, the oxygen pressure, the age of the core, and the degree of carbon deposit, according to Eq. (A.15).

The experiments of Dahl[1] on grade TSX graphite and Bunnel[12] on grade CSX appear to offer the best basis for evaluation of the constants A and activation energy, E. The average activation energy from these two experiments is 45,500 cal/mol (compared with the theoretical value of 60,000).

The average value of the constant, A, from these two data sets is 1.52×10^7 min^{-1} (9.12×10^8 hr^{-1}). A factor 4.76 (reciprocal of 0.21) must be applied to account for the fact that the original equation did not contain the term $P(O_2)$, which equals 0.21 for the tests. A burnoff correction needs to be applied because Dahl, and evidently also Bunnel, acquired their data after performing some oxidation as pretreatment. Dahl states that approximately 5% of the graphite mass was burned off to achieve a stable oxidation regime. According to Eq. (A.2), a 5% burnoff elevates the reaction rate by a factor of 3.55 relative to an unoxidized specimen. Therefore, a factor of 0.282 (reciprocal of 3.55) is applied to the expression. These two correction factors applied to constant A_g yield a value of 2.04×10^7 min^{-1}.

Summarizing, the values of the constants E and A in Eq. (A.15) are 45,500 cal/mol and 2.04×10^7 min^{-1} respectively. This expression requires that GRSAC retain prior oxidation histories of each block in order to calculate the burnoff factor f(B) and keep a record of the oxygen concentrations along the air flow path to determine $P(O_2)$.

3. The reaction rate for Zone III conditions is based on the exterior surface area of the block. It is assumed that the oxygen concentration at the graphite surface is zero, permitting the simple relation

$$R_{III} = h_m [O_2], \tag{A.16}$$

where R_{III} units are mol/(cm^2·min). h_m is the mass transfer coefficient in centimeters per minute, and $[O_2]$ is the oxygen concentration in the air for that particular location in moles per cubic centimeter. Implied in Eq. (A.16) is the assumption that the oxidation product is CO_2; that is, that one mole of CO_2 is produced per mole of O_2 delivered to the surface. (A factor of 12 g/mol converts moles of carbon into grams.) In general, h_m depends on the Reynolds number, Re, Schmidt number, and the surface roughness. A recommended evaluation method is given by standard relations summarized in items 4 and 5 below for laminar flow ($Re < 2100$) and turbulent flow ($Re > 2100$). For coolant channels, the value of Re is based on the hydraulic mean diameter, d_h, defined below.

4. If $Re < 2000$, h_m may be determined from a laminar flow relation from a theoretical development by Graetz (e.g., see Hines and Maddox[26]):

$$h_m = 60 \times 4.36 \times D/d_h, \tag{A.17}$$

where D is the diffusion coefficient of O_2 in air (square centimeters per second) and d_h is the hydraulic diameter of the tube (centimeters). The constant 4.36 applies to the case of a fully developed profile and constant mass flux. The factor 60 converts h_m to units of centimeters per minute.

The hydraulic mean diameter is defined as

$$d_h = 4 \times \text{flow area/channel perimeter} . \quad \text{(A.18)}$$

The value of D (oxygen in air) is 0.178 cm^2/sec at 298 K (Ref. 27). Theory predicts an increase with temperature according to $T^{1.75}$ with T in Kelvin (Ref. 28).

5. When Re > 2100, determination of h_m using the Reynolds Analogy is simplest and possibly best for turbulent flow of air in rough conduits (e.g., see Coulson and Richardson[29]). For mass transfer, the Reynolds Analogy may be written

$$h_m = f U , \quad \text{(A.19)}$$

where

h_m = mass transfer coefficient, cm/min;
f = friction factor, defined as the wall shear stress divided by the air density and velocity squared (Note, this is one-half of the more common Fanning friction factor.);
U = air velocity in conduit, cm/min.

For extremely rough tubes, as for the case of G-2 reactor coolant passages which contain transverse fins, the value of f is independent of Reynolds number, depending solely of the degree of roughness. For these deliberately roughened passages, f may take a value between 0.01 and 0.05.

6. It is assumed that CO_2 is the principal oxidation product and that the oxidation heat is deposited in the graphite at each node.* The oxidation heat varies with temperature according to the relation

$$\Delta H(T) = (-93{,}780 - 1.218T) + (2.29 \times 10^{-3}T^2) - (1.55 \times 10^{-6}T^3) . \quad \text{(A.20)}$$

Units are calories per mole of graphite oxidized and Kelvin. (In this convention, a negative ΔH means heat released by oxidation.) Equation (A.20) is based on an oxidation heat for the reaction $C + O_2 = CO_2$ of –94,050 cal/mol at 298 K. Extension to higher temperatures is based on standard thermochemical methods.[30]

A.6.3 Determination of Local Oxygen Pressure

The local oxygen pressure is required as a multiplier in the graphite oxidation rate correlation in the chemical control regime [Eq. (A.15)]. Similarly, the local oxygen concentration is required as an input for mass transfer control conditions [Eq. (A.16)]. Therefore, the gas composition is tracked along the flow channel from inlet, at the normal air composition and low temperature, through regions of increasing temperature, diminishing oxygen, and increasing carbon dioxide.

---

* Actually, CO production increases at elevated temperatures relative to CO_2, and progressively less oxidation heat is deposited locally. The balance is released where the CO burns, a portion of this heat being deposited in adjacent solid and the balance in the gas. Adding this sophistication would require models for (1) the ratio of CO/CO_2 oxidation product, (2) determination of the location(s) for CO burning, and (3) partitioning of the CO oxidation heat between gas and solid.

The following general approach is used for tracking the gas composition along a flow channel:

1. The gas space of each node is treated as a completely mixed volume.

2. It is assumed that the sole product of graphite oxidation is CO_2. (Provision for including CO requires a correlation for CO/CO_2 production as a function of temperature, testing for combustible CO/O_2 composition, and axial transport of CO into regions of combustible composition.)

3. A mass balance for O_2, CO_2, and N_2 is performed assuming known nodal temperatures from the previous time step. (The balance equations also include metal oxidation. See Appendix B for oxidation of the Magnox metals, magnesium and uranium. Also see Appendix E for the additional metals involved with the Windscale reactor accident evaluation.)

4. GRSAC then executes a heat balance to determine the new nodal temperatures.

5. The total gas pressure in the node is corrected to 1 atm, as required for an open system. To accomplish this, gas may either be exhaled from the node as a result of pressure rise due to increasing temperature or inhaled from surrounding nodes as oxygen depletion or temperature decrease results in a loss of pressure. If gas inhalation is required, it is assumed that surrounding nodes supply gas of the same composition as the node in question.

These assumptions lead to the following O_2, CO_2, and N_2 nodal mass balance equations based on temperatures for the previous time step:

$$[O_2]_2 = [O_2]_1 - (R_G + R_{Mg} + R_U)/(V/\delta t + Q) \quad \text{(A.21a)}$$

$$[CO_2]_2 = [CO_2]_1 + R_G/(V/\delta t + Q) \quad \text{(A.21b)}$$

$$[N_2]_2 = [N_2]_1 \quad \text{(A.21c)}$$

where

subscripts 2 and 1 refer to the new and old nodal compositions, respectively;
[ ] indicate concentration, mol/cm^3;
R_G, R_{Mg}, R_U = graphite, magnesium, uranium oxidation rates in node, mol/min;
V = node gas volume, cm^3;
δt = time step, min;
Q = local volumetric flow through node, cm^3/min.

The local nodal volumetric flow, Q (cm^3/min), is approximated by the following relation,

$$Q = m_{inlet} \times (N_{chan}/N_{node}) \times 22{,}400T_2/(29.1 \times 298) \quad \text{(A.22)}$$

where

m_{inlet} = inlet mass flow to core, g/min;
N_{chan}/N_{node} = ratio of flow channels in node to the total number of channels;
22,400 = gas volume per mole at 298 K, 1 atm;
29.1 = molecular mass of air, g/mol;
298 = assumed inlet temperature, K.

Equation (A.22) is an approximation that neglects the loss of oxygen to metal oxidation products and the alteration of molecular mass due to partial replacement of O_2 with CO_2. Since most of the volume flow is unaltered nitrogen, the approximation should be fairly accurate.

The new compositions and the new nodal temperature determined from the GRSAC heat balance result in a total pressure other than 1 atm. To correct to 1 atm, per assumptions listed above, determine required total gas concentration for the new conditions, $[n]_2$,

$$[n]_2 = 1/(R2 \times T_2) \tag{A.23}$$

where

R2 = gas constant, 82.06 $(cm^3 \cdot atm)/(mol \cdot K)$;
T2 = new nodal temperature, K.

The pressure-corrected gas compositions are then determined from

$$[O_2]_{2,corr} = X_{O2} \times [n]_2 \tag{A.24a}$$

$$[CO_2]_{2,corr} = X_{CO2} \times [n]_2 \tag{A.24b}$$

$$[N_2]_{2,corr} = X_{N2} \times [n]_2, \tag{A.24c}$$

where X_{O2}, X_{CO2}, and X_{N2} are mole fractions based on concentrations calculated from Eqs. (A.21a), (A.21b), and (A.21c).

A.6.4 Outline of Calculation Procedure

1. At time zero following introduction of air, and for the first tier of exposed blocks, determine the active oxidation volume in the graphite from Eq. (A.9) and the geometry of the block.

2. Assume Zone I oxidation occurs; determine the oxidation rate using Eq. (A.15), knowing that B = 0 at time zero. Determine the moles of carbon oxidized during the time step.

3. Repeat, assuming Zone III oxidation occurs.

   a. Determine the Reynolds number based on the hydraulic mean diameter of the conduit.
   b. If laminar flow exists, determine h_m using Eq. (A.17).
   c. For turbulent flow, use Eq. (A.19).
   d. Determine the oxidation rate from Eq. (A.16), using $[O_2] = 8.59 \times 10^{-6}$ mol/cm^3 for the oxygen concentration of normal air at standard conditions corrected for ambient temperature by the factor (298/T). Determine the total moles of carbon oxidized in the time step using the total exposed surface of graphite per node.

4. Select the smaller value between the Zone I and III determinations as controlling.

5. Determine the new nodal temperatures from a heat balance.

6. Determine the new oxygen, carbon dioxide, and nitrogen pressure-corrected concentrations by the method outlined in the above section. These are the concentrations which enter the next tier of nodes.

7. Repeat steps 1 through 6 for the second time step, using the new O_2 concentrations for the newly exposed second tier of blocks, and the calculated burnoff values, B, for the first tier that has experienced some oxidation (provided it was in Zone I oxidation regime). Note, the relation between oxygen concentration, $[O_2]$, and partial pressure is

$$P(O_2) = [O_2] \times R2 \times T,$$

where P is in atmospheres, $[O_2]$ is in moles per cubic centimeter, and T is in Kelvin. The gas constant *R2* takes the value 82.06 $(cm^3 \cdot atm)/(mol \cdot K)$.

8. For locations consistently in the Zone I regime, it is necessary to move the active reaction width inward to the next Δh when the burnoff is completed, considered to occur when B = 0.9. A reasonable procedure needs to be selected to account for variation of Δh due to a change in temperature. A simple method is to keep Δh constant with time until the burnoff is complete in Δh, and subsequently select a new Δh at the current temperature.

9. The oxidation regime at a particular location may change from Zone I to Zone III due to increasing temperature or reduced flow. In such case it is necessary to retain the record of the burnoff history and to base the new R_{III} $(mol/cm^2 \cdot sec)$ on the current density of the reaction zone. The reverse transition should not present a problem. However, several transitions back and forth between oxidation regimes could severely tax a program.

A.7 INTEGRAL SCALE GRAPHITE OXIDATION EXPERIMENTS

As stated in Section A.1, graphite oxidation models in GRSAC are necessarily based on small specimen data taken under controlled laboratory conditions. The experimental conditions need to be sufficiently broad to enable derivation of a predictive empirical correlation. However, a number of integral experiments have also been performed which may indicate general oxidation behavior of large graphite masses, and which may be used to check the GRSAC code. Their limitation as a GRSAC test lies with the fact that they contain only graphite; that is, there would be no interaction with cladding or uranium oxidation as existed in the complex Windscale sequence, or to a much less degree in the French channel fire experiments.

A.7.1 Integral Oxidation Tests at Hanford

Dahl[13] describes integral oxidation tests on Experimental Gas Cooled Reactor graphite. Dahl's follow-on report[31] summarizes the test results. By careful selection of heater power and air flow rate, Dahl was able to create conditions of spontaneously increasing temperature for bulk graphite temperatures above about 750°C, provided the air flow rate was sufficiently high. Reducing the air flow rate had the effect of terminating the transient. (This experiment would be informative as a graphite-only GRSAC test if sufficient operational information is available.)

A.7.2 Integral Oxidation Tests at Brookhaven

A series of integral oxidation tests performed at Brookhaven National Laboratory are described by Schweitzer et al.[3-5] A summary discussion of combined effects of flow, geometry, and chemical reactivity is presented by Schweitzer.[6] The tests were performed on channels of diameters ranging from 0.5 to 2.67 in. cut in 4- by 4-in. blocks of BNL-grade graphite. The motive for the tests was demonstration of the safety of the BNL graphite reactor, although study of the then recent Windscale fire must have been a secondary objective. Tests focused on predicting the maximum length of a

heated graphite channel which can operate under stable temperature conditions. (This experiment would be informative as a graphite-only GRSAC test if sufficient operational information is available.)

A.7.3 Integral Oxidation Tests at Windscale Laboratories

Robinson and Taylor[32] describe integral tests conducted following the fire in the Windscale reactor. As in Dahl's tests, they were able to create conditions of increasing graphite temperatures when the graphite temperature was raised beyond about 600°C, provided the air heater power was kept on and when sufficiently high air flow was present. A companion paper[33] describes a simplified analysis of conditions required for inducing continually increasing temperatures. (This experiment would also be informative as a graphite-only GRSAC test if sufficient operational information is available to permit a mock-up.)

A.8 REFERENCES

1. Dahl, R. E., *Oxidation of Graphites Under High Temperature Reactor Conditions,* HW-68493 (1961).

2. Robinson, P. J., and J. C. Taylor, *Thermal Instability Due to Oxidation of a Graphite Channel Carrying an Air Flow,* TID 7597, Vol. II (1960).

3. Schweitzer, D. G., et al., "Oxidation and Heat Transfer Studies in Graphite Channels: I. The Effect of Air Flow on the C-O_2 and CO-O_2 Reactions," *Nucl. Sci. Eng.* **12**, 39–45 (1962).

4. Schweitzer, D. G., et al.,"Oxidation and Heat Transfer Studies in Graphite Channels: II. Thermal Changes with Time and Distance in Air-Cooled Graphite Channels," *Nucl. Sci. Eng. 12,* 46–50 (1962).

5. Schweitzer, D. G., et al.,"Oxidation and Heat Transfer Studies in Graphite Channels: III. The Chemical Reactivity of BNL Graphite and Its Effect on the Length of a Channel Cooled by Air," *Nucl. Sci. Eng.* **12**, 51–58 (1962).

6. Schweitzer, D. G., et. al., "Oxidation and Heat Transfer Studies in Graphite Channels, IV. Combined Effects of Temperature, Flow Rate, Diameter, and Chemical Reactivity on the Length of the Channel Cooled by Air," *Nucl. Sci. Eng.* **12**, 59–62 (1962).

7. Clark, T. J., et al., "Gas Graphite Systems," Chap. 14 in *Nuclear Graphite*, R. E. Nightingale, Ed., Academic Press (1962).

8. Lewis, J. B., "Thermal Gas Reactions of Graphite," p. 139 in *Modern Aspects of Graphite Technology*, L.C.F. Blackmun, Ed., Academic Press (1970).

9. Lewis, J. B., Ibid, p. 155.

10. Bhatia, S. K., and D. D. Permutter, "A Random Pore Model for Fluid-Solid Reactions," *AIChE J.* **26**, 379–386 (1980).

11. Fuller, E. L., et al., *Corrosion of Nuclear Grade Graphites: Air Oxidation of H-451*, ORNL/NPR-91/27 (1992).

12. Bunnell, L. R., et al., *Oxidation of TSX Graphite from 450 to 1200C,* UNI-SA-207 (PNL-SA-14925) (1987).

13. Dahl, R. E., *Experimental Evaluation of the Combustion Hazard to the Experimental Gas Cooled Reactor–Preliminary Burning Rig Experiments*, HW-67792 (1961).

14. RHASD V800: *User Guide*, ITD/NP1/RHASD/91/3, MGFSG/P(91)7, Nuclear Electric (1991).

15. Hopkinson, K., AEA Technologies, personal communication to R. P. Wichner, February 18, 1997.

16. IAEA, "Directory of Nuclear Reactors, Vol. IV," *Power Reactors*, revised and supplemented addition to Vol. I, International Atomic Energy Agency, Vienna (1962).

17. Best, J. V., W. J. Stephen, and A. J. Wickham, "Radiolytic Graphite Oxidation," *Prog. Nucl. Energy* **16**(2), 127–178 (1985).

18. Lewis, J. B., "Thermal Gas Reactions of Graphite," p. 174 in *Modern Aspects of Graphite Technology*, L.C.F. Blackmun, Ed., Academic Press (1970).

19. Lewis, J. B., Ibid, p. 179.

20. Glassman, I., *Combustion*, Academic Press, Table 1, Appendix E (1987).

21. Lewis, J. B.,"Thermal Gas Reactions of Graphite," Chap. IV in *Modern Aspects of Graphite Technology*, L.C.F. Blackmun, Ed., Academic Press (1970).

22. Helsby, G. H., and M. R. Everett, *Some Graphite Corrosion Problems Related to Helium Cooled HTRs*, Dragon Project Report 566 (1968).

23. Cowan, H. C., et al., "The Rate of Oxidation of Large Blocks of Graphite in Air," pp. 359–373 in *Proc. of the U.S./U.K. Meeting on the Compatibility Problems of Gas-Cooled Reactors, Oak Ridge, February 1960,* TID-7597 (1960).

24. O'Brien, M. H., et al., *Combustion Testing and Thermal Modeling of Proposed CIT Graphite Tile Materials*, EG-FSP-8255 or DE90 013090 (1988).

25. Kuchta, J. M., et al., "Combustion of Carbon in High Temperature, High Velocity Air," *Ind. Eng. Chem.*, pp. 1559–1563, July 1952.

26. Hines, A. L., and R. N. Maddox, *Mass Transfer Fundamentals and Applications*, Prentice-Hall, p. 177 and following (1985).

27. *CRC Handbook of Chemistry and Physics, 70th ed.,* CRC Press, Inc., P.F-50 (1989).

28. Perry, R. H., *Chemical Engineer's Handbook*, McGraw-Hill, p. 3-285 (1984).

29. Coulson and Richardson, *Chemical Engineering*, Vol. I, McGraw Hill (1954.)

30. Hougen, O. A., et al., *Chemical Process Principles*, John Wiley and Sons, 2nd ed., Part I, p. 345 and following (1959).

31. Dahl, R. E., *Summary Report–Hanford Studies of EGCR Combustion Characteristics*, HW-71296 (1961).

32. Robinson, P. J., and J. C. Taylor, "Thermal Instability Due to Oxidation of a Graphite Channel Carrying Air Flow," in *Proceedings of the U.S./U.K. Meeting on the Compatibility Problems of Gas Cooled Reactors*, Oak Ridge, Feb. 24–26, 1960, TID-7597 (1961).

32. Nairn, J. S., and V. J. Wilkinson, "The Prediction of Conditions for Self-Sustaining Graphite Combustion in Air," in *Proceedings of the U.S./U.K. Meeting on the Compatibility Problems of Gas Cooled Reactors*, Oak Ridge, Feb. 24–26, 1960, TID-7597 (1961).

APPENDIX B. URANIUM METAL AND MAGNOX CLADDING OXIDATION MODELS

B.1 INTRODUCTION

In this section, models are presented for determining Magnox cladding and uranium metal oxidation rates. Since the model must be used at each node in GRSAC and for each time step, an important criterion for suitability is rapid run time. The main assumptions that permit straightforward adoption are (1) avoidance of elaborate mathematics (e.g., solution of a set of differential equations) and (2) maintenance of a regular geometry (i.e., no material relocation). The models are intended to apply to the class of Magnox-clad, uranium metal–fueled, gas-cooled reactors, for example, the British Calder Hall class and French G2/G3 types of gas-cooled reactors.

Two broad categories of oxidation are defined: heterogeneous oxidation, which requires transport of oxygen from the free stream to the metal surface, and true burning, a vigorous gas-phase oxidation of vaporized metal. Benchmarking tests using the French channel fire tests (see Appendix F) clearly show the need for a true burn model for graphite reactors containing large quantities of magnesium cladding material. A burn model is also developed in this appendix. All chemically active materials, including uranium and graphite, may burn in the vapor phase, although at much higher temperatures than required for magnesium. Application of a burn model in GRSAC requires prediction of the ignition temperature and the resulting burning rate.

As in the case of graphite, the oxidation rate in the chemical control regime is obtained from published empirical formulae. Simultaneously, the mass transfer rate of oxygen to the surface is determined using standard correlations. Under heterogeneous oxidation rate conditions, the lower of the two rates (chemical or mass transfer) is selected as the controlling oxidation rate. Consideration of oxidation of metallic uranium fuel in a CO_2 atmosphere is also included.

Literature searches on bulk oxidation characteristics of both uranium and magnesium extended back to 1950 and covered all related DOE (and predecessor) reports plus publications cited in *Energy Abstracts, Chemical Abstracts,* and *Engineering Abstracts.* The search has located significant work on uranium oxidation, but only a few reports were found on the oxidation rate of bulk magnesium.

B.2 FUEL ELEMENT AND CORE DESCRIPTION

Some pertinent characteristics of typical Magnox reactor cores and fuel which relate to burning of the uranium or cladding metals are included in the databases of Appendix H. Although the coolant channels are horizontal in some Magnox designs, such as the G2/G3 reactors, natural convective drafts could occur in the event of a pressure vessel breach. In some cases the mass of magnesium, in terms of moles, amounts to 40% of that of uranium. Therefore, magnesium oxidation heat may be a significant factor that should be included in the model.

B.3 CHEMICAL AND PHYSICAL PROPERTIES OF URANIUM AND MAGNESIUM

Some properties pertinent to uranium and magnesium burning are given by Kubaschewski and Alcock[1] in Table B.1. For comparison, some properties of graphite are also included. Also in Table B.1, standard enthalpy changes and free energy changes (ΔG) are given per mole of magnesium, uranium, and carbon at 25°C. Reaction products are assumed to be U_3O_8, MgO, and CO_2, and UC_2 and MgC_2 for the carbides.

Table B.1. Some properties of uranium, magnesium, and graphite

	Uranium	Magnesium	Graphite
Melting point (°C)	1,132	649	None
Boiling point (°C)	4,135	1,090	Sublimes
Density (g/cm^3 at 25°C)	19.0	1.74	1.8
Heat of fusion (kcal/mol)	3.0	2.1	--
Heat of oxidation (kcal/mol)	–284.7	–142.7	–94.1
ΔG for oxide (kcal/mol)	–268.5	–143.8	–94.3
ΔG for carbide (kcal/mol)	–23.7	+21	--

As values in the table show, in a core overheat situation the Magnox cladding will melt first and could, in fact, reach its boiling point before uranium melting begins. Molten magnesium is essentially insoluble in uranium; so there will be no alloying of the molten magnesium in uranium. The positive free energy of the carbide (+21 kcal/mol) indicates that magnesium will not react with graphite to form MgC_2. Since magnesium may ignite at about 600°C, one possibility is for low-temperature magnesium oxidation to result in melting or ignition of the uranium.

A measure of relative oxidation tendencies is the magnitude of the negative free energy of oxidation per unit mole of oxygen. From the values in the table and the stoichiometry of the reactions, one obtains –201 kcal/mol as the free energy of oxidation of U_3O_8 per mole of O_2 and –272 kcal/mol for MgO. High negative values signify that both metals are readily oxidizable, with the tendency for magnesium oxidation somewhat higher at low temperature. The large negative free energy of the oxide also indicates that U_3O_8 and MgO will form in preference to the carbides.

B.4 RAPID OXIDATION OF BULK METALS

B.4.1 Background

Several studies were done in the 1960s on the ignition and burning of bulk metals. However, the methodology has not yet developed to the point where it can be directly applied to clad, metallic fuel elements. Although a general approach is indicated, many important details on effects of solubility at high temperature, relative vapor pressure of metal and oxide, nature of the oxide film, material size, and transient heat transmission have not been generally treated.

Complex processes are involved in metal burning, perhaps more complex than for the burning of ordinary fuels, which entails mainly evaporation of volatiles, diffusive mixing with oxygen, and gas-phase oxidation. Theories of diffusion flames are well developed and described in texts (e.g., by Glassman[2]). Many more factors enter into metal burning. Interest in the subject was motivated by safety considerations for metal fuel reactors, which has since declined as a priority issue, and the use of powdered metals in rocket fuel.

B.4.2 Metal Burning Characteristics

The following five categories of metal combustion were developed by Brzustowski and Glassman[3] and by Gordon.[4] These have been reviewed by Markstein,[5] who also describes a series of metal burning tests which illustrate various types of phenomena encountered.

A. **Metals with High Volatility.** Relatively volatile metals, specifically magnesium, burn in the vapor phase by the processes of vaporization and diffusive mixing with oxygen. The major difference relative to organic fuels is that the combustion product is a high-melting-point oxide instead of a gas. As a result, this type of burning is marked by voluminous emission of smoke of the color of the oxide.

There is conflicting evidence whether or not aluminum falls into this category. (Aluminum was the cladding material for the Windscale reactor.) Harrison and Yoffe[6] state that aluminum also burns in the vapor phase, based on tests of burning wires. In contrast, Abbud-Madrid et al.[7] were not able ignite aluminum within limits of their apparatus, up to about 1500°C, and state that the ignition point should be the melting point of the oxide, 2050°C. The difference is the type of experiment; the normally protective aluminum oxide film failed to protect the base metal in the wire configuration of Yoffe but did so in the more quiescent tests of Abbud-Madrid, even well beyond the metal melting point of 660°C.

Therefore, the burning model for aluminum requires judgement if the situation is quiescent (oxide film protection) or aggressive. In the latter case, burning characteristics should be much like magnesium, a metal of similar properties.

B. **Nonvolatile Metals with Soluble Oxides.** Tests by Gordon[4] on small particles show that the effect of oxide solubility is to render the metal easily ignitable but slow burning. He places titanium and zirconium in this category.

C. **Metals with Protective Oxide Film.** As noted in group A, a protective oxide film under quiescent conditions may inhibit ignition and burning well beyond the melting temperature of the base metal. In addition to aluminum, beryllium and titanium fall into this category. These should exhibit the same degree of uncertainty with respect to burning rate as aluminum.

D. **Nonvolatile Metals with Volatile Oxides.** Boron and molybdenum are placed in this category. (This group should perhaps also include metals with nonadherent oxide films. The effect on burning rate appears to the same.)

E. **Alloys with Constituents That Differ in Volatility.** These may be observed to burn in successive stages due to differences in volatility. In addition, high temperature and alteration of composition can promote intermetallic compound formation. For example, Fassel, et al.[8] report that the burning rate of magnesium-aluminum alloys is increased when the compound $MgAl_2$ forms.

There are several omissions and inconsistencies in this categorization. Principally, no distinctions are made with respect to chemical affinity for oxygen; a more rational grouping should begin with chemical characterizations. There is a wide gulf between oxygen affinities of uranium, zirconium, and others at one end of the scale and the group of noble metals at the other which do not form stable oxides. Also, there is no group for low-volatility metals with nonadherent oxide coatings, hence the suggestion to expand group D to include metals of this type. Finally, the distinction between low-volatility or high-volatility metals is arbitrary. A so-called low-volatility metal, like uranium, could burn in the vapor phase (like magnesium) if the temperature were sufficiently high. But this early attempt to classify metals with respect to burning behavior does serve to illustrate the range of phenomena encountered.

It is interesting to note where our metals of interest are placed:

- Magnesium is clearly group A.
- Uranium fits best into the expanded group D, but at high temperature it can behave as group A.
- Aluminum, the Windscale cladding material, is placed in either group A or C, depending on conditions. This uncertainty presents a modeling problem.
- Lithium-magnesium alloy, a target material in the Windscale AM cartridge, combines properties of groups A and E.

B.5 DEFINITIONS—METAL BURNING AND METAL IGNITION

B.5.1 Burning vs Heterogeneous Oxidation

Intuitively, one associates burning (also combustion) with the familiar behavior of organic materials—vaporization of volatiles, diffusive mixing with oxygen, oxidation in the gas phase, generation of a visible flame, and vigorous reaction sustained by its own oxidative heat. All group A metals "burn" in this traditional sense, except that they make oxide smoke instead of water vapor and oxides of carbon. In fact, all chemically reactive metals can "burn" in this fashion given sufficiently high temperature.

The major departure for metals is the important regime of "heterogeneous combustion," which occurs at temperatures below the point where the metal vapor pressure is sufficient to generate a combustible mixture in the gas phase. Heterogeneous combustion requires the following steps in sequence: (1) diffusion of oxygen to the surface; (2) diffusion of oxygen through the oxide film, provided there is a protective oxide film; and (3) chemical reaction with the metal, perhaps involving diffusion of oxygen into the metal.

Depending on the particular conditions, any one of these three steps may be rate controlling. Several studies [e.g., by Reynolds[9]] derive burning models assuming control by step 2, which would render the theory valid for only the few metals that display protective oxide films. Other published theories assume step 1 control of the overall rate. In fact, in all cases the rate-controlling step will change as conditions change. The reason is that step 1 varies slowly with temperature, while steps 2 and 3 depend on a chemical activation mechanism and hence increase rapidly with temperature. Thus, in general, overall oxidation rate control will pass from step 1 to either 2 or 3 with increasing temperature.

Heterogeneous oxidation is generally slower than true burning due to transport resistance barriers of the gas or oxide film. It is also more difficult to self-sustain. Though experiments show that heterogeneous burning can progress spontaneously vertically along a thin wire,[6] it is not clear whether or not bulk burning can be sustained by this mechanism without some outside source of energy, such as a furnace or nuclear heat. In the absence of outside heating, heterogeneous oxidation of bulk samples is more typically represented by a glowing and gradually cooling mass.

B.5.2 Metal Ignition

The term *ignition point* implies a property of the material, like a melting point. Yet all reviewed reports on the ignition point of metals rely on measurement methods that affect the result. In each case the reported ignition temperature is simply the point at which oxidative heat exceeded heat losses for the specific conditions of the experiment. The term "pseudo-ignition temperature," or PIT, is used for these empirical values. The reported values of the PIT depend heavily on the experimental sample size and also on the rate of air or oxygen flow, the manner of heating, and for materials with a potentially protective film like aluminum, whether or not conditions are conducive for oxide film breakdown.

It is best to reserve the term *ignition point* for the possibility that a true property value can be developed. Two such theories have been proposed but have not gained acceptance. Epstein[10] proposed that the vapor pressure is related to the true ignition point for some metals (see Sect. B.5.3). Grosse and Conway[11] assert that the ignition point is a chemical property with demonstrable periodic behavior. The model adopted in GRSAC is closely related to Epstein's concept in that it is vapor pressure driven with, however, a higher initiating vapor pressure.

B.5.3 Metal Ignition Theory of Epstein[10]

Epstein presents an ignition correlation based on metal vapor pressure that is cited here because it is the only theory found with a potentially unifying physicochemical basis. The theory has not gained acceptance and has not been developed further since its inception. Although the correlation applies to ignition by steam, it may also apply to ignition in air.

According to Epstein, some metals (excluding low-melting alkali metals) ignite in steam at the temperature where the metal vapor pressure equals about 0.15 mm Hg. This prediction leads to the results shown in Table B.2 for magnesium, aluminum, zirconium, and uranium.

Table B.2. Predicted ignition temperatures of Epstein

Metal	Melting point (°C)	Predicted ignition temperature (°C)
Mg	649	539
Al	660	1150[a]
Zr	1857	2710
U	1133	2204[a]

[a] Data vary widely.

Epstein's postulate is insufficiently developed for any direct application. The concept that a metal ignites (i.e., begins to burn in the vapor phase) when its vapor pressure exceeds a certain value appears to be a sound beginning. However, 0.15 mm Hg vapor pressure appears to be far too low. Burning in the vapor phase requires on the order of 5 vol % metal vapor, which at 1 atm total pressure would occur at about 40 mm Hg vapor pressure. In addition, currently there appears to be no method for measuring a true ignition temperature. Therefore, testing the hypothesis would be difficult.

Uranium ignition temperatures cited in Sect. B.11, which are actually PITs since they depend on the conditions of the experiment, fall far below the predicted ignition point of Epstein. In contrast, measured ignition temperatures for magnesium (Sect. B.14) fall fairly close to Epstein's predicted values.

B.6 SUMMARY OF OXIDATION REGIMES AND MODELING APPROACH

The above review indicates that for the purposes of GRSAC, the oxidation of metals may be catalogued into four regimes.

- **Low-Temperature Heterogeneous Oxidation Regime.** In this regime, heat losses from the oxidation zone by conduction, radiation, and convection exceed the heat addition by oxidation. As a result, temperatures remain steady near the ambient level. The oxidation mode is heterogeneous, and since the temperature is low, the overall oxidation rate is most likely chemically controlled.

- **Mass Transfer Controlled Heterogeneous Regime.** As the temperature rises, the intrinsic chemical rate rises more rapidly that the heat removal rate. At some point, the overall oxidation rate becomes controlled by the mass transfer rate of oxygen to the surface.

- **Burning Regime.** True burning occurs when the metal vapor pressure is sufficiently high that a combustible mixture is produced in the gas phase. (This would occur above the true ignition temperature, if there were such a material property.) When true burning begins, a jump in oxidation rate occurs because the mass transfer inhibition inherent in the delivery of oxygen to the surface, as required for heterogeneous oxidation, is removed. The burn model is described in Sect. B.7.3. Further description and application to the French channel fire experiment are given in Sect. F.4.2 of Appendix F.

Parameters for selection of the appropriate oxidation mode are calculated by GRSAC at each time step and each node. The selection criteria are described in Sect. B.8. Therefore, the following general approach for determining magnesium and uranium oxidation rates has been adopted in GRSAC:

1. An oxidation rate is calculated for magnesium and uranium at each time step and node in three ways: (1) assuming surface oxidation controlled by the intrinsic chemical rate, (2) assuming surface oxidation under oxygen mass transfer control, and (3) true burning (i.e, vapor-phase oxidation of vaporized metal).

2. The appropriate oxidation rate for the node at the particular time step is selected by means of criteria described in Sect. B.8.

B.7 HETEROGENEOUS OXIDATION AND BURNING RATE MODELS

B.7.1 Heterogeneous Oxidation—Chemical Control

Expressions for the surface oxidation rate as a function of temperature are determined using physical chemistry techniques on small specimens. Sections B.10 and B.13 describe results for uranium and magnesium, respectively. Usually such experiments do not extend to sufficiently high temperatures, and the rate expressions need to be extrapolated. In addition, tests are generally performed either in air or pure oxygen. Rarely is an oxygen pressure dependency given. In GRSAC, which requires such an oxygen concentration dependence for regions of oxygen depletion, it is assumed that the reported rate would be directly proportional to the oxygen pressure. Very little data in this area was found on magnesium, and none was found for aluminum (the cladding material in Windscale, used for benchmarking; see Appendix E).

Chemically controlled heterogeneous oxidation rates are significant for the overall oxidation model, despite their low value in their region of dominance, because they determine the point of temperature instability, when the heat source exceeds the heat removal rate.

B.7.2 Heterogeneous Oxidation—Oxygen Mass Transfer Control

Chemically controlled surface oxidation rates increase rapidly with temperature and soon reach the point where oxygen delivery to the surface limits the rate. At this point, the oxidation rate is given by

$$R = n\, h_m\, [O_2] \tag{B.1}$$

where

R = surface oxidation rate, mol/(cm^2·min);
n = number of oxide molecules produced per O_2;
h_m = the mass transfer coefficient, cm/min;
$[O_2]$ = oxygen concentration in the free stream, mol/cm^3.

The value of h_m depends on the nature of the flow (laminar or turbulent) and is of course sensitive to geometry. The models in GRSAC use correlations appropriate for air flow in long ducts of not necessarily circular cross-section. The hydraulic mean diameter is used to determine the Reynolds number. If the flow is laminar, the Graetz or Nusselt solution is used (constant Nusselt number) to determine h_m. The nature of this solution is such that h_m does not depend on free stream velocity but does increase temperature due to the increase of oxygen diffusivity.

For turbulent flow, the Reynolds Analogy with an assumed friction factor is used. In this correlation, h_m is directly velocity dependent. For a given mass flow rate, the increase in h_m with temperature due to reduction in gas density (consequently increasing the velocity) is exactly compensated by the reduction in oxygen concentration. Therefore, a feature of oxygen mass transfer in turbulent flow is a rate that depends on velocity but not on temperature. The mass transfer correlations also apply to the surface oxidation of graphite and are more fully discussed in Appendix A.

B.7.3 The Burn Model

The presence of large amounts of magnesium cladding in graphite reactors fueled with uranium metal requires inclusion of a true burn model for oxidation evaluation. The French channel fire tests (used in Appendix F as a benchmark exercise for GRSAC) clearly show that magnesium can readily ignite under conditions of air exposure at bulk metal temperatures as low as 630°C. In principle, uranium metal and graphite can similarly ignite and burn in the gas phase, however, at much higher temperatures. A true burn model is required whenever combustion is possible because oxidation rates increase sharply in the transition from surface to gas-phase oxidation due to removal of the oxygen mass transfer constraint.

The model that is presented is based on a realistic, though simplified, mechanistic view of the transition from surface oxidation to true burning. Benchmarking comparisons in Appendix F indicate that predicted burning rates for magnesium approximate the observed values.

The burning model used in GRSAC is based on the concept that gas-phase oxidation will dominate over surface oxidation when metal vapor pressures are sufficiently high to generate a critical concentration of vaporized metal near the surface.[12] At such time, the mass transfer rate of metal vapor to the free stream exceeds the transport of oxygen to the surface, leading to increased oxidation and further increase of the metal vapor pressure. In such case the burning rate is given by

$$R = h_m\, [M]_s \tag{B.2}$$

where

R = the burning rate, mol/(cm^2·min);
h_m = mass transfer coefficient for transfer of metal vapor to the free stream, cm/min;
$[M]_s$ = concentration of vaporized metal at the surface, mol/cm^3.

The discussion for evaluation of h_m given for Eq. (B.1) also applies here, with the exception that the diffusivity of the metal vapor must be used in laminar flow rather than oxygen.

The value of $[M]_s$ is determined from the vapor pressure of the metal,

$$[M]_s = P_v/R_2T, \tag{B.3}$$

where

P_v = metal vapor pressure, atm;
R_2 = gas constant, 82.06 cm^3·atm/mol·K;
T = metal surface temperature, K.

The model tacitly assumes that when metal vapor transfer to the free stream dominates, the metal atoms combine rapidly and completely with the oxygen available within the node. In actuality, for this to occur, metal vapor and oxygen concentrations must be within specified ranges in the free stream. Such data for metal vapor oxidation do not appear to exist, and hence this criterion is not applied. In addition, rapid reaction requires the presence of specific free radicals to initiate the chemical chain reaction typical of vapor-phase burning. The assumption in the GRSAC model is that gas-phase kinetics is rapid and complete.

B.7.4 Regimes of Applicability of the Burn Model

According to the above model, gas-phase burning when the coolant flow is turbulent may be expected when the metal surface temperature is sufficiently high to generate vapor pressures of the level of oxygen in the air coolant, about 0.2 atm. (In laminar flow, allowance must be made for the diffusivity of the metal vapor in air). Temperatures at which this may be expected for magnesium, aluminum,* uranium, and graphite are indicated by the estimated vapor pressures listed in Table B.3. [Values for the three metals are based on formulae in Kubachewski and Alcock,[1] and values for graphite are taken from Hultgren et al.[13]]

As shown in the table, magnesium metal is the most volatile of the four materials, and according to the burn model described above, susceptible for gas-phase burning at true surface temperatures of about 900°C. Corresponding temperatures for aluminum, uranium, and graphite are much higher—approximately 2100°C, 3300°C, and 3400°C, respectively.

Comparisons with measured (pseudo-) ignition temperatures are given in Table B.4. It must be emphasized that the measurements are all [except Martin[14]] based on the technique developed by Fassel et al.,[15] which is highly dependent on details of the experiment, particularly the sample size, air flow rate, and method of temperature measurement. As a result, they are more properly called "pseudo-ignition temperatures," or PITs. Note that wide variations are reported in PITs, probably due to inappropriate measurement methods. In some cases, Fassel's method yields impossibly low values (e.g., the 600°C temperature for uranium). Uranium molds are routinely poured at much higher temperatures and do not burst into flame. Also note the range for magnesium. Martin's value is based on visual observation of Magnox cladding in the French channel fire experiments (see Appendix F).

---

* The cladding alloy in the Windscale reactor. See Appendix E.

Table B.3. Vapor pressures of key materials in graphite reactors

Vapor pressure (atm)				Temperature	
Magnesium	Aluminum	Uranium	Graphite	K	°C
2.56E-07	2.30E-21	4.66E-34	4.60E-55	600	327
2.39E-04	1.15E-14	3.54E-24	2.00E-39	800	527
1.35E-02	1.15E-10	2.81E-18	5.20E-30	1000	727
1.89E-01	5.13E-08	2.31E-14	9.80E-24	1200	927
1.20E+00	3.92E-06	1.41E-11	3.30E-19	1400	1127
4.71E+00	9.94E-05	1.68E-09	8.40E-16	1600	1327
1.33E+01	1.21E-03	6.83E-08	4.00E-13	1800	1527
3.02E+01	8.87E-03	1.30E-06	6.00E-11	2000	1727
5.82E+01	4.48E-02	1.44E-05	3.76E-09	2200	1927
9.94E+01	1.71E-01	1.05E-04	1.22E-07	2400	2127
1.55E+02	5.30E-01	5.64E-04	2.32E-06	2600	2327
2.25E+02	1.39E+00	2.36E-03	2.92E-05	2800	2527
		8.09E-03	1.42E-04	3000	2727
(BURN		2.37E-02	1.80E-03	3200	2927
REGIME)		6.08E-02	9.82E-03	3400	3127
		1.40E-01	4.42E-02	3600	3327
		5.73E-01	5.70E-01	4000	3727

Table B.4. Measured pseudo-ignition temperatures of magnesium, aluminum, and uranium (°C)

Reference	Magnesium	Aluminum	Uranium
Epstein[10]		1170	2200
Baker et al.[16]			600
Abbud-Madrid[7]	977	2054	
Fassel[15]	623		
Martin[14]	625–650		
Burn model prediction	900	2100	3300

B.8 SELECTION CRITERIA FOR DETERMINING MODE OF OXIDATION

The selection criteria are best illustrated by referring to Fig. B.1, which shows the variation of oxidation rate with the true surface temperature at constant cooling rate for three controlling mechanisms. (Since both the chemical rate and the vapor pressure are highly sensitive to temperature,

use of a bulk average temperature, such as the nodal average temperature in GRSAC or a measurement based on a thermocouple embedded in a metal specimen, will give incorrect results.) The horizontal line shows the rate when dominated by the mass transfer of oxygen to the surface assuming turbulent flow in the free stream. In such case, the oxygen mass transfer rate to the surface is relatively independent of temperature. The curve, "chemical rate," shows the steep rate of increase with temperature typical of an Arrhenius rate expression. The "metal vapor transfer" curve also rises steeply with temperature due to increasing vapor pressure of the metal.

As temperatures increase, oxidation regimes change as indicated by the bold line in the figure. Below T_1 is the regime of chemical control. At this condition, there is ample oxygen delivery to the surface; oxidation is limited by the intrinsic oxidation rate of the metal. Metal vapor transfer to the air is low due to low vapor pressure. Above T_1 (but below T_2), the oxidation rate is restricted by oxygen transfer to the surface and, therefore, remains approximately steady with increasing temperature. In both "chemical control" and "oxygen mass transfer control" regimes, oxidation occurs at the metal surface. Transition to the "burning regime" occurs above T_2, when metal vapor transfer to the free stream exceeds oxygen transfer due to the high vapor pressure of the metal.

This is executed in GRSAC as follows: Oxidation rates from all three mechanisms are calculated at each time step and node. The appropriate heterogeneous rate is selected by comparing the chemical control or oxygen mass transport control rates. The smaller one is selected as controlling. This heterogeneous rate is added to the estimated burning rate. In other words, heterogeneous and vapor-phase burning are assumed to occur simultaneously. However, above temperature T_2 (Fig. B.1), true burning begins to dominate over the rate-controlling mode of heterogeneous oxidation.

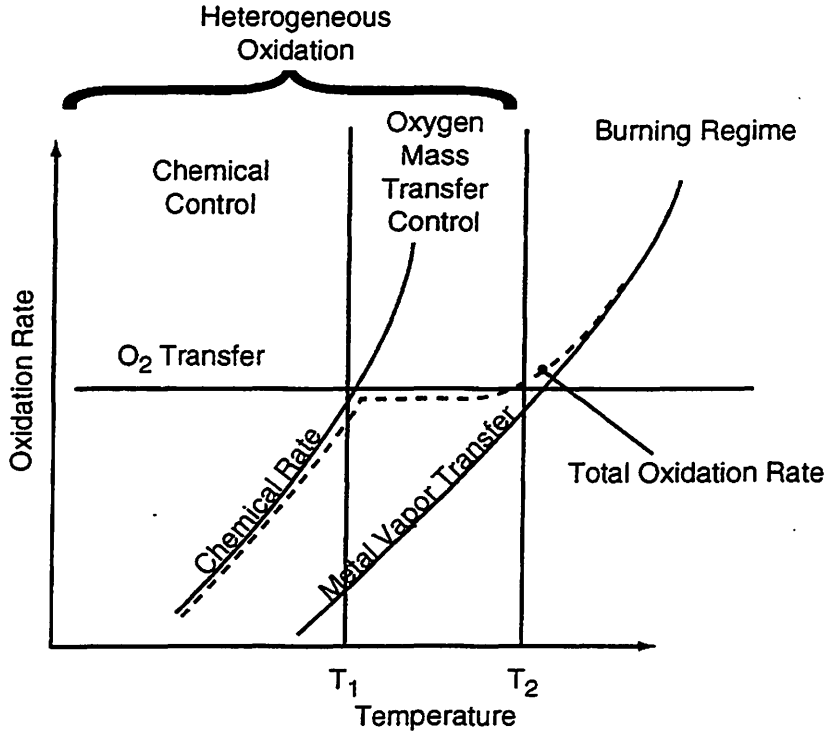

Fig. B.1. Metal oxidation regimes for fixed cooling rate.

B.9 OBSERVED FEATURES OF URANIUM BURNING

Uranium metal burning has been observed by fire safety personnel and by designers of the uranium burning facility at the Oak Ridge Y-12 Plant[17] This experience is that uranium metal ignition depends largely on the surface area per unit mass of material. Fine powders ignite spontaneously on exposure to air. At the other extreme, full density billets of several kilograms are routinely heated to 630°C and transported in air without difficulty. Walnut-sized pieces, heated to cherry red (about 700°C), will stop burning when allowed to cool in quiescent air.

In the intermediate size regime, machine turnings spontaneously ignite on exposure to air when the water-based cover liquid evaporates. In such cases, generation of increased surface area by slow oxidation, hydride formation by reaction with water, or sparking due to a breaking chip may all enhance ignition. Magnesium should have the same general burning behavior, except at correspondingly lower temperatures, because of its similar chemical affinity for oxygen. Another similarity is that neither metal produces a protective oxide film. A major difference is the much higher vapor pressure of magnesium, which causes it to burn in the gas phase compared with predominantly heterogeneous oxidation for uranium.

B.10 URANIUM OXIDATION RATE EXPERIMENTS

B.10.1 Baker and Bingle[18]

These tests are the most complete set in defining the oxidation characteristics of uranium in the low-temperature regime. Isothermal oxidation rates were measured in this study by placing a 1-cm^3 sample of uranium in a furnace, clamped to a large heat capacity holder so that oxidation heat would not alter the temperature. An oxidizing gas (usually a mixture containing 200 mm Hg oxygen pressure) was passed through the chamber. A survey is presented that showed no significant difference in oxidation rate between air and pure oxygen from 200 to 1400°C. (This implies that oxygen concentration did not limit the overall rate for the conditions of this experiment and the six others which are referred to. Independence of oxidation rate from oxygen partial pressure cannot be generally true.)

Preliminary tests showed that above 450°C, minor amounts of alloying can significantly alter the oxidation rate by forming (or destroying) a protective surface layer. Small amounts of copper (about 1%) were found to retard oxidation by forming a U-Cu protective layer. Small amounts of aluminum had the opposite effect, which is significant because it is a common alloy additive to uranium metal fuels. Oxidation rates of "pure" uranium metal were between these extremes.

The following three oxidation rate equations are given. The major presumption is that the tests were conducted in the chemical controlled regime. This is not shown definitely to be the case. (If conditions were mass transfer controlled, the results would be meaningless as they would apply only to the specific conditions of the experiment).

$$m^{4/5} = 1 \times 10^5 \, t \exp(-16{,}800/RT) \qquad T < 450°C \qquad \text{(B.4)}$$

$$m = 0.84 \, t \qquad T = 450°C \qquad \text{(B.5)}$$

$$m^{6/5} = 1.7 \times 10^4 \, t \exp(-14{,}300/RT) \qquad T > 450°C \qquad \text{(B.6)}$$

where

m = mass of oxygen in the sample, mg;
t = time, min;

T = temperature, Kelvin;
R = gas constant, 1.987 cal/(mol·K).

As for the graphite rate expression given in Appendix A, these equations will be modified into rate equations with the convenient units—moles for mass, time in minutes, and temperature in Kelvin as required for the Arrhenius expression. (Otherwise, temperatures will be shown in the more convenient Celsius.) Also for convenience, pressure in atmospheres and length in centimeters will be used throughout.

Note that after differentiating with respect to time, Eq. (B.4) predicts a gradually rising rate with time below 450°C, and Eq. (B.6) predicts a gradually reducing rate with time above 450°C. This is difficult to reconcile since given sufficient elapsed time, Eq. (B.4) for T < 450°C can predict a rate exceeding that given by the constant rate predicted for 450°C. Therefore, for numerical purposes it is best to assume linearity on sample mass with time for Eqs. (B.4) and (B.6). An additional necessary assumption is that the oxidation rate is first order with respect to oxygen pressure for oxygen pressures equal to or lower than that of air. To account for the phenomenon of oxygen depletion, GRSAC computes the oxygen concentration at each time stem and in each node as air flows axially from the inlet. It is also assumed that oxidation rates diminish in ratio to the oxygen pressure. It is noted that these tests were conducted mainly using 200 mm Hg oxygen pressure (0.263 atm). With these assumptions, the following oxidation rate equations for uranium are obtained. For T < 450°C,

$$R = 9.01 \exp(-16{,}800/R_1T)\, P(O_2) \qquad \text{(B.7)}$$

where R is the rate in moles U/(cm^2·min), t is the time from start in minutes, T is the temperature in Kelvin, and R_1 is the gas constant, 1.987 cal/(deg·mol). For T > 450°C,

$$R = 1.57 \exp(-14{,}300/R_1T)\, P(O_2)\,. \qquad \text{(B.8)}$$

B.10.2 Hayward et al.[19]

Tests were performed on foil and small disk samples of pure uranium metal in 25% oxygen, balance argon, from 190 to 610°C. After a short induction period, the following rate was observed:

$$R = 2.52 \times 10^{-4} \exp(5.169 - 6640/T) \qquad \text{(B.9)}$$

with R in units of moles U/(cm^2·min). Above 300°C, the principal oxidation product was U_3O_8. This paper reviews many other low-temperature experiments which are not of interest here. A small dependence on flow rate through the glassware apparatus was observed.

B.10.3 McGillivray et al.[20]

This study measured oxidation rates in moist and dry air below 300°C.

B.11 PSEUDO-IGNITION TESTS ON URANIUM METAL

Tests performed at Argonne National Laboratory (ANL) in the 1960s are briefly described. In general, these show "ignition" temperatures of uranium metal far below that predicted by Epstein and also far below the routine experience in handling uranium metal at the Y-12 Plant. The probable reason is that only bulk temperatures were measured, not surface temperatures, which should have been much higher. Also, the tests were conducted in a furnace, which added to the oxidation heat. In the discussion above on metal oxidation regimes, this was termed the pseudo-ignition temperature

(PIT). The PIT is a function of the test geometry, air flow rate, and furnace power, as well as chemical reactivity.

B.11.1 Baker et al.[18]

An 8.5-mm cube of uranium metal was placed in a furnace with air or oxygen flow. Temperatures were increased at a 10°C/min rate. *Ignition* was defined as the point where the bulk sample temperature rose sharply. It was found that such ignition occurred at about 600°C under the conditions of this experiment in both air and oxygen and for two types of pure uranium metal.

A transient heat balance verified that at about 600°C for this experiment, oxidation rates reached a point where heat losses could not keep up with the oxidative heat input. Since oxidation rates increase exponentially with temperature (as long as the oxygen supply holds out), an unstable situation results with rapid temperature increase in the sample. Temperatures rose rapidly above the PIT, in one case to 2150°C. It was not recorded when or if the uranium metal actually started to burn and produce a visible flame. Oxygen depletion was not monitored.

B.11.2 Schnizlein et al.[21]

Tests showed that the PIT of 8.5-mm cubes of uranium metal may be modified by small amounts of alloying. Additions of aluminum, carbon, and many other metals inhibited formation of surface oxide and therefore lowered the PIT from about 600°C to the 400–500°C range.

B.11.3 Schnizlein and Fischer[22]

Tests showed that the PIT of 8.5-mm cubes of uranium are lowered by irradiation, from about 600°C to 360°C for 1.71 at. % burnup.

B.12 URANIUM BURNING EXPERIMENTS IN THE UNITED KINGDOM

B.12.1 Picton and Sackman[23]

A technique similar to the ANL method for determining the PIT was used for U-Pu-Fe alloys of approximate composition 70-20-10. Observed PITs ranged from 100 to 315°C.

B.12.2 Other Uranium Oxidation Experiments in the United Kingdom

Antill and Peakall[24] refer to several U.K. references on oxidation of uranium and UC by oxygen, steam, and CO_2.

B.13 MAGNESIUM OXIDATION RATE DATA

B.13.1 Inouye[25]

This technical status report includes some earlier magnesium oxidation rate measurements by Leontis and Rhines[26] taken in pure oxygen from low temperatures (<450°C) up to 623°C. It is reported that below 450°C, the oxidation rate is quite low due to a protective oxide film. Between 450 and 575°C, the following oxidation rate equation describes the data:

$$R = 4.28 \times 10^7 \exp(-53{,}570/R_jT)\, P(O_2) \qquad \text{(B.10)}$$

where

R = rate, mol/(cm^2·min);
T = temperature, K;
R_1 = gas constant, 1.987 cal/(mol·K);
P(O_2) = partial pressure of oxygen, atm.

At higher temperatures, magnesium is reported to autoheat, by means of its own oxidative heat, to its ignition point, given as 623°C. [The original source is Fassel et al.[15]] At the ignition point, the oxidation rate is said to increase sharply and a flame appears. The product of combustion is MgO. (These comments are for tests in pure oxygen.) The reported ignition temperature decreases at lower oxygen pressures to about 600°C at 0.4 atm. Various reports are cited with ignition temperatures ranging from 591 to 645°C.

B.13.2 Fassel et al.[15]

Pure magnesium at 475°C is reported to oxidize at 0.01 mg/(cm^2·hr) in pure oxygen. [Alloying with aluminum markedly increased the rate, consistent with the observation of Baker and Bingle.[18]] An activation energy of 50,500 cal/mol is reported. This leads to the following oxidation rate equation, assuming first-order dependence on oxygen partial pressure:

$$R = 1.19 \times 10^7 \exp(-50{,}500/R_1T)\, P(O_2)\,, \qquad \text{(B.11)}$$

where R is mol/(cm^2·min), T is in Kelvin, R_1 is 1.987 cal/mol, and P(O_2) is the oxygen partial pressure in atmospheres. The agreement is fairly good with that reported by Inouye given in Eq. (B.10).

B.14 MAGNESIUM IGNITION TESTS

B.14.1 Fassel et al.[15]

Ignition temperatures are reported for pure magnesium and many binary alloys by the method later adopted by ANL researchers. An ignition temperature (properly, the PIT) of 623°C was measured for pure magnesium in oxygen. This is somewhat higher than predicted by Epstein's model, 623°C measured vs 539°C (812 K) predicted. Most alloy additions were observed to reduce the ignition temperature.

B.14.2 Darras et al.[27]

This study on magnesium and uranium oxidation is noted but not extensively reviewed because no oxidation rate equations are given. An ignition temperature of 645°C is given for magnesium, in good agreement with Fassel and Inouye. Following ignition, temperatures are reported to rise to above 1200°C, the maximum measurable. Ignition delays are reported: 85 min at 585°C, 10 min at 590°C, 5 min at 595°C, and 2 min at 600°C. Instantaneous ignition occurs at 645°C.

B.14.3 Martin et al.[14]

Channel fire tests conducted by the French used visual observation to record the ignition point of magnesium (see Appendix F for further description). Generally, these tests showed that magnesium ignites in air at magnesium bulk temperatures from 625 to 650°C, depending slightly on the rate of

air flow. Observation showed that ignition started at specific points on the surface that were hotter than the bulk temperature.

B.14.4 Abud-Madrid[7]

This study surveyed ignition points of several metals, including magnesium, using basically the method of Fassel except that the specimen was heated by an infrared lamp rather than a furnace. An ignition point of 977°C is reported for magnesium, significantly higher than other reports.

B.15 FUEL ELEMENT MELTING EXPERIENCE IN MAGNOX REACTORS

Martin et al.[14] describe the result of a fuel overheat accident that occurred in a G1 reactor in October 1956. Laboratory tests were conducted to duplicate the conditions of the accident. The out-of-pile tests showed that the course of the event depended largely on the air flow rate in the overheated channel. Air flows up to 15 g/s resulted in oxidation of the magnesium but generated temperatures of only 800°C on the surface of the uranium. Magnesium temperatures oscillated up to 1050°C. A test at 60-g/s air flow through the channel caused essentially complete magnesium and uranium burning along the 30-cm specimen. These tests as described by Martin, used for benchmarking GRSAC, are more fully discussed in Sect. E.2 of Appendix E.

Examination of the actual channel melting case showed that it was a relatively mild event which lasted about 20 min. Temperatures of 650°C were attained which melted the magnesium and blocked gas flow in the channel. All the cladding oxidized "along a certain length," but the uranium was attacked only superficially. The experiments showed that if the channel had not become blocked, a more severe event would have occurred. These observations show that oxidation of the Magnox cladding occurs first because it is the outer layer. Also, it has a higher vapor pressure, lower melting point, and is slightly more oxygen acquisitive than uranium. As cladding temperatures increase from the normal 400°C maximum, magnesium oxidation rates will rise rapidly, further accelerating the temperature rise.

B.16 GRSAC OXIDATION MODEL

B.16.1 Assumptions and General Method

1. Regular geometry of the fuel element is retained (i.e., no fuel element material relocation occurs). GRSAC does not have the capability for fuel element material relocation.

2. As indicated by data, neither the magnesium cladding nor the uranium is assumed to develop a protective oxide film. The magnesium cladding is assumed to protect uranium from oxidation until it is 90% oxidized or melts at 649°C.

3. Three estimates of the metal oxidation rate are made at each node and time step:

    a. assuming heterogeneous oxidation in the chemical control regime [i.e., using Eqs. (B.7) or (B.8) for uranium and (B.10) for magnesium] (R1),
    b. assuming heterogeneous oxidation, controlled by the mass transfer rate of oxygen to the surface (R2),
    c. simulating true burning (vapor-phase oxidation), controlled by the mass transfer rate of metal vapor to the bulk air (R3).

4. The controlling oxidation rate is selected by comparing the three rates. The appropriate heterogeneous rate is selected by comparing the chemical control or oxygen mass transport control rates. The smaller one is selected as controlling. This heterogeneous rate is added to the estimated burning rate. In other words, heterogeneous and vapor-phase burning are assumed to occur simultaneously. However, above temperature T_2 (see Fig. B.1), true burning begins to dominate over the rate-controlling mode of heterogeneous oxidation.

5. Several features of graphite oxidation, described in Appendix A, are also required for metal oxidation:

   a. The mass transfer coefficient, determined by a method described in Appendix A, is required for determination of metal oxidation rates R2 and R3.
   b. The oxygen concentration at each node and time step, determined by the method described in Appendix A, is required for metal oxidation rates R1 and R2.

6. When vapor-phase burning occurs via the above test, it is assumed that the oxidation reaction goes to completion within the node where the metal evaporation has occurred, with the energy of combustion also deposited in that node.

7. For the G2/G3 core, placing all the magnesium in a cylinder would result in a cladding OD of 33.6 mm and ID of 29.0 mm over the 8400-mm active core length (i.e., a pseudo cladding thickness of 4.6 mm). These dimensions include the material in the end caps; there are 28 elements per channel. All fuel element diameters are assumed to be 29 mm. (There are 28- and 31-mm-OD fuel elements.) The channel diameter is 70 mm.

8. The chemically controlled magnesium and uranium oxidation rates are assumed to be first order with respect to oxygen partial pressure. This assumption has been incorporated in the equations cited [i.e., Eqs. (B.7), (B.8), and (B.10)].

B.16.2 Properties Required for Determination of Mass Transfer Rates

- **Vapor pressure of magnesium and uranium** (Kubachewski and Alcock[1]).

$$P(vap) = A/T + B \log_{10} T + C \times T + D \qquad (B.12)$$

where

	A	B	C	D
Uranium	–25,580	–2.62	0	18.58
Magnesium	–7550	–1.41	0	12.79

and P(vap) is given in millimeters of mercury and T in Kelvin.

- **Diffusivity**. Diffusivities of magnesium and uranium vapor in air are required in the burn model for determining metal vapor mass transfer coefficients under laminar flow conditions. Measurements evidently do not exist, and predictive correlations must be used. Although correlations exist for binary gas phase diffusion coefficients,[28] they are difficult to apply to uranium and magnesium because of missing information. Instead, a method will be used which keys the diffusivities to an available measured value (e.g., oxygen in nitrogen at 298 K). If the Gilliland modification[29] of Maxwell's equation is assumed to apply, the required coefficients can be estimated by appropriate ratios of molecular properties. The application is as follows:

The Gilliland equation is given by

$$D = 0.0043\ T^{1.5}\ [1/MA + 1/MB]^{1.5}/[P(VA^{1/3} + VB^{1/3})^2] \quad \text{(B.13)}$$

where

D = diffusivity, cm^2/sec;
T = temperature, Kelvin;
MA = molecular weight of either magnesium or uranium, g/mol;
MB = molecular weight of air, g/mol;
VA = molecular volume of either magnesium or uranium, cm^3/mol (volume actually occupied by the molecular material, therefore given by MA/ρ, where r is the condensed phase density at the boiling point);
VB = molecular volume of air, cm^3/mol.

The handbook value [30] for oxygen in nitrogen is 0.181 cm^2/sec at 298 K. Atomic radii are given by Sargent-Welch.[31]

O	0.65 Angstroms
N	0.75
Mg	1.72
U	1.42 (not used)
C	0.77 (not used)

The value of the Gilliland parameter [the term in the brackets in Eq. (B.13)] for diffusion of O_2 in N_2 is determined to be 0.0287 in mixed units of angstroms and molecular weight in grams per mole. (Arbitrary units are permitted since only ratios are needed.) The molecular volume for each gas is assumed to be twice the atomic volume indicated by the atomic radius.

The Gilliland parameter for Mg atom in N_2 is determined to be 0.0153, in the same units. Therefore, the diffusivity of Mg vapor in nitrogen at 298 K is obtained from,

$$D(\text{Mg}) = 0.181 \times (0.0153/0.0287) = 0.0965\ cm^2/sec$$

The smaller value for magnesium in nitrogen relative to oxygen in nitrogen is due to its large atomic volume compared to the oxygen molecule. Since the Gilliland equation indicates a 1.5 power dependence on temperature,

$$D(\text{Mg}, T) = 0.0965 \times (T/298)^{1.5} \quad \text{(B.14)}$$

- **Oxidation model methodology.**

1. At time zero following the introduction of air, determine three estimates for magnesium oxidation rate [in moles Mg/(cm^2·min)]:

   a. R1 using Eq. (7)
   b. $R2 = 2\ h_m\ [O_2]$ (factor appears because the product is MgO)
   c. $R3 = h_m\ (P_{Mg}/R2 \cdot T)$

   where

h_m = mass transfer coefficient, cm/min, determined per method given in Appendix A;
$[O_2]$ = oxygen concentration, mol/cm^3;
$[O_2]_{initial}$ = $0.21/R2 \cdot T$, where 0.21 is the oxygen partial pressure, atm;
P_{mg} = vapor pressure of magnesium in atmospheres, per Eq. (B.12) converting pressure units;
R2 = universal constant, 82.06 (cm^3·atm)/(mol·K).

2. Select controlling rate:

   If R3 > R1 or >R2, then rate = R3; otherwise,
   If R1 < R2, then rate = R1; otherwise, rate = R2.

3. Record the new thickness of unoxidized magnesium cladding. The loss of magnesium thickness due to oxidation in the control volume over the time step is

   thickness loss (mm) = (mg of Mg oxidized)/[100 × ρ × exposed Mg area (cm^2)].

   The density, ρ, is 1.74 g/cm^3.

4. Determine the new concentration of O_2 leaving the control volume, reduced by the amount of MgO produced. The relation is

   moles Mg oxidized = $2Q([O_2]_{in} - [O_2]_{out})$,

   where Q is the volume flow rate, cm^3/min, and $[O_2]$ is the concentration, mol/cm^3. Convert to the new partial pressure,

   $P(O_2)_{out} = [O_2]_{out}/R2 \cdot T$,

   where *R2* is the gas constant, 82.06 (cm^3·atm)/(mol·K), and T is the gas temperature in Kelvin.

5. Determine the heat released by magnesium oxidation in each control volume during the time step by

   q_{Mg} (kcal) = (moles Mg oxidized)(–143.8).

   A negative indicates heat released in this convention. T is in Kelvin. Add this heat to the radioactive decay heat in the metal for calculation of a new T.

6. Repeat steps 1 through 5 for the remaining tiers, using the steadily diminishing values of $P(O_2)$, depleted by oxidation.

7. For each succeeding time step after initial exposure of a control volume to air, check remaining thickness of magnesium cladding. For the G2/G3 geometry, the relation is

   remaining thickness (mm) = 4.6 – mg of Mg oxidized/(100 × ρ × area),

   where ρ is the density (g/cm^3), and area is the exposed magnesium surface in the control volume, cm^2. As long as remaining thickness is positive, continue steps 1 through 6.

8. When all the magnesium cladding has oxidized in a control volume, substitute the uranium metal oxidation equations for the magnesium equations. Proceed as before, with the following exceptions:

   a. R1 using either Eq. (B.7) or (B.8), depending on the temperature
   b. $R2 = h_m [O_2]$ (product is UO_2)
   c. $R3 = h_m (P_U/R2 \cdot T)$

   where P_u is the vapor pressure of uranium in atmospheres, from Eq. (B.11) converting units to atmospheres.

9. Select controlling rate, R1, R2, or R3, according to step 2.

10. Add heat of uranium oxidation to heat balance, assuming the product is UO_2,

    $$q_U \text{(kcal)} = \text{(moles U oxidized)}(-259).$$

    As before, a negative signifies heat release. Keep track of amount of uranium oxidized in each control volume, and terminate oxidation when there is no more.

11. The oxygen balance along the node is the following, assuming the product is UO_2,

    $$\text{moles U oxidized} = Q([O_2]_{in} - [O_2]_{out}).$$

12. Repeat steps 8 through 11 until uranium is depleted or sequence terminates.

B.17 CONSIDERATION OF OXIDATION OF METALLIC URANIUM FUEL IN A CO_2 ATMOSPHERE

Accidents which do not result in a breach of the reactor vessel, permitting air inleakage to the core, may still result in release of fission products from fuel due to oxidation of any exposed metallic uranium by CO_2. Therefore, GRSAC has provision for estimating oxidation of the fuel in a CO_2 environment. The methodology is identical to that used for release due to oxidation by air, with the difference that chemically controlled uranium oxidation rates are set lower than the air rates. The fission product release rate correlations themselves remain the same since as in the case of air, the release is due to oxidation of uranium.

Parker et al.[32] have shown that chemically controlled oxidation rates of metallic uranium in CO_2, while lower than in air, become comparable at high temperature, i.e., about 1200°C. For example, Fig. B.2 reproduced from Parker shows the weight increase in air and CO_2 of uranium metal at 1000°C. It is appropriate to compare curves for "irradiated U in Air" and "Irradiated U in CO_2." Note that a weight increase of 17% in air, occurring at about 3 hours, represents 100% oxidation of U to UO_2, whereas an approach to a weight increase of 13% in CO_2 represents full oxidation to U_3O_8.

A rough comparison of relative oxidation rates in air vs CO_2 is made by selecting conditions near the beginning of the oxidation before scale formation or cracking of the specimen begin to effect the observations. Selecting the initial 20 minutes for the rate comparison yields the results in Table B.5, i.e., irradiated U in air (20% oxidant concentrations) vs irradiated U in CO_2 (100% oxidant concentration).

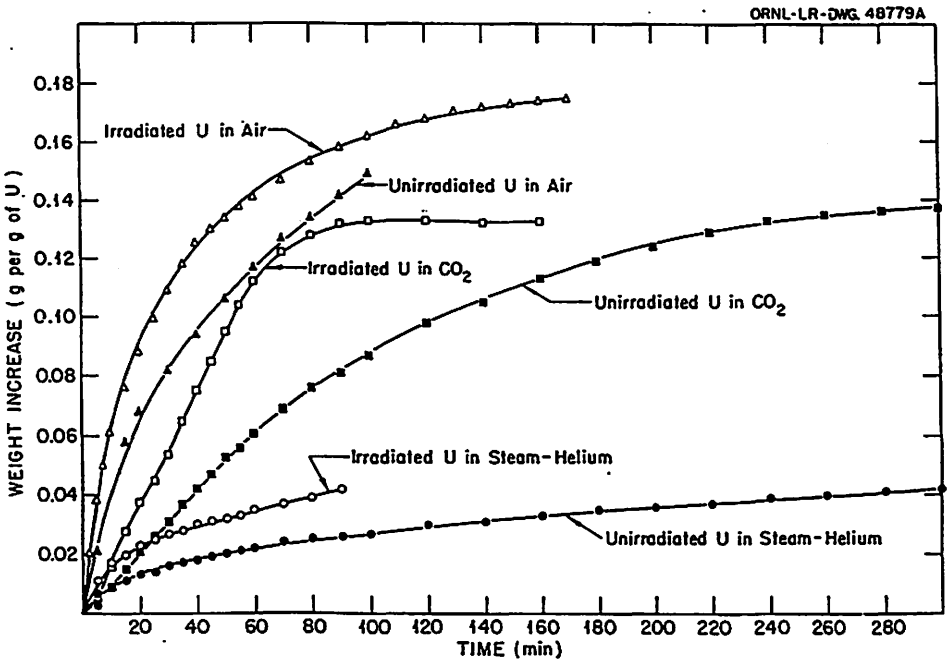

Fig. B.2. Comparisons of oxidation of irradiated and unirradiated uranium in steam, air, and CO_2 at 1000°C. *Source:* Parker et al.[32]

Table B.5. Comparison of U-metal oxidation rates in air vs CO_2 (Parker et al.)[32]
(Presumably in the chemical control regime—based on oxidation occurring in the first 20 min of the test)

	Initial percent weight increase		
Temperature (°C)	In air (U_3O_8)	In CO_2 (UO_2)	Oxidation rate ratio of air:CO_2
800	4.8	0.3	16
1000	9.3	3.8	2.4
1200	9.1	6.2	1.5

Note, that the rate ratio approaches unity at temperatures of 1200°C and above, which is expected since there is more free oxygen in CO_2 at elevated temperatures.

An alternate approach to modeling the reaction is to consider the longer-term effects rather than just the response within the first 20 min of exposure to the CO_2. Typically, longer-term effects are more pertinent to GRSAC accident calculations. The Parker data for the three oxidation temperatures noted in Table B.5 showed equilibrium taking place within one to two hours, and within that temperature range, the oxidation rates required to reach 90% of equilibrium for the CO_2 case were, on the average, 70% of those for air oxidation. Hence, the rate multiplier used in GRSAC for CO_2 oxidation of the metal fuel (vs air) was 0.7. The heat released per mole of uranium oxidized is also less for the CO_2 vs air oxidation, since the final product for CO_2 is UO_2 (vs U_3O_8 with air). The heat release multiplier used for CO_2 oxidation is 0.43.

B.18 REFERENCES

1. Kubaschewski, O., and C. B. Alcock., *Metallurgical Thermochemistry,* Int. Ser. Mat. Sci. Technol., Pergamon Int. Lib., tables in Appendix (1973).

2. Glassman, I., *Combustion,* Academic Press (1987).

3. Brzustowski, T. A., and I. Glassman, "Vapor Phase Diffusion Flames in the Combusion of Magnesium and Aluminum," pp. 117–158 in *Heterogeneous Combusion,* H. G. Wolfhard et al., Eds., Academic Press (1963).

4. Gordon, D. A., "Combustion Characteristics of Metal Particles," pp. 271–278 in *Solid Propellant Rocket Research,* M. Summerfeld, Ed., Academic Press (1960).

5. Markstein, G. H., "Combustion of Metals," *AIAA J.* **1,** 550–562 (1963).

6. Harrison, P. L., and A. D. Yoffe, "The Burning of Metals," *Proc. Roy. Soc. (London)* **A261,** 357–370 (1961).

7. Abbud-Madrid, A., et al., "Experimental Results on the Ignition Temperature and Combustion Behavior of Pure Bulk Metals," presented at the Spring Meeting of the Western States Combustion Institute, Salt Lake City, March 1993.

8. Fassel, W. M., et al., "Combustion of Metallic Powders," *Progress in Astronautics and Rocketry,* Vol. I, p. 259–269 (1960).

9. Reynolds, W. C., *Investigation of Ignition Temperatures of Solid Metals,* NASA TN-D-182 (1959).

10. Epstein, L. F., *Correlation and Prediction of Explosive Metal-Water Reaction Temperatures,* GEAP 3335 (1960).

11. Grosse, A. V., and J. B. Conway, "Combustion of Metals in Oxygen," *Ind. Eng. Chem.* **50,** 663–672 (1958).

12. Daw, C. S., personal communication to R. P. Wichner (1996).

13. Hulgren, R., et al., *Selected Values of the Thermodynamic Properties of the Elements,* American Society of Metals, Metals Park, Ohio (1973).

14. Martin, D., et al., "Inflammation dans L'Air D'Elements Combustibile," pp. 3–12 in *Reactor Safety and Hazards Evaluation,* Proceedings Sponsored by the IAEA, May 14–18, Vienna (1962).

15. Fassel, M. J., et al., "Ignition Temperatures of Magnesium and Magnesium Alloys," *J. Metals,* 522–528, July (1951).

16. Baker, L., et al., "The Ignition of Uranium," *J. Nucl. Mat.* **20,** 22–38 (1966).

17. Duerksen, W., "U Fire Hazard," electronic mail to J. Prazniak, May 23, 1995.

18. Baker, L., and J. D. Bingle, "The Kinetics of Oxidation of Uranium Between 300 and 625°C," *J. Nucl. Mat.* **20,** 11–21 (1966).

19. Hayward, P. J., et al., "Oxidation of Uranium in Argon–25% Oxygen at 190–610°C," *J. Nucl. Mat.* **187,** 215–222 (1992).

20. McGillivray, G. W., et al., "Kinetics and Mechanism of Uranium in Dry and Moist Air," *J. Nucl. Mat.* **208,** 81–97 (1994).

21. Schnizlein, J. G., et al., "Ignition of Binary Alloys of Uranium," *J. Nucl. Mat.* **20,** 39–47 (1966).

22. Schnizlein, J. G., and D. F. Fischer, "Ignition of Irradiated Uranium," pp. 227–223 in *Chemical Engineering Semiannual Report,* ANL-6925 (1965).

23. Picton, G., and J. F. Sackman "The Corrosion and Ignition Behavior of Some U/Pu/Fe Alloys," *J. Nucl. Mat.* **18,** 292–304 (1966).

24. Antill, J. E., and K. A. Peakall, "Oxidation Behavior of Defective Fuel Elements," *J. Nucl. Energy* Parts A/B, 935–947 (1965).

25. Inouye, H., *Reactions of Magnesium and Magnesium Alloys with Gases at High Temperature,* ORNL Central Files Report, External Transmittal Authorized, ORNL CF 58-1-93 (1958).

26. Leontis, T. E., and F. N. Rhines, "Rates of High Temperature Oxidation of Magnesium and Magnesium Alloys," *Trans. AIME* **166,** 265–292 (1946).

27. Darras, R., et al, "Inflammabilite du Magnesium et de L'Uranium Chauffes dans Divers Milieux Gazeaux," in *Third Metallurgical Symposium, Saclay Center for Nuclear Studies, June 29 to July 1, 1959,* NP-9715.

28. Reid, R. C., and T. K. Sherwood, *The Properties of Gases and Liquids,*2nd ed., McGraw Hill Chemical Engineering Series, Chap. 11 (1966).

29. Gilliland, E. R., "Diffusion Coefficients in Gaseous Systems," *Ind. Eng. Chem.* **28,** 681 (1934).

30. Perry, R. H., and D. W. Green, *Perry's Chemical Engineering Handbook,* 6th ed., McGraw Hill, Table 3-318 (1984).

31. Sargent-Welch, "Table of Periodic Properties of the Elements," Sargent-Welch Scientific Co. (1980).

32. Parker, G. W., et al., *Out of Pile Studies of Fission Product Release from Overheated Reactor Fuels at ORNL 1955–1965,* ORNL-3981 (1967).

APPENDIX C.
FISSION PRODUCT RELEASE MODELS FOR URANIUM METAL FUEL ELEMENTS

C.1 INTRODUCTION

Correlations are presented for fission product release from magnesium-alloy-clad, metallic uranium (Magnox) fuel elements under conditions representing core overheat events with air ingress. Eight correlations were developed, one for each of eight fission product groups defined by the NRC for severe light water reactor (LWR) accidents. Uncertainties associated with the correlations are quite large due to the traditionally high scatter exhibited by fission product release experiments and the incomplete understanding of release mechanisms. The degree of uranium oxidation is an important parameter governing radioactivity release. Therefore, release correlations must be used in conjunction with the metal oxidation models in GRSAC.

C.2 APPROACH—RELEASE FROM FUEL VS RELEASE TO ENVIRONMENT

The models described here are restricted to the prediction of radioactivity release from Magnox fuel elements to the reactor primary system. The larger issue of release to the atmosphere is very much dependent on the design and the event sequence and involves many other complex phenomena. Identification of release pathways depends on details of the reactor system and the failure mode; estimation of the trapping along the escape pathway requires evaluation of chemical change, prediction of local environments, and reactions of fission products with materials. Simplified models have been incorporated into GRSAC which are now used to interface with the HASCAL code[1] for plume and dose predictions. This work is currently in the development stage and will be reported later.

The nuclide selection used in GRSAC follows NRC guidelines and is taken from McKenna and Glitter,[2] who in turn acquired it from the major reactor safety study of the 1970s, WASH-1400.[3] The selection criterion is based on importance for early health effects. The methodology now required by the NRC for licensing purposes is described by Soffer et al.[4] The new NRC method is based on fission product groups (see next section) rather than on individual nuclides, which has certain advantages. Also, there is a failure time consideration, permitting radioactivity decay during the event.

The NRC methodology for release predictions is embodied in the RASCAL code.[5] Further development of RASCAL by the Defense Special Weapons Agency (DSWA) Hazard Prediction and Assessment Capability (HPAC) led to the creation of the HASCAL code (Hazard Assessment System for Consequence Analysis) and its associated transport model, the Second-order Closure Integrated PUFF (SCIPUFF) code.[1] This new code package provides a user-friendly PC-based hazard assessment capability for plumes of materials released in incidents or accidents, incorporating the modeling of winds over complex terrain.

C.3 CATEGORIES OF FISSION PRODUCTS

C.3.1 Fission Product Groups

Grouping fission products into sets of chemically similar elements makes maximal use of limited data and simplifies release calculations. The idea is that a data set or calculation for a nuclide can be representative of all elements in the group. The most recent grouping is given by Soffer et al.[4] in Table C.1. However, this grouping should not be taken as final even though it appears in the most

recent NRC severe accident publication.* The elements zirconium and yttrium are included in the lanthanide group because, like the lanthanides, they are strongly oxygen acquisitive and will usually form refractory oxides when oxygen is present. Hence, their transport properties outside the fuel should be similar. Actinides plutonium and neptunium are included in the last group.

Table C.1. Fission product groups recommended for LWR safety evaluations

Group	Group title	Elements in group
1	Noble gases	Xe, Kr
2	Halogens	I, Br
3	Alkali metals	Cs, Rb
4	Tellurium group	Te, Sb, Se
5	Alkaline earths	Ba, Sr
6	"Noble metals"	Ru, Rh, Pd, Mo, Tc, Co
7	"Lanthanides"	La, Pr, Nd, Pm, Sm, Eu, Zr, Y, Cm, Am
8	Cerium group	Ce, Pu, Np

Source: Soffer et al.[4]

Any grouping scheme is an attempt to reduce the labor of inputting a large number of elements and contains some compromises; no two elements contained in the fuel, moderator, etc., behave completely alike. The advantage of the grouping scheme selected for GRSAC is that it is restricted to materials contained in the fuel, and thus subjected to at least approximately similar environmental conditions.

C.3.2 General Group Behavior

Although the NRC methodology was developed for LWRs, the chemical similarities within each group make it useful for other cases, even though chemical speciation may differ. Generally, core release factors decrease from group 1 to group 8, mainly because vapor pressures of the expected chemical species decrease.

Group 1 elements (noble gases) exist in uranium metal as trapped interstitial atoms or as microbubbles. Since they form no chemical attachments, complete release from fuel is expected on melting, metal degradation, or oxidation.

Group 2 elements (halogens) can form uranium halides, and hence tend to be retained in uranium metal despite their high vapor pressure. However, they have only a weak attraction for oxides. On oxidation they should be released from fuel as readily as the noble gases. The chemical form once

* There are a few inconsistencies in the listing shown in Table C.1. Most glaring, ruthenium and molybdenum are listed as noble metals, even though they not only oxidize readily but have highly volatile oxides. Also, the radiologically important element silver is missing from group 6. It is not clear why the actinides curium and americium are placed in group 7 and not with the other actinides, plutonium and neptunium, in group 8. Also, it is not clear why the lanthanide cerium is not included in group 7. These uncertainties may not be significant for common postulated accidents where releases to air from groups 6, 7, and 8 are low, but they may be significant for lower probability energetic events.

outside the fuel is predominantly I_2 gas, which may adsorb on low-temperature (<400°C) metal surfaces.

Group 3 elements (alkali metals) evolve more slowly from uranium metal than group 2 due to lower vapor pressure. In addition, they may react with oxidized uranium to form compounds such as cesium uranate. Hence, release from oxidized fuel is also slower than group 2.

Group 4 elements (tellurium group) have relatively high vapor pressure but tend to be retained in uranium metal by chemical attraction as evidenced by the formation of compounds like uranium selenide and telluride. There is no such attraction withuranium oxide. Therefore, group 4 elements should be readily released from oxidized uranium.

Group 5 elements (alkaline earths) exist as metallic inclusions in uranium metal. As such they have relatively high vapor pressure but are held encased by solid uranium. Boiling points are 1380 and 1640°C, respectively—close to the melting point of uranium metal. On release from fuel and exposure to air, they rapidly form low-vapor-pressure oxides which may stay in place. Hence, for air accidents, release from fuel may appear to be low.

Group 6 elements ("noble metals") are so named to indicate they remain as metals and tend to be retained due to their low metallic volatility. This is true for reducing environments but is definitely not true for air ingress accidents. On exposure to air, both ruthenium and molybdenum form highly volatile oxides. The boiling point of RuO_4 is 135°C, and MoO_3 sublimes at 700°C. (Metal boiling points are 4250 and 4300°C, respectively.) We should expect strong retention of these elements in uranium metal but rapid evolution on uranium oxidation.

Group 7 (lanthanides) and 8 (cerium group) elements are retained as low-vapor-pressure metallic inclusions in uranium metal. On release and exposure to air, they form low-vapor-pressure oxides. Hence, retentions in fuel are expected to be high.

C.3.3 Radiological Importance

Accident evaluations generally place highest importance on groups 2, 3, and 4. Many nuclides in these groups have the highest combination of volatility, dose factor, and potential for biological concentration. This judgement needs to be reevaluated for extremely energetic accidents (explosions) which can release low-volatility material from groups 5 to 8. Many nuclides in these latter four groups have high inhalation dose factors.

C.4 RADIOACTIVITY RELEASE FROM URANIUM METAL FUEL: EXPERIMENTS AND REPORTS

C.4.1 Parker et al.[8]

A series of experiments over a 10-year period dealt with (1) oxidation of uranium metal in air, carbon dioxide, and steam, and (2) release of fission products from uranium metal fuel in helium, air, carbon dioxide, and steam. Many uranium oxidation tests were run but remain unanalyzed and are probably unanalyzable due to missing information. The most interesting qualitative result is that burnups up to 1000 MWd/MT had small effect on the oxidation rate in air. Rates increased with surface-to-volume ratio but not in a regular fashion. Table C.2 lists observed releases from partially oxidized uranium heated in air at 1000 and 1200°C. Table C.3 lists releases from completely oxidized uranium heated in air at 800, 1000, and 1200°C. In both cases the burnup is 0.1 at. % (about 1000 MWd/MT). This data set was used by Birney et al.[6] to develop Hanford N Reactor release correlations and also by Cronenberg[7] for the same purpose. (Birney's review is summarized below.) Principal results from Parker[8] follow.

Table C.2. Fission product release from irradiated uranium[a] incompletely oxidized in air[b]

Furnace temperature (°C)	Time (min)	Uranium oxidized (%)	Percentage of total activity released							
			Xe-Kr	I	Te	Cs	Ru	Zr	Ce	Sr
1000	<1	11.1	–	3.1	–	0.01	0.004	0.003		
1000	10	46.9	~100	–	–	2.4	0.1	0.007	0.001	0.05
1000	20	53.2	~100	67.3	–	2.8	0.13	0.005	0.008	0.055
1000	40	86.9	~100	79.5	–	18.4	5.2	0.018	0.006	0.05
1200	<1	25.0	–	12.5	–	1.62	0.019	0.17		
1200	5	43.6	97.7	31.9	8.1	18.5	0.035	–	–	0.024
1200	8	66.2	99.2	23.3	12.7	14.5	0.16	–	–	0.028
1200	10	94.0	100			11.2	0.51	0.05	0.06	2.7
1200	10	68.0	98.7	39.9	24.8	17.1	0.22	–	–	0.6
1200	12	77.5	99.8	46.4	23.0	–	–	–	–	0.9
1200	15	72.0	99.8	52.8	51.6	28.6	4.3	–	–	3.1
1200	15	64.8	99.6	71.5	68.0	13.65	2.0	–	–	1.1
1200	20	65.4	99.4	57.3	71.3	13.0	1.8	–	–	0.85
1200	30	72.3	–	62.1	77.4	19.2	2.34	–	–	1.77

a. 0.1% burnup, preheated in helium.
b. Velocity 120 cm/min, measured at room temperature.
Source: Parker (1967).

Table C.3. Activity released by complete oxidation of irradiated uranium[a] in air[b]

Experiment number	Temperature (°C)	Percentage of activity released							
		Xe-Kr	I	Cs	Ce	Te	Ru	Zr	Sr[c]
68	800		48	0.06	0.001	2.9	73	0.05	0.002
81	1000	97.1	89	0.4	0.002	80	77	0.02	0.002
83	1200	99.2	90	14	0.0006	96	85	0.01	0.02
32	1200		99.2	16	0.03	84	78	0.08	0.005

a. 0.1 atom % burnup.
b. Air flow velocity, 220 cm/min measured at room temperature.
c. Values probably low due to chemisorption of SrO by the mullite furnace tube.
Source: Parker (1967).

1. Release of noble gases (group 1) is essentially complete by 1000°C, independent of degree of oxidation. (However, this may not be accurate at low burnup. See Fig. C.1.)
2. Fractional release of iodine (group 2) at 1000 and 1200°C appears to be equal to the degree of oxidation. Table C.2 indicates that fractional release is less than the degree of oxidation at lower temperatures.
3. Release of cesium (group 3) at 1000 and 1200°C appears to be proportional to degree of oxidation above about 25%, but there is significant retention even at 100% oxidation. Table C.3 shows that cesium release drops sharply with temperature at 100% oxidation.
4. Release of tellurium (group 4) appears to be similar to iodine at 1000 and 1200°C and oxidation above about 25%. Table C.2 shows significantly less release than iodine at 800°C.
5. Release of strontium (group 5) shows no trend with degree of oxidation at 1000°C, where it is about 0.05%. At 1200°C there is a rough proportionality with oxidation, ending at about 2% release at 100% oxidation.
6. Ruthenium release (group 6) appears to be erratic, possibly due to formation of the volatile oxides, RuO_4 or RuO_3, under some conditions. For this reason, complete oxidation of uranium results in high release, about 75% at 800, 1000, and 1200°C. Long time at temperature may also enhance release (see 40 minute run, Table C.2). Clearly, ruthenium does not belong in the "noble metal" category for air ingress accidents.
7. Zirconium release (group 7) data are fragmentary, usually <0.05%.
8. Cerium release data (group 8) are also fragmentary but comparable to zirconium, as expected from its properties.

C.4.2 Birney et al.[6]

This review was conducted to support a severe accident study for the Hanford N Reactor, a graphite-moderated, natural-water-cooled, aluminum-clad, natural uranium metal–fueled reactor. Release in a steam environment was of principal interest. For this purpose, Birney used Parker's air exposure data cited above, the rationale being that air and steam are both oxidizing environments. (Birney did not make use of Parker's limited steam data which show much lower releases than for air.)

Birney proposed the following simple release model based on Parker's data:

(2)	iodine	$R = F$
(3)	cesium	$R = 0.3\ F$
(4)	tellurium	$R = F$
(5)	strontium or barium	$R \leq 0.01\ F$
(6)	ruthenium	$R \leq 0.05\ F$
(7)	zirconium	$R \leq 0.01\ F$
(8)	cerium	$R \leq 0.01\ F$,

where R is the fraction released from the fuel element and F is the fraction of uranium oxidized. Group numbers are given in parentheses at left.

This is a highly simplified rendition of Parker's data. No temperature dependence is included though data in Table C.3 clearly indicate lower releases for iodine, cesium, and tellurium at lower temperatures. Also, data showing high ruthenium release at complete oxidation for all temperatures are ignored even though there is a chemical rationale for the observation (i.e., the high volatility of ruthenium oxides). A detailed analysis by Cronenberg[7] on fission product transport in the primary system of the N Reactor accepts Birney's fuel release model as its starting point.

C.4.3 Hilliard (1959)

In this test series, 11.5-gram samples of trace-irradiated uranium metal were heated in air; the released fission products were captured in downwind traps. The irradiation level was extremely low—2.4×10^{14} nvt, roughly 10^{-7}% FIMA or 10^{-3} MWd/MT. Temperatures were predominantly 1250°C, with a few others ranging between 425 and 1400°C. Time at temperature ranged up to 232 minutes and degrees of oxidation up to 100%. The degree of oxidation was not measured; it was estimated by correlation from earlier tests. Therefore, oxidation values could be biased. Also, releases from very low fission product concentrations obtained by trace irradiation should be less than expected from realistic burnup levels.

Principal results from Hilliard[9] follow.

1. Figure C.1 shows a rough correspondence of xenon release to the degree of fuel oxidation at all test temperatures, 535 to 1440°C.
2. Figure C.2 shows the relation between iodine release and degree of oxidation. At 1215 and 1440°C the degree of release roughly equals the degree of oxidation. At lower temperatures, there is strong indication that releases are significantly less than the degree of oxidation, although there is a great deal of scatter. This feature agrees with Parker.[8]
3. Cesium releases were much less than expected from Parker's data (Table C.4). Moreover, no strong trend appears with temperature or degree of oxidation. The highest observed cesium release was 6% at only 620°C and 70% oxidation.
4. Figure C.3 shows that tellurium release approximately equals the degree of oxidation at the high temperatures, 1215 and 1440°C, but is significantly less at the lower temperatures. Only a few percent release is seen at 535 and 620°C at complete oxidation. This is generally in accord with Parker's data.
5. Barium and strontium releases were mostly scattered in the range 0.02 to 0.1%, generally below that observed by Parker.
6. Ruthenium releases scattered from 1 to 16% with no clear trends. The high releases observed by Parker (73–85%) at full oxidation were not seen.
7. Zirconium releases for two measurements were consistent with Parker, 0.01 to 0.07% at 1215°C.

C.4.4 Hilliard and Ried[10]

This study extended the earlier work by investigating the effect of higher irradiation levels. Burnups ranged from 10^{-3} to 1340 MWd/MT. Also, five additional elements were monitored for release: molybdenum (group 6); cerium, neptunium, and plutonium (group 8); and uranium. Most tests were conducted at 1200°C, 68 degrees above the melting point of uranium. There were a few tests at 1000 and 1400°C. Uranium oxidation ranged from 65 to 90%.

Test Conditions:	(a)	1000°C	45 min	10^{-3} to 1340 MWd/MT
	(b)	1200°C	24 min	10^{-3} to 1340 MWd/MT
	(c)	1400°C	10 min	10^{-3} to 1340 MWd/MT

Graphical results are shown in Sect. C.8. A brief summary is as follows:

1. Xenon release increased with burnup from 70 to 100% for all three test conditions.
2. Iodine release increased with burnup from about 65 to 95% for test conditions (b) and (c) and from 15 to 90% for test condition (a).
3. Cesium release increased with burnup from about 30 to 80% at test condition (b).
4. Tellurium release did not vary with burnup. (Note: legends are given as in the original report, but are probably switched for tellurium plot in Sect. C.8.)

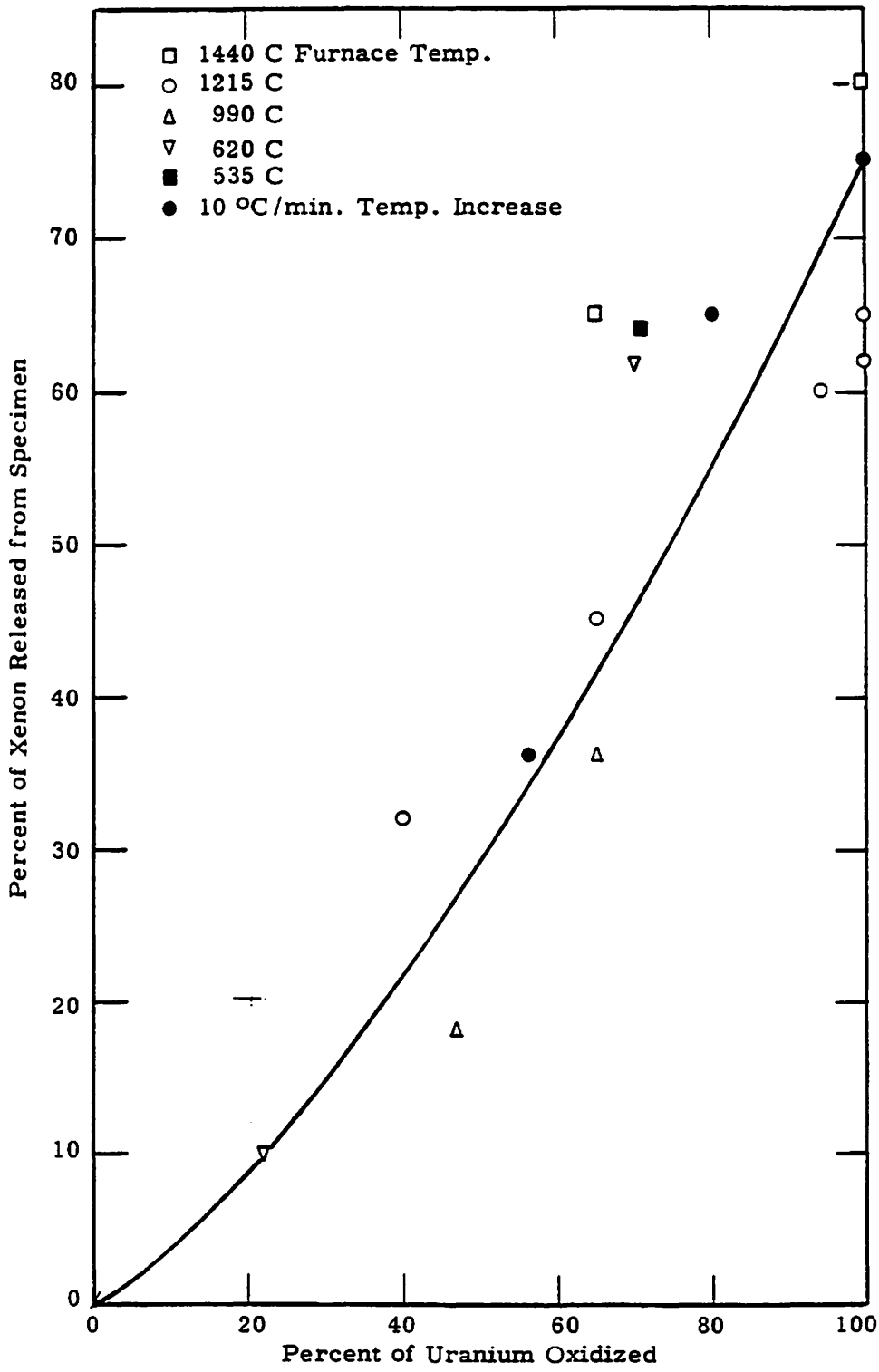

Fig. C.1. Release of xenon as a function of uranium oxidation. Source Hilliard.[9]

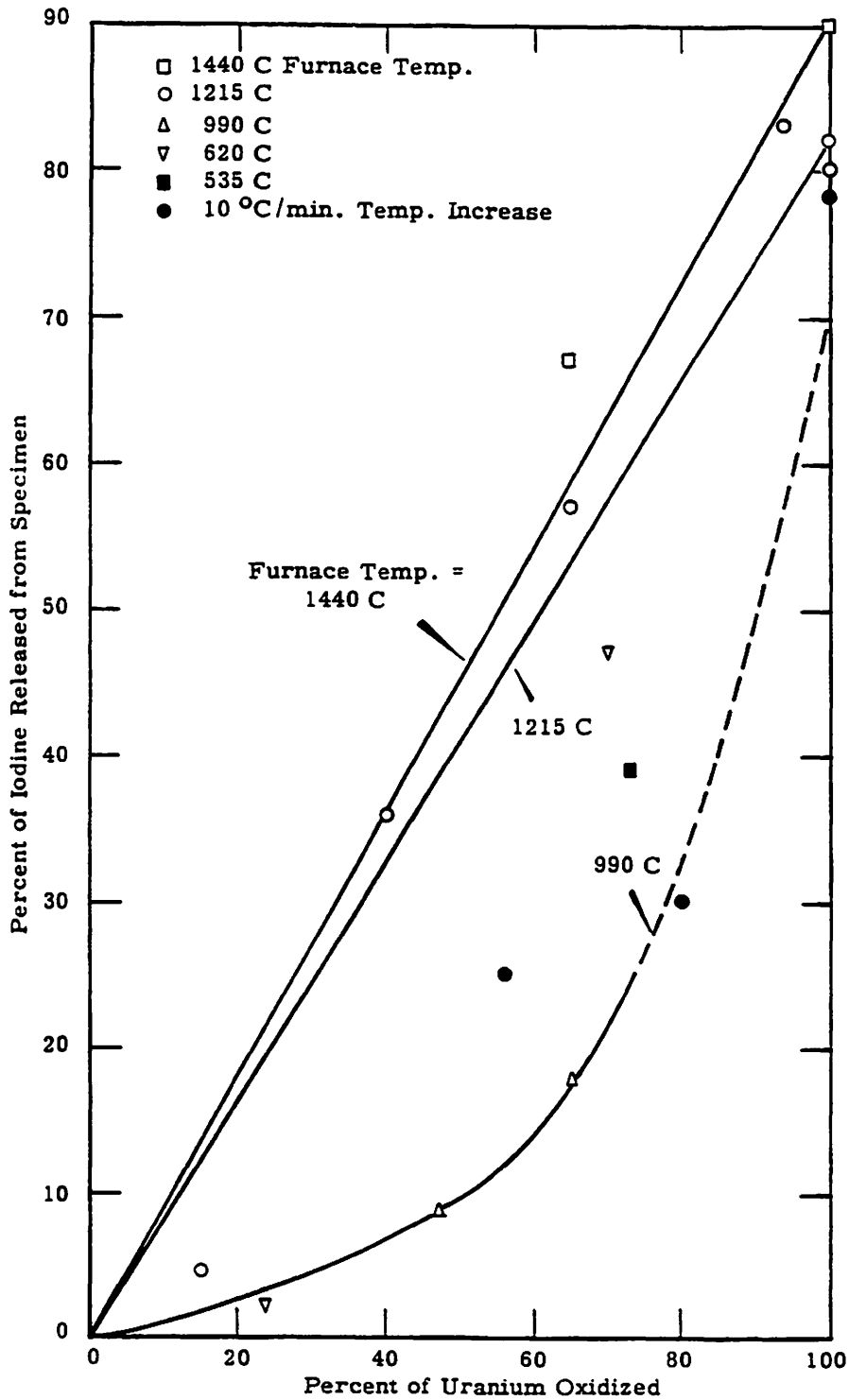

Fig. C.2. Release of iodine as a function of uranium oxidation. Source: Hilliard.[9]

Table C.4. Relationship between fission product release and percentage of uranium oxidized

Run number	Uranium oxidized[a] (%)	Furnace temperature (°C)	Percentage released from specimen						
			^{131}I	^{132}Te	^{133}Xe	^{89}Sr	Cs	^{103}Ru	^{140}Ba
A-20	65	1440	67	47	65	0.07	0.5	2.3	0.14
A-13	100	1440	90	76	80	0.07	1.1	2.8	0.15
A-19	100	1325[b]	78	70	75	0.02	0.9	12	0.03
A-10	15	1215	4.6	9.1	d	0.001	0.1	d	0.03
A-1, A-2, A-22	40	1215	36	34	32	0.03	0.4	1.0	0.05
A-6, A-16, A-18	65	1215	57	55	45	0.04	1.0	0.7	0.08
A-7	94	1215	84	81	55	d	0.6	1.6	0.13
A-3, A-8, A-12	100	1215	80	75	57	0.03	0.8	1.0	0.16
A-9, A-11, A-23	100	1215	82	76	65	0.02	1.0	3.4	0.03
A-31	80[c]	1170[b]	30	40	66	d	d	d	d
A-30	56[c]	1030[b]	25	9.3	36	d	d	d	d
A-14	47	990	8.6	8.9	18	0.03	0.2	1.0	0.04
A-24	65	990	18	18	36	0.01	d	1.4	0.01
A-15	22	620	2.2	0.54	10	0.004	0.6	0.38	0.004
A-21	70	620	47	0.50	62	0.05	6.0	7.2	0.02
A-27	73	535	38	0.67	64	0.03	0.7	16	d

a. Percentage of metal oxidized estimated from ref. 8 of Hilliard (1959).
b. Maximum temperature attained.
c. Percentage of metal oxidized determined by pickling and weighing residue.
d. Not analyzed.
Source: Hilliard (1959).

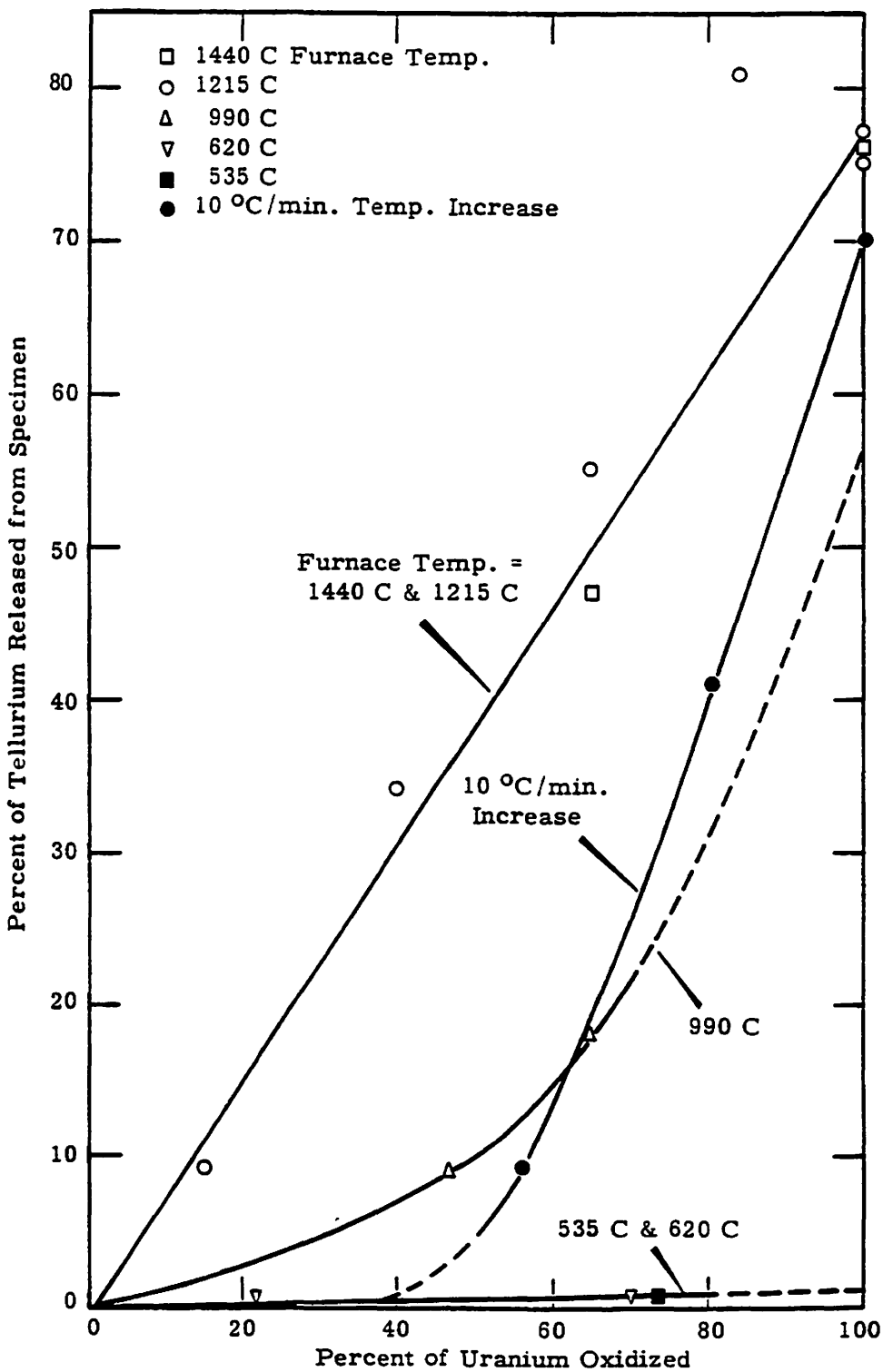

Fig. C.3. Release of tellurium as a function of uranium oxidation. Source: Hilliard.[9]

5. Strontium and barium releases averaged about 0.5% for the three test conditions.
6. Ruthenium and molybdenum release appeared to increase with burnup from a fraction of a percent to perhaps 4%.
7. Group 7 and 8 elements did not show any consistent trend with burnup. Very roughly, releases scattered around 0.04% for all three test conditions.

C.5 SUMMARY OF FISSION PRODUCT RELEASE REPORTS

The data indicate that generally fission product release rates from uranium metal under oxidizing conditions depend on (1) degree of uranium oxidation, (2) temperature, (3) irradiation level, and probably (4) time at temperature, which is difficult to separate from degree of oxidation. Moreover, these parameters can have a different effect for each fission product group. The data are included here in their original published form.

These types of experiments have always shown large error bands, as should be expected when fission product release and transport mechanisms are not fully understood. Even partial knowledge of the basic chemistry of release would be extremely helpful in interpreting the highly scattered data. Data scatter and the complex physicochemical mechanisms work against formulation of anything but a fairly crude model. However, the model proposed by Birney[6] for the N Reactor safety analysis, wherein the integrated release of each fission product group is assumed to depend solely on the degree of uranium oxidation, is perhaps overly simplified. All variations with temperature are neglected in Birney's models—most importantly, reductions in release at lower temperatures (i.e., <1000°C) and low burnups.

One should also note that a bias for some fission product groups may be introduced by the necessary use of certain selected isotopes to represent the group behavior. Experimental necessity requires use of a readily detectable, fairly long-lived isotope, meaning that ^{103}Ru is often used as the only representative of fission product group 6, the noble metals. However, ruthenium is unfortunately not representative of the noble metals group in air because it has a highly volatile oxide. Therefore, release estimates for group 6 are undoubtedly biased on the high side.

C.6 GRSAC MODEL

C.6.1 General Approach

The simple model of Birney[6] (see above) assumes releases proportional to the degree of uranium oxidation for all fission product groups. A strong dependency on uranium oxidation is reasonable for the iodine and tellurium groups, which form chemical bonds with the metal but not with the oxide. The noble gases appear to be completely released well before complete oxidation. Also, Parker's data[8] indicated a temperature dependence for most of the fission product groups, while Hilliard and Ried[10] show some to have a burnup dependence. Therefore, some enhancements to Birney's model are needed for this study. Our approach, then, is to follow the Birney model format but to include temperature and burnup dependency where appropriate. The selected form of the release model is given below:

$$FR_i = A_i \, f1_i(BU) \, f2_i(T) \, F^n{}_i \qquad (C.1)$$

where

FR_i = percent release of group i fission products from fuel,
A_i = empirical constant for group i,
$f1_i$ = an empirical function of burnup for group i, given by Eq. (C.2),

$f2_i$ = an empirical function of temperature for group i, given by Eq. (C.3),
F = percent oxidation of uranium fuel,
n_i = empirical constant for group i.

Equation (C.1) could be called an expanded Birney release model in the sense that the releases are still assumed to be proportional to the degree of uranium oxidation, now raised to the *n*th power. The multiplicative functions f1 and f2 modify the release by accounting for the influences of burnup and temperature. It was found that including an empirical exponent of F improved the accuracy of the correlation.

The advantage of using a release equation such as Eq. (C.1) is that well-behaved functions f1 and f2 may be selected with maxima of unity. Hence, extrapolations to extreme temperatures or burnups, if necessary, may be accomplished yielding releases within the 100% bound or less. A major drawback of Eq. (C.1) is that cross-correlations of burnup, temperature, and degree of oxidation are not taken into account.*

Figures shown in Sect. C.8 from Hilliard and Ried[10] illustrate the dependence of release on fuel burnup. From these figures it may be seen that a function f1 of the form given by Eq. (C.2) may reasonably describe the data of all fission product groups.

$$f1_i(BU) = m_i \log(BU/BU_0) + y_i \qquad (C.2)$$

where

m_i, y_i = empirical constants for fission product group i,
BU0 = selected minimum value of burnup, 10^{-3} MWd/MT,
BU = fuel burnup, MWd/MT.

As seen from the figures in Sect. C.8, release of fission product groups 1, 2, and 3 show significant burnup dependence while groups 5 through 8 show little effect.

The temperature dependency, f2(T), will be assumed in the form

$$f2_i(T) = 1 - \exp[-(T - T1_i)/(T2_i - T1_i)] \qquad (C.3)$$

where $T1_i$ and $T2_i$ are empirically selected temperatures for fission product group i, °C.

This assumed temperature dependency increases smoothly from zero, at T equal to T1, to unity for high values of T, making it more suitable for extrapolation than polynomial fits that may diverge widely beyond the data range. Data that show small effects of temperature may be modeled by selecting proximate values of T2 and T1. Numerical tests showed that arbitrary selection of reasonable values of T1 between 100 and 400°C had small effect on the rms error of the fit.

C.6.2 Evaluation of Model Constants

Release equation (C.1) plus the definitions of functions f1 and f2 given by Eqs. (C.2) and (C.3) contain six empirical constants for seven of the eight fission product groups. However, numerical tests showed that arbitrary selection of reasonable values for T1 between 100 and 400°C had little effect on the rms value of the fit. Therefore, only five release constants for each of the eight fission product groups need to be evaluated; that is, A_i, m_i, y_i, $T2_i$, and n_i. These constants must be evaluated from

---

* A release correlation in the form of a quadratic regression equation was tested in an attempt to account for cross effects of temperature, burnup, and degree of oxidation; for example, FR = a BU + b T + c F + d T BU + e T F + f F BU + g BU^2 + h T^2 + i F^2. This effort was discarded when improbable, negative effects of the independent variables, T and BU, were determined for several cases, probably due to data scatter. Also, extrapolation of a release equation of this form would be highly uncertain.

the release data given in Tables C.2, C.3, and C.4 and the data presented in graphical form in Sect. C.8.

The constants were evaluated using program RANOPT.[11] Program RANOPT starts with an assumed set of the six empirical parameters and calculates a revised set of parameters by a gradient search method that minimizes the value of an objective function, in this case the root mean square of difference between the measured and calculated percentage release of group i fission product. This yields a local optimum based on the assumed initial set of values. RANOPT then hunts for a global optimum by selecting a specified number of random initial parameter sets; for these runs, 2000 random sets were used. The global optimum is selected as yielding the minimum objective function for all selected sets of parameters. Table C.5 lists the optimized values of the release constants calculated by RANOPT.

Figures C.4 through C.11 illustrate the comparison of measured and calculated release for each data set given in Tables C.2, C.3, and C.4 and the data graphically shown in Sect. C.8.

Table C.5. Optimized release constants for Equation (C.1)

Fission product group	A	m	y	T1	T2	n	rms error (%)
1	4.347	0.1061	0.1379	100	202.8	0.7719	9.9
2	1.085	0.05933	1.299	400	2406	1.038	17.3
3	2.683	0.2218	0.2181	400	3590	0.7203	25.6
4	1.87	–0.007986	0.6662	400	2087	1.051	21.8
5	1.211	0.123	0.08845	400	2922	0.5862	0.65
6	0.06688	0.01398	–0.1277	400	436.1	2.24	15.6
7	0.009705	0.3057	1.973	400	1638.0	0.0731	0.04
8	0.01585	–0.1785	5.217	400	2480	0.3071	0.14

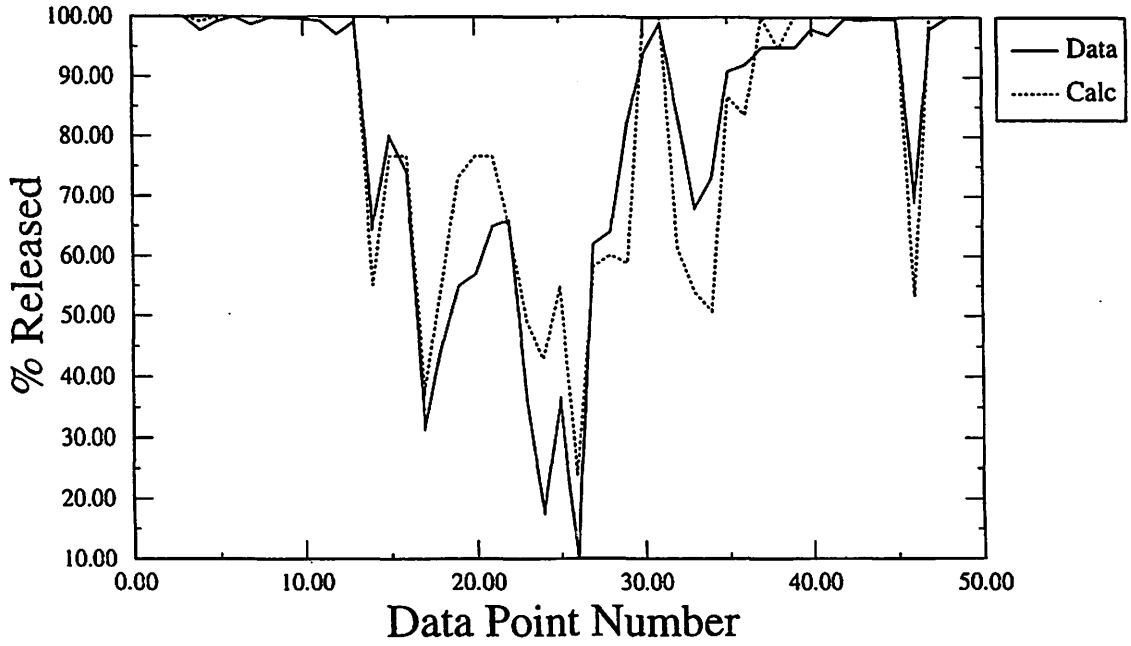

Fig. C.4. Measured vs calculated releases for fission product group 1.

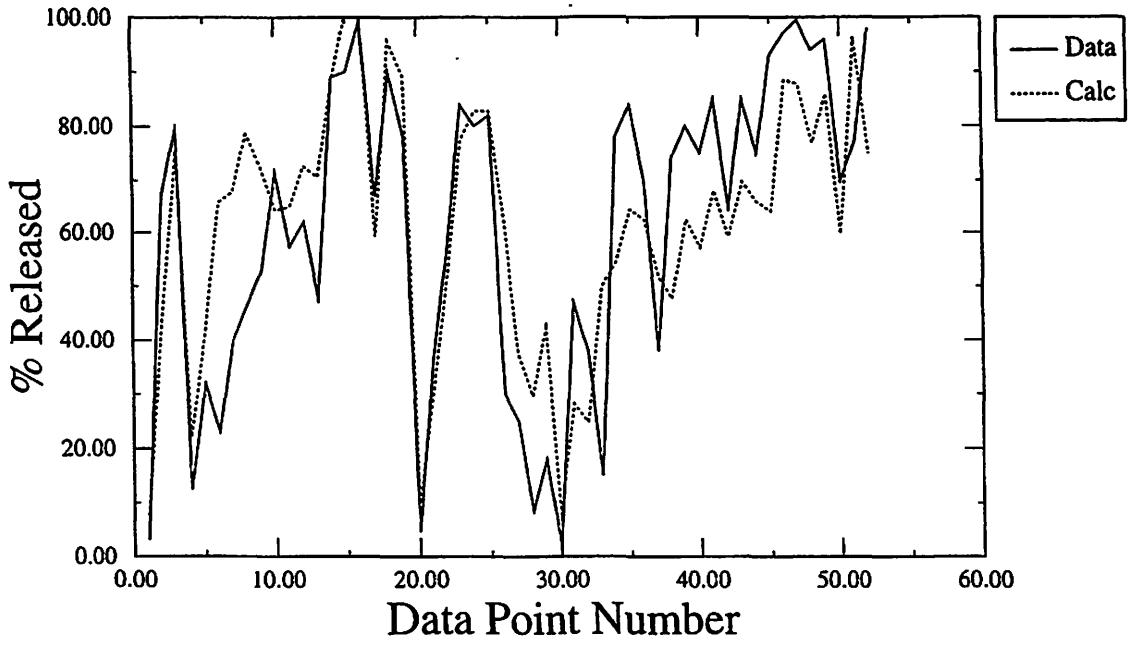

Fig. C.5. Measured vs calculated releases for fission product group 2.

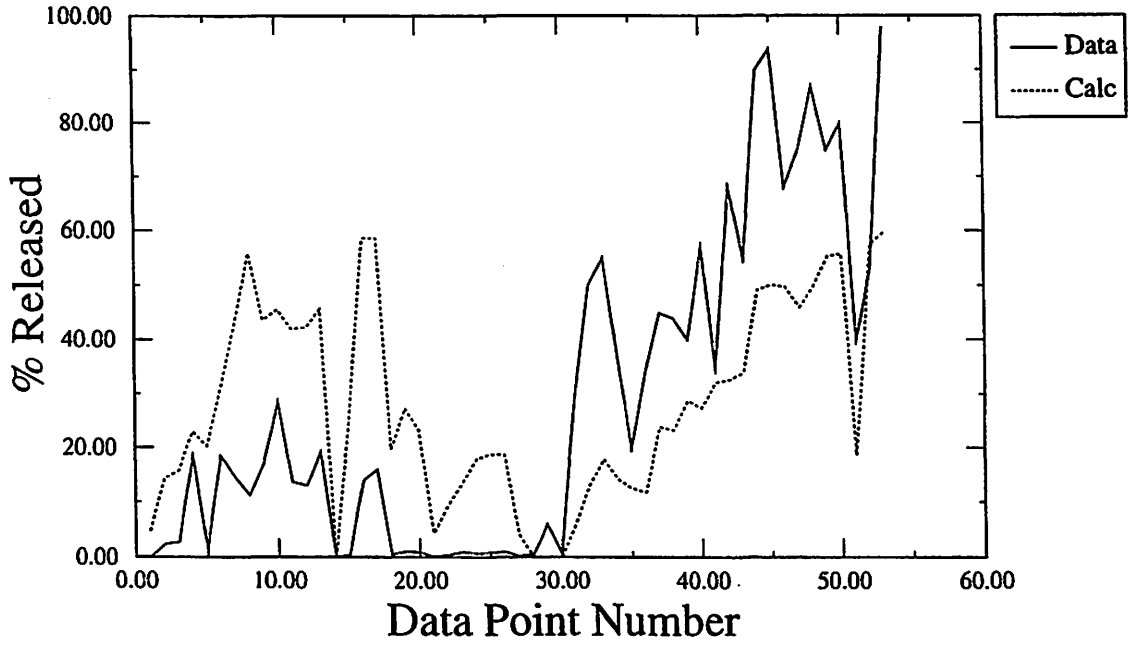

Fig. C.6. Measured vs calculated releases for fission product group 3.

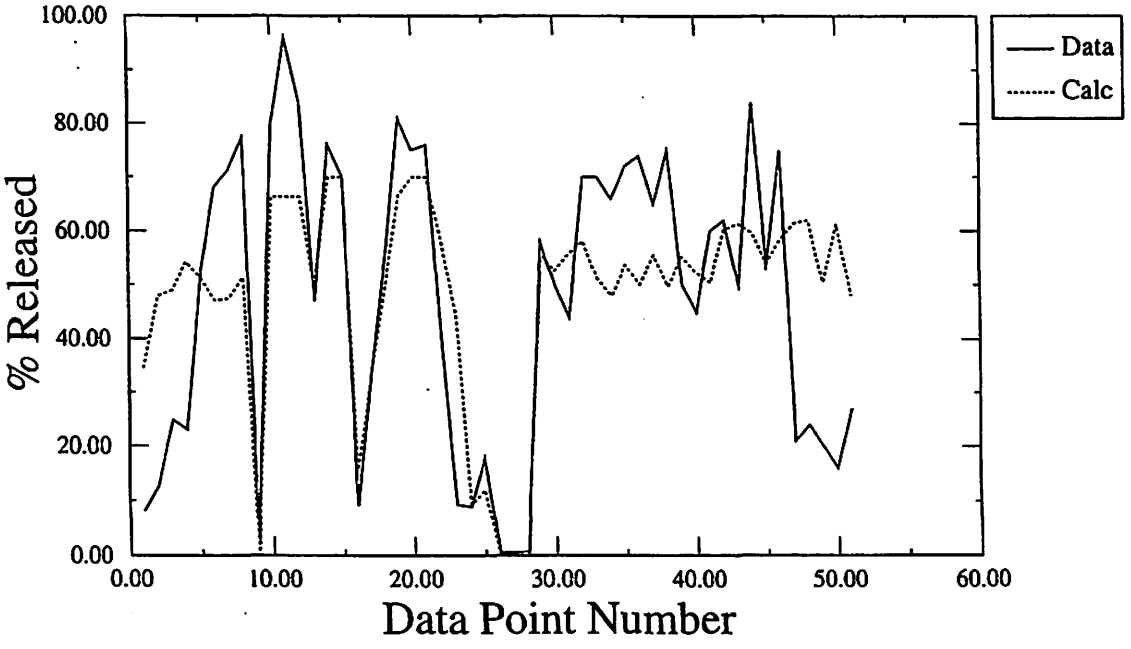

Fig. C.7. Measured vs calculated releases for fission product group 4.

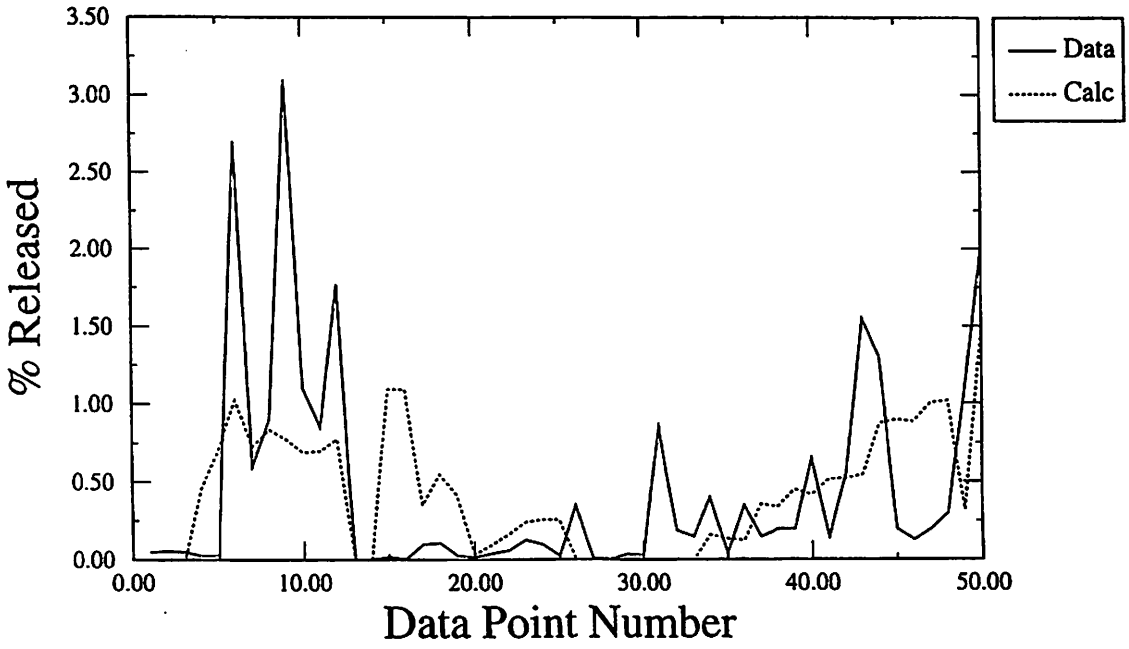

Fig. C.8. Measured vs calculated releases for fission product group 5.

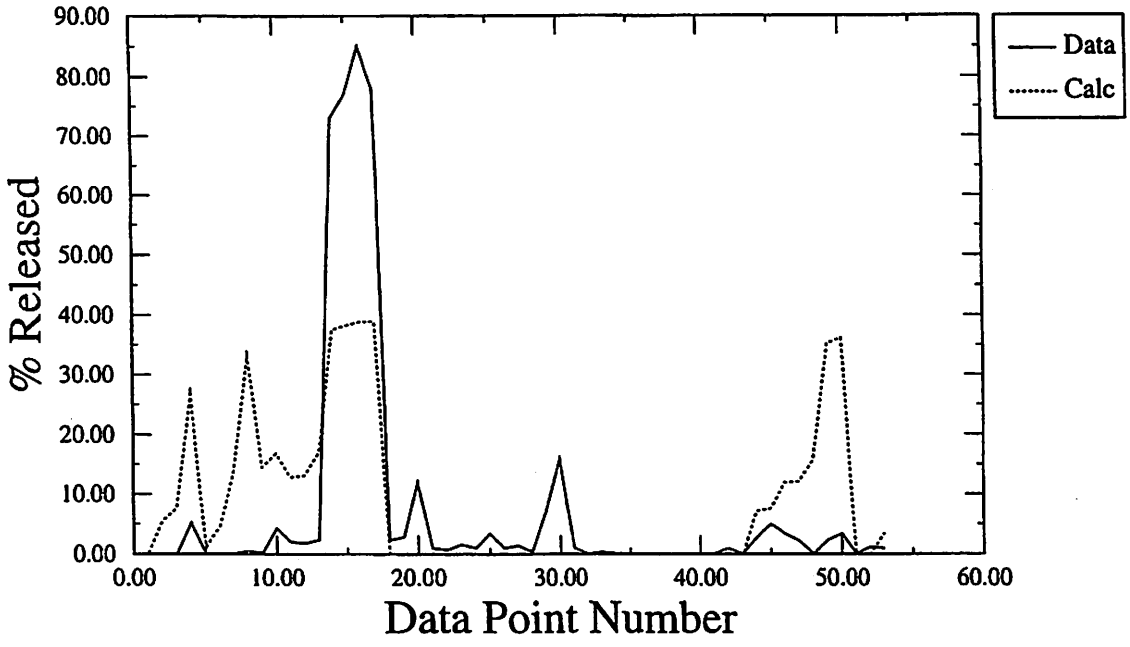

Fig. C.9. Measured vs calculated releases for fission product group 6.

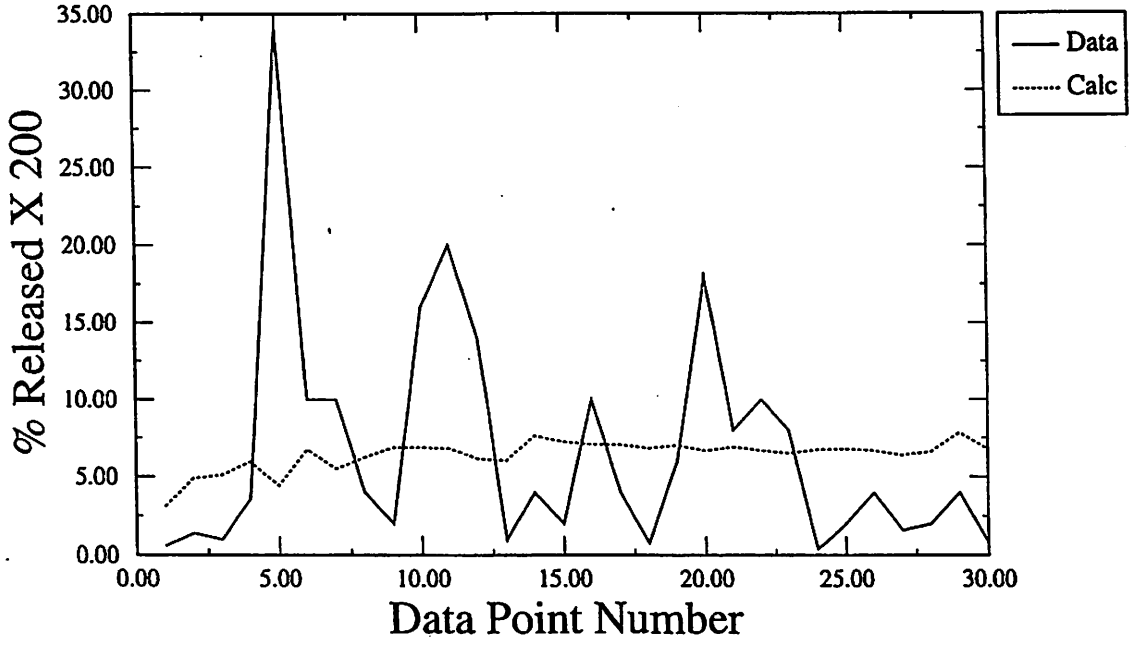

Fig. C.10. Measured vs calculated releases for fission product group 7.

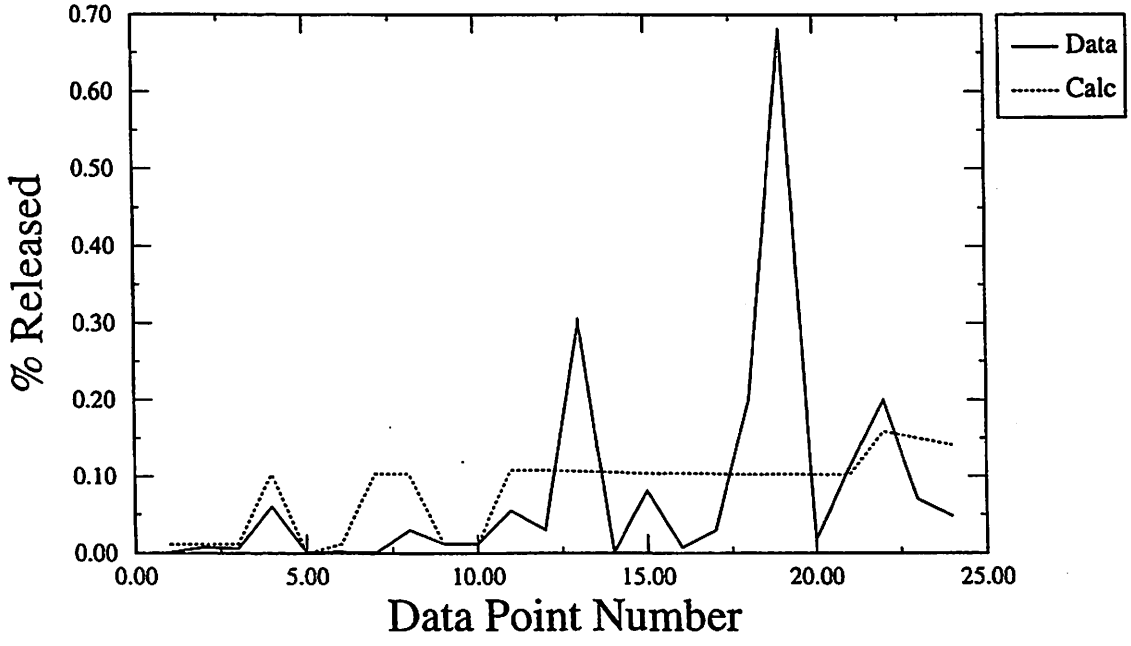

Fig. C.11. Measured vs calculated releases for fission product group 8.

C.6.3 Fission Product Release Model Predictions

Figures C.12 through C.19 illustrate the percent release from fuel vs degree of oxidation of each fission product group, as predicted by Eq. (C.1) using the constants given in Table C.5. Curves are given for an assumed high burnup (for metallic uranium) of 1000 MWd/MT at temperatures of 800 and 1200°C, and for a trace irradiated fuel at 1200°C.

For cases in which the optimized value of T2 is determined to be close to the assumed value of T1, such as for the noble gas and tellurium groups, very little temperature dependence of release is predicted. Likewise, a range of burnup effects are exhibited, the most pronounced being for the noble gas, cesium, and lanthanide groups, as per Figs. C.12, C.14, and C.18.

It is worthwhile emphasizing the uncertainties associated with use of Eq. (C.1), or any other derived correlation, for predicting fission product release from fuel. There is an inherently large degree of scatter historically exhibited for this sort of experimentation. Moreover, combining three data sets from three different experiments, as was done in the development of Eq. (C.1), amplifies the effective scatter. Finally, a bias may be introduced by the selection of specific elements as representing the entire group. Most flagrant is the choice of ruthenium and molybdenum to represent the noble metals. Both these elements exhibit high volatility when heated in air, and thus certainly bias the derived equation for noble metals to the high side.

C.7 REFERENCES

1. Defense Special Weapons Agency (DSWA), "HASCAL/SCIPUFF User's Guide" (March 1997).

2. McKenna, T. J., and J. G. Glitter, *Source Term Estimation for Severe Nuclear Power Accidents,* NUREG-1228 (1988).

3. Reactor Safety Study: An Assessment of Accident Risks in U.S. Nuclear Power Plants, U.S. Nuclear Regulatory Commission, WASH-1400MR, NUREG-75/0140 (October 1975).

4. Soffer, L., et al., *Accident Source Terms for LWRs,* NUREG-1465 (1995).

5. Sjoreen, A. L., et al., *RASCAL Version 2.1 User's Guide,* NUREG/CR-5247 (1994).

6. Birney, K. R., et al., *Correlations for Fission Product Release from N Reactor Fuel under High Temperature Accident Conditions,* WHC-SP--0017-3 (DE90 009487) (1988).

7. Cronenberg, A.W., *Scoping of Fission Product Transport in the Primary System for Postulate N Reactor Severe Accidents,* WHC-SP-0071 (DE90 009489) (1988).

8. Parker, G. W., et al., *Out of Pile Studies of Fission Product Release from Overheated Reactor Fuels at ORNL 1955–1965,* ORNL-3981 (1967).

9. Hilliard, R. K., *Fission Product Release from Uranium Heated in Air,* HW-60689 (1959).

10. Hilliard, R. K., and D. L. Ried., *Fission Product Release from Uranium—Effect of Irradiation Level,* HW-72321 (1962).

11. Ball, S. J., personal communication to R. P. Wichner, February 1997.

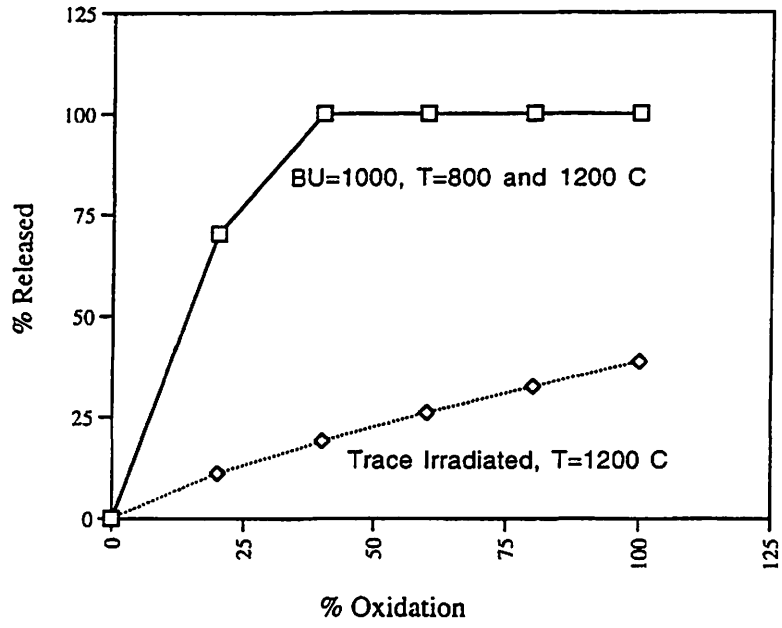

Fig. C.12. Noble gas release vs degree of oxidation.

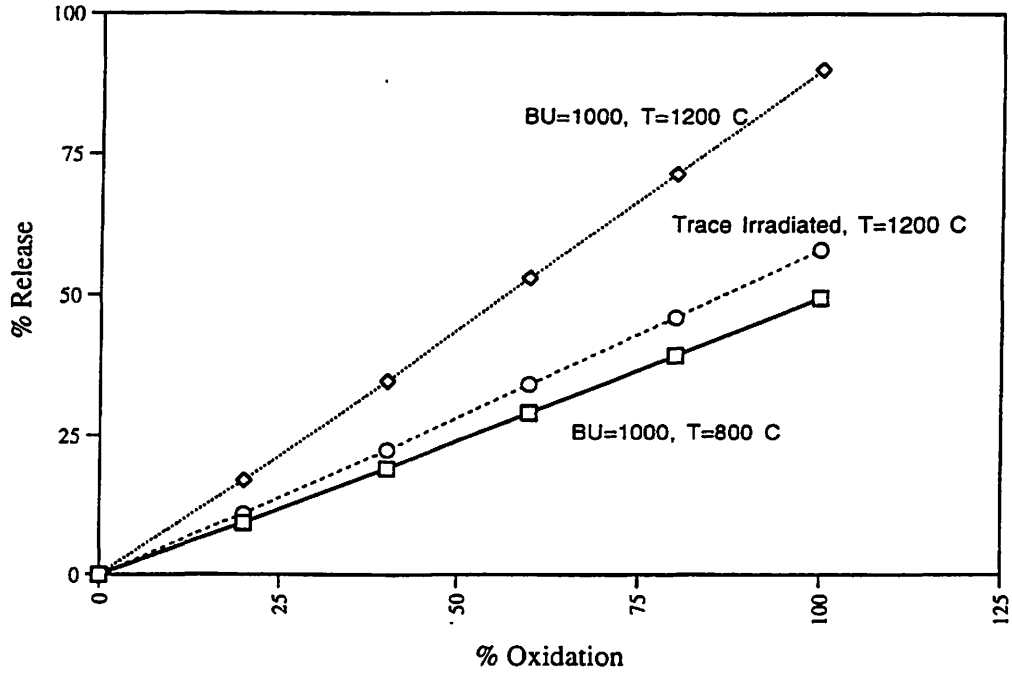

Fig. C.13. Iodine release vs degree of oxidation.

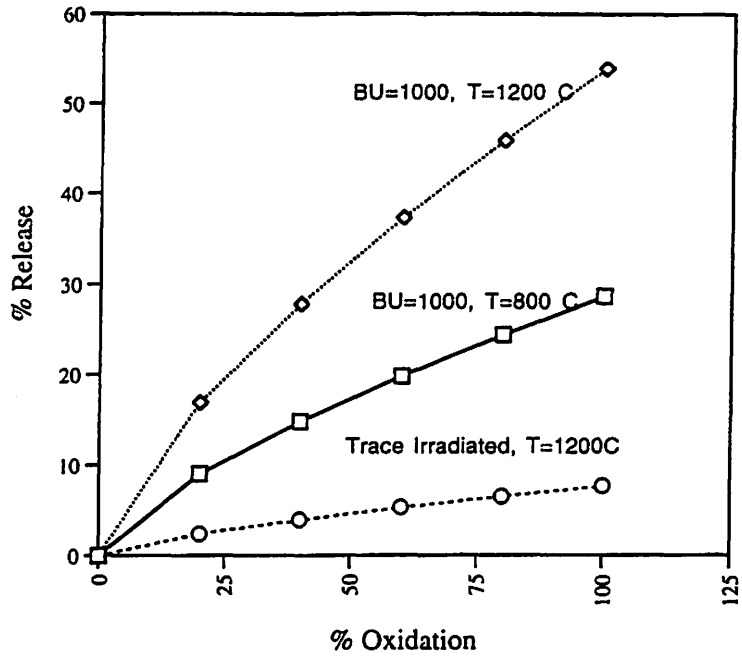

Fig. C.14. Cesium release vs degree of oxidation.

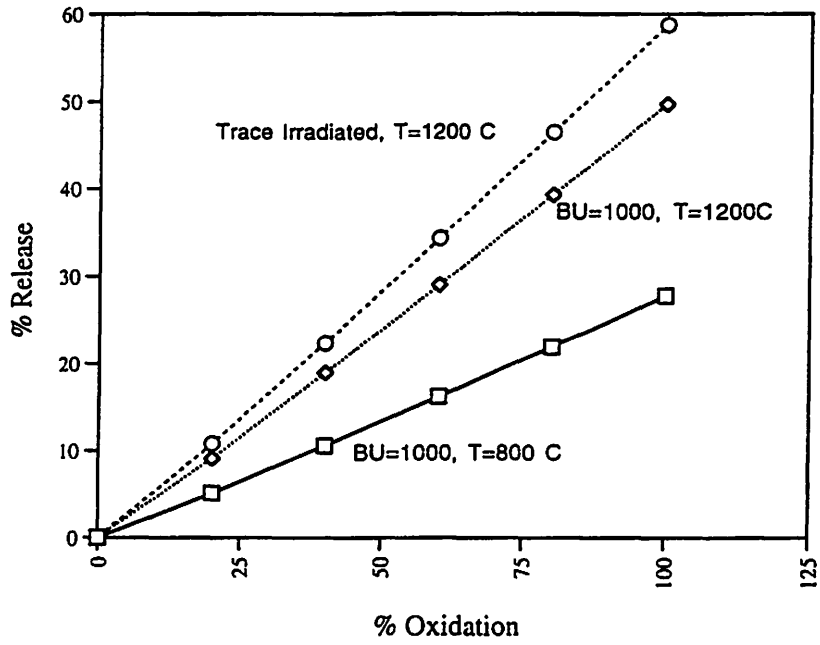

Fig. C.15. Tellurium release vs degree of oxidation.

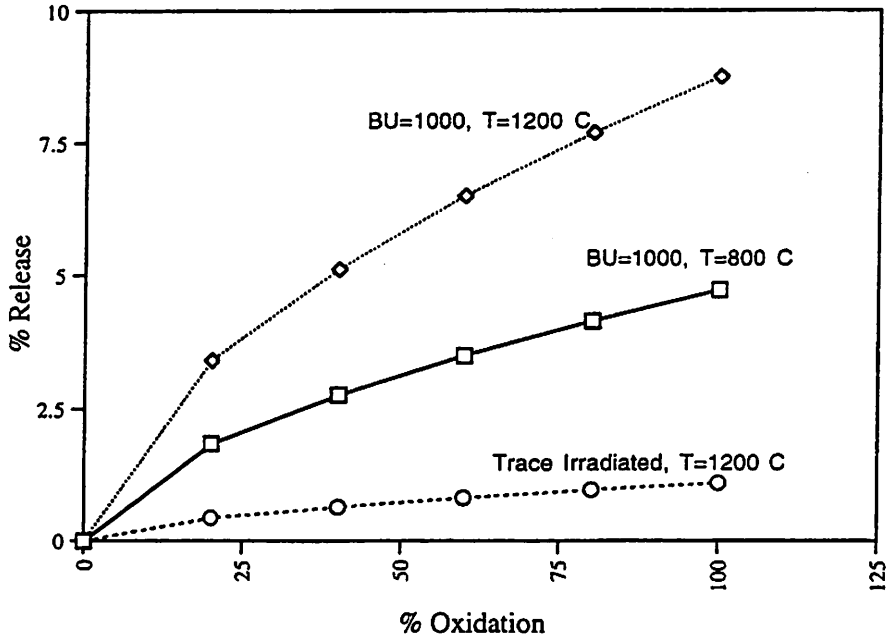

Fig. C.16. Strontium release vs degree of oxidation.

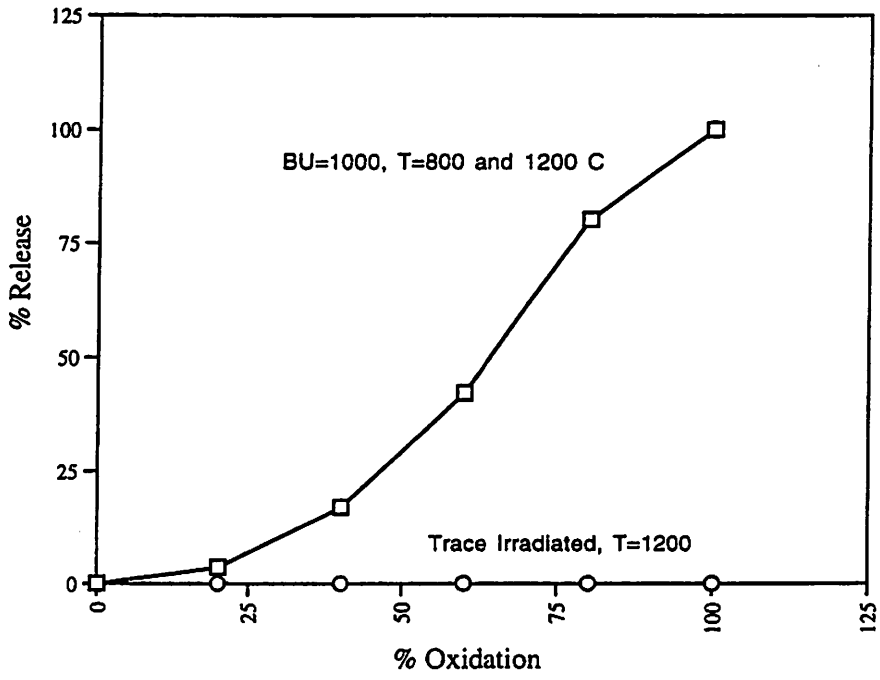

Fig. C.17. Noble metal release vs degree of oxidation.

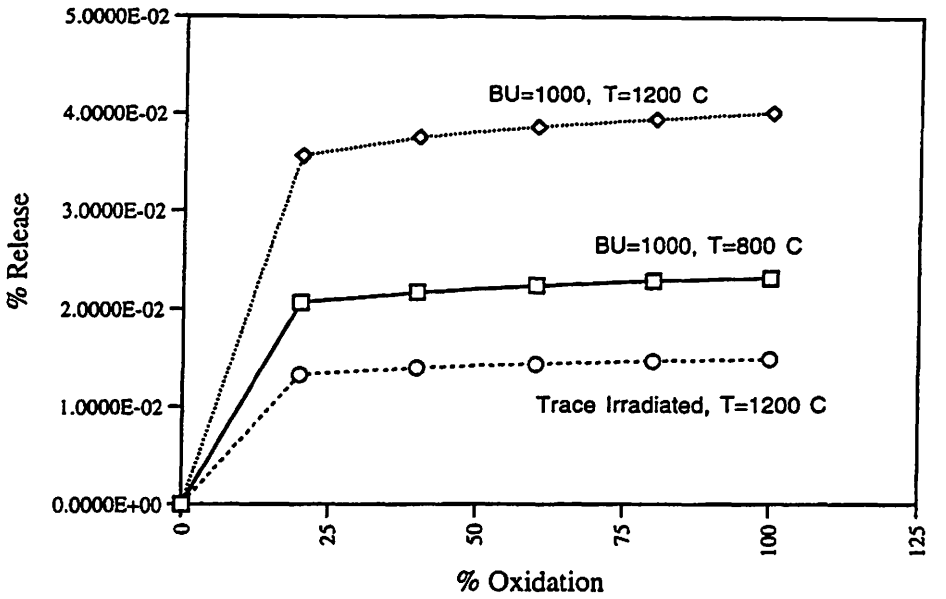

Fig. C.18. Lanthanide release vs degree of oxidation.

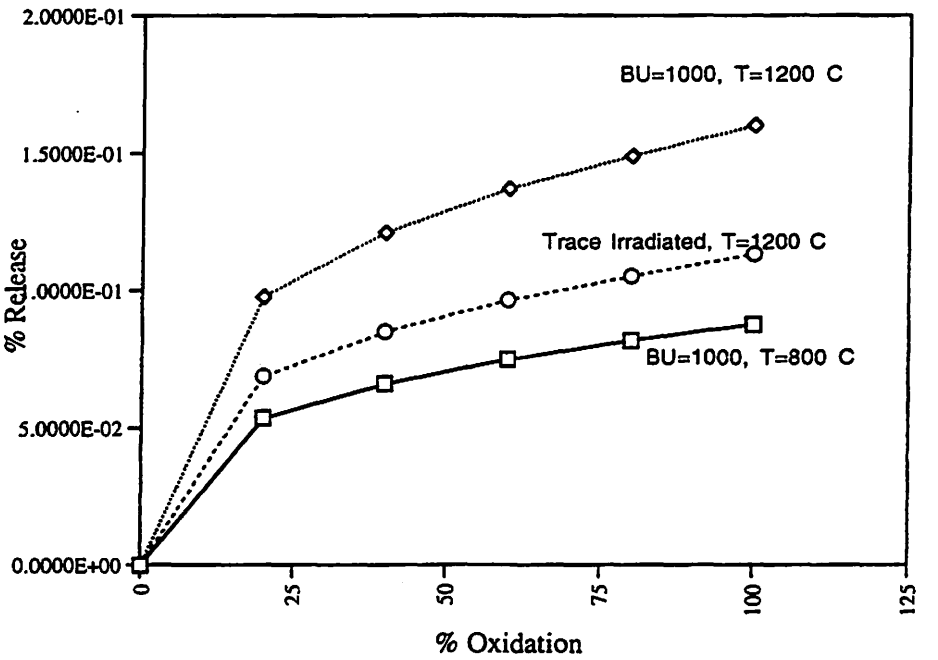

Fig. C.19. Cerium group release vs degree of oxidation.

C.8 FISSION PRODUCT RELEASE FIGURES FROM HILLIARD AND RIED (1962)

The figures on the following pages, taken directly from Ref. 10, illustrate the dependence of release on uranium metal irradiation.

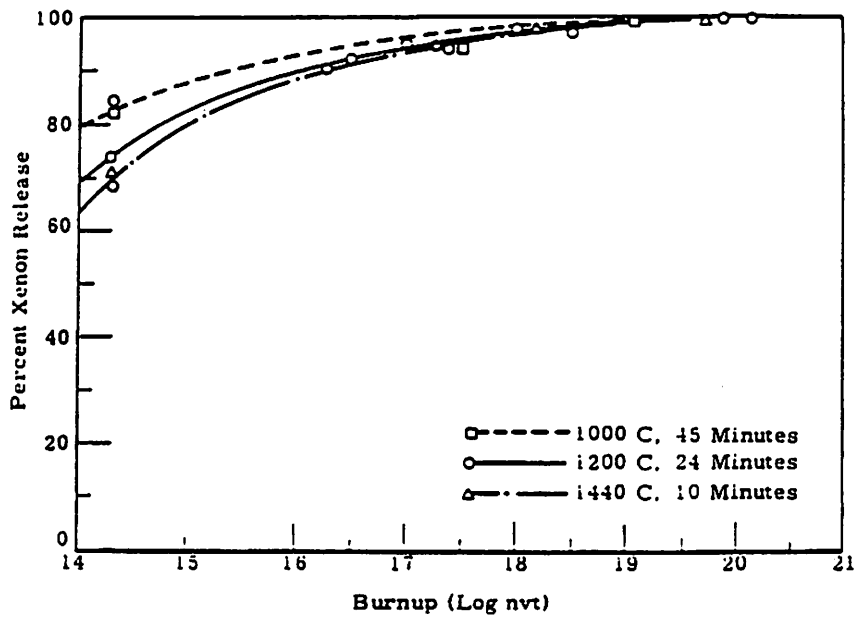

FIGURE 7

Release of Xenon as a Function of Burnup

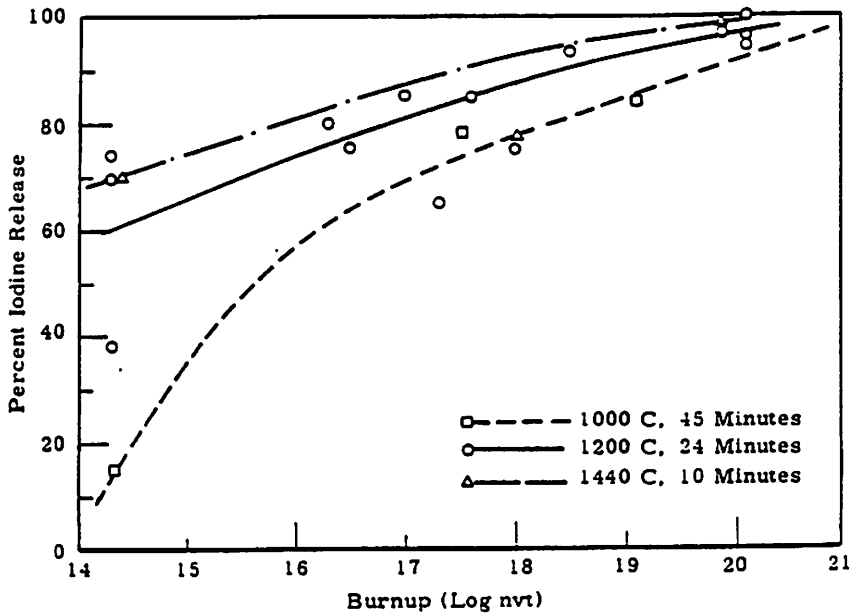

FIGURE 8

Release of Iodine as a Function of Burnup

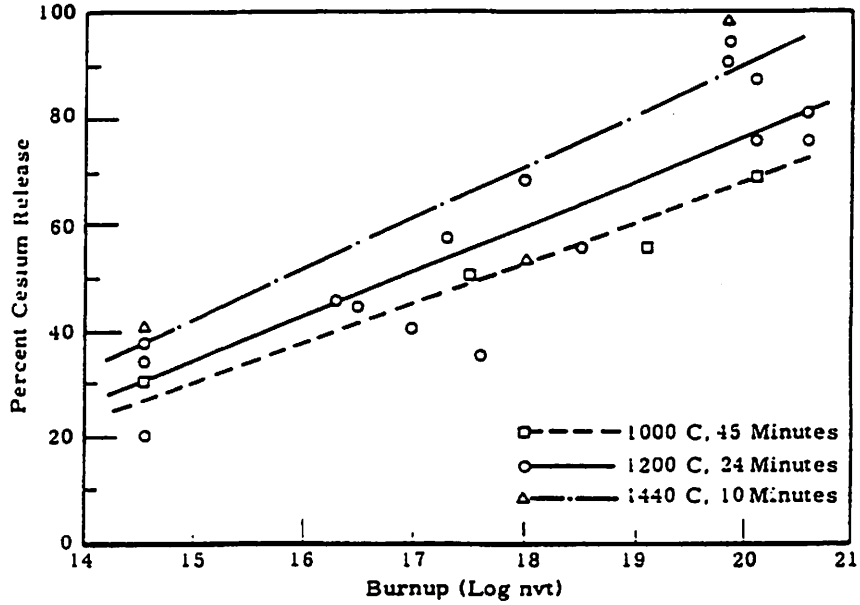

FIGURE 9

Release of Cesium as a Function of Burnup

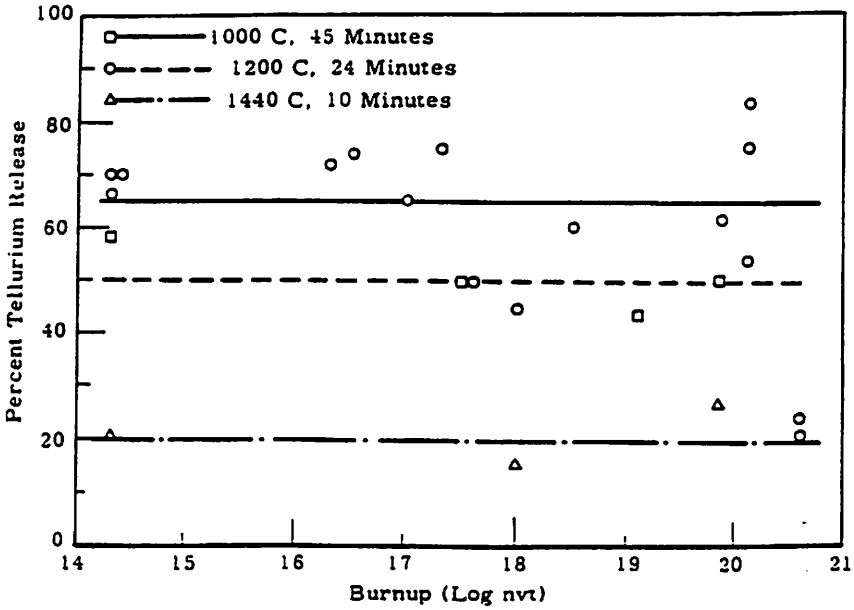

FIGURE 10

Release of Tellurium as a Function of Burnup

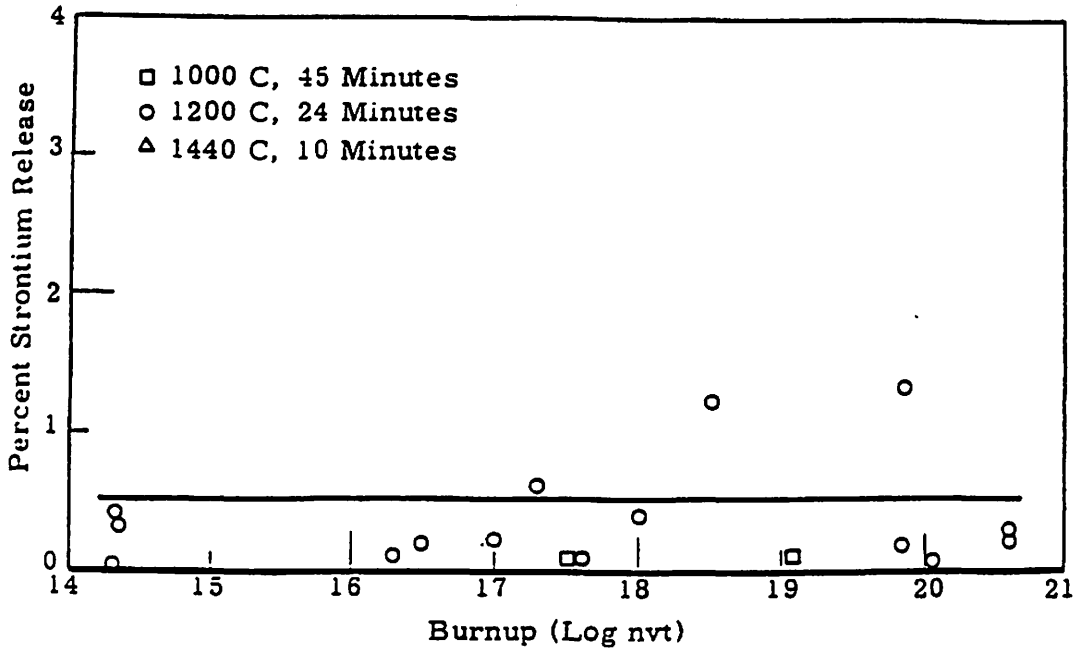

FIGURE 11

Release of Strontium as a Function of Burnup

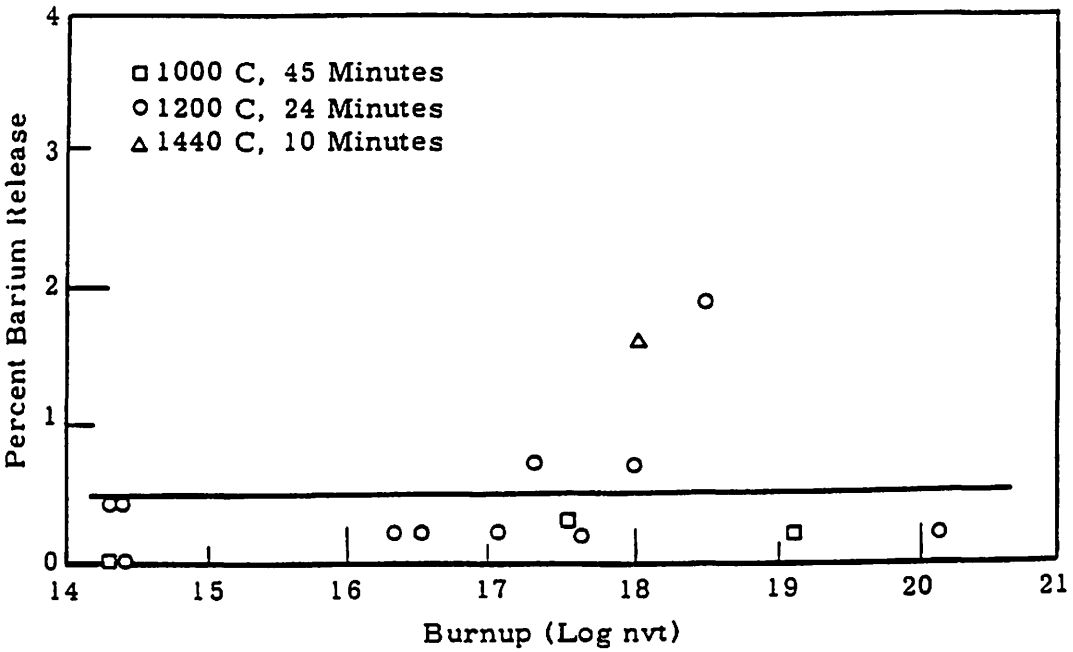

FIGURE 12

Release of Barium as a Function of Burnup

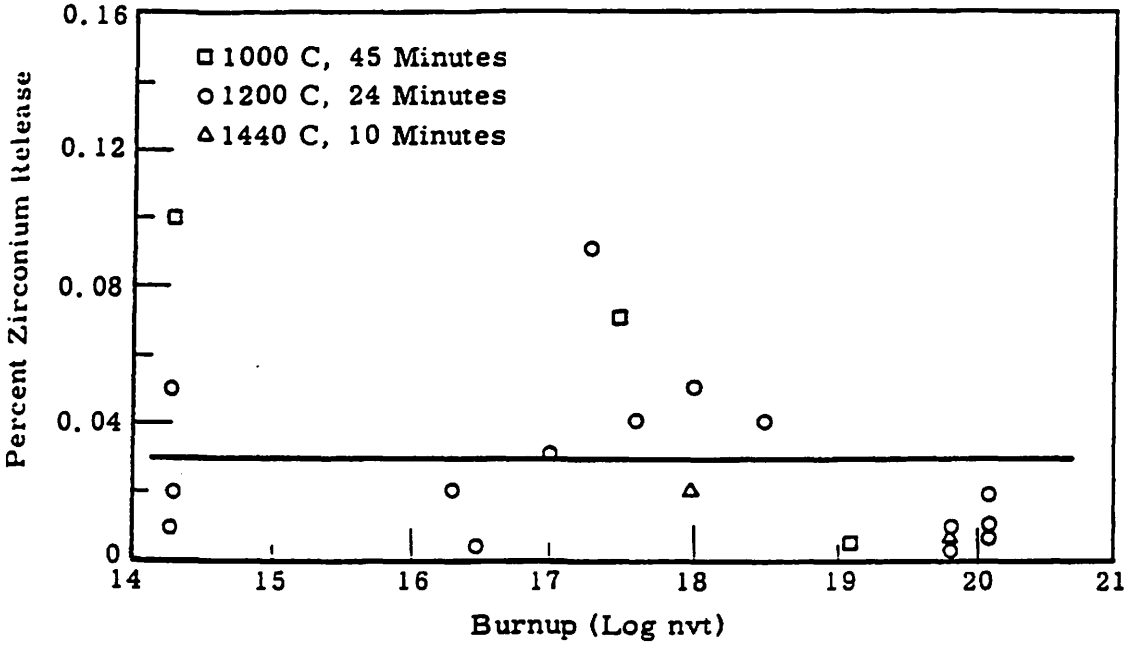

FIGURE 13

Release of Zirconium as a Function of Burnup

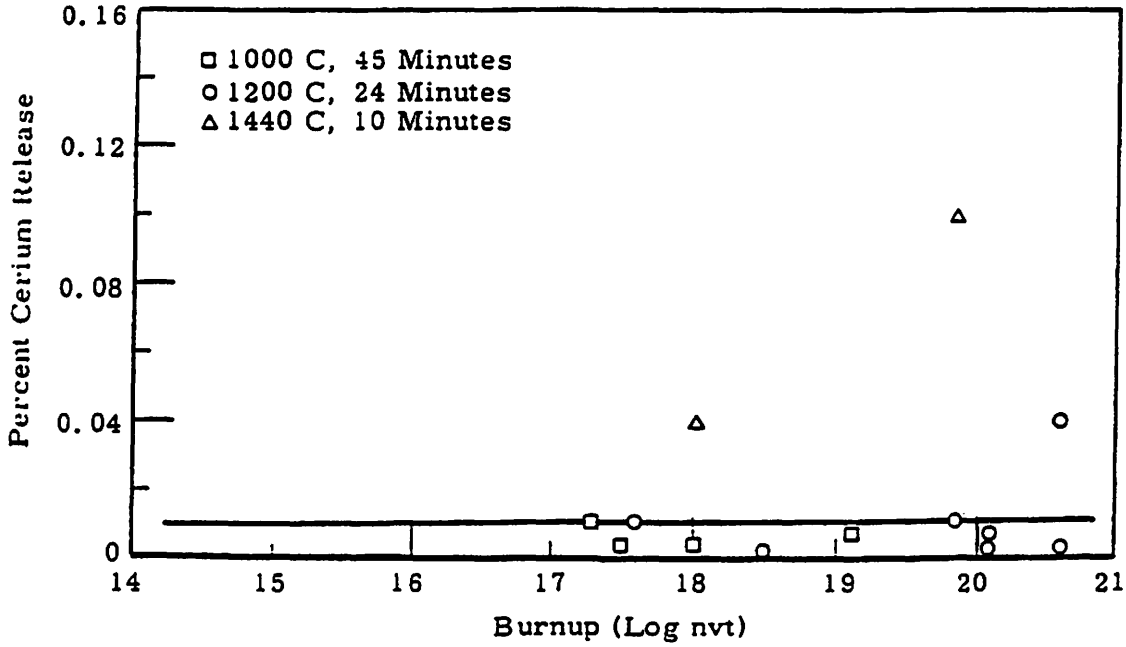

FIGURE 14

Release of Cerium as a Function of Burnup

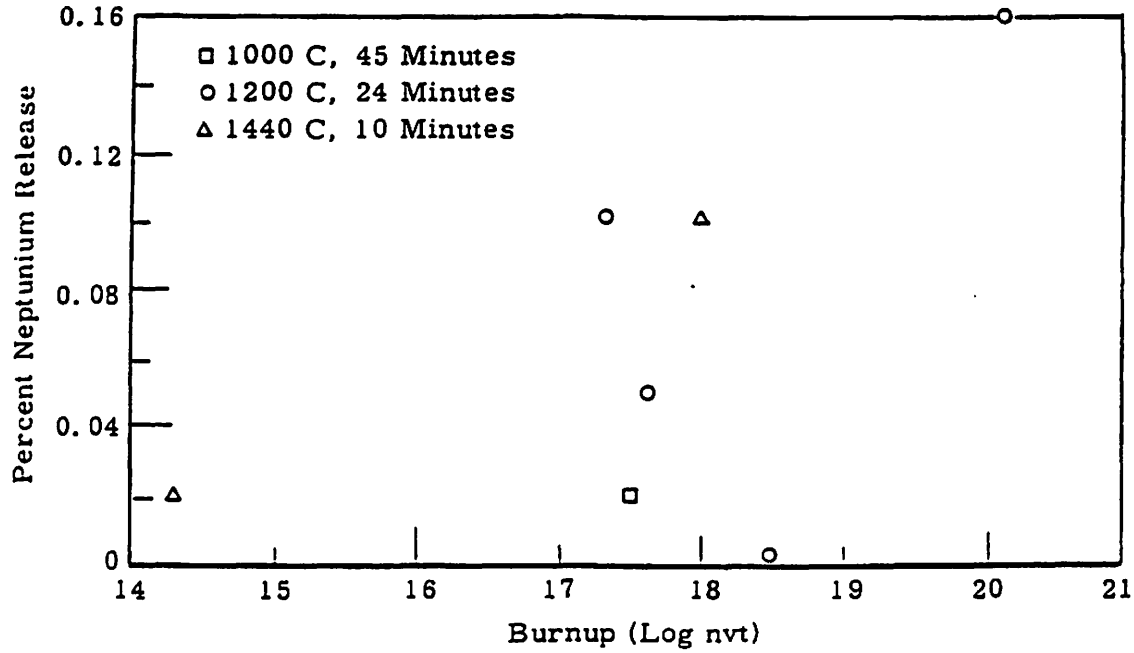

FIGURE 15

Release of Neptunium as a Function of Burnup

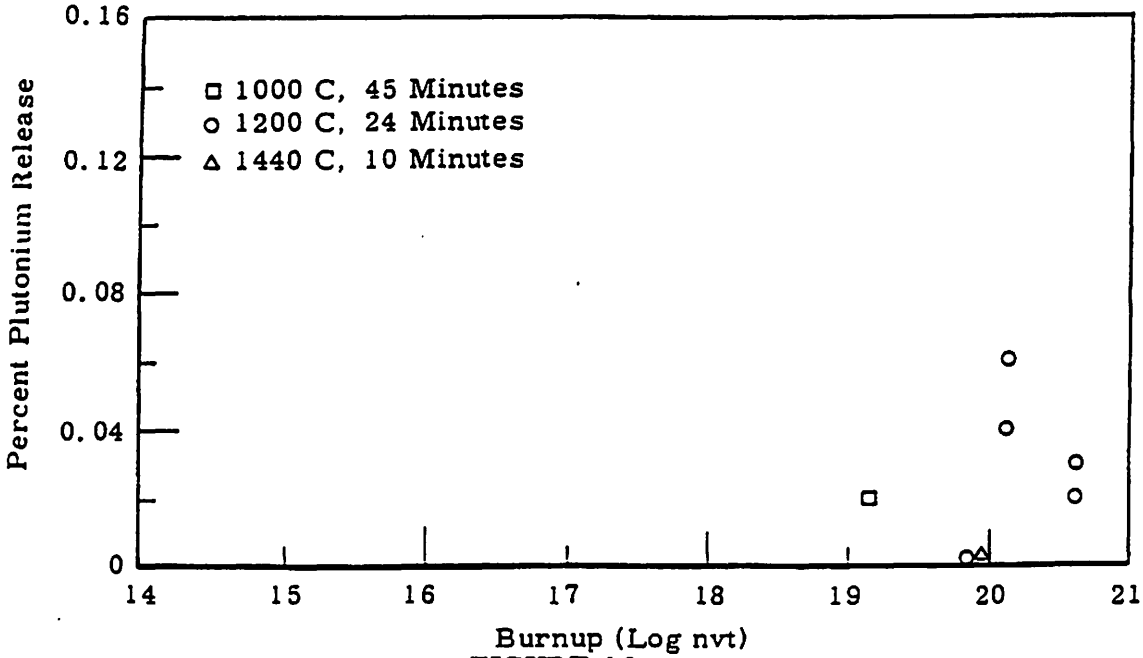

FIGURE 16

Release of Plutonium as a Function of Burnup

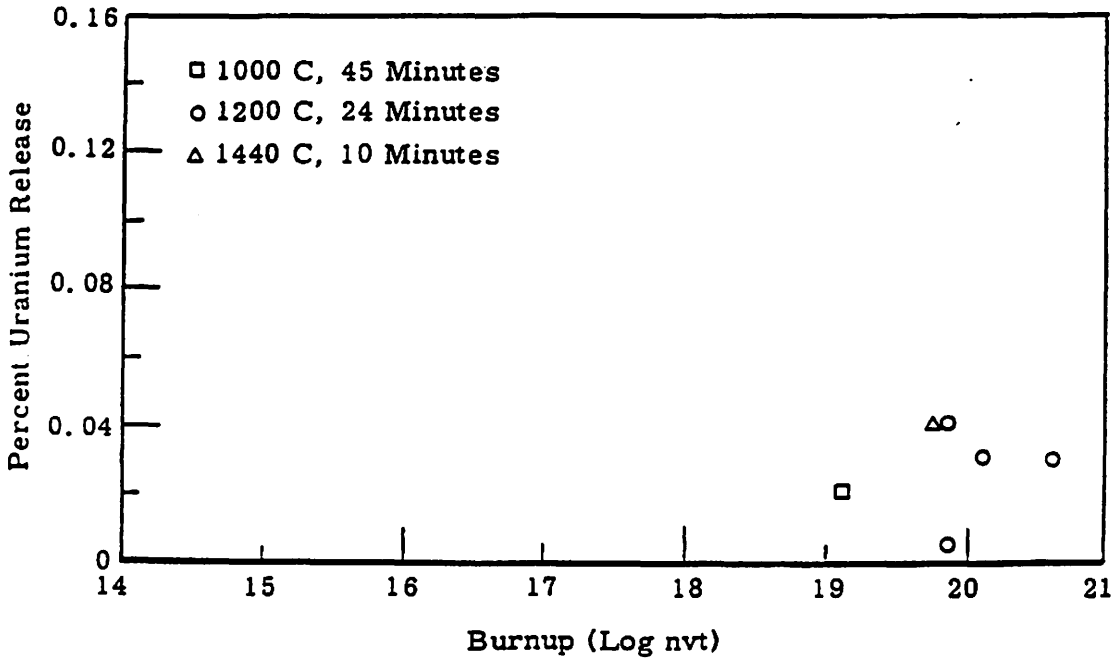

FIGURE 17

Release of Uranium as a Function of Burnup

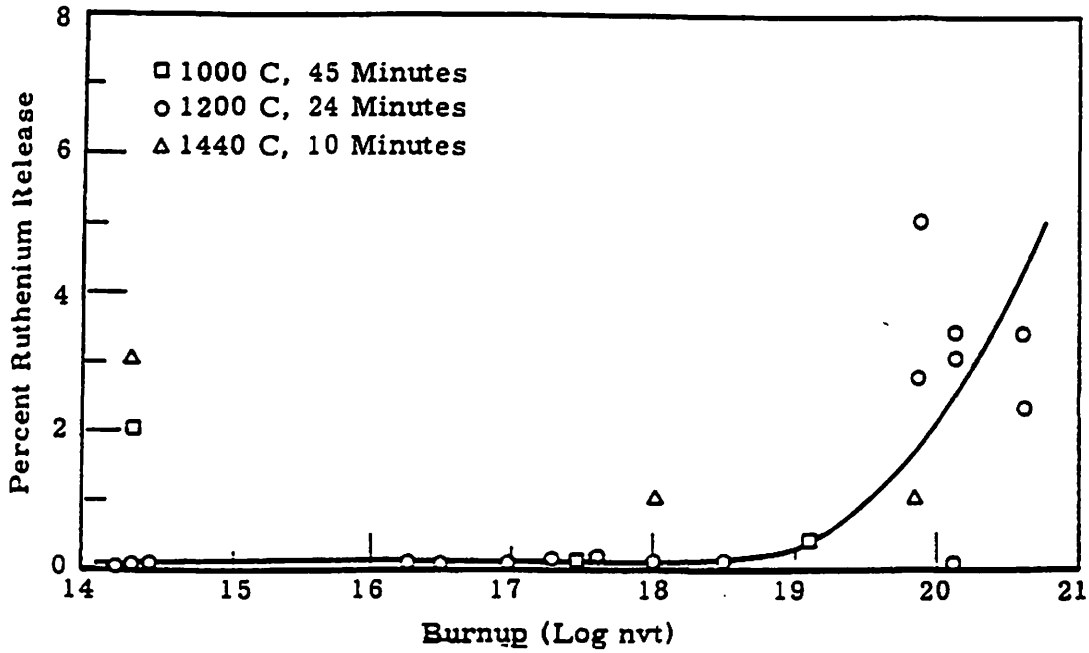

FIGURE 18

Release of Ruthenium as a Function of Burnup

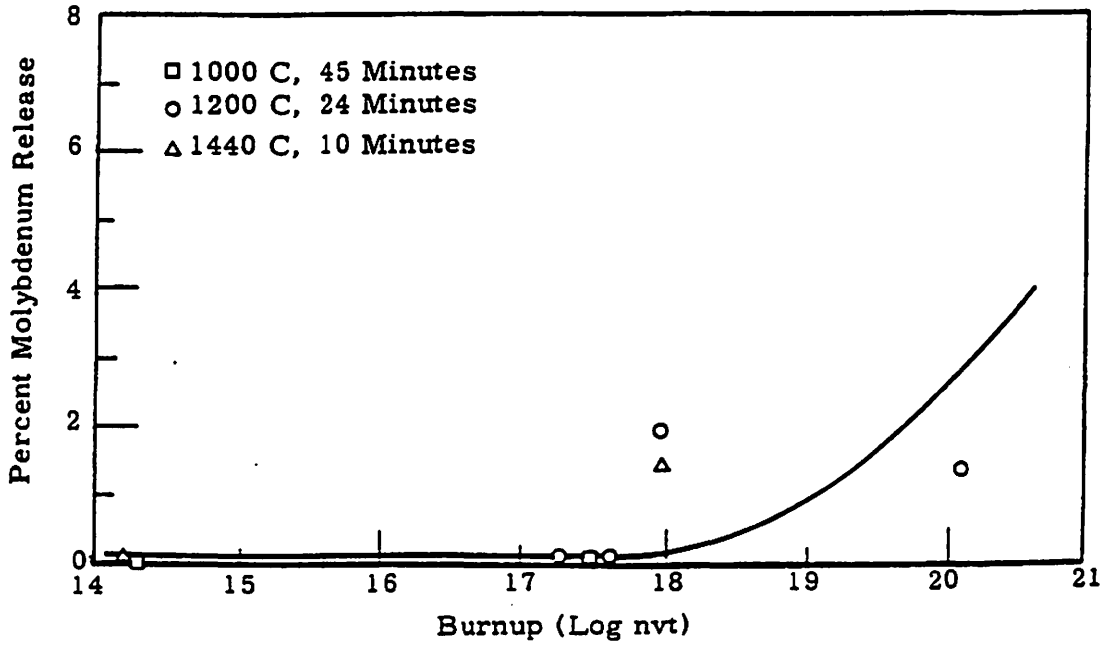

FIGURE 19

Release of Molybdenum as a Function of Burnup

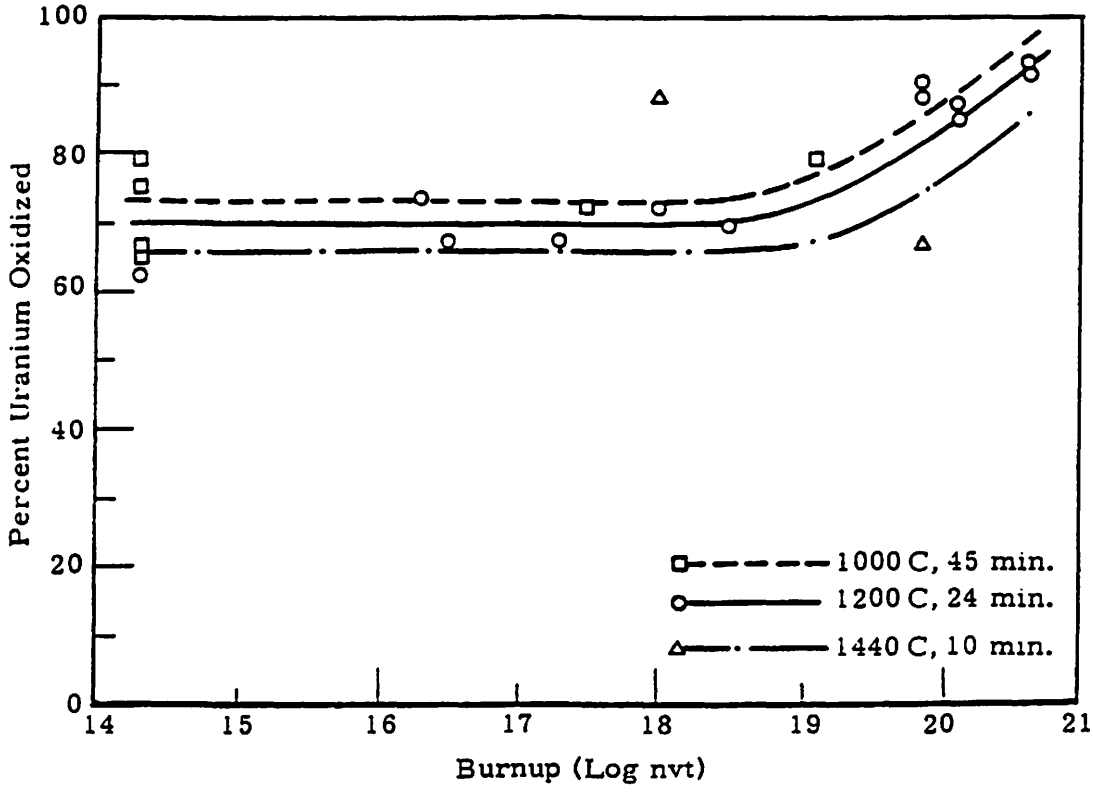

FIGURE 20

Effect of Burnup on Percent of Uranium Oxidized

APPENDIX D. WIGNER STORED ENERGY RELEASE—PHYSICAL BASIS AND MODEL

GRSAC incorporates a model for simulating effects of Wigner stored energy release in the graphite moderators of gas-cooled reactors. Low irradiation temperatures characteristic of air-cooled reactors generate a large amount of stored energy (SE), and its release with temperature, dS/dT (cal/g°C), can significantly exceed the specific heat of the graphite in the annealing region around 200°C. Stored energy release is of lesser safety concern in the higher-temperature CO_2-cooled reactors, and there it is expected only in the cooler zones of the core, but again it is not negligible in accident analyses. In helium-cooled HTGRs and other reactors whose graphite moderators operate at very high temperatures, very little stored energy is generated in the graphite moderator and it can be ignored.

Direct-inlet, air-cooled (or water-cooled) reactors incur the greatest stored energy build-up because their graphite moderators operate at low temperatures, and there is a strong sensitivity to radiation damage at low temperatures. GRSAC was benchmarked primarily against the extensive experimental data on graphite stored energy, and the well-documented features of the air-cooled Windscale 1 reactor accident in 1957. In this case, the release of stored energy played a significant part in the accident evolution.

In Windscale piles 1 and 2, stored energy releases occurred unexpectedly twice during shutdowns early in life.[1] Thereafter, due to safety concerns about further unplanned releases, procedures were instituted to periodically anneal the graphite moderator. Windscale operators used low-power nuclear heating, in the absence of air cooling, to initiate releases of stored energy that then further raised the graphite temperatures. These routine annealing operations were usually terminated when core temperatures reached about 350°C, although one annealing produced a localized graphite temperature of 420°C. Similar practices were adopted elsewhere in the U.S. and Europe for periodically annealing air-cooled, graphite-moderated reactors, using heat supplied either by nuclear heating or electrically heated inlet air. It was during a routine anneal to relieve built-up stored energy, that Windscale 1 suffered its very serious accident, which caused further stored energy releases as higher temperatures were reached, augmented by serious damage and oxidation (with consequent heat release) of the cladding, fuel and graphite.

The approximations used in GRSAC simulate stored energy release in reactors with differing amounts of stored energy and annealing characteristics. To understand the models implemented in GRSAC, some discussion of the complexity of the Wigner energy storage mechanisms in graphite will hopefully show what lead to the choices made in developing the models. These mechanisms are described in the following sections.

D.1 STORED ENERGY CONSIDERATION IN THE GRSAC MODEL

In its simplest form, the mechanism for energy storage in graphite is a displacement of carbon atoms from their equilibrium positions in a graphite lattice, where carbon atoms are trapped between the layer planes. The interstitial carbon atoms give up their energy when they recombine with lattice vacancies. The trapped carbon atoms, which are relatively immobile at low temperatures, thus "store" energy. High exposures at low irradiation temperatures produce even more complex damage to the graphite, with large values of stored energy release extending up to very high temperatures. Table D.1 shows the considerable potential for stored energy release to 1800°C for samples that were highly irradiated at a low temperature (30°C).[2]

Table D.1. Energy stored in graphite by low-temperature irradiation

Exposure at 30°C (MWd/AT)	Total stored energy (cal/g)	Up to 800°C (cal/g)	From 800 to 1300°C (cal/g)	From 1300 to 1800°C (cal/g)
575	210	160	35	5
2023	423	280	100	40
4965	630	275	170	175

The characteristics of graphite damage are particularly sensitive to irradiations at lower temperatures, from 30 to 150°C. Stored energy in graphite irradiated at 30°C can reach saturation values of about 650 cal/g. In most cases, the amount of stored energy released will not be this high. Power densities sufficient to generate such large amounts of saturated stored energy were found only in the Hanford reactors, although several hundred calories per gram could be stored in air-cooled reactors in the cooler regions of the graphite.

During a low-temperature irradiation, stored energy accumulates first in the lower annealing activation energy (temperature) regions and progresses to higher temperature regions, such that when all temperature regions are filled, at saturation, the stored energy release spectrum values approach the specific heat of graphite for all annealing temperatures.[3] Because of irradiation temperature sensitivity, more stored energy is found in the cooler regions of a moderator than in the center of the reactor where the neutron flux is actually higher. Thus, for air-cooled or water-cooled reactors, the largest amount of stored energy is found in the inlet fringe graphite, about 2 m from the inlet, where temperatures are low, yet where there is appreciable damaging flux. Coolant temperatures in an air-cooled reactor such as Windscale rise from 25°C at the inlet to 160°C at the outlet. The higher temperatures in the rear-most portions of the graphite stack nearly eliminate generation of stored energy there, as seen in Fig. D.1 for samples from Windscale measured at Chalk River.[4]

Direct-inlet, air-cooled reactors such as the Oak Ridge Graphite Reactor (ORGR), the Windscale reactors, and the French G1 all accumulated much less stored energy in their moderators than occurred in graphite irradiated in Hanford cooled test holes at 30°C. Recirculating CO_2-cooled reactors with higher graphite temperatures, such as the Calder reactors and the French G2 and G3 reactors, accumulated less stored energy per unit exposure because of higher operating temperatures. Moreover, graphite in these later reactors most importantly lacked a dominant 200°C annealing peak because of the higher operating temperatures.

If the temperature of irradiated graphite is raised above the irradiation temperature and if the release spectrum of the stored energy exceeds the specific heat of graphite, sufficient stored energy can be released to cause a spontaneous temperature rise in the graphite. This effect has been observed to be rate sensitive, where the faster the induced temperature rise, the more likely it is for the spontaneous release to occur.[5] This self-propagating temperature rise occurs quite rapidly and continues until the amount of energy excess, relative to the specific heat of graphite, is exhausted. During annealing of an actual reactor moderator, however, delays in the propagation can occur because of stack geometry, gaps between bars, and differences in stored energy remaining from previous anneals, such that a typical annealing may not be complete even after 24 hours. Latent stored energy releasable at temperatures higher than those achieved in the heatup remain after the annealing process, and stored energy can continue to build up with further irradiation. This accumulated stored energy is important for accident consequence prediction when temperatures encountered during an accident are higher than those reached during planned annealings.

GRSAC considers both the heat generated by the neutron moderation processes as well as the release of stored energy that builds up because of displacement damage.

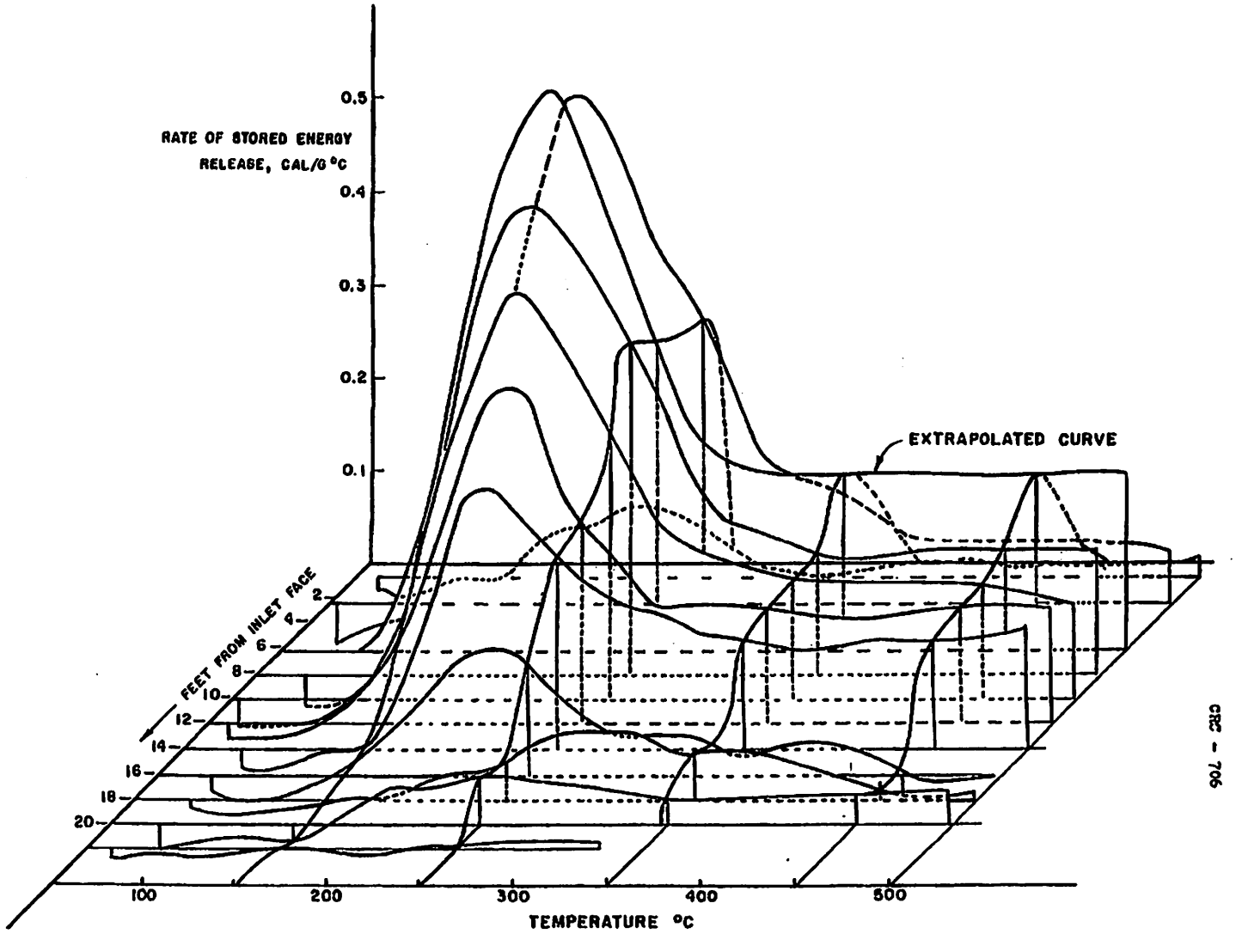

Fig. D.1. Stored energy release spectra spatial distribution in Windscale 1. *Source:* Attree et al.[5]

Wigner stored energy behavior is quite different for cases where graphite irradiation takes place at higher temperatures. In such cases, the total stored energy and its annealing characteristics are primarily related to total integrated exposure, and much less to the temperature of exposure. In addition, the stored energy is more uniformly distributed over all annealing activation energies as the exposure proceeds. As a result, the saturation values of stored energy (cal/g) are less in CO_2-cooled reactors than in air-cooled reactors, although the actual total energy accumulation can be large for cores with long exposures with no special annealing procedures.

Reductions in stored energy are achieved by elevating the graphite operating temperatures via design features, such as using gas gaps and insulating sleeves to separate the graphite from the cooling gas stream, as well as by increasing the core inlet gas temperature. These features were incorporated into the Calder Hall reactors.[6] Raising the inlet gas temperatures of the Calder reactors to ~145°C significantly limited the rate of stored energy buildup, changed its characteristics, and, particularly, avoided generation of a large 200°C release peak anywhere in the moderator. The optimum solution to this (and other problems) was, of course, the HTGR, where the entire core is above ~350°C and essentially no stored energy accumulates.

D.2 IMPLEMENTATION OF A STORED ENERGY MODEL IN GRSAC

The stored energy model used in GRSAC has the versatility to account for various conditions of exposure, including the spatial dependence of flux and irradiation temperature.[7] This model is based on data from many sources, including stored energy data reported on samples that were annealed and reirradiated.[8] This report provides insight on the 200°C peak regeneration after an annealing operation, which can occur after few hundred additional MWd/AT exposure.

Saturation of total stored energy (TSE) occurs when in-situ annealing completely offsets any further generation of Wigner damage. Saturated TSE varies with irradiation temperature, as shown in Fig. D.2, derived using data from several sources. The upper limit of total stored energy is ~650 cal/g for an irradiation temperature of 30°C. In this approximation, the saturated stored energy decreases linearly with increasing temperature, down to zero at 340°C. The GRSAC model first computes the saturation values of total stored energy for the irradiation temperature of each node in the core model. It is assumed that the total stored energy available for release is some fraction of the saturation value, and further reductions are usually made for other considerations (e.g., less than full-saturation exposures, or prior annealing). The overall reduction factor for total stored energy release can be modified via a user-input multiplier. The equilibrium value for stored energy in each node multiplied by this reduction factor controls the maximum total energy that can be deposited in that node during a GRSAC run.

Typical dS/dT stored energy release curves (cal/g°C) from Quetier's work are shown in Fig. D.3 and present data for several irradiation temperatures and exposures. These curves are characteristic of low-exposure, low-temperature graphite stored energy. The maximum exposures in Fig. D.3 do not exceed 300 MWd/AT, but such conditions for 200°C peak regeneration might represent the stored energy built up upon similar exposure after an annealing. While peak energy release is located at about 200°C, residual release tails extend to significantly higher temperatures. Also shown is the relationship between the release spectrum at each temperature and the corresponding value of graphite specific heat. If dS/dT exceeds the specific heat, the effective heat capacity of the graphite is negative and the temperature will rise quite rapidly until a thermal equilibrium is reached. GRSAC calculates the actual heat released whether or not dS/dT is greater than the specific heat.

The peak and tail values of dS/dT vary widely with different conditions of irradiation temperature and total exposure. In the 3-D stored energy release spectra representation for Windscale 1 (Fig. D.1), showing values from front to rear (inlet to outlet), values are inferred from samples irradiated in a test channel and measured by Attree. The samples were in isotope channel 27-50 (in the lower periphery

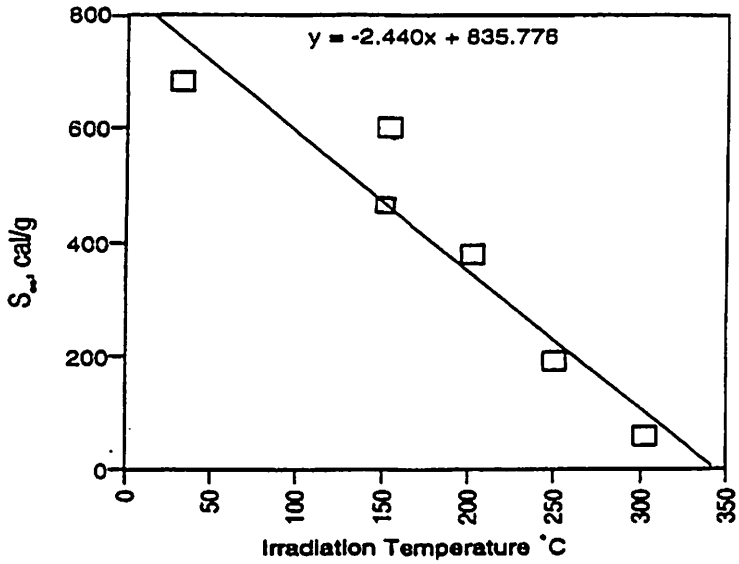

Fig. D.2. Saturation stored energy as a function of irradiation temperature.

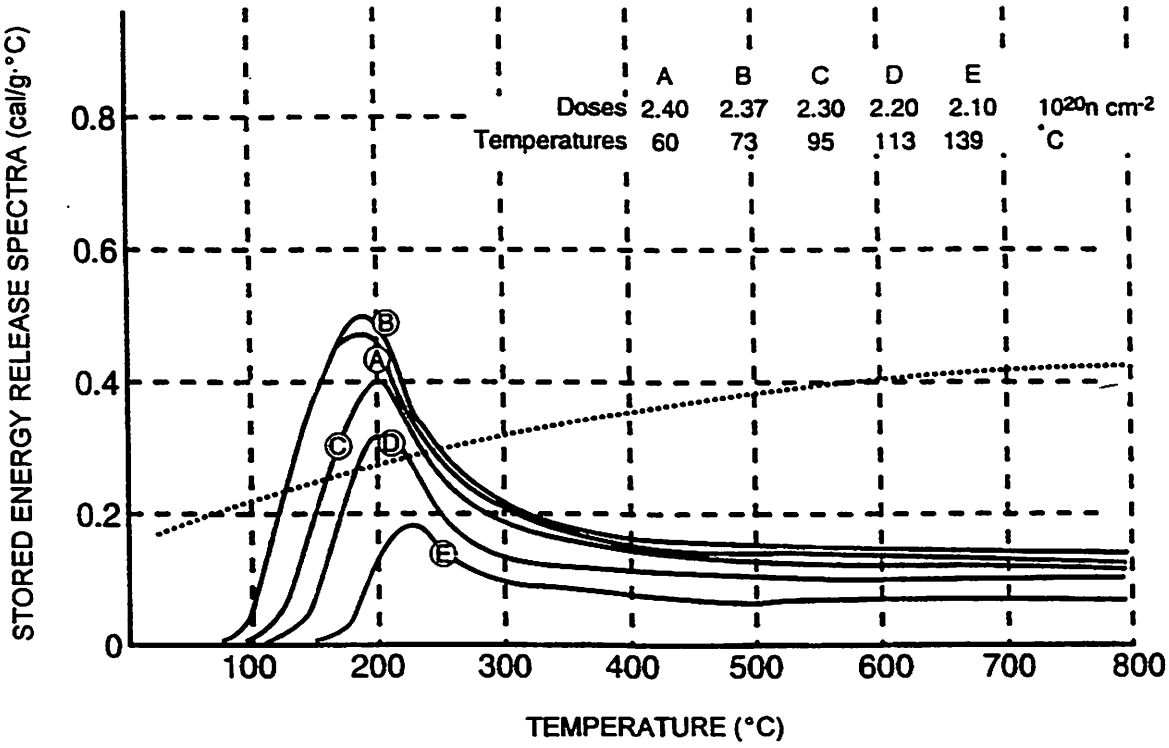

Fig. D.3. Stored energy release spectra for graphite irradiated at low temperatures.

of the active core), irradiated for 177,000 cumulative-pile MWd, and removed during planned anneals. The largest amount of stored energy measured in this set was 100 cal/g, taken from a sample located 2.1 m from the inlet where the temperature was typically 30–40°C.

The 200°C peaks in the dS/dT function are approximated in GRSAC with a triangular shape using an initial (leading edge) slope in dS/dT of 0.56 per 100°C, and a return (trailing edge) slope of 0.22 per 100°C towards a tail value. The peak diminishes both with increases in irradiation temperature and exposure, and can disappear completely. For a graphite node lacking a 200°C peak, the tail function continues to provide for the stored energy release. A dead band for the initiation of energy release has been observed in many experiments; that response is considered in GRSAC with stored energy release inputs beginning only after the calculated graphite temperature exceeds its irradiation temperature plus a dead band increment. The Reference Case in the Windscale 1 benchmark analysis used dead band for initiation of stored energy release set at 50°C.

Two functions are used in GRSAC to approximate the tail values of the dS/dT function for variations in exposures (expressed in MWd/AT) and irradiation temperature. Figure D.4 shows the stored energy function dS/dT (cal/g°C) vs irradiation temperature for the case where the graphite exposure was 2000 MWd/AT. Then to account for different exposures, the function shown in Fig. D.5 is used. This gives the ratio of dS/dT at the desired exposure to the dS/dT value calculated in Fig. D.4 for a 2000 MWd/AT exposure. The calculated stored energy function using Fig. D.5 (using the solid lines) is the most conservative (high value) representation of the data and would best apply to the Windscale benchmark calculation, accommodating the 30°C irradiation temperature data. Hence for Magnox (higher temperature) reactors, the user-input reduction factor should be applied. For example, the dashed (high temperature) line in Fig. D.5 represents a large amount of data from Calder reactors,[9] where the effect of a 200°C peak is greatly reduced (or absent), giving lower fractional values.

The flux distribution for steady state operation is used to derive multipliers that calculate exposure values for each core node. Because the "tail" portion of stored energy is not removed by temperature-limited annealing operations, a core average long-term exposure factor (in MWd/AT) is used (user input) to account for stored energy in the tail region. Because the dS/dT curve in the region of the 200°C peak may be annealed out periodically, however (e.g., Windscale annealing runs), a different core average short-term exposure factor (in MWd/AT) can also be used (user input) in such cases.

In the GRSAC model, stored energy release is delayed for a while after the graphite node reaches an annealing temperature. The calculated instantaneous release energy is added to an energy release "storage reservoir" with a 20-min time constant and is subsequently added to each node, incrementally, for every degree Celsius the node exceeds the irradiation temperature. This process is continued until all available stored energy is released. The maximum temperature attained in each time step is "remembered" by the program so that if this temperature is exceeded in subsequent time steps, additional energy will be added to the reservoir proportional to that temperature difference, then released into the graphite node, delayed by the 20-min time constant.

The GRSAC algorithm for stored energy is implemented for all graphite in the active core and side reflector, and in the nodes adjacent to the core in the inlet and outlet reflector. The total stored energy release rate is displayed on the computer accident screen in kilowatts, with plots of the release available via on-line dynamic plots or post-run plots.

D.3 REFERENCES

1. Arnold, L., *Windscale 1957—Anatomy of a Nuclear Accident*, St. Martin's Press, New York (1992).

2. Nightingale, R. E., J. M. Davidson, and W. A. Snyder, "Damage Effects to Graphite Irradiated up to 1000°C, *Progress in Nuclear Energy, Series V—Metallurgy and Fuels,* Pergamon Press, New York (1961).

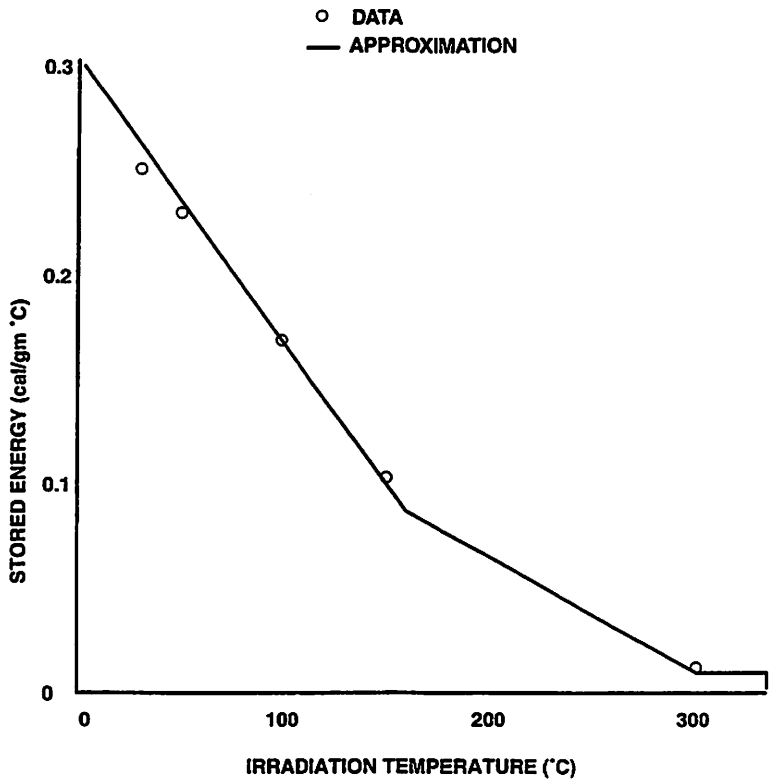

Fig. D.4. Wigner high-temperature ("tail") stored energy vs irradiation temperature for exposure of 2000 MWd/AT.

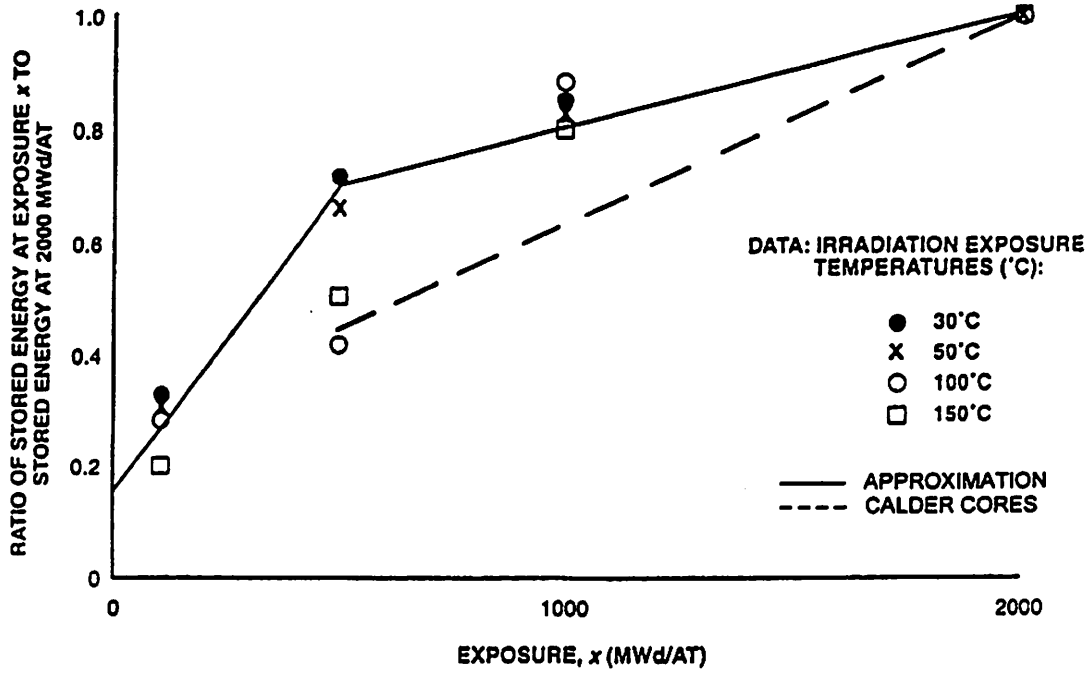

Fig. D.5. Wigner stored energy vs exposure: ratio of stored energy at exposure x to stored energy at 2000 MWd/AT.

3. Davidson, J. M., "Stored Energy in Irradiated Graphite," US/UK Graphite Conference, St.Giles Court, London, December 16–18, 1957, USAEC Report TID-7565 (Pt. 1) (1959).

4. Attree, R. W., R. L. Cushing, and J. Pieroni, "Stored Energy in Graphite Irradiated at Windscale and at Hanford," CRC-706, Chalk River, Ontario (1957).

5. Davidson, J. M. (Los Alamos National Laboratory), personal communications, May 1998.

6. Cottrell, A. H., and M. W. Thompson, "Stored Energy in Graphite," Informal Document, HS.9875X (1961).

7. Burchell, T. D, "A Simple Model for the Release of Stored Energy from Irradiated Graphite (draft)," internal correspondence, Nov. 30, 1995.

8. Quetier, M., and J. Rappeneau, "Energy Stored by Irradiated Graphite Variation of the Energy as a Function of Successive Annealings," pp. 208–218 in *Properties of Reactor Materials and the Effects of Radiation Damage,* D. J. Littler, ed., Butterworths, London (1962).

9. Bell, J. C., H. Bridge, A. H. Cottrell, G. B. Greenough, W. N. Reynolds, and J. H. W. Simmons, "Stored Energy in the Graphite of Power-Producing Reactors," *Proc. Royal Society,* Vol. 254(A), 1043 (1962).

APPENDIX E.
GRSAC BENCHMARK USING THE WINDSCALE ACCIDENT, OCTOBER 1957

E.1 DESCRIPTION OF WINDSCALE

E.1.1 Reactor Cooling Characteristics

Work on the first of two Windscale reactors began in 1947, about four years after the Manhattan Project's Clinton Reactor, later called the Oak Ridge Graphite Reactor. At that time, higher power water-cooled production reactors were already in operation at Hanford. The British were aware of both air-cooled and water-cooled technologies and preferred water cooling for their production reactors. However, they chose air cooling because of both safety concerns and siting difficulties in the UK for water-cooled reactors. The air-cooled Windscale reactors are similar to the Oak Ridge Reactor, with common features of once-through air cooling, horizontal flow, aluminum cladding, and metallic uranium fuel. Figure E.1 shows the loading face,[1] which has the appearance of a larger version of the Oak Ridge Reactor. A major improvement was use of extended surfaces as an integral part of the fuel element cladding, enabling improved heat transfer and higher power density.

Cooling air was forced into a plenum at the charge face, passed horizontally through the core into an exit plenum at the discharge face, through a duct containing fission product detectors, and into the base of a 400-ft stack capped by a set of particle filters. There was one blower house on each side of the main building, each containing four main blowers and two shutdown fans. Full-rated flow was about 1000 m^3/sec or about 1200 kg air/sec.

When essentially zero cooling was desired, as during a Wigner energy anneal, flow dampers at the outlet of each fan were shut and a hatch at the base of the chimney was opened, thereby breaking the vacuum created by the stack. Under these conditions, an estimated 0.01 to 0.05 kg/sec of air would pass through the core due to natural convection. Closing the hatches at the base of the chimney while keeping the dampers closed would, we assume, increase the cooling flow to about 0.3 kg/sec. The next step up in the air flow was achieved by opening the dampers, which raised the flow to an estimated 7.5 kg/sec. Turning on the four shutdown fans would create a flow of about 120 kg/sec through the core, about 10% of the full flow using seven of the eight main circulators.

E.1.2 Reactor Parameters

Not a great deal has been published regarding dimensions, power levels, and core loadings of the Windscale reactors. Moreover, sources often differ somewhat regarding particulars (e.g., precise dimensions, rated power level, and isotope channel loadings). Data gleaned from various sources are given in Appendix H.

E.1.3 Nodal Geometry

The GRSAC simulation uses 1630 nodes to approximate the Windscale active core, 163 radial nodes times 10 axial nodes. Each node is 70 cm in axial length and consists of 21.1 fuel channels and 5.28 isotope channels.

E.1.4 Sources of Information on the Accident Sequence

A basic source of information on the Windscale fire is provided in the recent comprehensive description by Arnold.[2] Arnold also provides a valuable historical perspective as well as an extensive

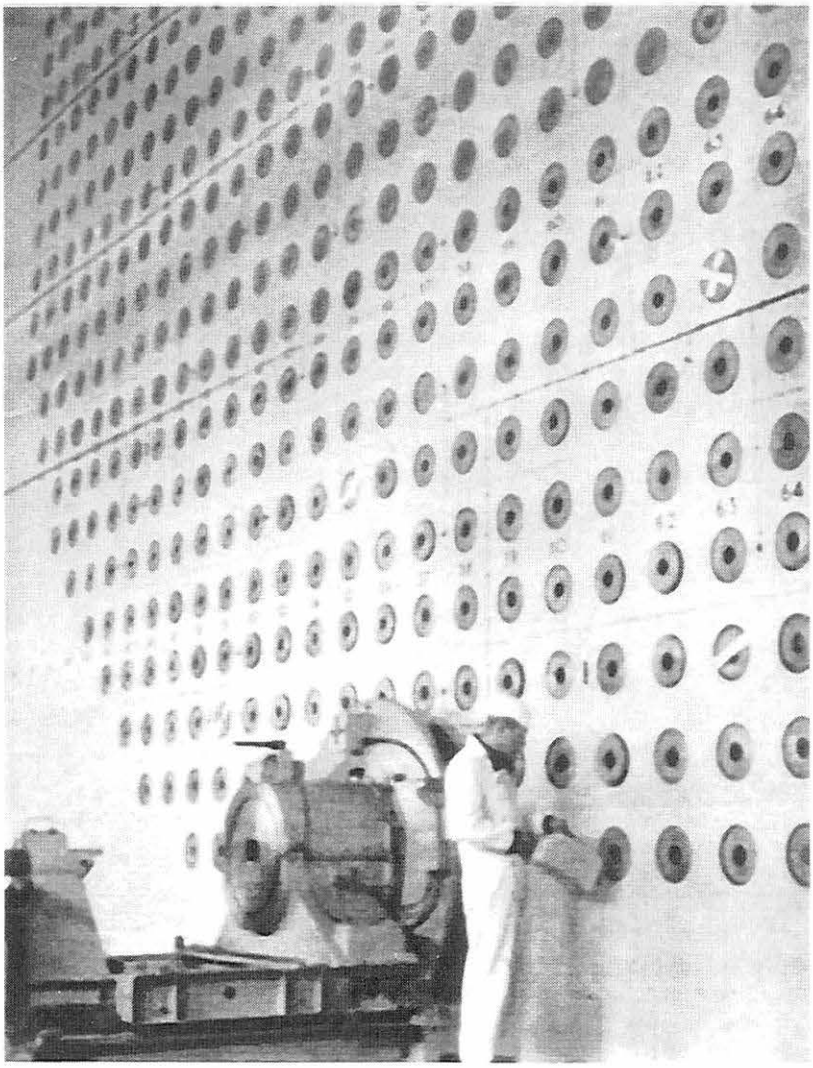

Fig. E.1. Loading face and charging machine.

list of references, much of which deal with details of the accident brought forward during a Court of Inquiry held only a few months later. Six other references,[3-8] all of which dealing with the accident sequence, were obtained from Arnold's book. Additional information on core loadings, stored energy release patterns, fuel element descriptions, AM cartridge failure, and other technical details exist at the Public Records Offices (PRO).[11] Material obtained from the PRO are given in the references, Section E.10, under the single designation of Ref. 9.

E.2 ACCIDENT DESCRIPTION AND CHRONOLOGY

E.2.1 Chronology

The five-day accident, from the first anneal through the termination of the fire, has been described in various publications, most recently in Chapter 4 of Arnold's *Windscale 1957.*[2] Her principal source appears to be the report of the Penney Inquiry[10] published in October 1957, several weeks after the accident. Command 302,[4] published in November, contains similar information. These reports in turn are based on testimony given in a "Court of Inquiry" conducted directly following the accident and on written statements by key personnel. The testimony and written statements have been preserved, though in rough form. In addition, several articles have been published describing the sequence of events, for example, "Windscale—The Committee's Report."[1]

Because of the sensitivity of the results to the details of sequence, an effort was made to verify the event chronology provided in summary reports with information given in testimony of the Court of Inquiry, with the written statements, and control room log data. A fairly complete record of occurrences is given in Sect. E.8, abstracted from the following sources: the Windscale Pile 1 Control Room Log,[11] Summary Table for the Event,[8] and the Testimony at the Court of Enquiry.[10] All three sources are integrated so that minor differences may be smoothed out. Additional items included from Arnold[2] are so identified.

It is beneficial to portray key events in a time line in order to visualize the interrelationships between observed events and operator actions. Figure E.2 shows critical events and actions in a the time line covering the full five-day period. The time line in Fig. E.3 focuses on the critical last 40 hours. Figure E.2 shows that there were two nuclear heatings, which was not a unique occurrence. Following the first heating, from Monday evening to early Tuesday, opinion was that a second heating was required as indicated by temperatures declining more rapidly than expected for a successful anneal.

The critical second nuclear heating was conducted from late Tuesday morning into the evening. A sharp rise in one of the measured uranium fuel element temperatures, from 80°C to 380°C, occurred within 15 min after the start of the second heating. (This particular peak was reduced by insertion of an adjacent control rod.)

The most readily combustible material in the core was the lithium component of the AM target cartridge alloy. The aluminum cladding of the cartridge begins to fail at 440°C (see Sect. E.4). Ignition of the target alloy occurs after a period of time that depends on temperature history. Therefore, it was concluded at the time that the most likely initiation was either burst or ignited AM cartridge(s) due to local temperatures exceeding 440°C during the second nuclear heating. A temperature spike of this magnitude was not observed at this time but may have escaped notice due to missing thermocouples.*

---

* The report of the Penney Inquiry[10] states a somewhat contrary opinion: "that the cause of the accident could conceivably have been the failure of the lithium-magnesium cartridge but that this was unlikely." Instead it states that, "the most likely cause of the accident was the combined effect of the rapid heating [during the second nuclear heating] and the high temperature reached by the fuel elements in the lower front part of the pile. In all probability, one or more end caps...were pushed off, and the uranium exposed." According to uranium oxidation rate models adopted in GRSAC, uranium oxidation would not contribute significantly to core heating below temperatures of about 700°C. On the other hand, lithium oxidation, if exposed by rupture of the AM cartridge, would significantly contribute heat at a much lower temperature, about 500°C. Our view is more in accord with later evaluations. The Hill Memorandum [summarized by Arnold[2] stated: "Oxidation of uranium had taken place fairly late in the chain of events." Also, "The AM cartridges were a principal factor . . . [A] single AM channel had led to oxidation of the graphite immediately around it, and this led to propagation of the fire." The Bowen Memorandum [summarized by Arnold[2]] is closest to our view that AM cartridge failure was the initial event, followed by a lithium and magnesium fire spreading to aluminum when its melting temperature was reached (660°C), a situation which turned critical when the shutdown fans were turned on.

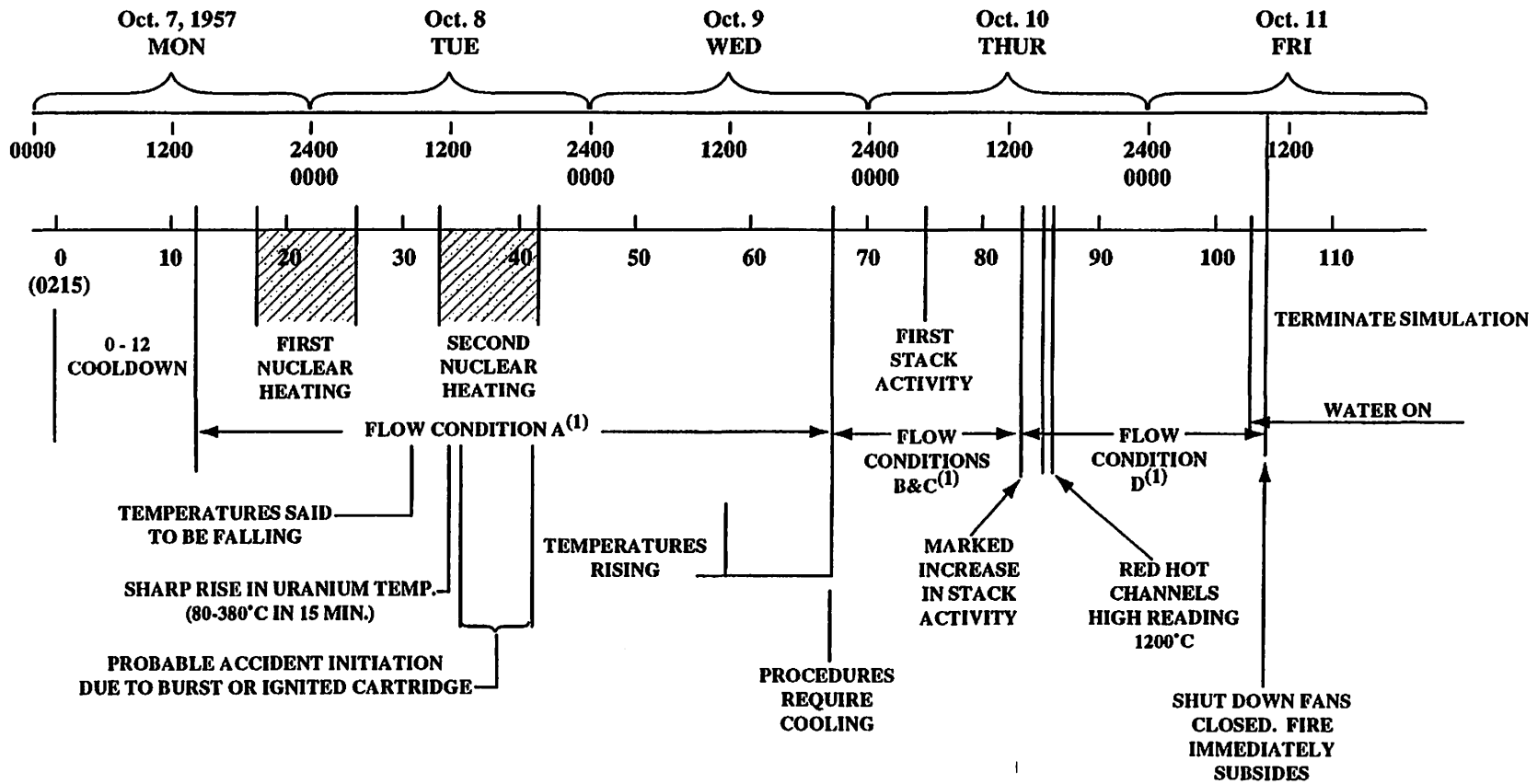

(1)FLOW CONDITIONS

A	0.01-0.05	kg/s	[Dampers Closed, Hatch Open]
B	0.3	kg/s	[Dampers Closed, Hatch Closed]
C	7.5	kg/s	[Dampers Open, Hatch Closed]
D	~120	kg/s	[Shutdown fans on]

Fig. E.2. Windscale accident time line—5-day overview.

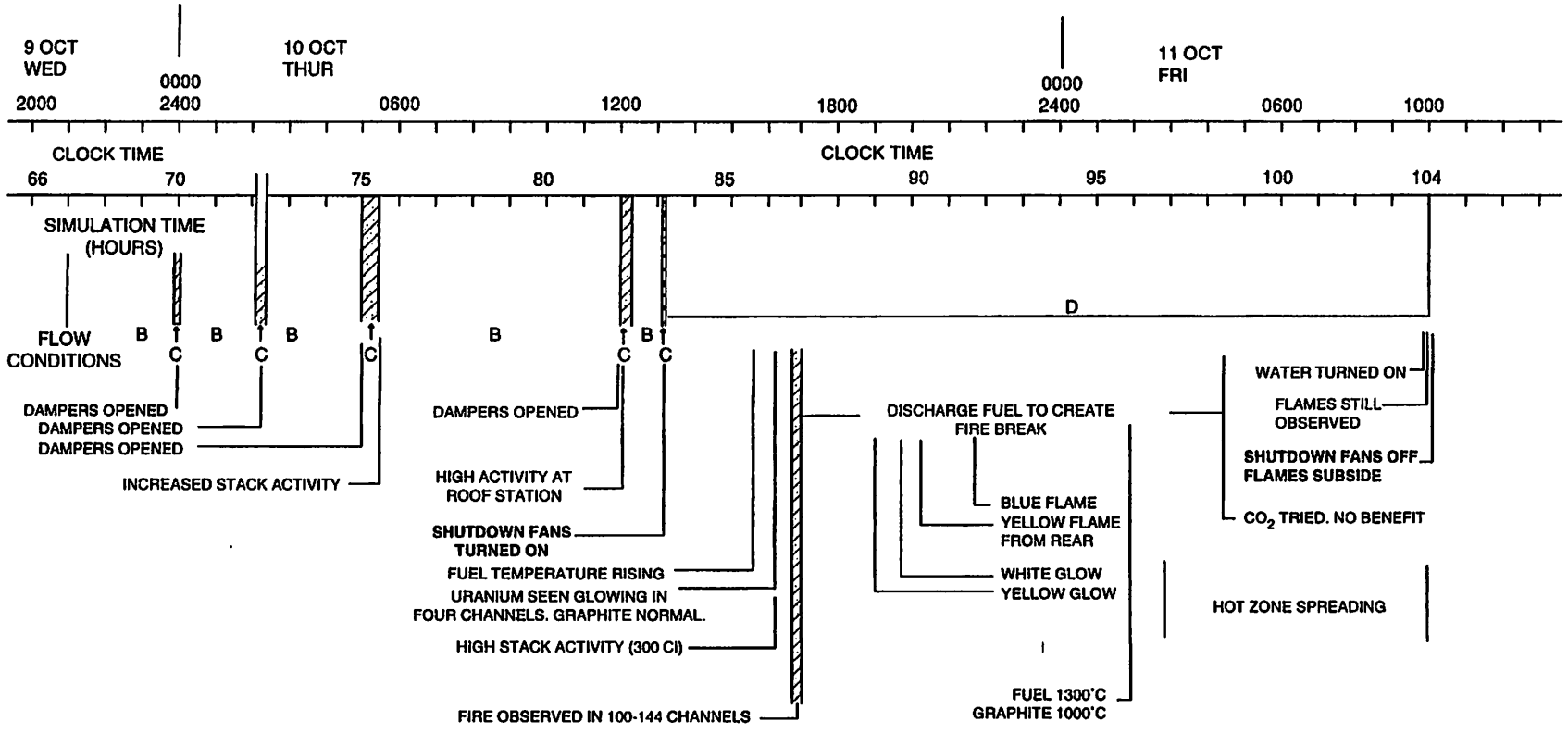

Fig. E.3. Windscale accident time line—final 40 hours.

As shown by the time line, no major operator actions occurred during the next 25 hours. Air flow through the core was maintained at its lowest possible level—flow condition A in the figure. Some thermocouples indicated a gradual rise in temperature during the latter half of this period, in retrospect caused either by local oxidation of leaking AM cartridges broken in the second nuclear heating or by a continuation of the Wigner energy release. In view of following events, the consensus at the time was apparently that the former was more likely. GRSAC estimates of Wigner release are considerably larger than what AM cartridges would have produced. In such cases of observed temperature excess above, procedures called for increased air flow to produce a cooling effect [see Appendix III of Ref. 2, and Section E.5]. Therefore, late Wednesday an incremental increase flow was generated by sealing the hatch at the base of the chimney causing a flow increase (assumed to be about 0.3 kg/sec, flow condition B in the time line).

In Sect. E.5, the effects of increased air flow on an overheated core are discussed qualitatively. Briefly, a cooling effect is achieved provided temperatures are below some specific value. Above this temperature, which depends on the particular geometry and materials, increased air flow has the opposite effect of generating increased oxidation, which intuitively may be called "fanning the flames."*

In retrospect, the subsequent period, from 2200 Wednesday to 1000 Friday, is just such a time of exacerbated oxidation resulting from periodic increases in air flow. This period is shown with more detail in Fig. E.3. From this time (2200 Wednesday), air flow was never reduced back to condition A. Instead, the chimney hatch was kept shut and the dampers were repeatedly opened (flow condition C) causing increased air flows assumed to be about 7.5 kg/sec. The increased air flow at 2200 Wednesday, by closing the hatch at the base of the chimney, followed by the three episodes of damper openings early Thursday, did not succeed in lowering core temperatures. A marked increase in stack activity was observed following the third damper opening. A fourth damper opening at about noon Thursday was similarly followed by high activity reading, this time at the meteorological station on the roof of the reactor.

Finally, at 1330 Thursday, the shutdown fans were turned on (flow condition D), increasing air flow to about 120 kg/sec. The shutdown fans remained on until the end, at 1000 Friday. It was hoped the fans would cool the pile, which momentarily seemed to be the case. However, there were soon reports of high activity readings at the roof station (at 1350), and the highest recorded uranium temperature began to rise, rapidly reaching 460°C. The previous concerns regarding pile behavior gelled at this point into the realization that a serious event was in progress.†

From the time that the shutdown fans were turned on (1330 Thursday), the core condition steadily deteriorated. Glowing fuel and graphite was observed at 1700 Friday involving from 100 to 144 channels, and progressively higher temperature flames were seen emanating from the rear face of the core. In addition, there were indications that the involved zone was spreading radially. As a calculated risk, water from a fire truck was introduced into the core at 0900 Friday. Flames continued emanating from the rear of the core. According to the Penney Inquiry,[10] the fire immediately subsided on shutting off the shutdown fans at 1000 Friday. This action cut off oxygen and suffocated the fire. Water flow continued, finally cooling the core.

E.2.2 Estimated Core Damage

A detailed description of the damage suffered by the Windscale core has not been published. What appears clear is that a relatively few fuel channels were involved, although there were

---

* Arnold (Ref. 2, p. 90) notes that "in 1954 there was reference to cooling air 'fanning the flames' if too high a temperature was reached."

† The account in Arnold[2] errs at this point by stating that the main blowers were turned on at 1430, Thursday. Instead, the "turbo exhausters" were turned on in preparation of scanning the pile for burst cartridges.

indications of gradual radial spreading towards the end of the accident. According to the Penney Inquiry,[10] 150 fuel channels out of the 3440 total were observed glowing red (at 1630 on Thursday), signifying temperatures of about 700°C. This indicates that 4.4% of the fuel was involved in the fire, counting the entire axial length of each channel, which was not the case. The fire involved a fairly slim axial column of material in the core.

According to a later reminiscence by Sir John Cockroft, a member of the Penney Inquiry, some 10 tons of uranium were melted during the accident, amounting to about 6% of the total amount of uranium (reported by Arnold[2]). There is no indication of the basis of this estimate. If based on noble gas release (see section below), it would be difficult to distinguish between molten or oxidized uranium. We have found no mention of the degree of aluminum damage.

A highly informative memorandum by Hill[6] written for the Penney Inquiry states that probably most of the AM cartridges were burned away in the observed area of red hot uranium, which, at the time the plugs were first removed (1400 Thursday), extended over an area 10 feet by 8 feet.

B. S. Smith et al.[12] tried to estimate the scale of core damage from noble gas concentrations monitored at air stations downwind. The method is a bit tricky, and possibly may be improved using modern software. The problem is that ^{131m}Xe, the isotope on which the estimate was based, is a decay product of ^{131}I. Therefore the source of ^{131m}Xe observed in the plume may have been (1) direct release of ^{131m}Xe from damaged fuel, (2) decay of ^{131}I released from fuel and escaping capture in the stack filters, (3) secondary release from ^{131}I deposited on the ground. A further complication is that correlations differ for release from damaged fuel differ for xenon vs iodine (see Appendix C). How these problems were sorted out is not made clear in the brief report; however, Table E.1 presents damage estimates based on three assumptions.

Table E.1. Windscale damage estimate based on noble gas release

Assumption	Quantity of fuel melted	Number of channels
1. No iodine retention on filters	8.9 tonnes	156
2. Filters retain 50% of iodine	9.3 tonnes	164
3. No iodine released	11.0 tonnes	193

Source: Smith et al. (Ref. 12).

Since the rate of xenon release from exposed uranium depends on the temperature of overheat, amount melted, and the amount of fuel oxidized (iodine release depends mainly on the degree of uranium oxidation; see Appendix C), the term in the table "quantity of fuel melted" properly should read "quantity of fuel overheated, molten or oxidized." But the estimate is consistent with both Cockcroft's recollection and the observed involvement of about 150 channels reported by the Penney Inquiry.

From the account by Arnold[2] (page 74) based on the Gausden Report,[7] inspection of the core after the accident by looking down fuel channels revealed that both fuel and graphite appeared undamaged for a distance of about 6 feet from the charge face. Further on, damaged graphite and blocked channels with "mangled and melted fuel" were visible. "Of 180 tonnes of uranium in the core, about 22 tonnes were not recovered; it was estimated that 5 tonnes had been burned, and that 17 tonnes remained in the core." In terms of percentages, these estimates are equivalent to about 3% of the uranium oxidized, and an additional 10% melted. No mention is made of degree of graphite damage. A concurring estimate is that 20 tonnes of uranium could not be removed from the core and remain in place to date.

E.2.3 Fission Product Release

Subsequent to the estimate of Smith et al.,[12] several surveys of radioactivity release were published which could serve as indicators of core damage. A good summary is given in Appendix IX of the Arnold book,[2] and some of the estimates are given in Table E.2. Noble gas data are most useful for unfolding the degree of core damage from monitored radioactivity release because there are no uncertainties introduced by adsorption on filters or other plateout effects. Volatile iodine, and the less volatile cesium, are also useful. Other fission products such as strontium, tellurium, and others become less useful for this purpose due to large uncertainties in degrees of plateout and fractional release from damaged fuel. Observed tritium release is useful for assessing damage sustained by the AM cartridges. Arnold [2] makes no note of noble gas release, though some estimates undoubtedly have been made. Arnold also notes that according to Command 1225,[5] 168,000 Ci of ^{131}I were retained in damaged fuel elements and 30,000 Ci ^{131}I were retained on the filters in the stack.

Table E.2. Estimated volatile fission product releases to the atmosphere, curies

	Command 1225[5]	Beattie[13]	Clarke[14]	Chamberlain[15]
Krypton	–	–	–	–
Xenon	–	–	–	–
Iodine-131	20,000	20,000	16,200	27,000
Cesium-137	600	600	1,230	–
Tritium	–	–	–	100,000 (?)

Source: From Arnold (Ref. 2, Table A.4, p. 185.)

E.3 WIGNER ENERGY RELEASE MODEL FOR WINDSCALE

The stored energy release model used for Windscale has been described in Appendix D. The same basic model is also used for Magnox reactors, with different input parameters—that is, radial and axial power peaking factors and graphite temperatures.

E.4 WINDSCALE-SPECIFIC OXIDATION RATE EQUATIONS

Use of aluminum cladding in combination with the lithium/magnesium alloy as target material for production of tritium is unique to Windscale as an early plutonium production reactor. Later reactors use magnesium cladding for its lower absorption cross-section and avoid a volatile metal like lithium for safety reasons. In addition, the irradiated Windscale graphite was clearly more reactive to oxidation than the nuclear graphites used in the derivation of the GRSAC oxidation model. (Appendix A describes the graphite oxidation model used in GRSAC for other reactors.) These three Windscale-specific items are discussed below.

E.4.1 Windscale Graphite Oxidation

Nairn and Robinson[16] measured the oxidation rate of numerous sets of Windscale graphite, including one set acquired immediately prior to the accident. Figure E.4 shows a summary of test results. The upper set of data labeled "AG x /P" refers to graphite samples removed from pile 1

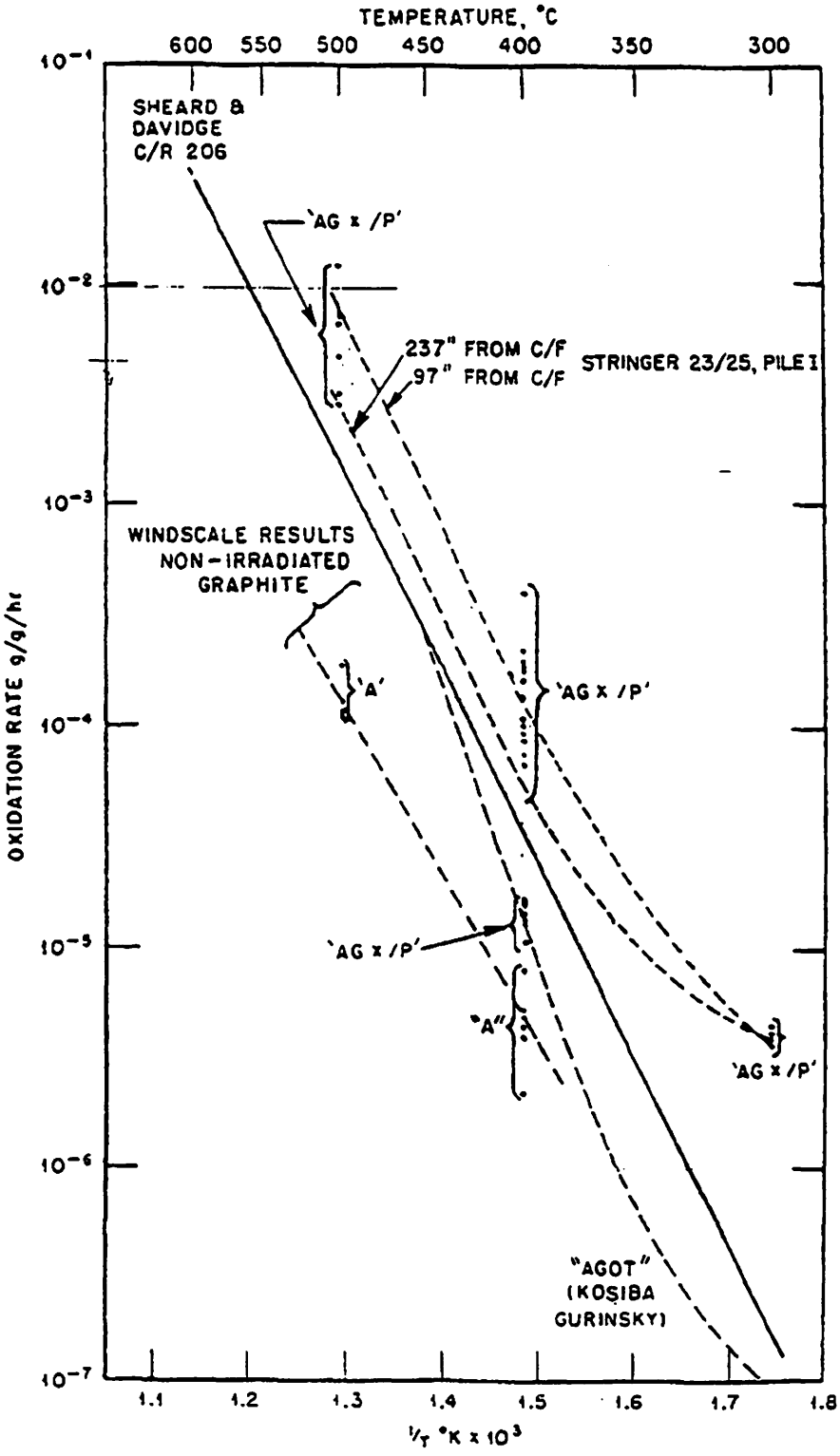

Fig. E.4. Windscale graphite oxidation rates. Source: Nairn and Robinson (Ref. 16).

directly before the accident. The solid line through these points represents the starting point for the correlation used in GRSAC for oxidation of Windscale graphite in the chemical control regime. This line is represented by the following equation:

$$R = 2.12 \times 10^7 \exp(-20{,}277/T) \qquad \text{(E.1)}$$

where R is the oxidation rate [g/(g·min)] and T is the graphite temperature (K).

Equation (E.1) predicts an oxidation rate (Windscale graphite) that is 244 times higher at 400°C and 28 times higher at 1200°C than predicted for the graphite samples from which the GRSAC reference-case oxidation model were derived (see Section A.5). As discussed in Appendix A, these extremely high intrinsic rates may not actually be achieved because of inhibition by the rate of oxygen transport to the surface. Besides the effects of long-term irradiation, the higher oxidation rates observed are commonly believed to have been aggravated by sea spray and oil-based contaminants from blower lubricants. However, published references supporting this theory have not been found.

The upper points in the figure labeled "AG x /P" at temperatures 400 and 500°C are for irradiated Windscale graphite removed just prior to the accident. Note, there is a range of about a factor of two in the data. The lower set of points labeled "AG x /P," for unirradiated graphite, exhibited about a factor of ten lower oxidation rate. Equation (E.1) represents the solid line drawn to the irradiated graphite data. Equation (E.1) needs to be augmented to account for depth of oxidation penetration into a large block and variation of oxygen pressure with time and along the channel. For the latter, it will be assumed that the reaction rate is first order with oxygen pressure, as in Appendix A. Since these tests were performed in air, multiplying by the oxygen pressure of air, $P(O_2)$, and dividing the premultiplier by 0.21 accounts for the variation of oxygen pressure according to this assumption.

Accounting for the depth of oxidation is more problematic. Large moderator blocks do not oxidize uniformly as a mass except at extremely low temperatures. As a result, units of R in terms of grams oxidized per gram mass per time are inappropriate for large blocks. Conversion to surface units of moles/(cm^2·time) is accomplished by multiplying R(1/time) by the factor (ρ Δh/MW), where

ρ = graphite density, g/cm^3 (about 1.5 g/cm^3 for Windscale graphite);
Δh = depth of oxidation penetration, cm;
MW = molecular weight of graphite, 12 g/mol.

For the value of Δh, post-accident testimony by Wright (Ref. 17, p. 1-39) offers the following snippet:

> "Q: . . . were [these experiments] done with graphite 7 inches thick?
>
> Wright: . . . the experiments were done on quite small samples, but we found no effect of sample size.
>
> Q: This is in fact a deduction on your part that air would get into 4 inches into the graphite and that the CO_2 would get out again.
>
> Wright: It is an extrapolation from some experiments made on specimens. I think as thin as 1/2 inch and as thick as 3 or 4 inches."

The reports describing these tests, if indeed there were any, are likely well buried in archives. We interpret Wright's response to mean that oxidation was uniform throughout 3-in.-thick samples tested at 400°C (400°C was mentioned several times in earlier testimony). Assuming the same functional dependence of Δh on temperature as used for later nuclear grade graphites [Appendix A, Eq. (A.3)] yields the following for Windscale graphite:

$$\Delta h(\text{Windscale}) = 6.9 \times \Delta h(\text{reference}), \quad \text{(E.2)}$$

that is, the oxidation reaction penetrates 6.9 times deeper in the graphite, according to this assumption than in the reference nuclear-grade graphite. These considerations lead to the following graphite oxidation rate equation for Windscale graphite:

$$R = 1.01 \times 10^8 \exp(-22{,}899/T)\, P(O_2)\, (\Delta h\, \rho/MW) \quad \text{(E.3)}$$

where

R = oxidation rate, mol/(min·cm^2);
$P(O_2)$ = oxygen pressure, atm.

E.4.2 Aluminum Oxidation

Finned aluminum cladding was used for the fuel elements; unfinned cladding was used for the isotope targets. Magnesium is to be preferred due to lower neutron absorption, but fabrication technology was not fully developed at this early date. On the other hand, aluminum does have a better oxidation resistance than magnesium.

A significant feature of aluminum oxidation as an important factor in the propagation of the Windscale fire was use of extended surfaces to enhance heat transfer. There was an estimated 3.2 m^2 of aluminum fin surface in each cooling channel plus 0.6 m^2 cladding surface, providing a high surface-to-volume ratio. We have found no specific, dimensional description of the aluminum fins. Arnold (Ref. 2, Appendix V) states that six different designs were used. Some reports show these included both longitudinal and transverse fins. The later designs, Mark VI and X, used longitudinal fins with about 160 grams of aluminum per element.

The general method for metal oxidation used for uranium and magnesium, described in Appendix B, applies as well to aluminum. Namely, (1) acquire a heterogeneous oxidation rate correlation from the literature, obtained under conditions that ensure chemical control, and (2) test at each location and time step if mass transport of oxygen to the surface limits the rate. An additional step, required for magnesium, is testing for "true burning"—that is, vaporization and gas-phase oxidation. This appears not to be required for aluminum due to its lower (than magnesium) vapor pressure. Thus far we have not found a correlation for aluminum oxidation in a temperature regime that may be extrapolated to temperatures seen in the Windscale fire. Possibly the reason is that often the rate of aluminum oxidation reflects the diffusion rate of oxygen through the adherent oxide film rather than the inherent oxidation rate of the metal. In such case, the observed rates depend mainly on the thickness of the film.

An example of this behavior is the widely divergent values reported for the ignition temperature of aluminum. For example, ignition tests conducted by Abbud-Madrid et al.[18] on various metals failed to ignite aluminum. They cite earlier tests in which aluminum was ignited at 2054 °C, approximately the melting temperature of the oxide. In agreement, Markstein[19] reports an ignition temperature of 2303 °C. In contrast, Grosse and Conway[20] report 580 °C, based on an earlier work. Epstein[21] reports 1170 °C.

Clearly, the ignitability of aluminum depends on whether or not conditions permit an intact oxide film. Under quiescent conditions, the film appears to protect the base metal well above the melting point of the metal. Under vigorous conditions, aluminum may ignite in the vicinity of its melting point, 660 °C. In view of these factors, we have adopted the following approach based on the view that Windscale conditions were closer to physically aggressive rather than quiescent:

1. We assume that the aluminum oxide film is protective of the base metal up to 640°C, or 20°C below the melting temperature. Oxidation rates below 640°C are assumed sufficiently slow such that oxidative heat addition to the accident is insignificant.

2. Above 640°C, we currently use the heterogeneous oxidation rate correlation for magnesium [Eq. (B.7), Appendix B], since we have not found an equivalent correlation for aluminum.

3. The above relation is used when oxidation is not inhibited by O_2 diffusion to the surface. The method for estimating O_2 diffusion to the surface is described in Appendix A.

Data reported in Appendix B indicate that aluminum vapor pressures around 1000°C are about 10^{-5} that of magnesium. Therefore, the "true burning" model described in Appendix B for magnesium is likely not required for aluminum.

E.4.3 AM Cartridge Failure and Oxidation Model

An approximate model for the failure, subsequent oxidation and energy release for the AM isotope cartridges in Windscale was developed based on information supplied in the Windscale Court of Enquiry testimony (Saddington testimony in Ref. 17, p. 2.5 and following). Arnold (Ref. 2, Appendix VI) summarizes the out-of-pile AM cartridge tests succinctly:

The cartridges resided in isotope channels located at the center of each block of four fuel element channels. For one isotope channel for every four fuel channels, that gives a total of 3444/4 = 861 isotope channels. The information we have to date is not clear on how many of these 861 channels had AM cartridges in them, or what else was in the channels besides the AM cartridges. Currently, we are assuming that all of the space for isotope cartridges was occupied by AM cartridges containing lithium/magnesium alloy for the production of tritium. Although some lead weights were used in the channels to keep the cartridges from getting blown away by the main blowers, these should not have had any effect on oxidation behavior. The target material in the AM cartridge was a 1-in.-diam rod of lithium/magnesium alloy consisting of 11.5 to 13.0 wt % lithium (about 30 to 40 at. %).[17] The rod was sheathed by a 30-mil aluminum tube.

Both liquid lithium and magnesium are incompatible with aluminum, which accounts for failures being initiated at 440°C, well below the melting temperature of the alloy, 588°C. (The phase diagram for these alloys shows a convergent two-phase liquidus/solidus temperature at 588°C at this composition.) Initiation of failure at 440°C was undoubtedly caused by intimate contact of magnesium and aluminum creating an alloy with a broad eutectic at 450°C. As temperatures increase, the time to failure is expected to be reduced.

To account for the time-at-temperature dependence of failure illustrated in Table E.3, for the variable-temperature situations in the accident, a counter algorithm is implemented for the cartridges in each core node. The counts per time step fed to the counter is a function of temperature, as shown in Fig. E.5. When the count reaches 12,000/DT (where DT is the time step, min), the cartridges in that node are assumed to have failed. For example, with a 5-min time step and a steady core node temperature of 450°C (corresponding to 100 counts per time step), failure would occur after 2 hours.

The heat of oxidation released from oxidation of the alloy of the given composition due to a failed cartridge was estimated to be between 71,305 and 61,314 Btu (total, including the cladding) by witnesses at the Enquiry.[17] A value of 64,000 Btu is used in GRSAC. Experiments showed the capsules to oxidize completely (in air) in about 1 hour. Due to the likelihood that oxygen is depleted in the isotope channels during the critical heatup period, the oxidation period (after failure) was arbitrarily assumed to be 4 hours (at a uniform rate).

Table E.3. Mark III AM cartridge failure rates[2,17]

Temperature	Failure and ignition behavior
550°C	All failed in 30 minutes. One ignited.
450°C	All failed in 1–10 hours. Some caught fire.
440°C	All failed after 34 hours.
425°C	All intact after 59 hours.

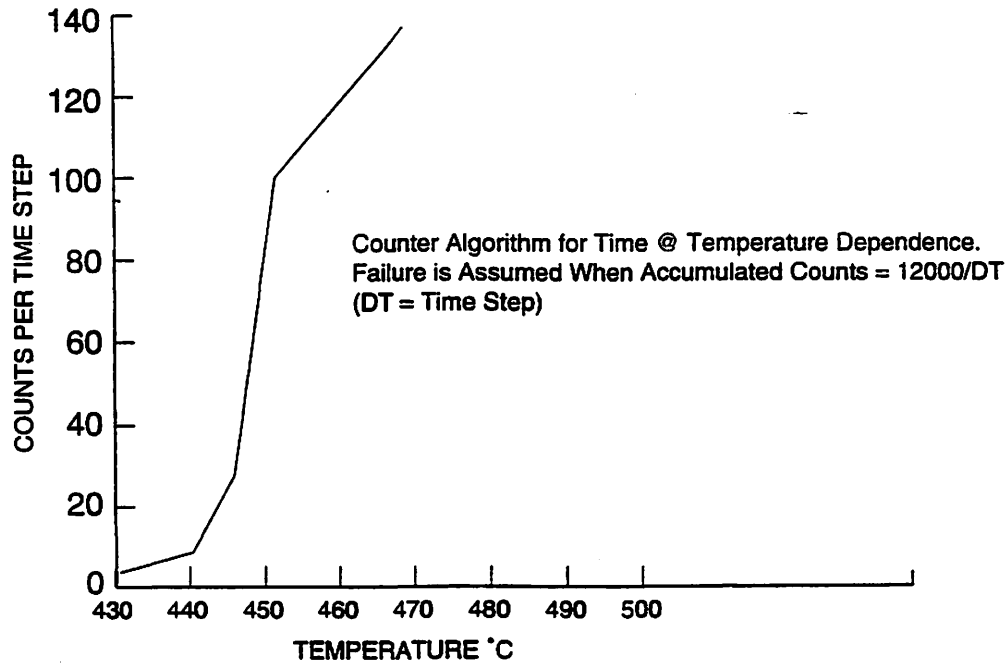

Fig. E.5. Lithium-magnesium cartridge oxidation model.

E.5 QUALITATIVE DISCUSSION OF THE ACCIDENT

E.5.1 Sequence of Initiating Events According to Post Accident Studies

Several evaluations soon after the accident sought to gain an understanding of its initiation and progression. Arnold (Ref. 2, Chapter 8) summarizes these, including the Report of the Penney Inquiry,[10] the closely related White Paper,[4] the Bowen Memorandum,[3] and the Hill Memorandum.[6] All place the initiating event in the time of the second nuclear heating, beginning 1100 Tuesday. The first two cite fuel cartridge failure and uranium ignition as the most likely first source of fire. The latter two studies disagree, citing AM cartridge failure as a more likely initiator. The memorandum by J. M. Hill[6] is especially forceful, having the advantage of firsthand experience. It is worthwhile quoting from portions of this memorandum to highlight several important features of the accident.

> "During the whole of the period between the end of the second nuclear heating and the discovery of the fire it is clear that the whole reactor was finely balanced between safety and catching on fire. At the time the fire was discovered it is clear that heat was being produced from the burning of the AM cartridges, the oxidation of graphite and the combustion of uranium metal."
>
> "[O]xidation of uranium did, in fact, take place fairly late on in the chain of events and I do not believe there was any substantial oxidation of uranium prior to the increase in activity on the stack filter chambers which was recorded at about five o'clock on the morning of Thursday, 10 October."
>
> "[W]hen the charge plugs were first removed and the red hot uranium was discovered [at about 1700 Thursday] there was no apparent center for the fire but rather we had a large area of the pile, perhaps ten feet by eight feet, over which all the channels were at very nearly the same red hot temperature. At the edge of this zone, the temperature fell rapidly over perhaps a distance of two pitches from being red hot to quite undamaged. . . . This could have resulted in two ways, either the second nuclear heating burst within a few minutes several hundred cartridges, . . . or, the mechanism which spread the fire or defined the area of the fire was extremely temperature dependent. . . . I do not see how a few uranium cartridges, slowly oxidizing could readily have led to the uniform temperature distribution that was observed."
>
> "The AM cartridges have a very sharp eutectic at 436°C, and the extreme temperature dependence of the integrity of these cartridges leads me to believe that they were the principal factors in determining the extent of the fire zone."
>
> "The AM cartridges could not have been the sole cause of the fire. . . . I believe that it was the oxidation of graphite in the area immediately surrounding the fire in a single AM channel that provided the bulk of the heat necessary to propagate the fire to adjacent channels."
>
> "On the cause of the rapid rise in temperature during the second nuclear heating it is clear that this was due to the abnormal manner in which the pile was being started up . . . to deliberately . . . produce a distorted flux pattern. The pile did come to criticality more rapidly than had been expected . . . ."

There is one omission in this account, and also one contrary observation that casts doubt on the full exposition expressed in this memo. The omission, apparently common to the three other studies cited at the beginning of this section, is failure to account for aluminum oxidation. Scoping GRSAC runs show that oxidation of aluminum, beginning at about 640°C, is a significant factor in propagating the fire to uranium. According to correlations used in GRSAC, uranium oxidation would not contribute significantly up to temperatures of roughly 800°C. Aluminum oxidation achieves such temperatures by virtue of its large surface-to-volume ratio embodied in the extended surface (fins) on each fuel cartridge. There are uncertainties regarding aluminum oxidation due to its adherent oxide film (see Sect. E.4). However, under the vigorous conditions of the core under incipient fire, particularly with the shutdown fans turned on, the oxide film would very likely not be completely protective as the base metal approached and surpasses its melting temperature of 660°C.

The contrary observation is cited in the testimony of the Court of Inquiry[17] by the operator first observing the glowing red fuel cartridges at 1700 Thursday. The operator stated that the uranium glowed red but the graphite surrounding the glowing fuel appeared at its normal black color. This first

hand observation clearly runs counter to the view expressed by the Hill Memorandum that the fire was propagated (from a burning AM cartridge) by means of a progression from graphite oxidation to fuel.

E.5.2 Effect of Varying Air Flow

Further understanding of the events leading to the fire requires examination of the complex relationships between varying air flows and overheated or smoldering material in the core. Procedures prescribed cooling down the core by means of increasing the air flow when observed temperatures reached certain levels. As noted in the time line, Fig. E.3, the heating and anneal periods were usually conducted in a regime of quite low air flow, estimated as 0.01 to 0.05 kg/sec (flow condition A), achieved by opening the hatches at the base of the chimney and shutting the dampers on each blower.

According to Arnold (Ref. 2, Appendix III), operating staff were instructed to shut the chimney hatches, increasing the flow to about 0.3 kg air/sec (flow condition B), if the highest graphite or uranium temperature reached 380°C. If temperatures of 400°C were observed, instructions called for opening the dampers on all circulators located in the blower houses, further increasing air flow to about 7.5 kg/sec (flow condition C). If temperatures of 415°C were observed, instructions called for activating all four shut down fans, elevating the flow to about 120 kg air/sec (flow condition D).

As noted in the time line, a campaign of increased air flow began at 2100 Wednesday, with alternating flow conditions B and C until 1330 Thursday, when the four shutdown fans were turned on. The fans stayed on until 1000 Friday, when the fire was terminated by shutting them off. Cooling the core with increased air flow had worked in all previous cases, but the concept fails when temperatures exceed some critical value. This was noted by an unknown designer in 1954, but not followed up; e.g., Arnold (Ref. 2, p. 90) states, "in 1954 there was reference to cooling air 'fanning the flames' if too high a temperature was reached."

The idea of a dividing line between cooldown and "fanning the flames" is illustrated in Fig. E.6. All lines drawn in this figure were generated in a side calculation using models in GRSAC, with the exception that normal air concentration of oxygen is assumed in all cases. The provision in GRSAC for depleting oxygen due to oxidation was not used, and flow redistribution among channels was not accounted for. (GRSAC provides for the reduction of flow in hotter channels due to higher flow resistance.) The figure is intended as an illustration of the concept of "fanning the flames" and not to quantitatively specify transition temperatures. The curved line shows the graphite oxidation rate as a function of temperature, as given by Eqs. (E.1) and (E.2). The horizontal lines illustrate the restrictions on the chemical rate due oxygen mass transport limitations under flow conditions A, B, C, and D. Beginning at 500 K (227°C) and assuming the upper limit of flow condition A is in effect, increasing temperature causes an increase in graphite oxidation rate up to the mass transfer limit of 2×10^{-5} mol/(cm^2·min). This limit is reached, according to the figure, at about 540 K (267°C). Further temperature increase cannot cause higher oxidation rate without flow alteration; that is, the rate moves parallel to the abscissa along the dotted line. However, if the air flow rate were increased to flow condition B while the graphite temperature is below this limit of 540 K (267°C), cooldown would occur. The enhanced oxygen mass transfer would have no effect, since it is not limiting, while the higher heat transfer coefficient at the elevated flow rate would affect cooling.

Progressing to higher temperature, if at 700 K (427°C) the hatch were closed initiating flow condition B, the graphite oxidation rate would jump about a factor of four to the new mass transport limit, 8.2×10^{-5} mol/(cm^2·min). Further temperature increase at this point would again not generate a higher oxidation rate; the rate moves parallel to the abscissa until the next step increase in flow to condition C. In other words, "fanning the flames" occurs whenever the air flow rate is increased under conditions of oxygen mass transport limitation. Cooldown occurs whenever the flow is increased while the oxidation rate is in the chemical control regime.

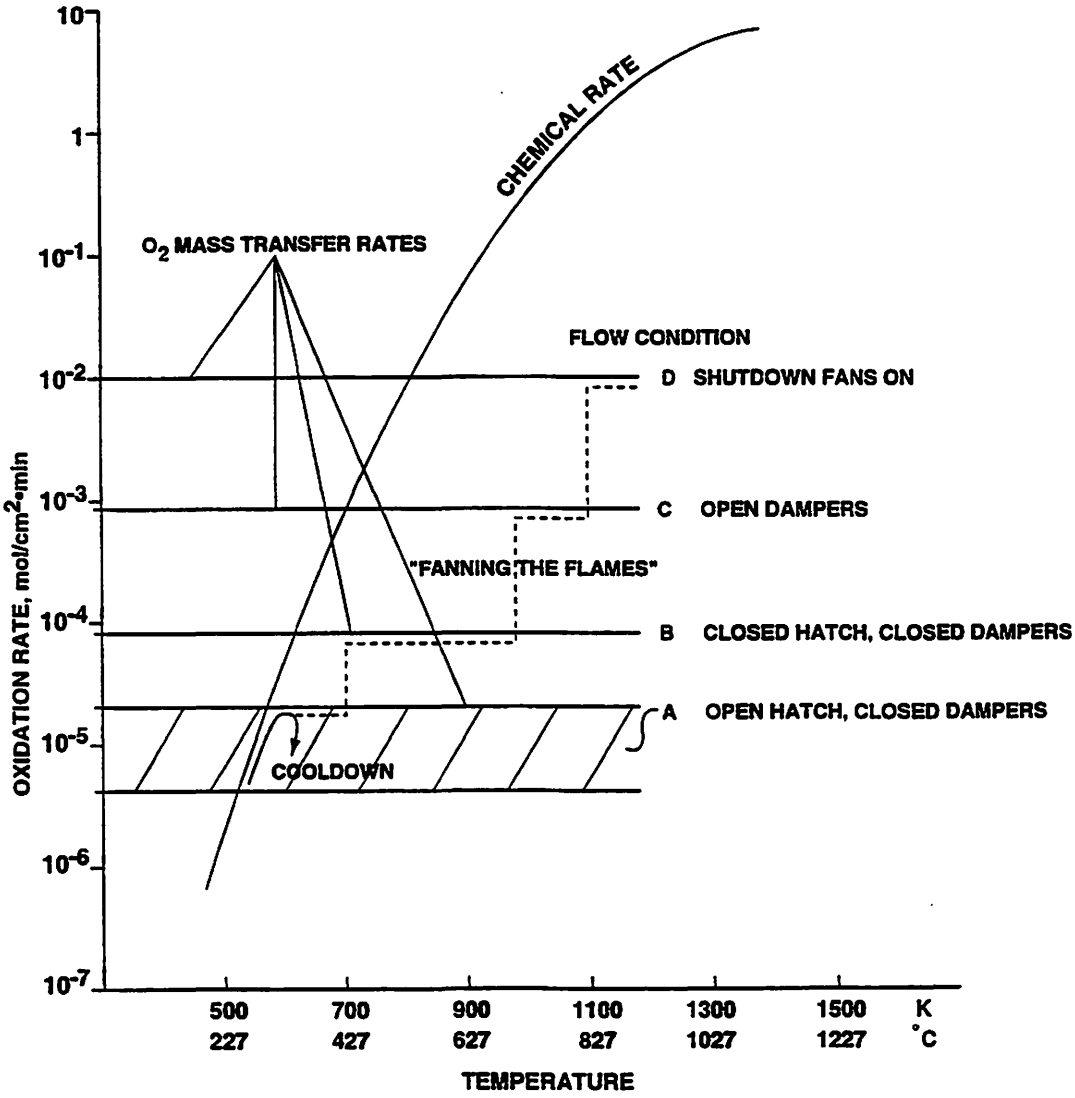

Fig. E.6. Comparison of graphite chemical control and mass transfer control oxidation rates.

E.5.3 Predicted Transition Temperatures

On these bases, the predicted transition temperatures (between cooldown and fanning the flames) for each flow transition are listed in Table E.4. The GRSAC prediction for the flow transition C to D was in the range 520 to 540°C.

Given the uncertainties in the graphite oxidation rate predictions for Windscale cited above, as well as the additional complications from AM cartridge oxidation, all of these predicted transition temperatures are somewhat uncertain. The important point is that the operational directives for increased shutdown cooling are at least near the predicted cooldown/fanning the flames transition temperatures for each required flow transition. In addition, graphite temperatures read by the operator were also uncertain due to an absence of thermocouples in some critical locations. Therefore, higher core temperatures than those indicated by the thermocouple readings may have existed.

Table E.4. Summary of Windscale operations directives (Arnold,[2] App. III)

Flow transition	Windscale operations directives	Predicted
Flow Condition A to B	380°C	267°C
Flow Condition B to C	400°C	337°C
Flow Condition C to D	415°C	427°C[a]

[a]GRSAC estimate ≈ 520°C.

Under these circumstances, a very likely supposition is that the operational requirement calling for increased shutdown cooling flow, based on a maximum thermocouple reading, occurred at a time when some portion of the core exceeded the cooldown/fanning the flames transition limit, the net result being higher core temperatures at the critical location rather than cooldown.

E.5.4 Summary Qualitative View of Windscale Accident Initiation and Early Propagation

In summary, the following are the most likely key events leading to the fire:

1. Prolonged nuclear heating concentrated near the central inlet section of the core.

2. Initiation occurred due to a combination of Wigner energy release and AM cartridge failure during the second heating period. Since the first observation of the hot zone showed an affected area of 100 to 140 channels, multiple AM cartridge failures must have occurred throughout this volume of the core.

3. The AM cartridge failures released a range of liquefied metals—mixtures of aluminum, magnesium, and lithium. The liquid metals may have attacked graphite integrity in the vicinity. Local ignition must have occurred.

4. In the 25 hours following the second nuclear heating, localized zones of oxidation spread, though quite slowly due to extremely low air flows during this period. The precise chemical nature of the incipient fire is not known, but it probably spread through the highly reactive Windscale graphite.

5. Increases in air flow beginning late Wednesday (but before the shutdown fans were activated) hastened the spread of the oxidation zone. Local zones must have been at sufficiently high temperature to be in the "fanning the flames" regime. Aluminum ignition probably occurred during this time, which in turn affected the uranium. Finally, after the third and fourth damper openings, radioactivity is detected in the stack. This is the first indication of uranium involvement.

6. The final step was turning on the shutdown fans which truly exacerbated the fire. The fire terminated on cutting off the shutdown fans.

E.6 SPECIAL MODIFICATIONS TO GRSAC FOR WINDSCALE ACCIDENT SIMULATIONS

E.6.1 Reference-Case Windscale Model Features

The Windscale reactor model is set up to represent a generalized air-cooled horizontal core, but with several special options to facilitate the modeling of Windscale-1 behavior in general and the October 1957 accident in particular. The Windscale default data set specifies air as the coolant, atmospheric pressure, and horizontal flow. A special Windscale accident screen is also implemented. Operator/analyst-controlled changes in fission power inputs (corresponding to annealing run inputs) and changes in the primary and shield cooling air flow can be done from the accident screen. Arbitrary programmed sequences of fission power and flow can be set up in advance of the run from the programmed input screen.

The shifting of the peak power (for the annealing heatup) to the inlet end of the core is done by adjusting the axial peaking factor (APF) curve accordingly before the start of the accident run. The curve used for the reference-case Windscale accident runs is shown in Fig. E.7. The corresponding input curve for the radial peaking factors (RPFs) is shown in Fig. E.8 (note that the four central RPF points are off scale). These peaking factors were derived from 1957 post-accident calculations by B. Cutts of Risley [Ref. 9 (AB ref. 86/61)]. For the Windscale accident case, the APFs and RPFs for normal Windscale operation (Figs. E.9 and E.10) are used to determine the distribution of afterheat power.

An annealing model for graphite node thermal conductivity is included as a GRSAC option. The model was developed and used for the MHTGR in the ORNL MORECA code,[22] which was GRSAC's predecessor. It was incorporated here because of the large (up to a factor of ~40) increases in Windscale graphite conductivity that can occur upon annealing and, hence, may be crucial in the predictions of Windscale annealing transients. In the MHTGR core, irradiation temperatures were in the range of 500°C, with the effective start of annealing at ~1000°C and with full annealing occurring at ~1300°C. Data presented by Nightingale[23] indicate that for the early Hanford (and Windscale) graphites with very low irradiation temperatures, the annealing effectively starts at much lower temperatures. Per a recommendation from Jim Davidson (LANL), data derived for CSF graphite from the Nightingale reference were used to approximate Windscale graphite. They were incorporated into the MORECA hysteresis model for both the radial and axial conductivities as functions of temperature (see Figs. E.11 and E.12). In the figures, TLO is a reference low temperature (85°F), TSA is the temperature for start of annealing (175°F), and TFA is the temperature for full annealing (2300°F). Values of conductivity K (in Btu/hr·ft·°F) are indicated on the figures at key points in the algorithm. Example heatup/cooldown paths on the figures are used to illustrate the hysteresis effect.

An approximate model was added to GRSAC to correct the core conductance heat transfer for the additional resistance due to gaps between elements. This model accounts for radiant heat transfer and conduction through the gas in the gap. The original MORECA code model was altered to account for the very low temperature conditions (with air as the coolant) seen in Windscale.

The inclusion of the annealing and gap models in the calculation is an option selected via the Wigner energy model flag (1 = Wigner energy only, while 2 = Wigner energy and thermal conductivity annealing with gap resistance models [both]; 0 = omit Wigner and annealing). The Wigner flag values of 1 or 2 are the reference or default cases for Windscale transients, where power and flow inputs are entirely "manual," that is, are input either as a preprogrammed input or changed during the run via the interactive accident screen. Setting the flag = 3 enables a preprogrammed approximation of the October 1957 accident sequence, as described below.

An approximate model for the failure and subsequent oxidation and energy release for the AM isotope cartridges in Windscale was developed based on information supplied in the Windscale Court of Enquiry testimony[17] and other data developed by Bob Wichner (ORNL) (see Sect. E.4.3).

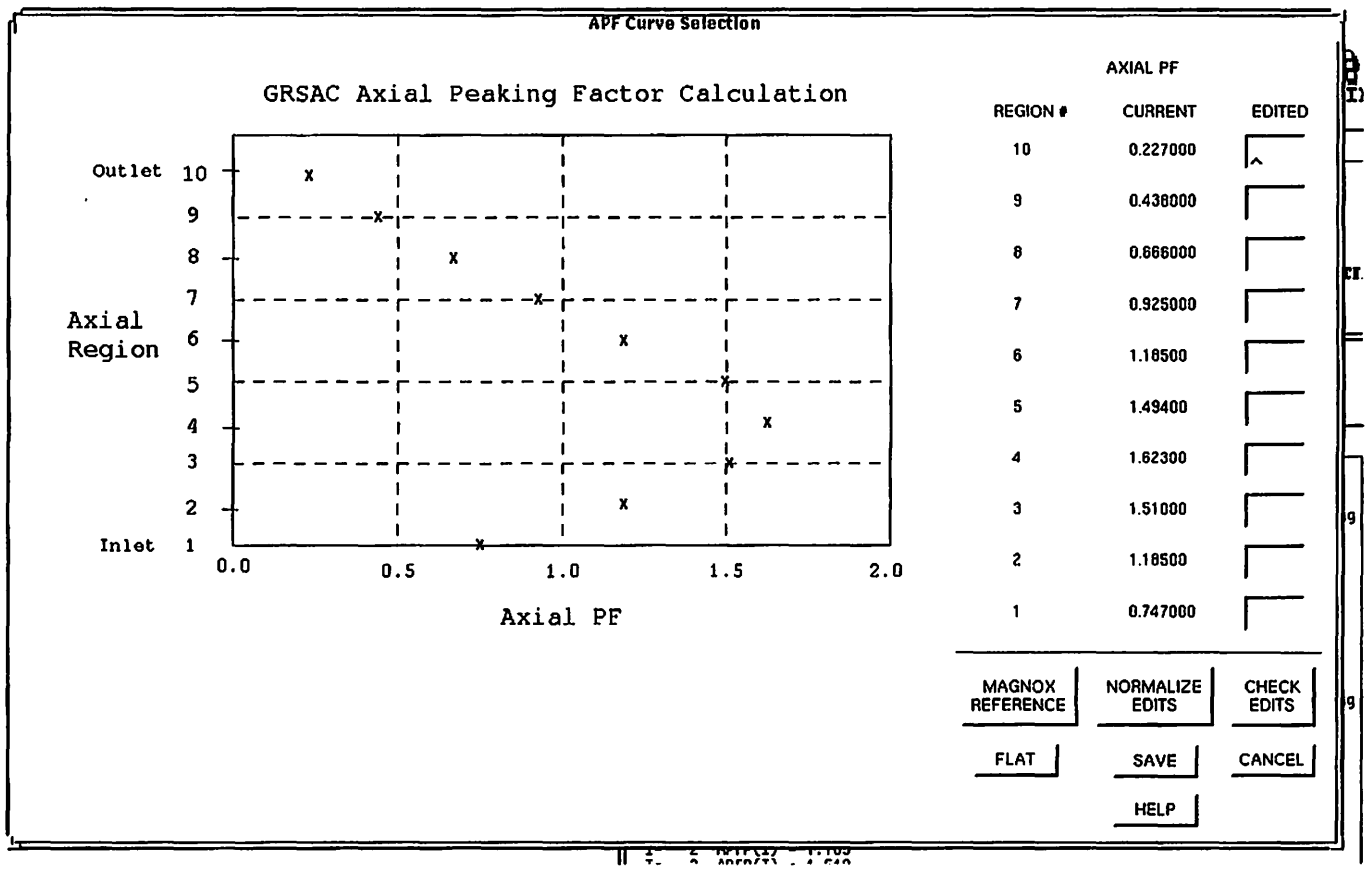

Fig. E.7. Windscale accident reference GRSAC case: Axial peaking factors (APFs) for fission power during the accident.

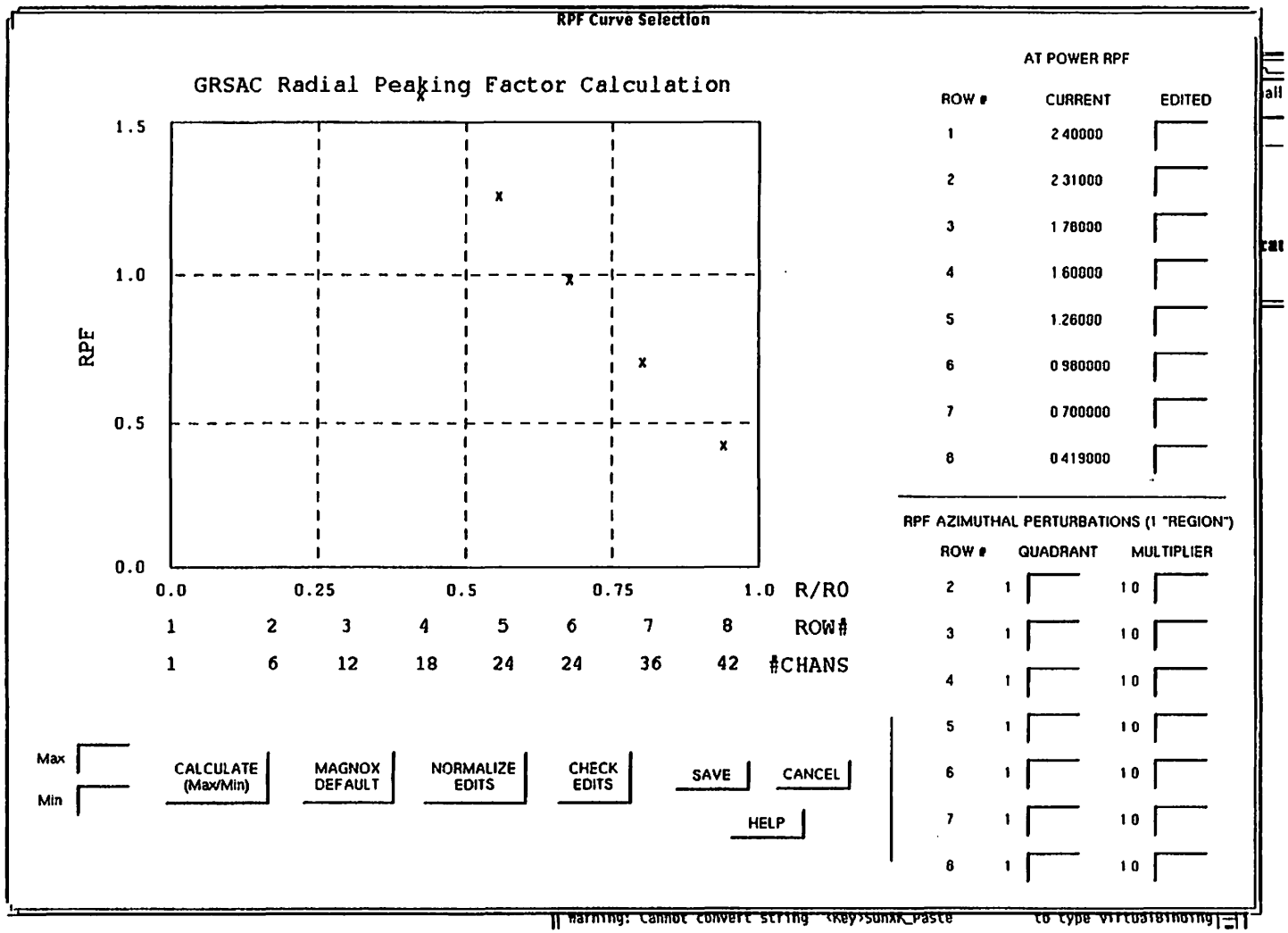

Fig. E.8. Windscale accident reference GRSAC case: Radial peaking factors (RPFs) for fission power during the accident. (Note: Points for rows 1 through 4 are off scale on the graph.)

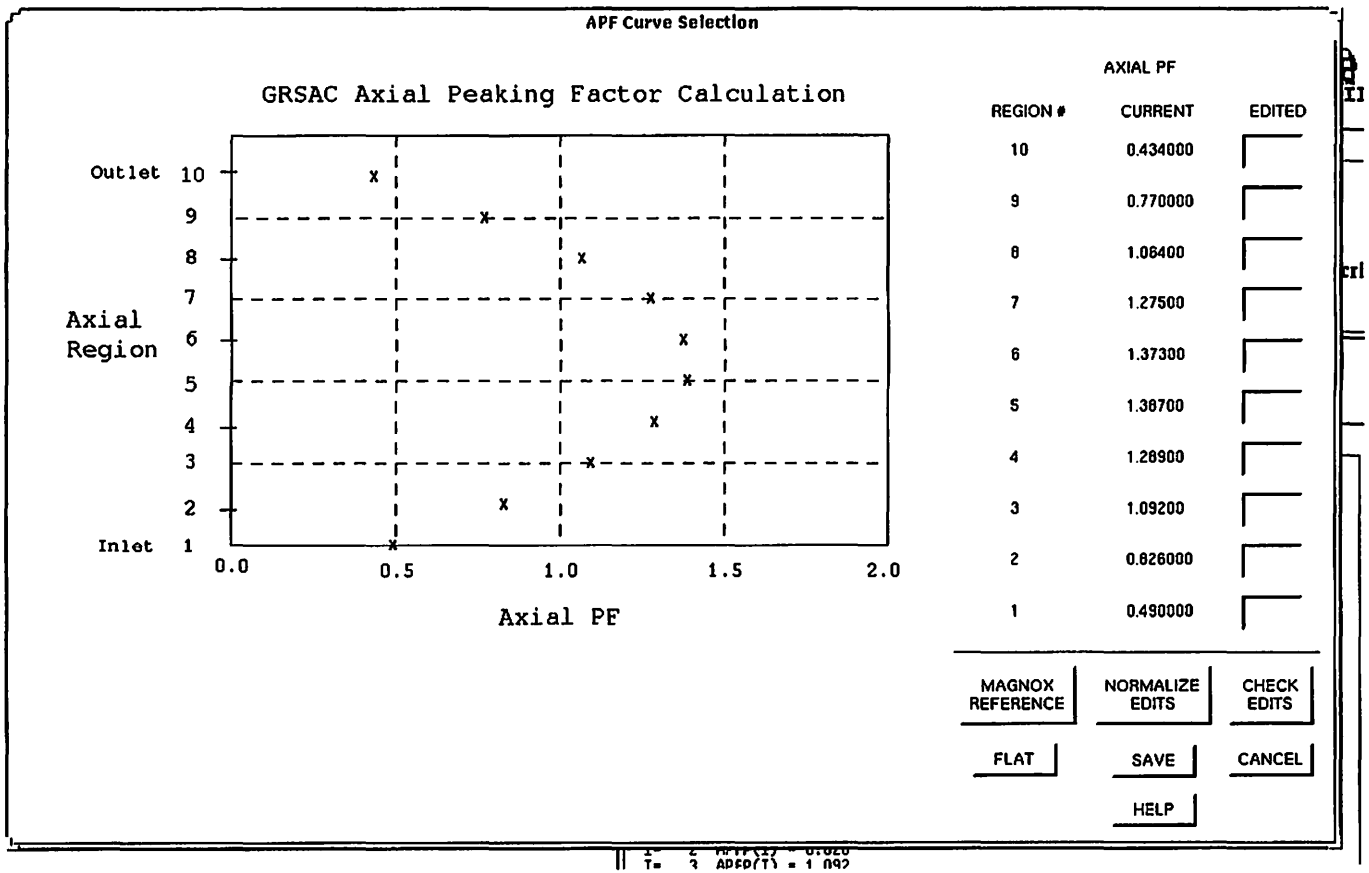

Fig. E.9. Windscale accident reference GRSAC case: Axial peaking factors (APFs) for normal operation.

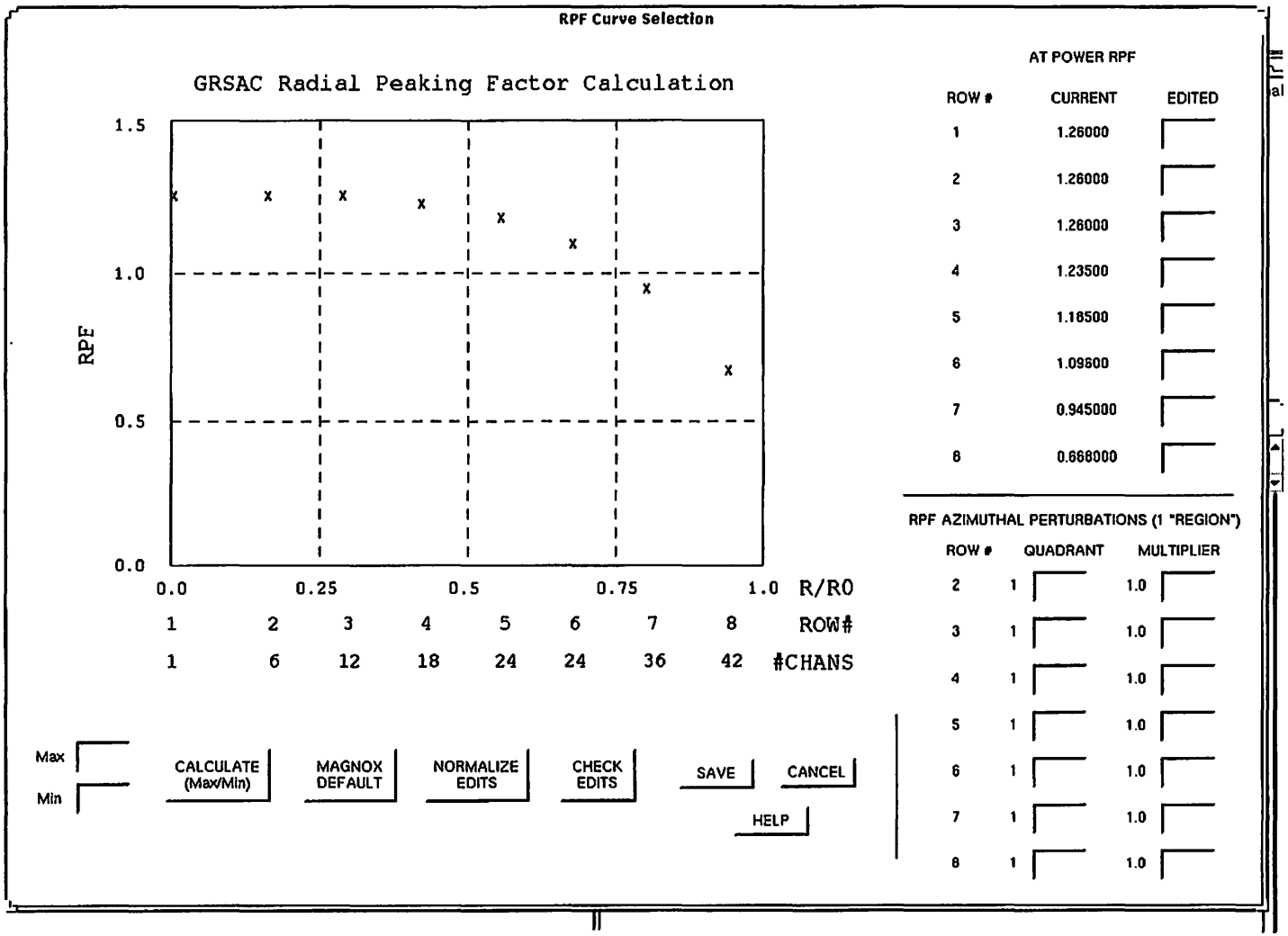

Fig. E.10. Windscale accident reference GRSAC case: Radial peaking factors (RPFs) for normal operation.

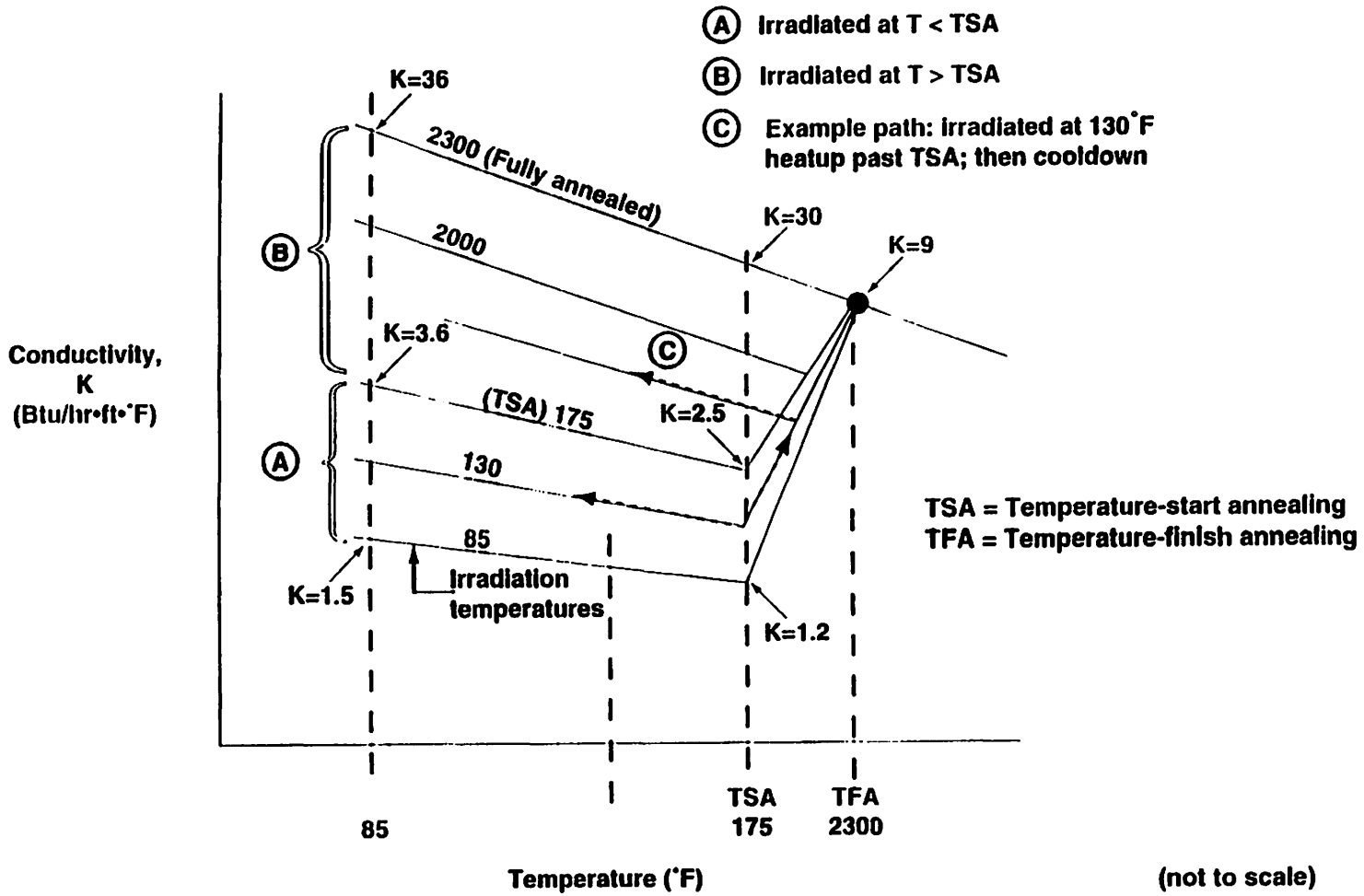

Fig. E. 11. Windscale accident reference GRSAC case: Annealing map for core radial conductivity.

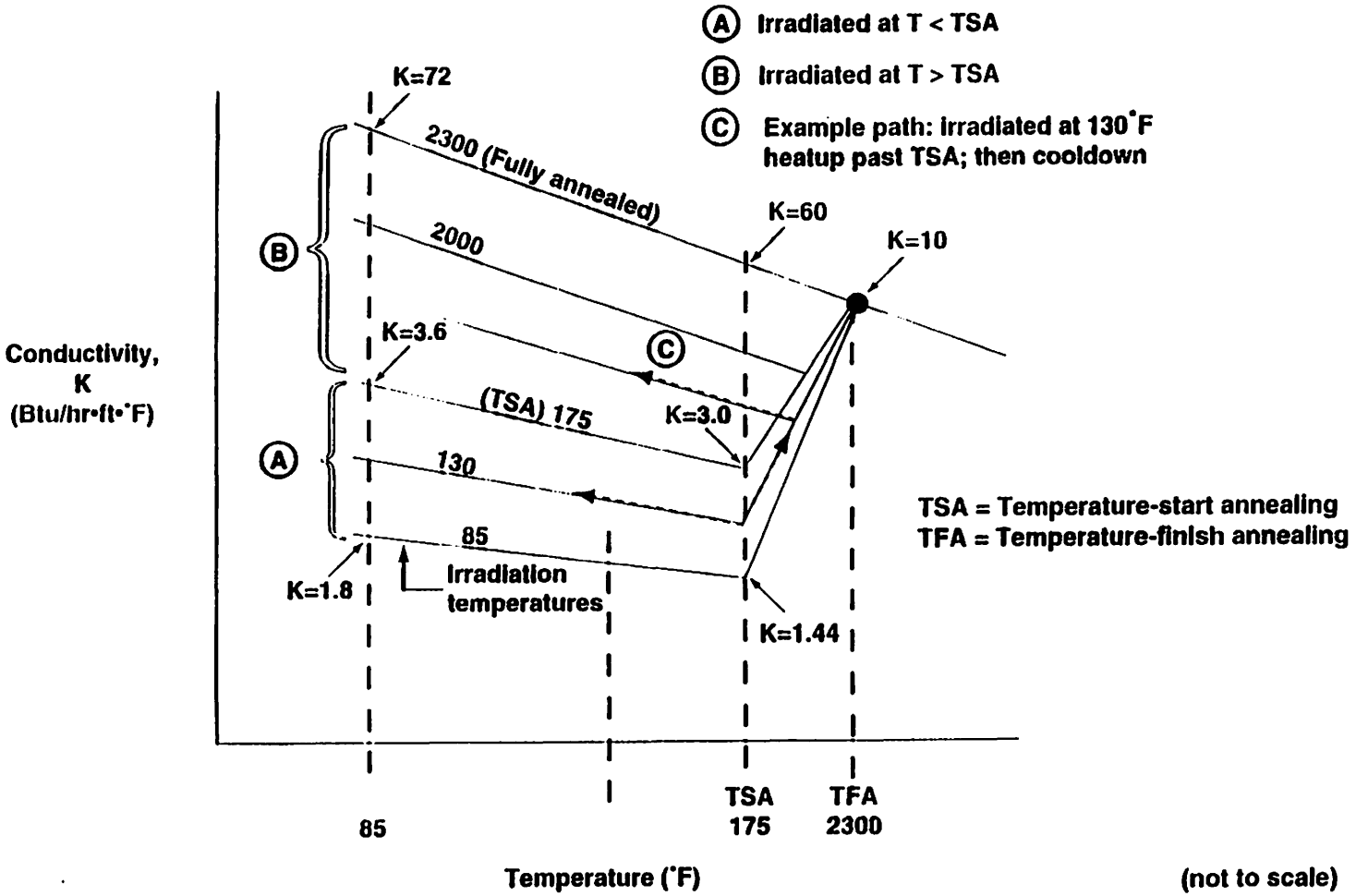

Fig. E. 12. Windscale accident reference GRSAC case: Annealing map for core axial conductivity.

E.6.2 Special GRSAC Setup to Model the Windscale Accident Sequence

A Windscale option in GRSAC introduces programmed core power and primary cooling flow sequences vs time that correspond roughly to those for the October 1957 accident scenario. This option is activated by setting the Wigner energy model flag = 3. For this option, the thermal conductivity annealing and gap resistance models apply.

The sequence begins with an arbitrary 12-hour cooldown period just prior to the time all the blowers were cut off (Monday, October 7, 1415 h). The purpose of this cooldown period is to make the initial core temperatures correspond approximately to those reported. The first of the two nuclear heatups began later that day (1925 h) and continued to early the next morning. The estimate for shutdown is October 8, 0225 h. The second nuclear heatup was assumed to be on October 8, from 1105 h to 1925 h. In the reference-case sequence, the fission power (added to the afterheat) was reported to be roughly 1.8 MW during each of the heatup periods.

It is assumed that ambient heat losses (via the "shield cooler" model) are minimal, and the flow is set to 1% for the reference case. This gives an air mass flow of about 1 kg/s and a nominal heat loss of about 100 kW at normal operating conditions. Nominal reactor power level for the period before the shutdown was assumed to be 160 MW.

The programmed core cooling flow during the accident sequence is more complex. The Windscale accident sequence begins (T = 0) at 0215 h on Monday, October 7. The sequence for the fission power heating periods (with the total power equal to the afterheat power plus 1.8 MW) is shown in Table E.5.

Table E.5. Fission heating sequence

	Start/stop times	
Heating period	Calendar	Simulation
1	Mon 10/7 1925 h to 10/8 0225 h	17.2 h to 24.2 h
2	Tue 10/8 1105 h to 10/8 1925 h	34.3 h to 42.7 h

The reference-case primary coolant air flows for the accident sequence are shown in Table E.6. Note that the cooling flow for the first 12 hours is arbitrary—enough to cool the core down to the reported temperatures. In the next period, the chimney hatch is open, which helps minimize flow through the core. For the final "cooldown," which in fact "fanned the flames," the normal four-fan shutdown flow is assumed.

Figure E.13 shows the core flow and reactor power input sequences assumed for the reference case. Note the time and magnitude scale changes in the three segments shown for the flow sequence: the initial 12-h cooldown, the rampup in leakage flow (as the core heats up) followed by the successive damper openings, and the final "cooldown" period. In the plot showing total power, the two (1.8 MW) fission power heatup periods are superimposed on the afterheat curve. In the reference case, the afterheat function is multiplied by 0.702 (sensitivity factor) to account for the actual amount of time that the reactor had been shut down prior to the start of the sequence.

E.6.3 Details of Reference-Case Results of the Windscale Accident Simulation

For the reference-case accident sequence, reference-case models and parameters are used as described in detail in the appendices, with the following exceptions:

Table E.6. Core cooling air flow sequence

Event	Start time			Duration (h)	Flow (kg/s)
	Calendar		Simulation		
Cooldown	Mon 10/7	0215 h	0.0 h	12	120
No fans on	10/7	1415 h	12.0 h	54.8	0.01–>0.05
Close hatch	Wed 10/9	2100 h	66.8 h	1.25	0.3
Damper openings: ("Hatch closed" flow = 0.3 kg/s assumed after each event)					
#1	Wed 10/9	2215 h	68.0 h	0.5	7.5
#2	Thu 10/10	0000 h	69.8 h	0.17	7.5
#3	10/10	0215 h	72.0 h	0.21	7.5
#4	10/10	0510 h	74.9 h	0.5	7.5
#5	10/10	1200 h	81.8 h	0.25	7.5
#6	10/10	1330 h	83.3 h	0.08	7.5
Cooldown	10/10	1430 h	84.3 h	19.5	120
Shutdown	Fri 10/11	1000 h	103.8 h	16.2	0.1
End of run	Sat 10/12	0215 h	120.0 h (5 days)		

- The algorithm used to calculate the Wigner energy dS/dT curve peak value at ~200°C was reduced from 0.7 to 0.6 cal/gm°C, and the total Wigner energy release factor (sensitivity input) was set to 0.2. The graphite long-term exposure value for calculating the "tail" of the dS/dT curve was 300 MWd/AT, and the short-term exposure value for calculating the peak was 250 MWd/AT.
- The sensitivity factor multipliers for graphite oxidation rate were reduced to 0.75. The multiplier for AM cartridge oxidation was reduced to 0.75 to account for the fact that other material was in the experiment channels. The summary of sensitivity factors used are as follows:

Clad:	Zone I = 1.0; Zone III = 1.0
Fuel:	Zone I = 1.0; Zone III = 1.0
Graphite:	Zone I = 0.75; Zone III = 0.75
AM cartridges:	0.75

E.6.4 Discussion of the GRSAC Code Reference-Case Windscale Run Results

Some interesting aspects of the reference accident run can be seen in the next sequence of figures. Figure E.14 shows the maximum fuel temperature and average core temperature heatup in the first 50 h of the transient, where the effects of the two 1.8-MW fission heating periods (beginning at 17.2 and 34.3 h) can be seen on the maximum fuel temperature transient. Note that just following the second fission heating period (at 42.7 h), the temperatures in the hottest regions were pushed into the range where AM cartridge failure (and oxidation) begins (>440°C). The upper right frame shows the axial profile of the maximum fuel temperature peaking near the inlet, where the fission heating is concentrated. In the lower left frame, the axial profile of graphite oxidation shows the start of the graphite oxidation, also near the inlet end. Fuel oxidation has not yet begun. The Wigner stored energy release is shown in the lower right frame. Note that there is a sustained release in the second heatup period of ~3 MW (plus a brief spike of >12 MW), which is comparable to the total of fission plus

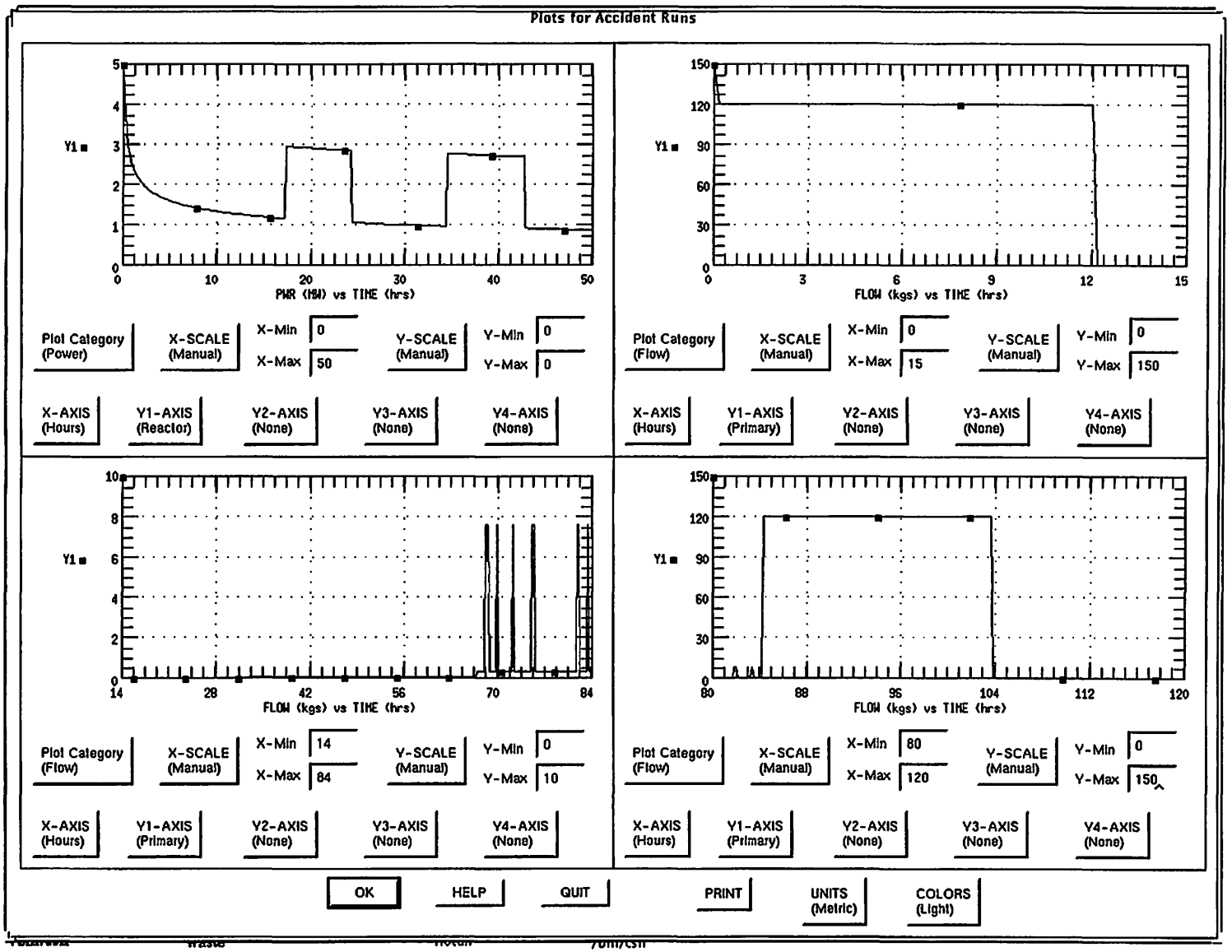

Fig. E.13. Windscale accident reference GRSAC case: Power and flow transients during the accident.

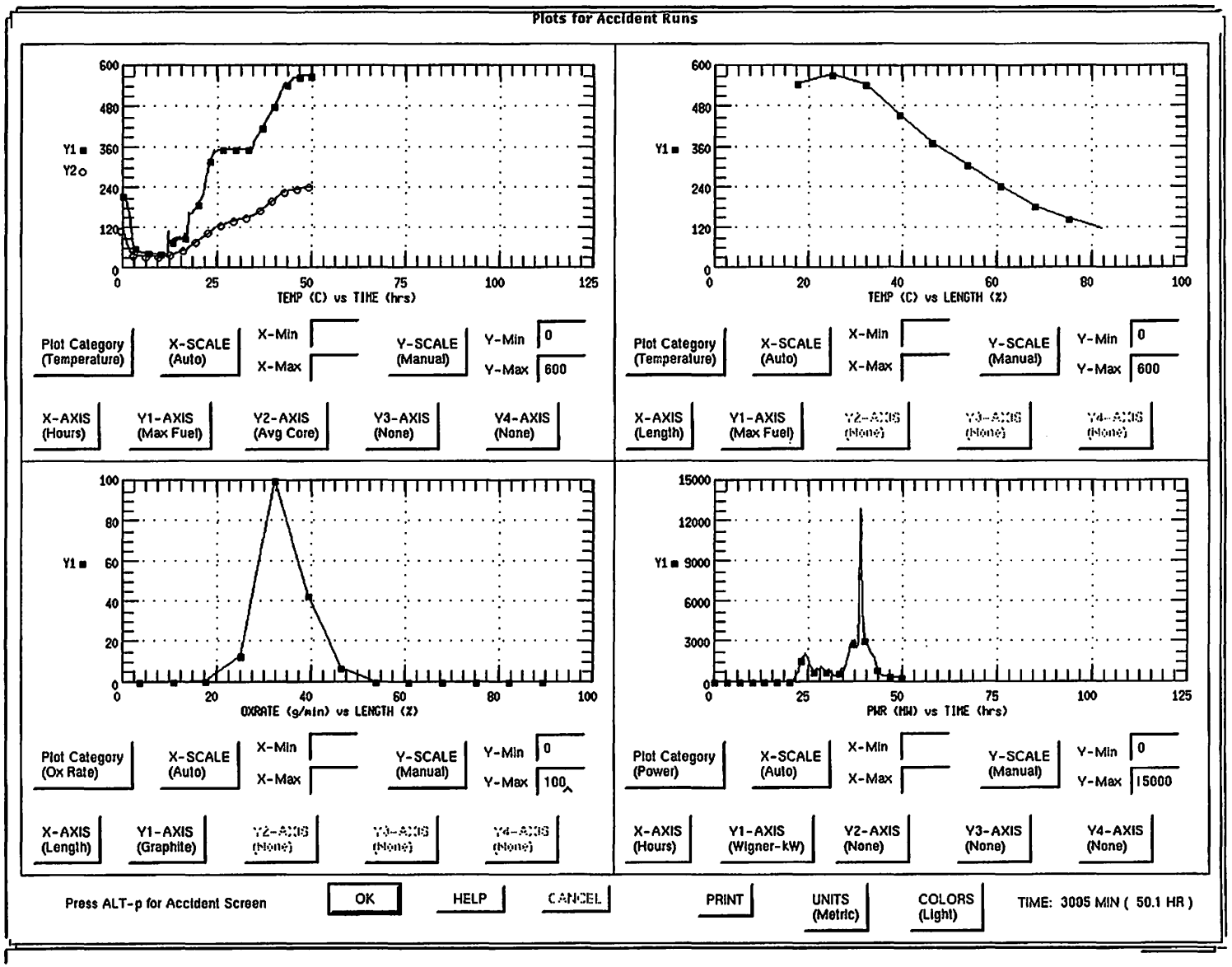

Fig. E.14. Windscale accident reference GRSAC case: Initial 50 hours of the accident sequence showing maximum fuel and average core temperatures vs time, maximum core temperature and graphite oxidation rate vs axial position, and Wigner stored energy release vs time.

afterheat power, and much larger than the graphite oxidation heating during this period. The next several figures show these and other parameters at subsequent times in the accident sequence.

Figure E.15 is a snapshot at 75 h, showing the very slow progression of the temperature and graphite oxidation fronts from inlet to outlet due to conduction, a very small amount of (assumed) convection flow, as well as a much larger graphite oxidation rate due to the higher (pulse) of flow during a damper-opening period. In the following case (82 h, Fig. E.16), fuel oxidation has begun for the first time (lower right frame). Likewise, the next case (84 h, Fig. E.17) shows high rates of fuel and graphite oxidation, again during a damper-open period.

Figure E.18 (at 88.4 h) is about 4 hours after the startup of the shutdown fans, and the huge increases in both fuel and graphite oxidation can be seen, along with the large shift of the maximum core temperatures towards the outlet. It can also be seen (upper left frame) that the average core temperature is very low, indicating that only in the hot spot region is the rapid oxidation occurring (corresponding to observations). In the next figure (Fig. E.19, 90 h) the action has been pushed further towards the outlet end, and the fuel oxidation rate has diminished to near zero. The entire 120-h transient (Fig. E.20) shows the peak fuel temperature of 1796°C occurring at 94.9 h. The power input contributions due to oxidation are shown for the AM cartridges (upper right frame), graphite (lower left) and clad and fuel (lower right—where the curve with the peak at ~16 MW is the fuel oxidation). In the early part of this sequence, relatively little energy was released by the AM cartridges; however, it was released in a crucial time period in the heatup and helped to raise the hot-region clad temperatures to a point where failures eventually occurred, allowing exposure of the fuel to oxygen during the later periods of higher flow.

Figure E.21 shows the entire run highlighting the overtemperature failures of the clad (16.3%) and fuel (11.4%) (upper right frame), the short 4-h period (84–88 h) of clad oxidation (lower left) immediately following the restart of the blowers, and the percentage of the total material oxidized vs time for the clad and fuel (15%) and graphite (3.5%) (lower right frame). During the final few hours, water was applied via fire hoses to the core (but not simulated).

Figure E.22 shows some details of the activity during the last three damper-opening events (t = 74–84 h). The maximum clad temperature (upper left frame) exceeds the aluminum melting point of 640°C at t = 77 h, and the progression of clad failure percentage is shown in the upper right frame. At this point (77 h), there is some noble gas release (lower right frame). It was in this time period when the stack activity was first observed to register high readings. The first sign of stack activity at this time would support the idea that the first clad failure may have occurred just before. Another theory proposed, however, was that some clad had failed earlier, but the air flow through the core was not sufficient, until later, to carry the fission products up the chimney to the detector.

In the period between the fourth and fifth damper openings, note that there was no fuel (or clad) oxidation, indicating clearly that the oxidation and damage rates were both controlled by oxygen availability. The first fuel oxidation events are shown during the final two damper opening periods. The calculated fission product release percentages for the eight groupings are shown beginning with the initial noble gas release at about t = 77 h (Fig. E.23). Releases for the lanthanide and cerium groups were very small (0.01%).

E.6.5 Sensitivity Studies

As noted, a major objective of this study is to get a better understanding of how the various features of the GRSAC Windscale reactor accident simulation, including both the model parameters and "external induced events," contributed to the predicted accident outcome in three ways: (1) getting the core temperatures to the point where fuel and target elements would fail and burn, (2) affecting how much damage (material oxidation and failure) was done, and (3) affecting the fission product release to the stack. Several studies were run to determine the relative importance of factors that

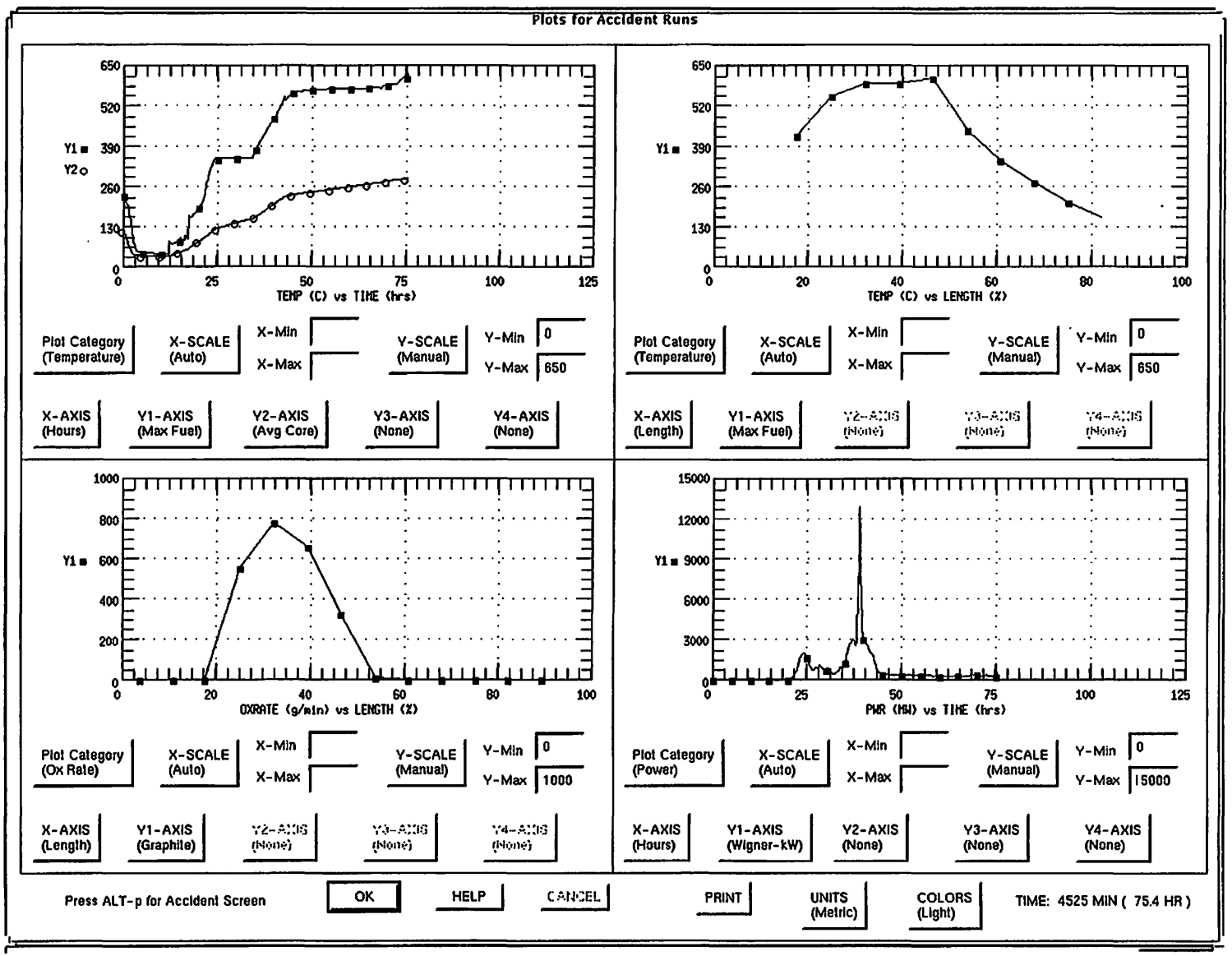

Fig. E.15. Windscale accident reference GRSAC case: Initial 75 hours of the accident sequence showing maximum fuel and average core temperatures vs time, maximum core temperature and graphite oxidation rate vs axial position, and Wigner stored energy release vs time.

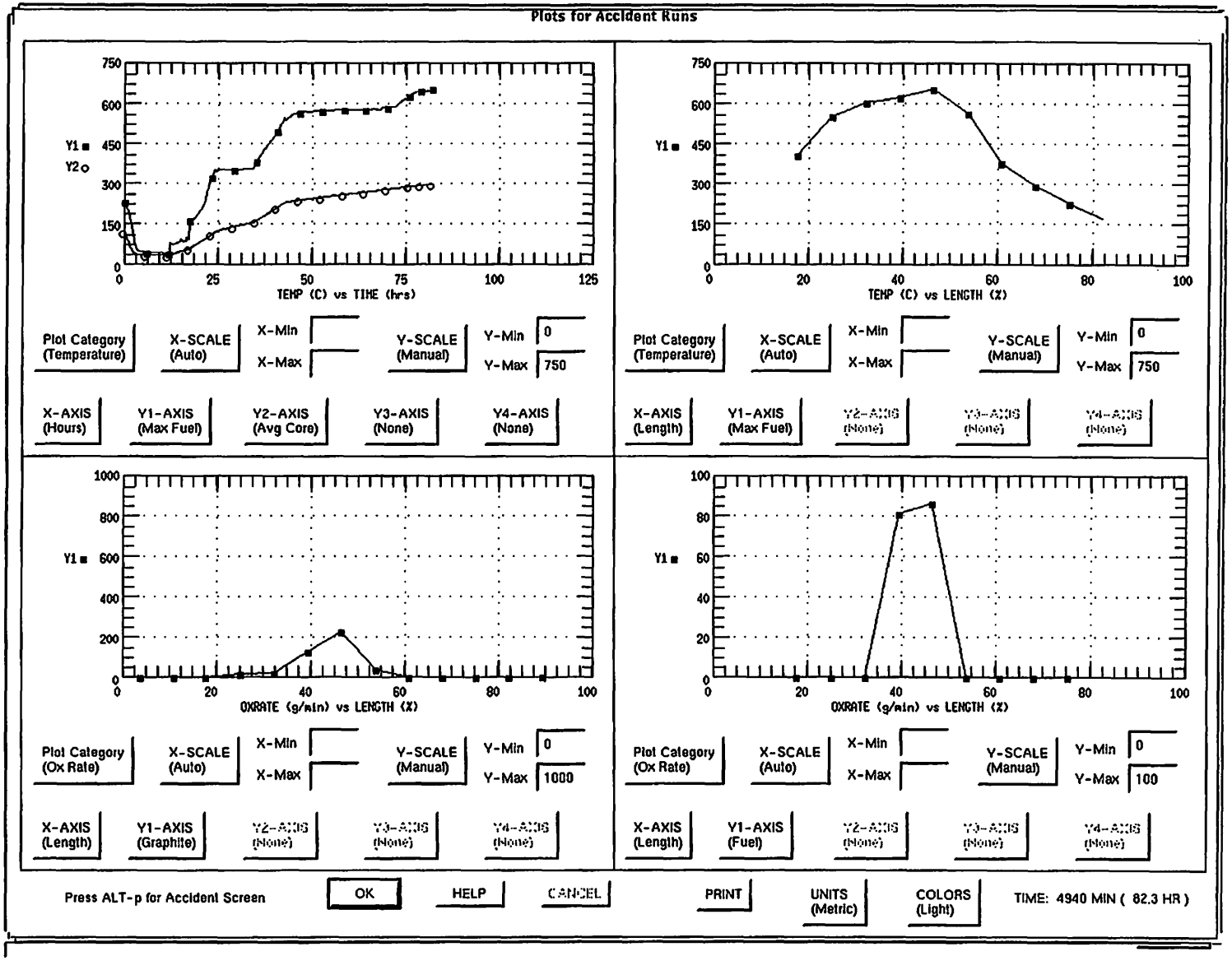

Fig. E. 16. Windscale accident reference GRSAC case: Initial 82 hours of the accident sequence showing maximum fuel and average core temperatures vs time, and maximum core temperature, graphite oxidation rate, and fuel oxidation rate vs axial position.

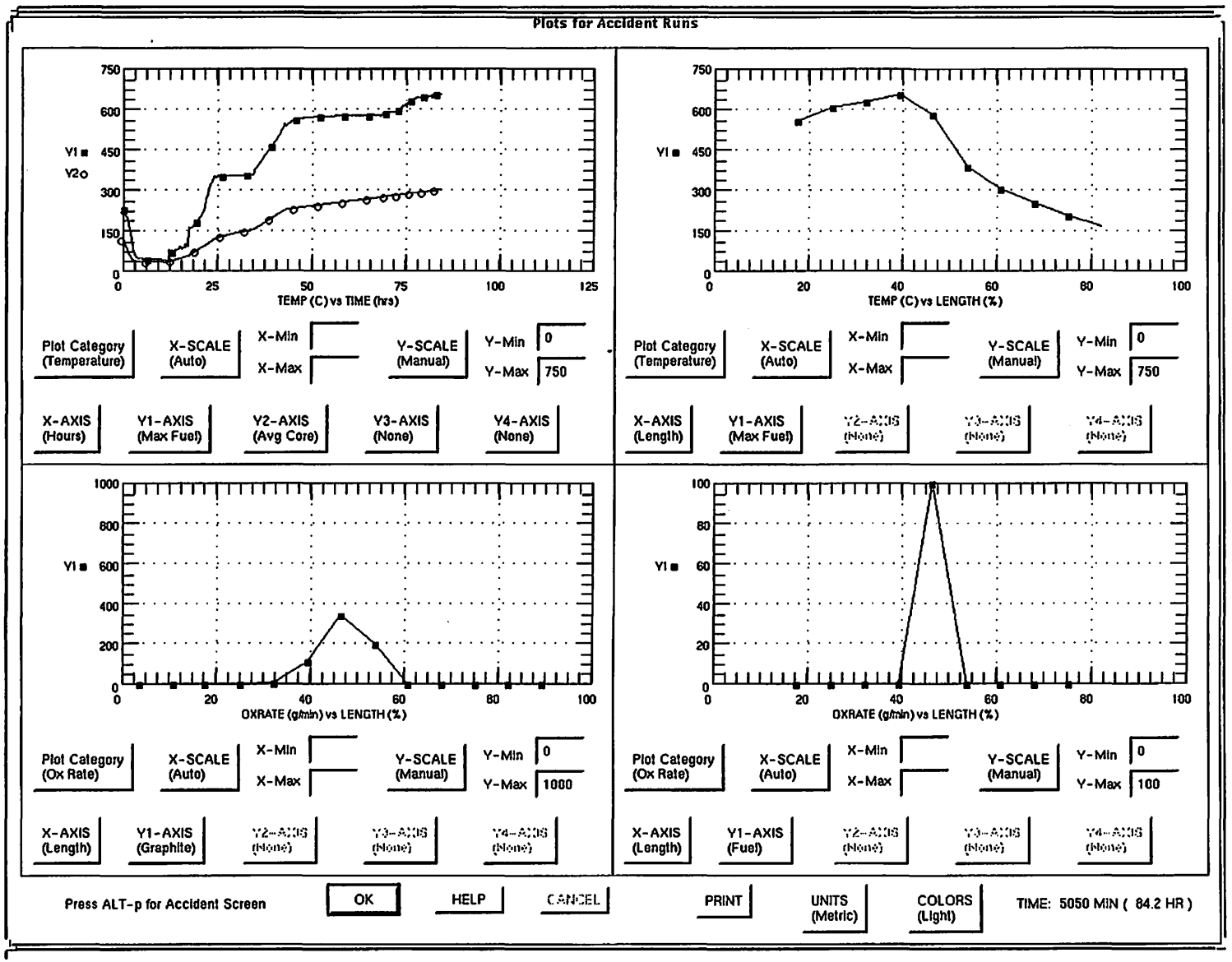

Fig. E.17. Windscale accident reference GRSAC case: Initial 84 hours of the accident sequence showing maximum fuel and average core temperatures vs time, and maximum core temperature, graphite oxidation rate, and fuel oxidation rate vs axial position.

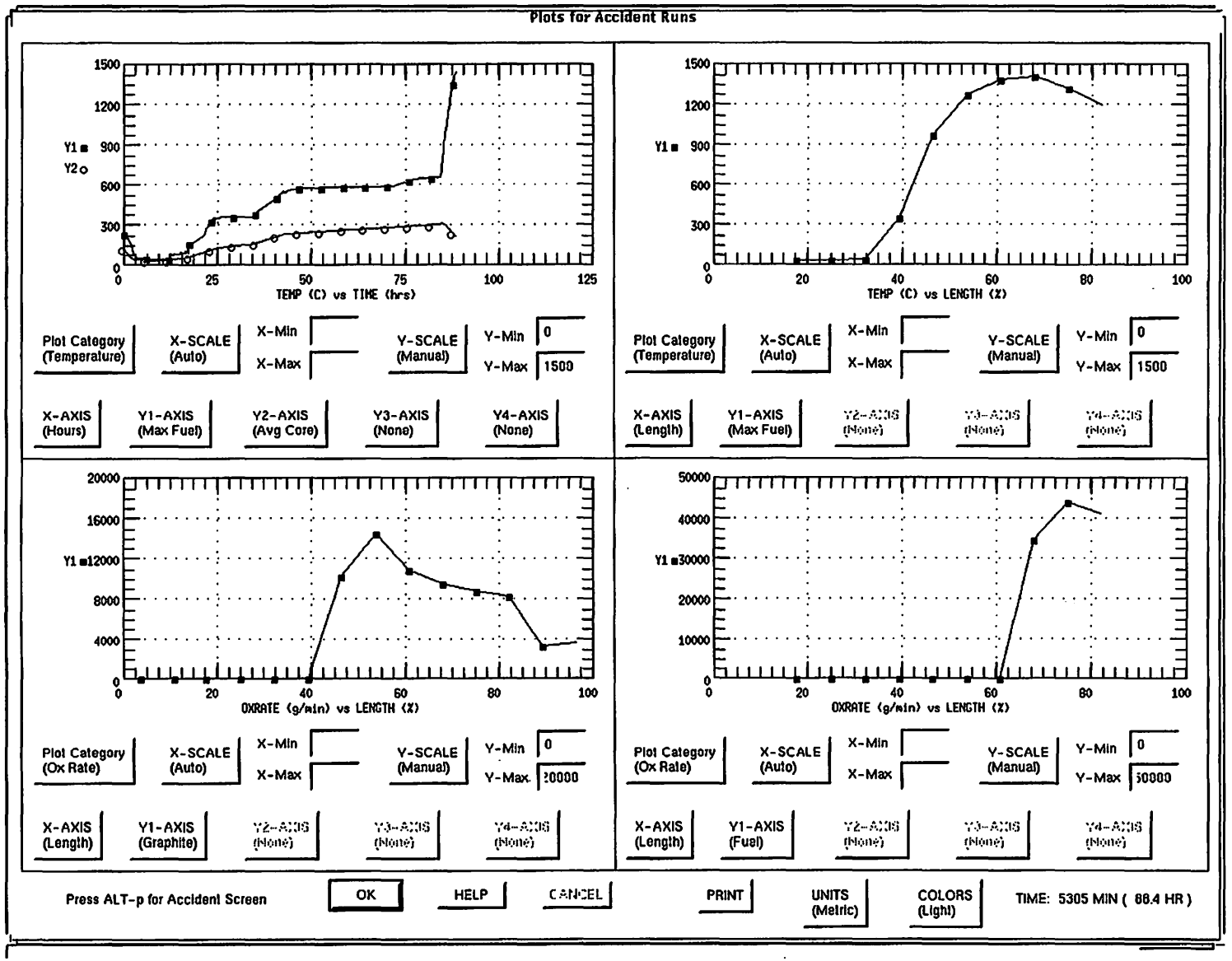

Fig. E.18. Windscale accident reference GRSAC case: Initial 88.4 hours of the accident sequence showing maximum fuel and average core temperatures vs time, and maximum core temperature, graphite oxidation rate, and fuel oxidate rate vs axial position.

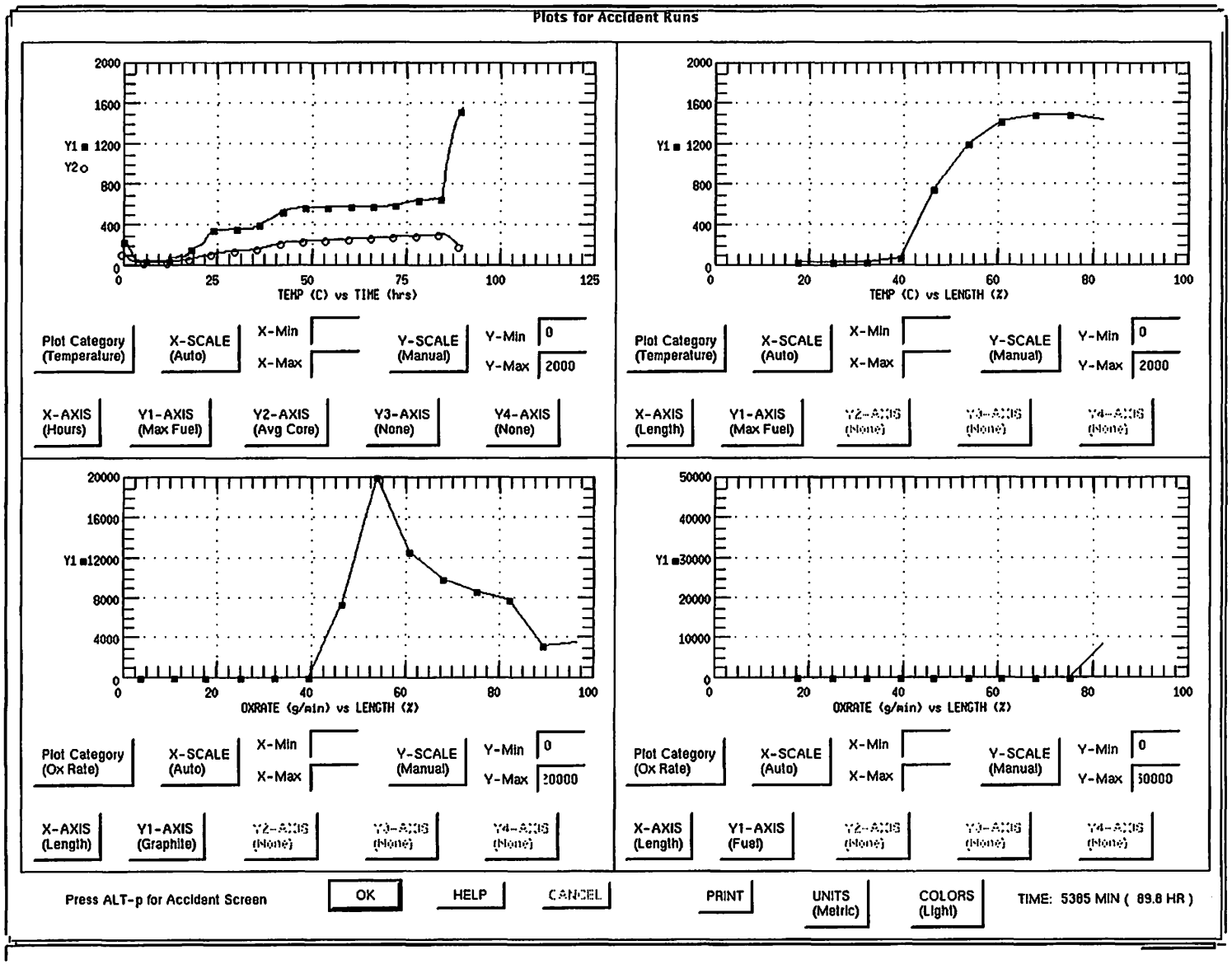

Fig. E.19. Windscale accident reference GRSAC case: Initial 89.8 hours of the accident sequence showing maximum fuel and average core temperatures vs time, and maximum core temperature, graphite oxidation rate, and fuel oxidation rate vs axial position.

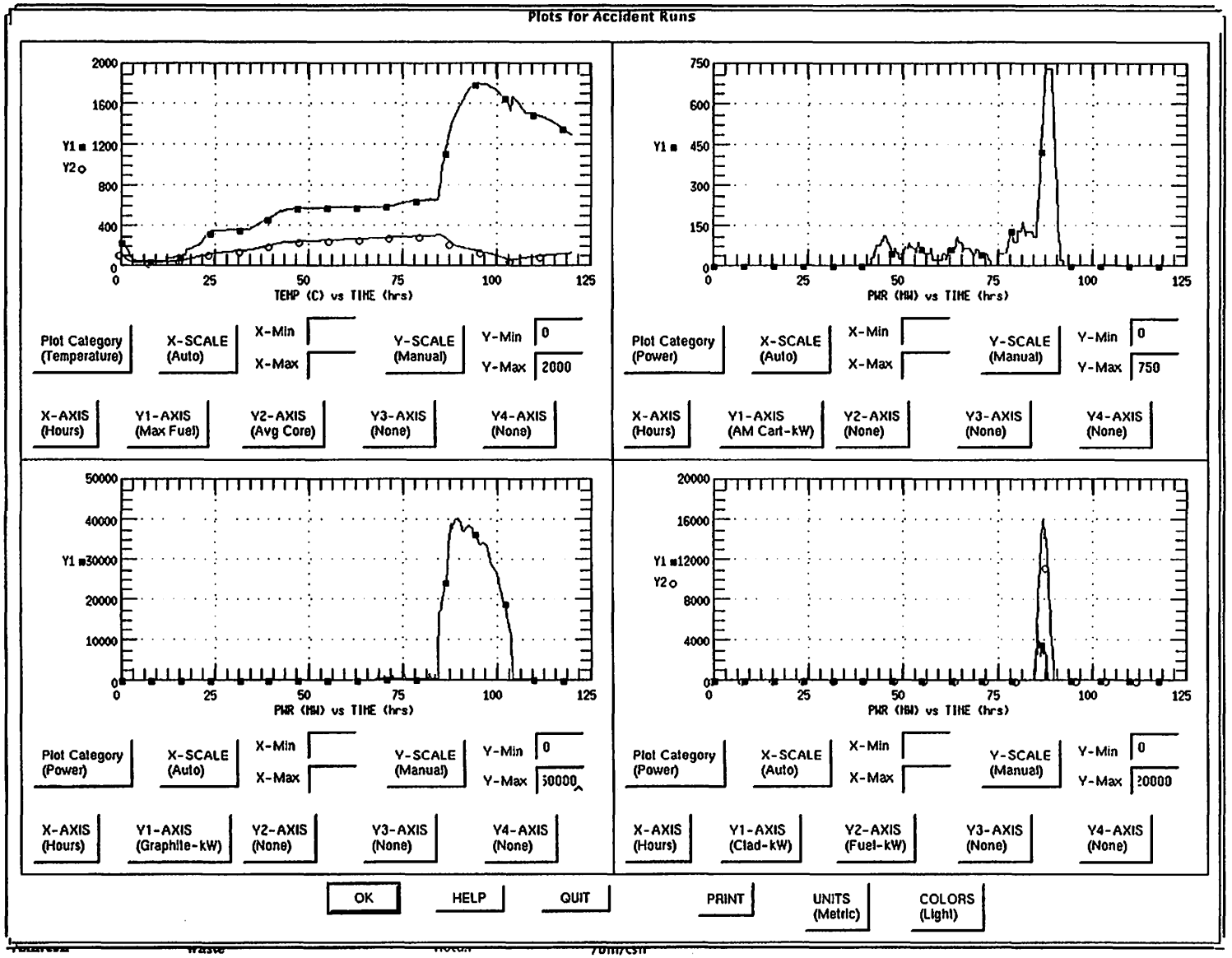

Fig. E.20. Windscale accident reference GRSAC case: Duration of the 5-day accident sequence showing maximum fuel and average core temperatures vs time, and AM cartridge, graphite, clad, and fuel oxidation heat release rate vs time.

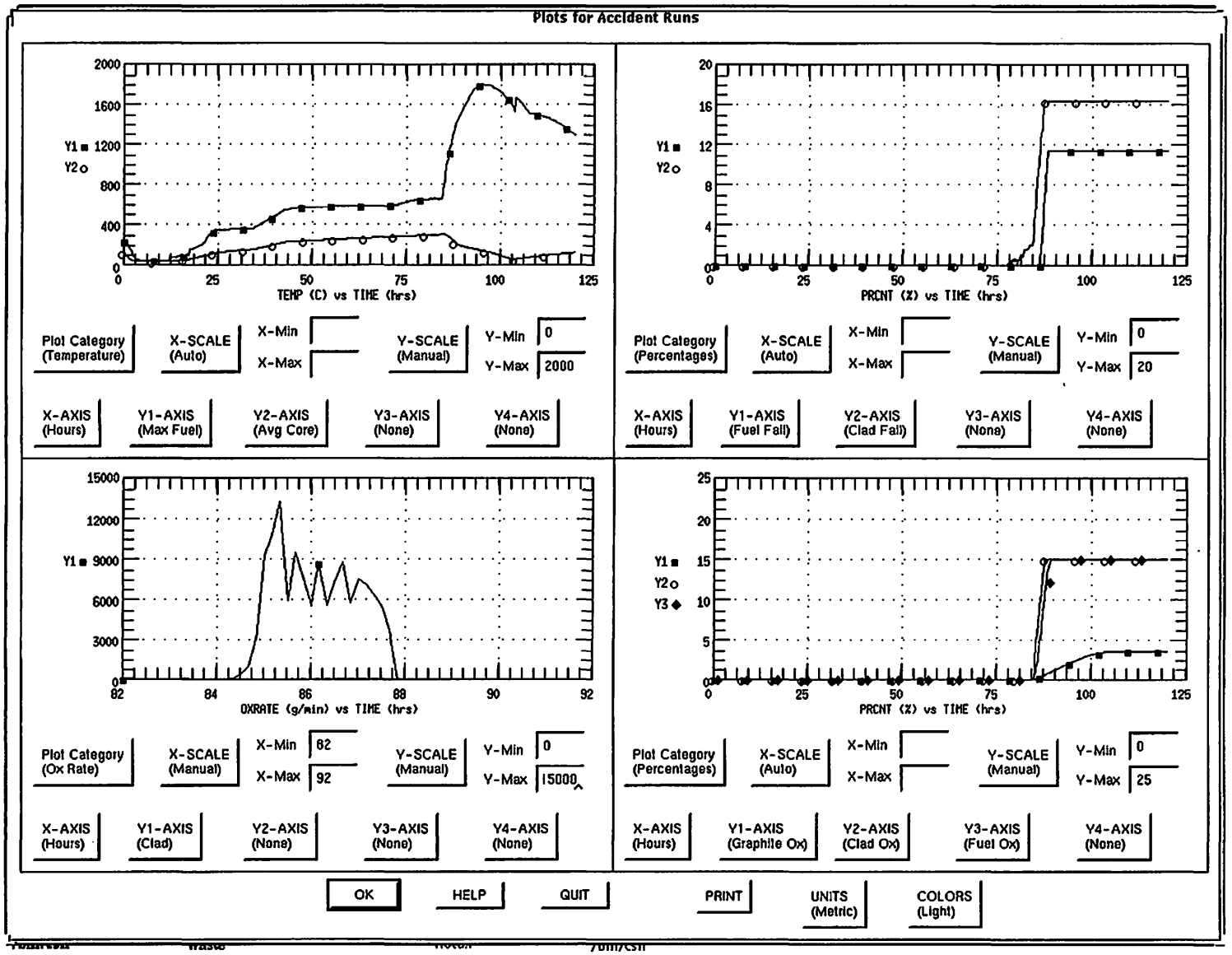

Fig. E.21. Windscale accident reference GRSAC case: The 5-day accident sequence showing: (upper right frame) fuel and clad overtemperature failure percentages vs time; (lower left frame) clad oxidation power just after startup of the shutdown fans; and (lower right frame) graphite, clad, and fuel oxidation percentages vs time.

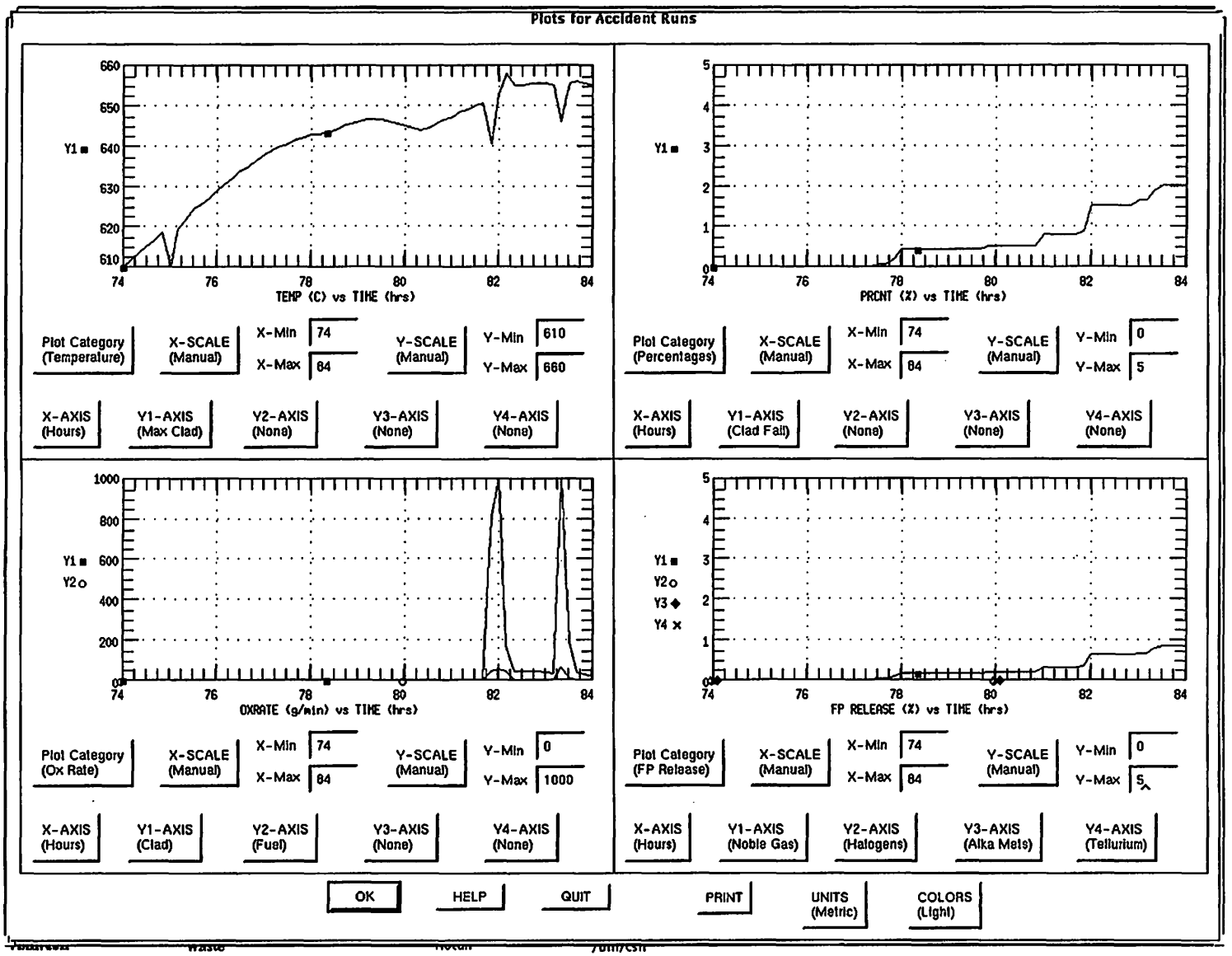

Fig. E.22. Windscale accident reference GRSAC case: Details of results during the period of the last 3 (of 6) damper openings showing: (upper left frame) maximum clad temperature vs time; (upper right) clad (overtemperature) failure vs time; (lower left) clad and fuel oxidation rates vs time; and percent releases of the first four fission product groups (only noble gases released in this period).

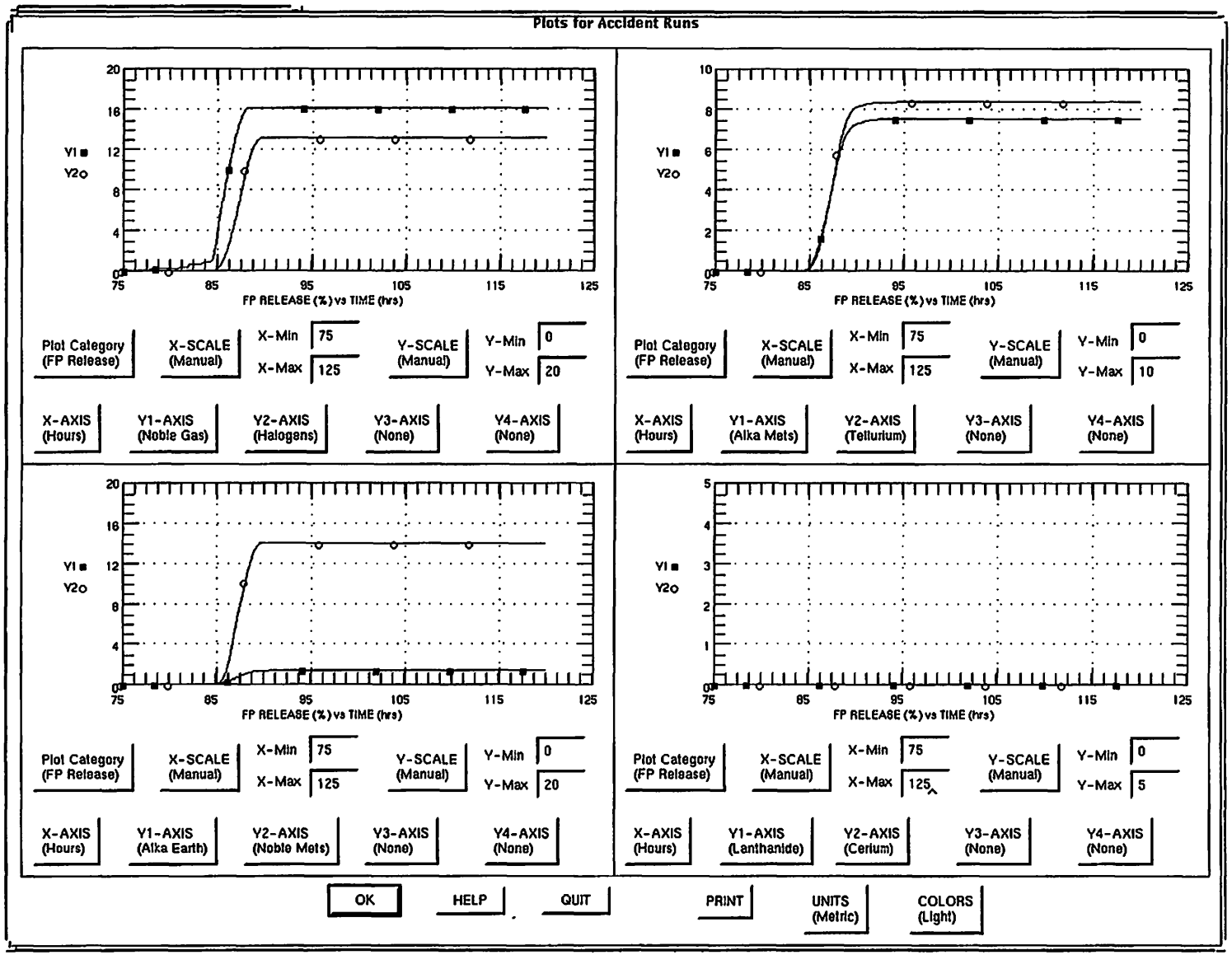

Fig. E.23. Windscale accident reference GRSAC case: The 5-day accident sequence showing percentage fission product releases (from the fuel into the primary system air) for all eight groups.

considered both model uncertainties and operational uncertainties (such as power levels and flows). There are numerous ways one could categorize and quantify the effects of these parameter variations, the most thorough and effective being detailed studies of the time histories of many variables. Instead, we have selected a few parameters that appear to be crucial, plus a few other results: percentage of total graphite, cladding, and uranium metal fuel oxidized; peak fuel temperature; percentage of cladding and fuel that exceeded their nominal melting temperatures; and the total release of fission products to the stack.

The sensitivity studies were done by using both GRSAC's automated sensitivity study feature and the manual approach (running a variety of cases) as follows:

- Automated: (1) core specific heat multiplier; (2) clad failure temperature (for the fuel elements); (3) radial peaking factor (RPF) smear or distribution factor for decay heat (set to 0.0 in the reference case, meaning that the power distribution for core heat input equals the at-power RPFs = "no smear"); (4) graphite oxidation rate multiplier; (5) afterheat power multiplier; and (6) flow sequence multiplier.

- Manual: (1) fission power multiplier (for fission nuclear heating) for the two heatup periods; (2) the oxidation time and total heat of oxidation per core node for failed AM cartridges; (3) the oxidation parameters (multipliers) for clad and fuel oxidation; and (4) Wigner energy release model variations, including:

  - the hysteresis temperature difference (or trigger delta-T) between the nominal operating temperature and the temperature at which stored energy release begins to occur,
  - the fraction of total Wigner stored energy available for release,
  - the maximum peak value in the Wigner energy dS/dT curve at ~200°C,
  - the graphite long-term exposure value for calculating the tail of the dS/dT curve, and
  - the short-term exposure value for calculating the ~200°C peak in the dS/dT curve.

E.6.6 Automated Sensitivity Study

The results of the sensitivity study are summarized in the Sensitivity Study Report Generator output (Table E.7) and the output screen (Fig. E.24). (Note that values in the report are given in English units.) Findings and follow-up studies are as follows:

A 10% increase in the assumed core specific heat reduced the initial temperature rise rates during the two nuclear heating periods and reduced the Wigner energy releases, such that when the higher flows occurred, less damage was done due to oxidation, and at the end of the accident sequence, the clad and fuel (overtemperature) failures were 3.0% and 1.8% vs 16.3% and 11.4% in the reference case. In a follow-up study, a 20% increase in assumed specific heat was found to be sufficient to prevent the maximum core temperatures from reaching the 440°C absorber element failure temperature, and no cladding failures occurred. Changing the assumed aluminum clad melting temperature from 640°C to 650°C delayed the clad failure time and reduced the total clad failure to 15.7% (vs 16.3% Reference).

Changing the RPF decay heat smear factor from the 0.0 reference case (which means that the RPF values maintain their original peaked values throughout) to 1.0 (which means the RPFs went 100% of the way towards approaching unity) resulted in lower maximum fuel temperatures. Furthermore, the wider, more uniform redistribution of the power throughout the core resulted in a slight decrease in the total clad and fuel overtemperature failures (15.7% and 10.1% vs 16.3% and 11.4% Reference).

Increasing the graphite oxidation rate multipliers (for Zones I and III) by 10% increased the clad and fuel failures to 18.8% and 13.6% (vs 16.3% and 11.4% Reference) and increased the maximum predicted fuel temperature from 1796°C to 1889°C. A 10% increase in the afterheat power multiplier

Table E.7. Report generated from Windscale accident GRSAC automated sensitivity study, showing results for variations in core specific heat multiplier, clad melting temperature, radial peaking factor decay heat smear term, graphite oxidation rate multiplier, afterheat multiplier, flow sequence multiplier, and changing all selected parameters to "worst case" values

GRSAC Sensitivity Study Report: 05/26/97 16:07 h

Reference Run: # Variables = 6 Reference O.F. = 230.523
T-max clad / fuel = 3265 / 3266 % fail clad / fuel = 16.32 / 11.41 Sum % FP rel = 60.56
Param #2 Core Cp multiplier
Param #5 Clad melting temperature
Param #9 Radial peaking factor decay heat smear
Param #10 Graphite oxidation multiplier
Param #27 Decay heat power multiplier
Param #28 Flow sequence multiplier

Run #1 Param #2 Default value = 1.000
New Param = 1.200 New O.F. = 104.348 d(O.F.)/d(Param) = –0.63087E+03
T-max clad / fuel = 3016 / 3016 % fail clad / fuel = 3.01 / 1.78 Sum % FP rel = 10.90

Run #2 Param #5 Default value = 640.000
New Param = 650.000 New O.F. = 224.572 d(O.F.)/d(Param) = –0.59510E+00
T-max clad / fuel = 3264 / 3264 % fail clad / fuel = 15.95 / 11.41 Sum % FP rel = 59.96

Run #3 Param #9 Default value = 0.000
New Param = 1.000 New O.F. = 185.222 d(O.F.)/d(Param) = –0.45301E+02
T-max clad / fuel = 3236 / 3237 % fail clad / fuel = 15.71 / 10.21 Sum % FP rel = 56.63

Run #4 Param #10 Default value = 1.000
New Param = 1.100 New O.F. = 325.895 d(O.F.)/d(Param) = 0.95372E+03
T-max clad / fuel = 3432 / 3432 % fail clad / fuel = 18.77 / 13.25 Sum % FP rel = 69.73

Run #5 Param #27 Default value = 1.000
New Param = 1.100 New O.F. = 249.543 d(O.F.)/d(Param) = 0.19020E+03
T-max clad / fuel = 3291 / 3291 % fail clad / fuel = 23.31 / 15.52 Sum % FP rel = 84.53

Run #6 Param #28 Default value = 1.000
New Param = 1.100 New O.F. = 148.414 d(O.F.)/d(Param) = –0.82109E+03
T-max clad / fuel = 3281 / 3281 % fail clad / fuel = 15.95 / 11.41 Sum % FP rel = 59.63

Run #7 All params set to give best O.F.
Param #2 Core Cp multiplier Param = 0.800
Param #5 Clad melting temperature Param = 630.000
Param #9 Radial peaking factor decay heat smear Param = 0.000
Param #10 Graphite oxidation multiplier Param = 1.100
Param #27 Decay heat power multiplier Param = 1.100
Param #28 Flow sequence multiplier Param = 0.900
Final (best) O.F. = 437.634
T-max clad / fuel = 3732 / 3732 % fail clad / fuel = 57.42 / 38.83 Sum % FP rel = 206.57

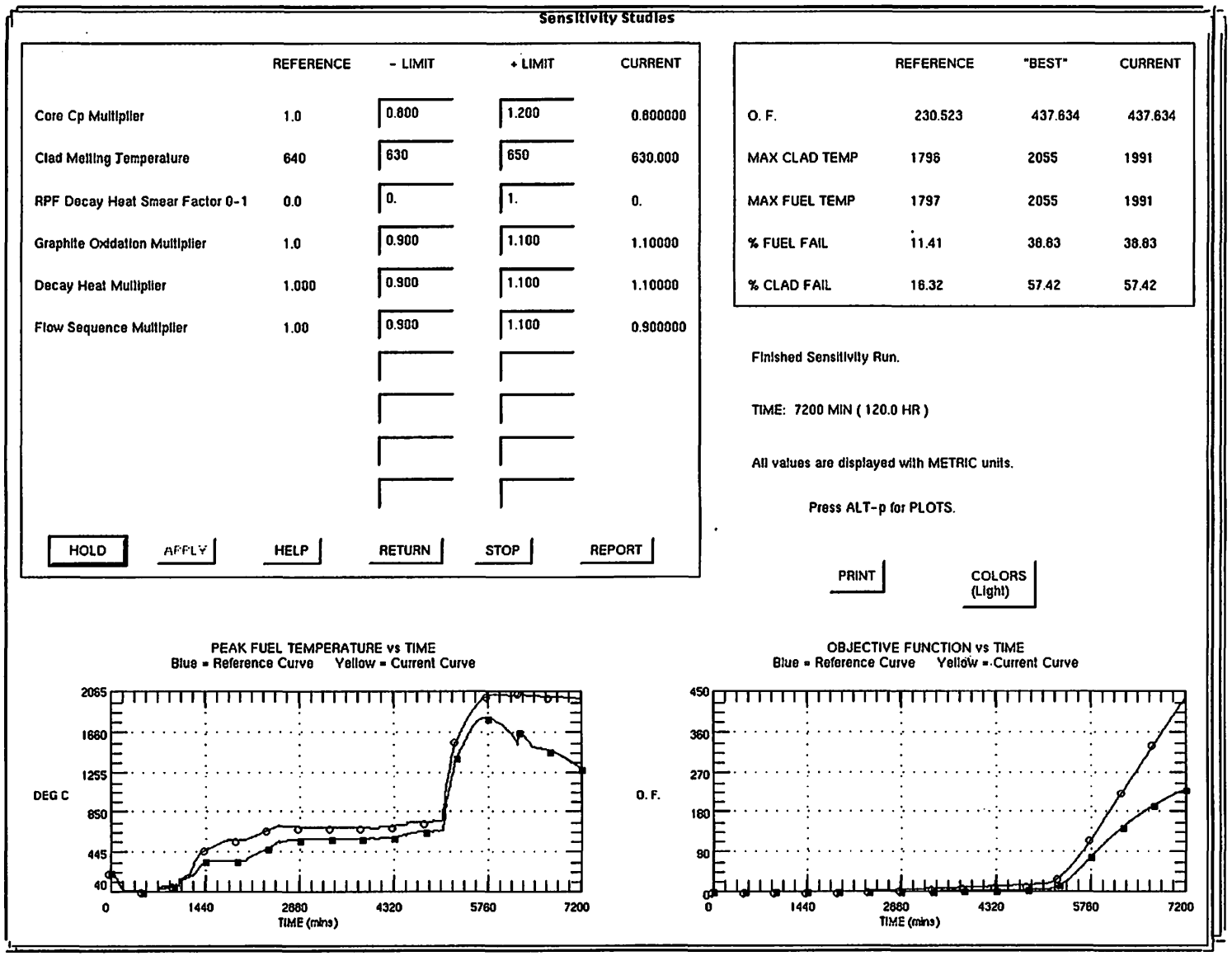

Fig. E.24. Windscale accident GRSAC sensitivity study case: Automated sensitivity study screen following completion of a sensitivity run with variations in core specific heat multiplier, clad melting temperature, and radial peaking factor decay heat smear term; graphite oxidation rate multiplier, afterheat multiplier, flow sequence multiplier, and then changing all selected parameters to "worst case" values.

from 0.702 to 0.75 boosted the temperature rise rate sufficiently to raise the core "cooking" temperature, and as a result, the clad and fuel failures were 23.3% and 15.5% (vs 16.3% and 11.4% Reference).

A 10% increase in the flow sequence multiplier (which affects the primary flow rate in all stages of the 5-day accident sequence) had no effect on the fuel failures but caused a slight decrease in clad failure percentage (15.95% vs 16.32% Reference). Hence for this small change, the benefits from increased cooling outweighed the drawbacks from increased oxygen availability. In the final run, a combination of all of the worst-case values was assumed and resulted in a considerable increase in clad and fuel overtemperature failure (57.4% and 38.8% vs 16.3% and 11.4% Reference), a 260°C increase in maximum fuel temperature, and an increase in total fission product release by a factor of 3.4.

E.6.7 Manual Sensitivity Studies

It had been shown previously that the changes assumed in the multipliers for core effective heat transfer coefficient (±40%) and core radial conductivity (±20%) had a relatively modest effect on the accident consequences, so they were omitted from the present sensitivity study.

Sensitivity to damper-open flow variations

It should be emphasized that the flow values used in the reference case are off-the-cuff estimates, especially for the hatch open, hatch closed, and damper open periods. Overall accident sequence flow changes are discussed above in Section E.6.6. Varying only the flows assumed for the six damper-open flow periods (between 66.8 and 84.3 h, per Table E.7), a 20% reduction in those flows resulted in only slight decreases (1–3%) in material oxidation and overtemperature failures.

Sensitivity to fission power in the heatup periods

In this case, the fission heating was increased 20% from the nominal 1.8 MW (to 2.16 MW). There was a major increase in accident severity vs the reference case. The total material damage and oxidation were ~40% greater than in the reference case. Also, the peak temperature was 26°C higher than the reference. On the other hand, a 20% decrease in the fission power resulted in only 5–10% decreases in material oxidation and damage.

Sensitivity to Wigner energy release modeling

Fraction of total stored energy available for release: Typically, not all of the Wigner stored energy is available for release when annealed. In the reference case, it is assumed that 20% is available, and in this case, the assumption was made that only 10% (maximum) is released. This resulted in only a very small decrease (1–4%) in the total material oxidation and failure, with a peak fuel temperature 13°C less than in the reference case.

Maximum value of the 200 °C peak in the dS/dT stored energy curve: This value was reduced from the reference case (0.6) to 0.4 and resulted in ~2 to 10% decreases in material damage and oxidation, with a peak fuel temperature of only 6°C lower than the reference value.

Exposures affecting the peak and tail values of the stored energy curve: Reduced exposures by 20% (200 MWd/AT for the short-term peak effect vs 250 reference, and 240 MWd/AT for the long-term tail effect vs 300 reference) resulted in ~5–10% decreases in material damage and a peak fuel temperature 7°C less than the reference.

The hysteresis temperature difference between the nominal operating temperature and the temperature at which stored energy release begins to occur: When the temperature difference was increased from 50°C (reference case) to 75°C, the material oxidation and damage was ~2–10% less

than in the reference case, while the peak fuel temperature was only 5 °C less than in the reference case.

Sensitivity to AM cartridge failure modeling

The time assumed for oxidation of a failed AM cartridge was reduced from 4 hours (reference case) to 1 hour, and the total heat released upon failure was increased from 75% to 100% (e.g., assumed 100% of the total space available in the experiment holes was occupied by AM cartridges). This resulted in an increase of ~12–14% in material oxidation and a peak fuel temperature 7 °C greater than the reference.

Sensitivity to material oxidation rate multipliers

The outcome of the accident appeared to be most sensitive to variation in the oxidation parameters (multipliers) for graphite. For only a 10% increase (from 0.75 to 0.825), the total graphite oxidation increased 53%, while the clad and fuel oxidation increased by ~15%. On the other hand, for a 10% increase in the clad and fuel multipliers, the material oxidation was only ~1% greater than the reference.

E.6.8 Sensitivity of GRSAC Results to Computation Time Step Changes

Another simulation variation of interest is the computation time step. The reference-case time step is 5 min. Comparison runs were done for the reference case with a smaller time step (2 min), since some of the oxidation rate equations are rather fast acting. At the end of the run for the smaller time step, the graphite oxidation was ~25% larger, and the clad and fuel failure and oxidation values were 2–7% larger than for the reference case. The peak fuel temperature was 19 °C higher than for the reference case. Results for 1- and 2-min time step cases were all within about 2% of each other.

E.6.9 Follow-up Sensitivities Studies Showing Relative Likelihood of No Accident

Several interesting follow-up studies indicated just how close the (simulated) accident was to being a non-accident. For example, the following combinations of changes resulted in a sequence with *no* clad or fuel damage occurring:

1. A 20% increase in core specific heat combined with a 20% reduction in fission heating power (from 1.8 to 1.44 MW).
2. An RPF smear factor of 1.0 plus a 30% reduction in afterheat plus a 20% reduction in fission heating power (from 1.8 to 1.44 MW) during the two nuclear heatup periods.
3. A 20% decrease in Wigner damage long-term exposure and 50% decrease for the short-term exposure values for the graphite (from 300 to 240 MWd/AT for the "tail" and 250 to 125 MWd/AT for the peak) plus a 25% reduction in afterheat plus a 20% reduction in fission heating power (from 1.8 to 1.44 MW).
4. A decrease in damage exposure values for the graphite (from 300 to 240 MWd/AT for the "tail" and 250 to 125 MWd/AT for the peak) plus a 25% increase in core specific heat.

These "non-accident" cases, which were relatively small changes away from the reference accident case, are strongly supported by the fact that the two Windscale reactors had both undergone many annealings where "no accident occurred" that were in fact very similar to the Windscale 1 October 1957 annealing sequence.

E.7 DETAILED CHRONOLOGY OF THE WINDSCALE ACCIDENT

The following Windscale accident sequence chronicles Monday, October 7, through Friday, October 11, 1957. The type font identifies the source: **Control room log (bold),** Summary Table (regular), and *Testimony (italics).* These sources are further identified in references 11, 8, and 10 for the control room log, Summary Table and Testimony, respectively. Additional sequence information, acquired from Arnold,[2] is so identified.

Day	Time	Event
Monday	0113	**Pile shutdown and the pile main blowers switched off.**
	1415	Thermocouples installed for observing the Wigner energy release followed by switching off the shut-down fans. The door in the base of the chimney opened and inspection plugs removed to minimize coolant air flow through the lattice
	1925	Pile made to diverge to generate nuclear heat for triggering off the energy release. *Gausden: Testimony, 1.2: The Pile diverged at 7:30 in the evening of Monday, 7th. The power level was gradually raised after 1.8 MW to about 0100 on Tuesday evening.*
Tuesday	0100	**Temperature rose to indicate first release of Wigner energy.** *Gausden: Testimony, 1.2: By that time we got our maximum uranium temperature, 250 °C in two places, 2557 and 2757. The graphite temperatures generally were somewhere between 50 and 80 °C with one particular exception which 2148 at 10 feet depth into the pile and was showing the characteristic signs of a release at that period.*
	0200	**Control rods slowly run in. The release proceed only very slowly, then temperatures started to fall and it was decided to boost the release by more nuclear heating.** *Gausden: Testimony, 1.3: From 1 o'clock to 4 o'clock on Tuesday morning we were running the rods back in and closing the reactor down because we had sufficient heating to start off the release and during this period the first good releases occurred in 2655 and 2661. 2665 was at 110 °C when the release started and finished up at 250 °C in about 3 hours, and 2661 was about 200 °C and finished up again in about 3 hours.*
	0400	*Gausden: Testimony, 1.3: The pile was shut down by 4 o'clock. . . . The Wigner release spreading heat to further points. At 1105 on Tuesday morning the general tendency was for the graphite temperatures to be dropping rather than rising, and it was obvious at that stage that unless we put in more nuclear heating the release would stop.*

	1105	**Control rods withdrawn till pile diverged to increase energy release.**
		Gausden: Testimony, 1.3: The pile was run up with the bottom rods and more nuclear heating put in to raise the maximum uranium temperature which was 300 °C at the time to 330 °C. (time for the run up not stated.)
		Gausden: Testimony, 1.3: Yes, the graphite temperatures rose in sympathy from a maximum of 310 to 330 °C in 2148.
	1400–1600	*Gausden: Testimony, 1.3: . . . but between 1400 and 1600 on Wednesday, this took a slight turn upwards, the rate of temperature increase was rising and by 2055 it was decided that we would have to exercise some control on this temperature and the first step was to replace the covers over the inspection holes behind the scanner gear on the top of the reactor. . . . This would provide the first measure of cooling.*
	1700	**Control rods run in, and release of energy continued.**
		Pile closed down and the release of energy continued.
Wednesday	2100	Inspection covers replaced.
	2155	Hatch at chimney base locked.
	2215	**Measured temperatures slowly rising and some greater than 400°C. The four shut-down fan dampers opened for 15 min to supply cooling air to reduce the temperatures.**
		Temperatures slowly rising and some greater than. The 4 shut down fan dampers opened for 15 minutes to supply air coolant and bring the temperatures down.
		Gausden: Testimony,1.3: At 2215 four shut down fan dampers were opened which gave a positive air flow through the reactor. . . . You will see that opening the 4 shut down dampers arrested the temperature rise and flattened it right off.
Thursday	0001	**Dampers opened for 10 minutes to reduce temperatures.**
		Gausden: Testimony, 1.3: Again at 1 minute past midnight the dampers were opened for ten minutes, but did not materially influence the temperature.
	0215	**Dampers opened for 13 minutes to again reduce temperatures.**
		Gausden: Testimony, 1.3: so at 0215 they were again opened for a longer period of 13 minutes and this did affect the temperature and it dropped.

Davey: Testimony, 6.22: My own opinion is that the incident started about 2000 on the Thursday morning. . . .but my opinion is that the first time the air went on, the incident had started.

0315 *Gausden: Testimony, 1.4: . . . but within an hour* [0215–0315] *the temperature again turned round and was beginning to rise again.*

0510 **Dampers opened for 30 minutes to again reduce temperatures.**

0540 **Reading on pile stack activity had increased.**

0540–0810 Stack activity falling

1200 **High activity reading on the meteorological station roof reported to Pile Manager. Pile 2 suspected since Pile 1 was shut down and also since there had been a high stack activity measurement the previous night on Pile 2. This high measurement on Pile 2 proved to be an instrument error.**

1210 Dampers opened for 15 minutes to again reduce temperatures.

1215 **Marked increase in pile stack activity after opening up dampers.**

Marked increase in pile stack activity noted after opening up the dampers.

1230 *Gausden: Testimony, 1.4: At 1210 the dampers were again opened for 15 minutes and shortly after this there was a marked increase in stack activity. I was informed of this immediately, and I gave instructions to open the dampers, put on shut down fans and blow the Pile cool.*

1340 **Dampers opened for 5 min to again reduce temperatures.**

1345 **Suspected burst cartridge. The four shut-down fans switched on to reduce temperatures before proceeding to inspect for burst cartridge.**

The 4 shut down fans switched on to reduce temperatures prior to looking for a burst which was now suspected on Pile 1 from the stack activity measurements. The graphite temperature fell and the fuel temperature rose until the fuel and graphite temperatures approached the same value, as expected.

Gausden: Testimony, 1.4: I would point out at this stage that the operator is operating from the roof and he was watching very closely this 2053 graphite temperature and trying to ensure that he kept that under control; and at the same time he was watching 2153 uranium temperature which was adjacent to this and noted that that reading was still round about the 350 °C mark.

[W]e expected two things to happen. We expected first of all the uranium temperature in 2153 to rise (because you are extracting heat from the graphite and passing it to the uranium which it did and it steadied off at

about the 400 mark. We would then have expected it to fall away as the graphite temperatures went down, which they all did. They began to fall and one would have expected the uranium temperatures to do the same. 2153 steadied off and then began to rise quite sharply as you can see from the graph and in the space of one hour rose from 340 to 400 °C. Then the rate of rise decreased somewhat over the next few hours up to 420 and then began to rise again quite rapidly at about the rate it had done just before the previous two hour period.

1350 Report of high readings at met station to Pile Manager. Small particles.

1430 Turbo exhausters switched on prior to scanning for burst. Switched off at 2020. Scanner jammed.

1400 *Hughes: Gausden called Hughes that he thought there was a burst.*

1415 *Hughes: Mr. Howells stated that an air count from 1100–1400 showed reading of 3000 dpm.*

1430 **Turbo exhausters switched on but on attempting to use the scanner gear it could not be moved.**

1440 Mr. Hughes and Factory management notified.

1515 Mr. Hughes informed W G III charge burst.

1545+ *Davey: Hughes phoned me that there was a bad burst.*

1550 Fuel temperature continued to rise higher than the graphite temperatures. This was not expected.

1600–1630 Locating the channel (2153) with the high fuel temperature, temperature up to 450°C by 1630. The slight delay in locating the channel was due to incorrect labeling of the temperature recorded.

1630 *Davey: Hughes phoned again and said he was quite concerned because the stack activity meter was showing of the order of 300 curies. He and Ross go to top of pile, where thermocouple read out showed rate of rise on 2153 was quite abnormal. Ordered discharge as soon as possible.*

1630+ *Davey: With particulate activity on site, Davey thought it undesirable to bring big blowers on in order to cool the pile. Ordered graphite plugs to close channels.*

1645est *Davey: Within 15 minutes, next information was that something like 100 channels were involved. (25 ports?). Later testimony by Peirson stated 36(ports) × 4, more exactly.*

1700 Decision to make a fire break by pushing out first one complete ring of groups of 4 channels and then a second ring. The discharge sequence is shown on the plan of the charge face. Some channels were discharged by

		"brute force" from the hot region. (Continued until about 0430 Friday morning)
	1845	Obvious glow on looking at pile rear face through the east inner inspection hole.
	1930	Much brighter glow.
	2000	Yellow flames.
	2130	Blue flames (under east inner or yellow under W inner).
		Davey: In answer to question of Schonland on whether he had the impression that the graphite was burning, stated that he certainly attributed the flames to material burning in the channel as distinct from graphite.
	2300	Hold up during discharge due to discharge dolly almost pulling cartridge out onto charge platform.
	2345	Skiptrain moved 20 ft towards pond to bring relatively empty trucks under regions being discharged.
Friday	0030	Temperatures above the isolated region rising. Decided to remove more rows above the region in preference to completing discharge of the lower half of the second isolating ring.
	~0055	Decided to use water cooling if temperatures continued to rise since it was unlikely that CO_2 cooling would be sufficiently effective. Equipment for enabling supply of CO_2 and of water to the fuel channels via the charge hoist was being made.
	Soon after midnight	Mr. Ross warned the Chief Constable of the possibility of an emergency.
	0133	Equipment being collected to permit water supply. People in buildings warned of an emergency with instructions to stay indoors and to wear face masks. (rising air counts)
	0138	Fuel channel temperature 1300°C measured by optical pyrometer. Graphite in channel 20/53—near top of "box" —1000°C.
	0158	Channels being discharged by brute force from "box."
	0223	Water pipes not yet ready. At least six channels pushed.
	0230	Instructions to remove face masks and hold them ready. Temperature 650°C graphite near 26/55—just below the box. This was 350°C at about 0015. Thermocouple 4 ft in the pile. 1000°C graphite at 20/53 (inside the box); thermocouple now US.

0235 Temperature below box at 26/55 had risen to 650°C. Tuohy on charge hoist to use discretion in continuing to discharge hot box but not to lose sight of probable need to use water. To request permission from Mr. Ross before using water.

0300 High count rate in pile forecourt. Fuel being discharged and new units being made to increase rate of discharge.

0318 20 channels pushed out and continuing. No indication of fire above or below box.

0344 Visit from Tuohy to HQ (Mr. Davey's office). Nearly all top row of box out. No signs of fire outside the box. Water hose can be coupled at 15 minutes notice and CO_2 supply at 45 minutes notice.

0403 TV camera to be inserted in RHS of charge face at outer edge subject to air temperature not being too high.

0419 Running out of steel poles to push out channels, to issue scaffolding poles from Calder. Skips to be pulled out because of criticality hazard from 1.28 Co fuel and to continue discharge into water duct. Criticality limit of 2.3 tons if graphite boats present, quoted for 1 skip.

0430 CO_2 fed into hole 20/56 with no appreciable effect. TV camera, no vision have to more nearer to box. (Not done)

0655 Temperature measurement of fuel in channel 16/57 showed increase in rate of temperature rise. Now at 270°C, 100°C rise in the last hour. Tuohy informed at Pile Administration Building.

0700 Decision to use water officially taken.

0717 Fuel in channel 16/57 now rising at 20°C/min.

0806 Discharging at rate of 90 channels/hour. Use of water postponed to 0830.

0830 Temperature measurements. Graphite 25/50 now rising rapidly, 30°C/hr.

0855 Water turned on in channels 14/54 and 14/57. The 2-in. N.B. tubes are directed at the isotope channels and terminate on the pile side of the charge plug. Flow rate stepped up to 800 gal/min. 50 to 75 to 100 max. pressure.

0956 Flames still feathering out back of pile.

1010 Shut down fans closed off to reduce air flow through the pile. The result was dramatic (Arnold 1992, p. 52). Touhy saw the flames rapidly dying out.
Water flow continued until 1510 Saturday.

E.8 OBSERVATIONS FROM GRSAC ANALYSES OF THE WINDSCALE ACCIDENT

As noted, the special GRSAC code Windscale sequence has preprogrammed changes in both the fission power (corresponding to the two "nuclear heatup" periods) and the primary air coolant flow. The course of events for the reference-case power and flow assumptions, along with the values entered in the design input file's many options for sensitivity coefficients, gives an outcome that bears a striking resemblance to the accounts (per our current information) of the actual accident. There are a lot of readily accessible parameters that can show sensitivities quite well.

The major parameters of particular interest to the accident sequence are as follows:

1. *The assumed fission power levels in the two nuclear heatups, along with variations in the radial and axial peaking factor (RPF and APF) shapes.*

   Because of the way the heatup was run, the operators had very little idea what the actual power level was—the detector was shaded by rods, the total power was very low (~1% of full scale), and the shape was distorted (purposely), but to an unknown extent. In the reference-case setup, the peaking factors accentuate the peaking in the central 140–160 fuel channel regions near the inlet (RPFs for rows 1 and 2). This results in core temperatures consistent with the observation during the accident that showed "glowing red" fuel elements in these channels, but with not much more of the core "involved" at least at that point. The actual "power control" used was to observe and manually control the rate of temperature rise of the fuel in the central core region via control rod manipulation. Variation of the assumed power in the critical regions can demonstrate that with relatively small variations from the reference values (well within the uncertainty bands), the accident might not have occurred at all (i.e., like in the case of previous anneals), or it could have been a lot worse (and perhaps readily detectable) near the start of the sequence.

2. *The very small net core flow values during the heatup and "cooking" periods.*

   The reference values selected are arbitrary, and probably not known to any reasonable accuracy since they are relative "trickles" compared to the nominal forced flow values. During the two heatup periods, however, they are crucial in that if they were much higher, they would have provided enough cooling, other factors being equal, to avoid the accident. Further along, however, had they been larger flows, the increased oxygen availability would have led to much higher temperatures.

3. *The Wigner energy release in the initial period.*

   Both the total and spatial variations in Wigner energy released early in the sequence are also crucial to the course of events. In the GRSAC reference-case simulation, Wigner energy release is a major early source of heat input.

4. *The oxidation of AM cartridges.*

   Cartridge oxidation is also crucial at the start, since the AM cartridges are known to fail and oxidize at a temperature lower than any other core component. The crucial parameters here are the time-at-temperature failure model and the rate of energy release (from oxidation) upon failure, all of which are input variables.

5. *The oxidation parameters for graphite, clad, and fuel.*

The parameters in the oxidation equations, particularly for graphite, also appear to be crucial at the start. Graphite oxidation appears to dominate the oxygen supply/demand picture in the early part of the accident, and may have provided enough extra heating to push some of the clad and fuel to the damage temperature. For the Windscale cases, the oxidation parameters for "Windscale graphite—irradiated" are used. These give much higher oxidation rates than those used for nuclear-grade graphites used to derive the GRSAC reference model. The rationale for cutting them back in the reference set of values, besides the fact that too much of the core burns up if they are not, is that the bulk of the core graphite may not have been damaged via irradiation as much as the (small) test samples were.

The oxidation model for the aluminum clad uses parameters for magnesium at this point, with the exception that the thin protective oxide layer is accounted for, and it is assumed to stay in tact until the aluminum melting temperature is reached. At that point, the fuel is exposed and begins oxidizing, and that creates additional heat that makes the clad oxidize faster, etc., and speeds up the whole oxidation process in the node considerably. For additional discussions of clad oxidation models, see Appendix F.

The reference-case oxidation model for the uranium metal fuel uses sensitivity (multiplier) coefficients of 1.0. In the early part of the accident transient, use of the high coefficients can be rationalized (or accommodated) by assuming less oxygen is available; otherwise, the predicted fuel temperatures at that time would be too high. However, in the last part of the accident, when the shutdown blowers are turned on, plenty of oxygen is available, and with the high values for oxidation rates, perhaps the prediction of total fuel oxidized is too high (data on total fuel oxidation have not been published). A possible explanation for overprediction of total uranium metal oxidized could be a "self-protection" effect that debris in the affected channels would have (i.e., limiting the flow in these channels and preventing access to "flame-fanning" oxygen-rich air).

6. *Range of applicability: physical property and oxidation rate equations.*

Another problem with the last part of the accident (with the blowers turned on), is that the predicted (and observed) temperatures in the core go very high (~1750°C), past the temperature limits where some of the correlations for heat and mass transfer, physical properties, and oxidation reaction rates (in particular) may be valid. Data for these high-temperature conditions may not be available for some of the materials. The difficulties in getting an accurate simulation in this part of the transient may not be crucial to the major objectives of the Windscale accident simulation, however, which are to determine the major contributors and factors involved in causing a serious accident and to see what effects intended mitigating actions would have on the outcome of the event.

E.9 WINDSCALE CONCLUSIONS

The GRSAC analysis of the October 1957 Windscale 1 reactor accident provided an opportunity to incorporate detailed models of the essential features of the accident and the means to study the interactions and relative importance of these various effects. There were obviously some characteristics and operational maneuvers that were different from the many similar annealing operations that had taken place without incident on both Windscale 1 and 2. Since there are so many variables involved, each with its own accompanying uncertainty band, it is not feasible to predict precisely how much each of the factors contributed to the accident. However, based on the testimony

of the Windscale operating and analysis teams and other observations, some conclusions can be drawn.

1. The two fission heating periods concentrating power in a selected core region, plus the resulting release of Wigner stored energy in the inlet region, were the two major factors in raising the temperature of the "lower central inlet" portion of the core to a higher-than-usual level.

2. Once this portion of the core was at the higher temperature level, the relatively "uncooled" core temperatures were high enough to cause the further release of energy from additional annealing (Wigner energy), failure and oxidation of AM cartridges (which were known to begin failing at temperatures in excess of ~440°C), and graphite oxidation. In this portion of the accident sequence, the heating process was "oxygen limited," i.e., small increases in air coolant flow would raise the temperatures in this hot region rather than provide a net cooling effect as was intended.

3. At this early point in the sequence, there was in fact a very delicate balance between an ultimate safe shutdown and an ultimate fiery accident. Sensitivity studies described in Section E.6.9 show how very minor changes in the models and/or the scenario could make the difference between the two extreme outcomes.

4. In the reference-case GRSAC sequence, the increased flow (due to closure of the chimney hatch and the successive damper openings) caused the initial cladding failure to occur just following the fourth damper opening. The release of fission gasses and the uranium metal fuel oxidation that occurs at this point correspond to the initial observation of chimney stack activity due to fission products noted in the testimony.

5. The relative timing of GRSAC predictions for the release of tritium (earlier in the sequence, due to AM cartridge failure), and of fission products due to clad failure, which began during the last part of the damper opening sequence, corresponds to the observations made in Germany, where the tritium "fallout" was detected about a day earlier than the fission product fallout.[15]

6. The vast majority of the damage to the fuel, cladding, and graphite occurred following the restart of the shutdown fans, which was a last-ditch attempt to cool the core. While the fans succeeded in cooling most of the core, the hot section of the core was at a high enough temperature such that the heat generated from oxidation of the clad, fuel, and graphite far exceeded the cooling effects. Most of the heat generated in this period was from graphite oxidation, although heat from fuel and clad oxidation, Wigner energy release, and AM cartridge oxidation also contributed to the problem as the high-temperature front was "pushed" through the core by the air flow. The abrupt cessation of flaming when the fans were turned off (in GRSAC) also corresponds to observations.

7. The GRSAC reference-case damage estimates for oxidation of clad, fuel, and graphite are predictably high compared to those in reports available to date. Certain limitations of the GRSAC analysis would tend to make its damage estimates higher than actual: removal of fuel, blockage of channels due to rubble from damaged elements (which would tend to protect channel components from oxidation), and water cooling effects were not modeled.

8. In a recent assessment of graphite behavior,[24] investigators addressing safety concerns about U.S.-design graphite reactors in light of the Chernobyl accident correctly noted that (Wigner) stored energy release would not be a factor in postulated accident scenarios for high-temperature gas-cooled reactors because of the higher temperatures at which they operate. However, that report came to a different conclusion about the role of stored energy release in the Windscale

accident from the one reached in this analysis; that is, Schweitzer et al. claimed there was "no evidence that stored energy release initiated or played a significant role in the evolution of the Windscale accident." That report's conclusion was apparently based on a detailed survey of data on the potential for stored energy release but not on a comprehensive simulation.

On the other hand, this analysis is based on the comprehensive GRSAC simulation that included (for the first time, to the best of our knowledge) all of the potential factors involved in the heatup. The GRSAC model for stored energy release was developed using many of the same data sources used in the Schweitzer assessment and, in addition, used data from graphite actually exposed in Windscale 1 just prior to the accident (Attree et al. 1957). The conclusion reached from the GRSAC study clearly indicated that the stored energy release and the two fission power heatup periods were both major factors in the heatup of a portion of the core to a temperature only slightly higher than "usual." This maximum (localized) temperature was high enough so that AM cartridge failure and some graphite oxidation occurred, and eventually significant clad failure and fuel oxidation took place when attempts were made to admit additional air into the core for cooling.

E.10 REFERENCES

1. "Windscale—The Committee's Report," *Nucl. Eng.* **2,** 510–513 (December 1957).

2. Arnold, L., *Windscale 1957, Anatomy of a Nuclear Accident,* St. Martin's Press (1992).

3. Bowen, cited in Arnold (Ref. 2), p. 128.

4. Command 302, "Accident at Windscale No. 1 Pile on 10th October, 1957," presented to the Parliament by the Prime Minister, November 1957. US documentation as NP-6539.

5. Command 1225, "Second Report to the Medical Research Council on the Hazards to Man of Nuclear and Allied Radiations," HMSO (1960).

6. Hill, J. M., "A More Detailed Assessment of the Early Stages of the Windscale Fire," memorandum to Sir Leonard Owen, Jan. 17, 1958.

7. Gausden Report. "Inspection of the Core," a portion of post accident testimony for the Penney Inquiry (1957).

8. Hand marked journal, "Windscale Pile 1 Incident: Summary of Events," written for Mr. Touhy immediately after the accident (1957).

9. PRO (Public Records Office), London (1996).

AB PRO Ref.	Date	Title
7/1655	1952	The unexpected temperature rise on Pile 1 on 30 September 1952.
7/6435	1957	Windscale pile incident October 1957 report of work carried out by R&D Branch Windscale from 10 October to 5 November 1957.
62/72	1950	Windscale general description of piles.

86/33	1957	Committee of Inquiry; Exhibit 9 reports tabled by Mr. Hall. Temperature of AM cartridges, and Effects of a fire in an AM channel on the surrounding graphite.
86/37	1957	Committee of Inquiry; Exhibit 14. Chart showing spread of Wigner reaction during the last five attempted anneals.
86/38	1957	Committee of Inquiry; Exhibit 15. Report dated 16 October 1957 by K. Saddington on AM alloy cartridges.
86/39	1957	Committee of Inquiry; Exhibit 16. Report by D. Hindley on fuel and graphite temperature measurements in the Windscale pile.
86/43	1957	Committee of Inquiry; Exhibit 20. Report on magnitudes of various heat sources in the Windscale pile.
86/46	1957	Committee of Inquiry; Exhibit 23. Effect of a fire in an AM channel on the surrounding graphite.
86/50	1957	Committee of Inquiry; Exhibit 27. The possible failure of Mark 10 cartridges due to a thermal shock.
86/54	1957	Committee of Inquiry; Exhibit 31. Drawing SK/45147C, cartridge Mark 10 arrangement; production pile, Windscale.

AB PRO Ref.	Date	Title
86/61	1957	Committee of Inquiry; Exhibit 37. Flux distributions for reactor with control rods, B. Cutts.
86/68	1957	Committee of Inquiry; Exhibit 44. Analysis of effluent in pile 1 stack up to 1530 hours on 10 October 1957, J. Moore.
86/70	1957	Committee of Inquiry; Exhibit 46. Summary of previous Wigner energy releases, piles 1 and 2.
86/84	1957	Committee of Inquiry; Exhibit 60. Paper AERE M/M 177 (RSRC/S 16), Uranium oxidation in relation to the safety of gas cooled reactor, B. E. Hopkinson.
86/88	1957	Committee of Inquiry; Exhibit 64. Chart of reactor showing zones 1, 2, and 3.
86/92	1957	Committee of Inquiry; Exhibit 68. Radiochemical Centre, isotope loading in pile 1, October 1957.

10. Penney Inquiry, "Report on the Accident at Windscale No. 1 Pile on the 10th October, 1957" Court of Inquiry, Sir William Penney, Chairman (October 1957).

11. Windscale Pile 1 Control Room Log, "Production," history obtained from the British Ministry of Defense (1995).

12. Smith, B. S., et al., "Some Estimates of the Scale of the Windscale Accident Based upon the Noble Gas Released," AERE HP/M 133 (1958).

13. Beattie, J. R., *An Assessment of Environmental Hazard from Fission Product Releases,"* U.K. Atomic Energy Authority, Authority Health and Safety Branch Report (5) R64 (1963).

14. Clarke, R. H., "An Analysis of the Windscale Accident Using the WEERIE Code," *Ann. Nucl. Sci. Eng.* **1,** 73–82 (1974).

15. Chamberlain, A. C., "Emission of Fission Products and Other Activities During the Accident at Windscale, Pile 1," AERE-M3194 (July 1981).

16. Nairn, J. S., and P. J. Robinson, "The Reaction of Graphite with Gaseous Coolants in the Windscale and Calder Reactors," presented at the US/UK Graphite Conference, London, December (TID 7565 171) (1957).

17. Testimony given at the Court of Inquiry, October 1957, for inclusion in the first Penney Inquiry report.

18. Abbud-Madrid, A., et al.,"Experimental Results on the Ignition and Combustion Behavior of Pure Bulk Metals," presented at the Spring Meeting of the Western States Section of Combustion Institute, paper 93.007 (1993).

19. Markstein, G. H., "The Combustion of Metals," *AIAA J.* **1**(3), 550–562 (1963).

20. Grosse, A. V., and J. B. Conway, "Combustion of Metals in Oxygen," *Ind. Eng. Chem.* **50**(4), 663–672 (1958).

21. Epstein, L. F., "Correlation and Prediction of Explosive Metal-Water Reaction Temperatures," GEAP-3335 (1960).

22. Ball, S. J., and D. J. Nypaver., *MORECA-2: Interactive Simulator for Modular High-Temperature Gas-Cooled Reactor Core Transients and Heatup Accidents with ATWS Options,* NUREG/CR-5945, ORNL/TM-12233 (1992).

23. Nightingale, R. E. (ed.), *Nuclear Graphite,* Academic Press, New York, pp. 329–330 (1962).

24. Schweitzer, D. G., et al., *A Safety Assessment of the Use of Graphite in Nuclear Reactors Licensed by the U.S. NRC,* NUREG/CR-4981, BNL-NUREG-52092 (1987).

APPENDIX F.
GRSAC BENCHMARK USING FRENCH CHANNEL FIRE DATA

F.1 REACTOR DESCRIPTION

The subject of this section is a channel fire that occurred in the French G1 reactor—a natural uranium–fueled, graphite-moderated, air-cooled reactor. The out-of-pile tests which simulate this channel fire are used here as a benchmark test of the GRSAC program.

The G1 reactor, which is described in detail in Appendix H, had a unique cooling flow arrangement. Air entered a vertical plenum located at the midplane of the core and passed in both directions from this central plenum into horizontal fuel channels, exiting the core from both the fuel feed and discharge faces.

F.2 DESCRIPTION OF CHANNEL FIRE IN THE G1 REACTOR

The GI accident is described by de Rouville et al.:[1]

> "The reactor was brought up to power . . . on 26 October 1956. . . . Following a level period of 5 hours at 15 MW, then 30 minutes at 30 MW, the power was increased at 1842 hr, reaching 40 MW at about 1850 hr."

During this time an adjustment to the dampers was carried out (they had been thrown out of adjustment by the reheating) in order to make the temperatures of air leaving the channels uniform.

> "At this power, the highest temperature on the cans . . . was 275°C. However, . . . hot spots [were] in the vicinity of 300°C on the jackets of the central cartridges.
>
> "The can break detection system . . . gave its first pre-alert signal at the loading side at 1907 hr.
>
> "The chambers . . . in the air channel downstream from the reactor indicated an alert at 1854 hours. Power reduction was ordered at 1915.
>
> "It was deduced that there had been a sudden increase in activity at about 1900 hours."

To assess the damage,

> "optical devices were built . . . to look through the loading face, the unloading face . . . and into the central slot. On the loading side it was noted that a great part of the magnesium can had burned up: the uranium bar rested on a bed of magnesia, the channel being completely obstructed. Furthermore, the cartridge appears to have shifted towards the slot. Examination through the slot confirmed that the edge of the cartridge protruded from it by about 6 cm."
>
> "The cartridge was removed by means of a tube equipped with end teeth like a trephine."

Later discussion by Martin et al.[2] provides further details.

> "Toward the end of the power-up phase, temperature in the duct experiencing low flow must have exceeded 630 to 640°C on the cladding. The fire started in the normally hot region and intensified because of the low flowrate. Oxidation of the magnesium formed a plug on this spot, and the duct became obstructed. The nuclear power then produced combustion of 5–6 kg uranium and caused about 2 additional kilograms to melt. Once the duct became obstructed, virtually all (99%) of the non-volatile combustion products remained in place, and the remainder were caught on the filters.
>
> "Remarkably, in the region in which the uranium was not affected, the cladding nevertheless burned up entirely, but damage to the fuel was only very superficial.
>
> "We should add that neither the graphite nor the adjoining elements suffered any damage on that occasion."

de Rouville et al.[1] cite three possible causes for the accident:

1. The sudden development of a can leak during a temperature rise.
2. The protrusion of the cartridge into the central slot, hence reducing the cooling flow into the affected channel.
3. The partial obstruction of the channel by a foreign body.

With regard to item 1, later tests showed that a major crack in the cladding could be a point of enhanced oxidation, probably due to air flow impinging on a roughened surface. A small failure of the cladding would likely have no effect, even if uranium is exposed to air (uranium is less oxidation prone than the cladding). Items 2 and 3, both of which diminish cooling flow and thus create higher-than-expected temperatures, are the more likely initiating cause. The event was also directly related to the ramp in power from 30 to 40 MW started at 1842 h and completed at 1850 h. A sudden increase in radioactivity was observed at 1854 h, which signaled the start of the event. Martin et al.[2] notes that the reactor remained at full power for about 20 min following the onset of the accident.

F.3 THE OUT-OF-PILE TEST

F.3.1 Physical Arrangement and Materials

Out-of-pile tests of the G1 channel fire are described by Martin et al.[2] Nuclear heating of a fuel element was simulated by enclosing an electrical resistance heater in a uranium tube of 2-mm wall thickness. The heaters were capable of generating a 12-W/cm^2 heat flux, representative of the G1 reactor power density, and had an upper limit temperature of 1050°C. The uranium cylinder was placed in a magnesium can simulating the cladding. However, an 18 fin cladding was used instead of the 8 fins shown in the Appendix H description. The length of the elements ranged from 30 to 60 cm. They were placed in graphite tubes measuring 40 to 80 cm in length. Presumably, cladding and fuel dimensions were typical of a G1 fuel element, except for the number of fins. Also presumably, the diameter of the graphite duplicated the G1 fuel channel diameter (i.e., 7.0 cm). Temperatures were measured on the cladding, the uranium, and the resistance heater. A test run proceeded by fixing an air flow rate and turning on the heater until the magnesium cladding reached a temperature between 625 and 650°C, at which point a location on the magnesium ignited. Progression of the fire was

followed by means of photographs taken along the axis. The final damage state was determined by photographs; degree of oxidation and melting were determined by weighing.

F.3.2 Test Results

Four tests are described, classified with respect to air flow rate.

1. **Zero air flow.** In a duct with no air flow and some degree of sealing to outside air, ignition of the magnesium occurred at one localized point when cladding temperature reached 640 to 650°C. The fire did not spread unless the surrounding cladding temperature exceeded 620°C. Even so, propagation was extremely slow. Evidently, the fire did not actually propagate, but the surface of the cladding oxidized a the relatively low temperature of about 700°C. (Slight addition of air to this condition caused an immediate flash and a renewed outbreak of the fire.)

2. **3–4 g/sec air flow (3% of normal).** When air was supplied at this rate, ignition of the cladding occurred at temperatures of 625 to 630°C. The fire was intense, characterized by flashes, and advanced at the rate of 2 cm/min. When the flame front reached a thermocouple location, cladding temperature fluctuations between 840 and 1050°C lasted for about 3 min. Uranium temperatures beneath the burning cladding reached 800°C. The uranium rod oxidized superficially (about 0.1 to 0.2 mm in depth) and lost 10 g mass. The 30-cm length of cladding was entirely burned to fine MgO powder. The air flow passage was almost completely obstructed.

3. **15 g/sec air flow, (15% of normal).** When the air flow was alternately stopped and restarted, the intensity of the fire was found to closely follow the air flow alterations. The average rate of fire propagation on the magnesium was 2–3 cm/min, the same as for the lower air flow rate. Cladding temperatures remained fairly low (790°C), uranium reaching 800°C about 1 mm beneath the surface. A slit cladding was used which exposed uranium along the line of the slit. A 1-mm burned groove in the uranium was observed along the slit. Rod length was 60 cm. The most affected rod lost 16 g uranium. The cladding completely oxidized over 25 cm of its 60-cm length. It was reasoned that the cool rod ends, at about 400–450°C, prevented complete oxidation of the cladding. It was also noted that oxidized cladding provided some protection for the uranium because the "magnesium burned in localized fashion."

4. **60–65 g/sec air flow (66% of normal).** This test was run using a 30-cm-long fuel element; iron was substituted for uranium. The fire in the cladding was extremely violent at this high air flow rate. The fire began "in calm air at 125–150°C" [?] and at about 645°C on the cladding. When the air flow was turned on, the fire became violent and quickly spread over the entire cladding, which was destroyed in less than 1 min. Rate of propagation was about 30 cm/min. Cladding temperatures rose to at least the upper limit of detection, 1200°C. Molten magnesium occurred in the duct which was entirely blocked at the inlet. Table F.1 summarizes the test observations.

F.4 MAGNESIUM IGNITION

F.4.1 Measured Ignition Temperatures

The most distinctive feature of these tests is the consistent ignition of magnesium at bulk temperatures between 620 and 650°C. In Appendix B, the term "pseudo-ignition temperature" is used to signify that measured ignition temperatures of all metals seem to depend on the particular situation. In this case, magnesium was heated by a resistance heater within a uranium tube with heat being transferred to the interior of the magnesium tube by radiation and conduction. Martin observed that

ignition occurred at highly localized points on the surface. Table F.2 summarizes reported magnesium ignition temperatures.

Table F.1. Summary of test observations

	Air flow (g/sec) (percent nominal)			
	0 (0%)	3–4 (3%)	15 (15%)[a]	60–65 (66%)
Magnesium ignition (°C)	640–650	620–625	620–625	645
Max. temp. magnesium (°C)	700	1050	790	1200
Magnesium oxidized (%)		100%	42%[b]	100%
Burning rate (cm/min)		2	2-3	30
Max. temp. uranium (°C)		800	800	NA[c]
Uranium oxidized (g)		10	16	NA[c]

a. Flow was "pulsed."
b. Probably would have been 100% if the ends had not been cool.
c. Iron used instead of uranium.

Table F.2. Survey of measured magnesium ignition temperatures

Reference	Pseudo-ignition temperature (°C)	Comments
Martin et al.[2]	620–650	Flow, visual
Darras et al.[3]	585–645	Quiescent, temperature break
Darras et al.[3]	610–650	For Magnox alloy
Fassel et al.[4]	623	Quiescent, temperature break, numerous alloys
Abbud-Madrid[5]	977	Quiescent, temperature break

Note that Darras reports ignition temperatures for a French Magnox alloy similar to those of commercially pure magnesium. The French Magnox alloy is reported by Blanchard et al.[6] have a composition of Mg–0.5% Zr.* The term "temperature break" in Table F.2 refers to a method developed by Fassel wherein the ignition temperature is defined by a distinct break in the metal temperature recording with respect to time. It appears to be a common procedure, used as late as 1993. The method, however, reports only a bulk temperature, and misses the true, localized ignition temperature.

* Reports show that alloying ingredients may have a marked effect on the burning characteristics of a metal. The effects with magnesium is most often to reduce the ignition temperature, possibly due to a reduction in solidus temperature. For example, see Fassel.[4]

Most studies report magnesium ignition at about 600°C, at which point its vapor pressure is 0.0013 atm. At the outlier reported by Abbud-Madrid, 977°C, the vapor pressure is 0.318 atm. This enormous difference is undoubtedly due to details of experimental technique; however, the exact cause is not known. An important consideration is whether the magnesium cladding will ignite at about 600°C or at about 977°C as reported by Abbud-Madrid. Oxidation rates increase at ignition because the mass transfer inhibition of oxygen delivery to the surface is removed. The majority of tests favor about 600°C as the ignition temperature, but 977°C seems more reasonable mechanistically; the 0.0013 atm vapor pressure at 600°C appears to be too low to generate burning (i.e., gas-phase oxidation).

F.4.2 Magnesium Ignition Model

There have been several ignition models reported based on a simple heat balance, wherein heat gain due to surface oxidation is compared against the estimated heat loss. When heat gain exceeds loss, temperatures rise sharply by virtue of the rapid rise in reaction rate with temperature. The reasoning is that ignition would inevitably occur soon after such an unstable temperature situation is developed.

It is important for this method to include all heat sources—for example, furnace heat (for an out-of-pile experiment), fission and decay heat, Wigner energy release, and oxidation of other materials (which is not usually done in the literature but which GRSAC does). Similarly, all modes of heat loss must be accurately represented. This concept illustrates that the pseudo-ignition temperature depends on the particular geometry, the coolant flow rate, and in some cases the type of metal (i.e., whether or not an adherent film exists and its thickness). However, use of this method alone is not sufficient because it does not provide the augmented oxidation rates above the ignition temperature.

The burning rate model adopted in GRSAC is described in Sections B.6 and B.16 of Appendix B. The method is based on a mass transport rate comparison rather than a heat balance. The principal assumption is that at high temperature, diffusion of metal vapor from the surface to the free stream may dominate the oxidation rate, assuming metal atoms rapidly oxidize in air under these conditions. The model is best illustrated by referring to Fig. F.1, which shows the variation of oxidation rate with temperature at constant cooling rate for three controlling mechanisms. The horizontal line shows the rate when dominated by the mass transfer of oxygen to the surface. When turbulent flow in the free stream is assumed, the oxygen mass transfer rate is relatively independent of temperature. The curve, "chemical rate," shows the steep rate of increase with temperature typical of an Arrhenius rate expression. The "metal vapor transfer" curve also rises steeply with temperature due to increasing vapor pressure of the metal.

As temperatures increase, oxidation regimes change as indicated by the bold line in the figure. Below T_1 is the regime of chemical control. At this condition, there is ample oxygen delivery to the surface; oxidation is limited by the intrinsic oxidation rate of the metal. Vapor transfer to the air is low due to low vapor pressure. Above T_1 (but below T_2), the oxidation rate is restricted by oxygen transfer to the surface, and therefore remains steady with increasing temperature. In both "chemical control" and "oxygen mass transfer control" regimes, oxidation occurs at the metal surface. Transition to the "burning regime" occurs above T_2, when metal vapor transfer to the free stream exceeds oxygen transfer due to the high vapor pressure of the metal.

Further details are given in Sect. B.16 of Appendix B, where the speculative nature and limitations of the model are emphasized. Here it is necessary to note that the model predicts a transition to the burning regime at about 800°C for magnesium, compared with approximately 630°C observed in the French channel fire tests. It is assumed that the reason for this is that the actual, highly localized, ignition spots observed on the magnesium surface[2] were hotter than the reported bulk temperatures obtained from thermocouples. In such case the burning rate is given by

$$R_b = h_m P_{vap}(T + \Delta T_{HS})/(R_2 T)\,, \qquad (F.1)$$

where

R_b = burning rate, mol/cm^2·min;
h_m = mass transfer coefficient, cm/min;
P_{vap} = vapor pressure at temperature $T + \Delta T_{HS}$, atm;
T = bulk temperature, K;
ΔT_{HS} = hot spot addition, K (set at 300 K for the French tests);
R_2 = gas constant, 82.06 cm^3·atm/mol·K.

Section B.7 of Appendix B includes vapor pressures of some other materials in the test. Clearly, only magnesium develops sufficient vapor pressure to burn in the gas phase for temperatures achieved in the French channel fire tests.

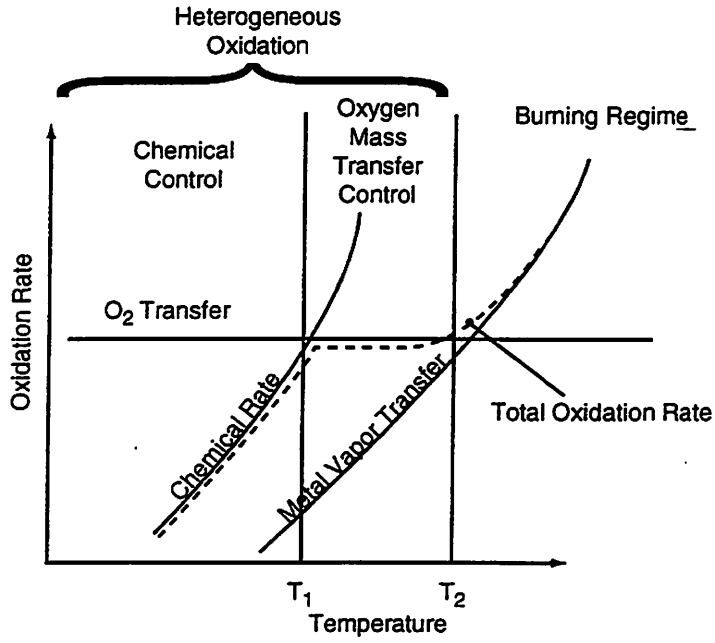

Fig. F.1. Metal oxidation regimes (fixed cooling rate).

F.5 GRSAC SIMULATION

F.5.1 Model Setup

The reference case GRSAC model used the French channel fire experiments is a small core with 163 channels (one per radial node), each with ten axial nodes. The simulated 60-cm-long test section consists of the five axial nodes at the outlet end of the active core, where each axial node is 12 cm long. The radial peaking factors (RPFs) are uniform (=1.0) to create the equivalent of an isolated (adiabatic) central channel. The axial peaking factors (APFs) are tailored to provide for heating the inlet gas to the test section, and to optionally provide (simulated electrical) heat for the test section, and to optionally provide (simulated electrical) heat for the fuel rods. Fuel and cladding oxidation is suppressed in all except this test section, and graphite oxidation sensitivity multiplier terms are set to very small values. The calculation of flow redistribution among the channels is suppressed so that the

test elements will receive the prescribed (input) amount of flow. The model for gas-phase oxidation of the magnesium cladding is activated for this experiment model.

While the French experiments used an oven and electrical resistance heating to heat the test fuel element mockups, in the GRSAC test we have the flow to the experiment nodes heated by the upstream nodes. Some "nuclear" (i.e., electrical) heating may be used, or not, in the test element section. The air cooling flow rate (%) is set manually via the accident screen, as is the nuclear heating input, in MW, for the entire core. The procedure used for these simulation runs is to pre-set the power and flow values to give reasonable heatup rates for the three experimental cases (3, 15, and 60 g/s test element flows).

F.5.2 Model Results

Previous attempts to duplicate the French test results without the magnesium gas-phase burning model were unsuccessful. Element temperatures were several hundreds of degrees hotter than the observed ignition values before high cladding oxidation rates were seen. With the addition of the gas-phase burning model, however, ignition and complete oxidation of the cladding occurs rapidly at temperatures closer to those observed in the tests. The algorithm for gas-phase burning is activated (for magnesium) and added to the expression for either the chemical reaction (Zone 1) or mass transfer (Zone III) type of oxidation, whichever is applicable under the local node circumstances. An arbitrary "hot spot" factor (temperature difference) of 300°C is added to the computed cladding temperature to use as a biased temperature in the calculation of magnesium burning. Hot spots on the cladding were in fact observed during the French experiments. In the reference case simulation, no rate limiting of the gas-phase burning is assumed.

There are two options available for activation of the fuel oxidation process: the first is to allow fuel oxidation to occur if either the cladding exceeds the melting temperature or if the cladding oxidation is 90% complete, whichever occurs first; the second option is to allow fuel oxidation to occur only when the cladding is >90% oxidized. There is also a second modeling option available (via Fortran program change) to reduce the 60-cm test section to a single long node (the outlet node) instead of the five nodes as in the reference case.

The results for the second oxidation option with the reference five-node test section model and the low air flow (3 g/s) (Fig. F.2*) show the very rapid oxidation beginning when the cladding reaches ~750°C, compared to the French observation of ~650°C. The upper left plot shows the cladding and fuel temperatures peaking between ~1800-1900°C due to the peaks in heat input from cladding oxidation (the taller peaks in the lower left plot). The smaller heat power curve in that plot is due to uranium metal fuel rod oxidation, which comes into play when the cladding oxidation is not dominating (in the algorithm, cladding oxidation takes precedence). The corresponding oxidation rates are shown in the upper right plots, and the cumulative oxidation weights in the lower right plots. The very rapid oxidation of the cladding in this case occurs in successive spurts. Ignoring the "dead time" periods, which are judged to be artifacts of the model, the total time for completion of the cladding oxidation is ~12 min, giving an approximate burning rate of ~5 cm/min, compared to the observed value of ~2 cm/min.

The "spurts" (periodic burns) seen in these results are assumed to be an artifact of the model, which does not include such effects as axial radiant heat transport between nodes, which would help to reduce the granularity of the predicted oxidation pattern. In the experiment, it was also observed that there was very little oxidation of the uranium fuel rod, while the simulation results (Fig. F. 3) show substantial fuel oxidation taking place in the periods where cladding oxidation does not dominate.

Using the GRSAC alternative one-node test section model (vs five nodes), the peak temperature for the 3 g/s low-flow case is ~1650°C (Fig. F.3), which is closer than the five-node model predictions

---

* Figures F.2 through F.6 are grouped together and begin on page F-9.

were to the observed value of 1050°C; however, the predicted burn rate is faster, ~7 cm/min vs the observed value of ~2 cm/min.

Results were also obtained for the first oxidation model option, where fuel oxidation is assumed to occur beginning either when 90% of the cladding has been oxidized or when the cladding melts (which generally comes first). Results for the 3 g/s flow case are shown in Fig. F.4. The rapid oxidation of the cladding takes place over about the same time period (9 min), but there is more uranium oxidation predicted, which is contrary to the observations. In all cases, it is assumed that the experiment is terminated just after the cladding burn is complete.

Cases were run with the one-node model for the higher flow experiments. For the 15 g/s flow case, the predicted burn rate was ~24 cm/min (Fig. F.5) vs ~2–3 cm/min observed. The "observed" value here is not considered to be a reliable estimate, however, since the Martin reference notes that the flow was "pulsed," not steady, and that only 42% of the cladding was oxidized. For the 60 g/s flow case, the predicted burn rate was ~60 cm/min (Fig. F.6) vs ">30 cm/min" observed, and the maximum predicted cladding temperature was ~1650°C vs ~1200°C observed. Results are summarized in Table F.3.

In a subsequent version of GRSAC, various oxidation-rate-limiting algorithms will be developed and evaluated in attempts to better match the observed burning rates in the French experiments. Additional rate-limiting mechanisms needing improvement in the model could be accommodation of a limited availability of localized oxygen supply at the point of burning, and a more sophisticated treatment of radiant and convective heat transfer from the cladding.

Table F.3. French channel fire test results

	Flow		
	3%	15%	60%
Observed magnesium oxidation rate (cm/min)	2	2–3	>30
Calculated magnesium oxidation rate[a] (cm/min)	16	65	90
Observed peak temperature (°C)	1050	790	1200
Calculated peak temperature (°C)	1650	1650	1650
Observed uranium oxidized (g)	66	16	c
Calculated uranium oxidized[b]	<5	<5	--

[a] Linearized rate from 20% to 100% magnesium oxidation.
[b] At test termination, when 100% magnesium oxidation occurred.
[c] Test used steel rod instead of uranium.

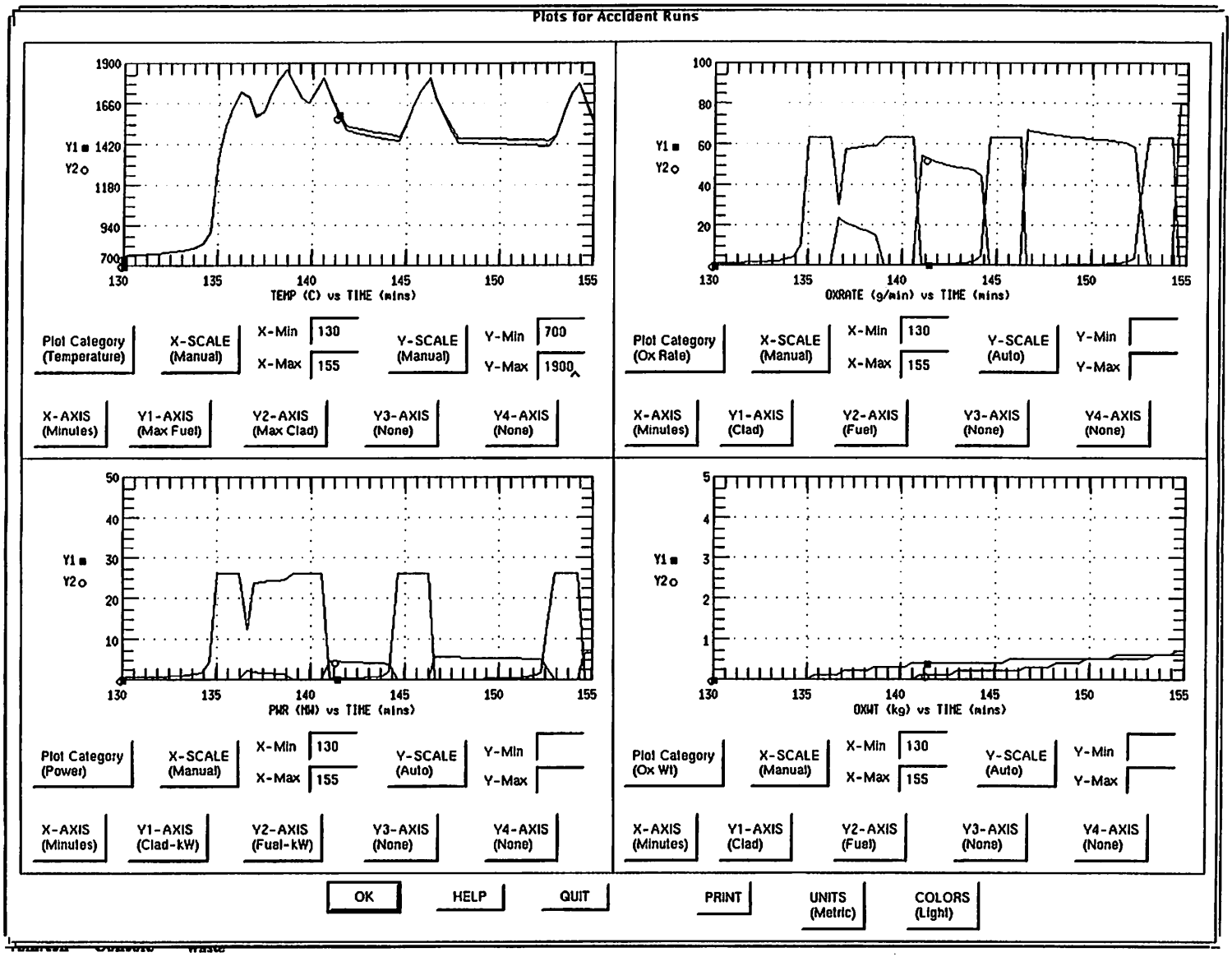

Fig. F.2. Results of French experiment simulation—five-node model, low-flow case (3 g/s). Fuel oxidation allowed only if the cladding oxidation is >90% complete.

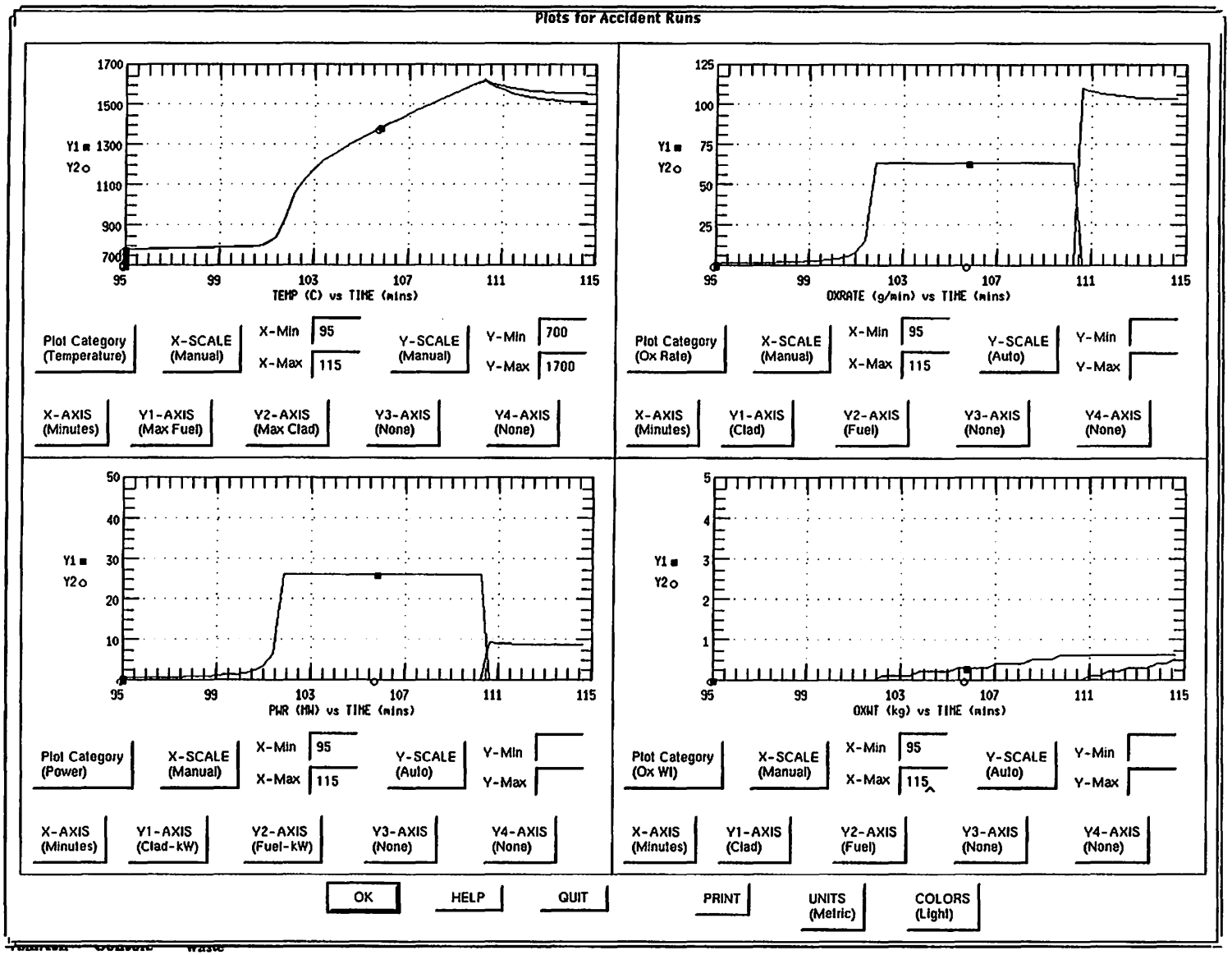

Fig. F.3. Results of French experiment simulation—one-node model, low-flow case (3 g/s). Fuel oxidation allowed only if the cladding oxidation is >90% complete.

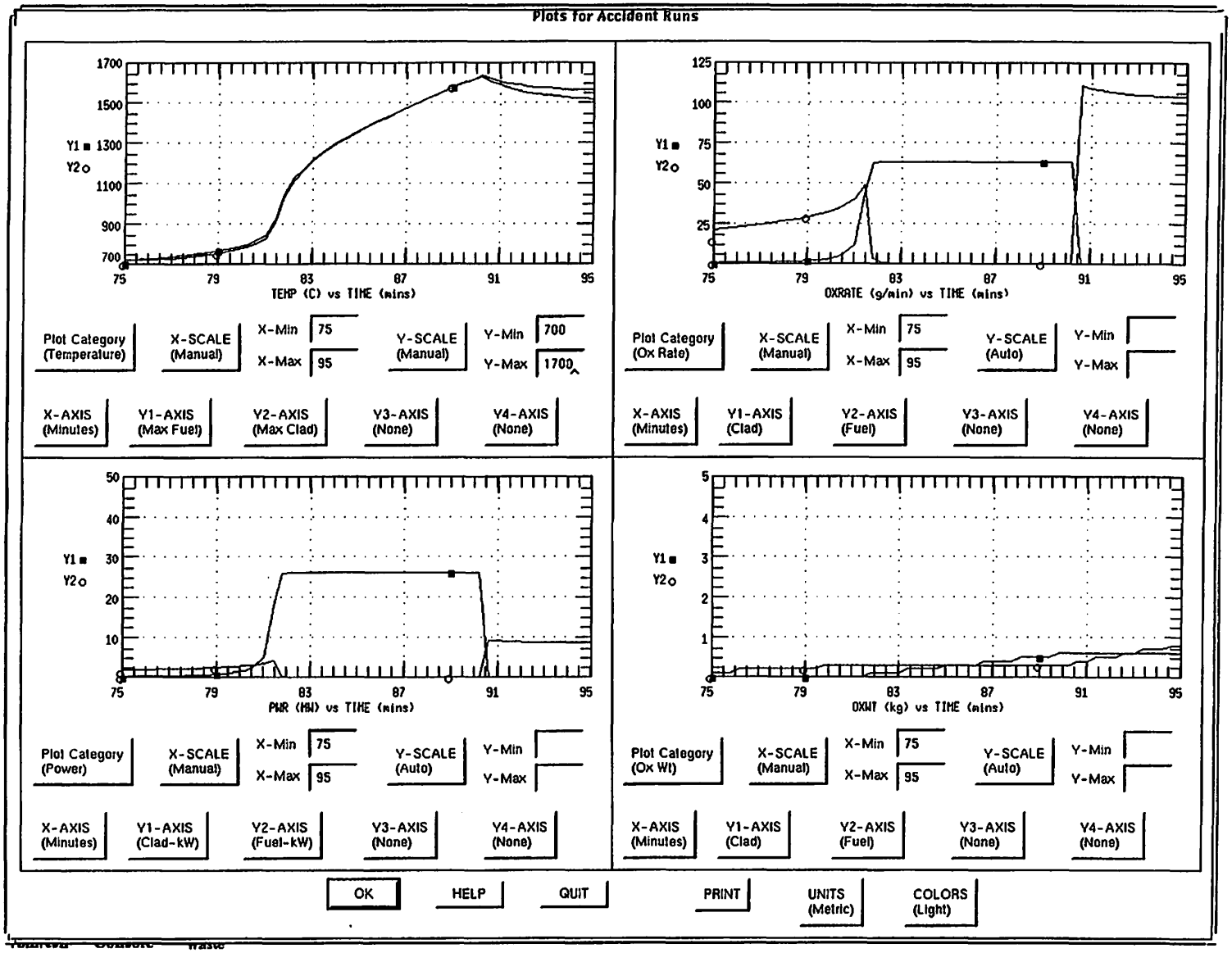

Fig. F.4. Results of French experiment simulation—one-node model, low-flow case (3 g/s). Fuel oxidation allowed if either the cladding exceeds the melting temperature or if the cladding oxidation is >90% complete.

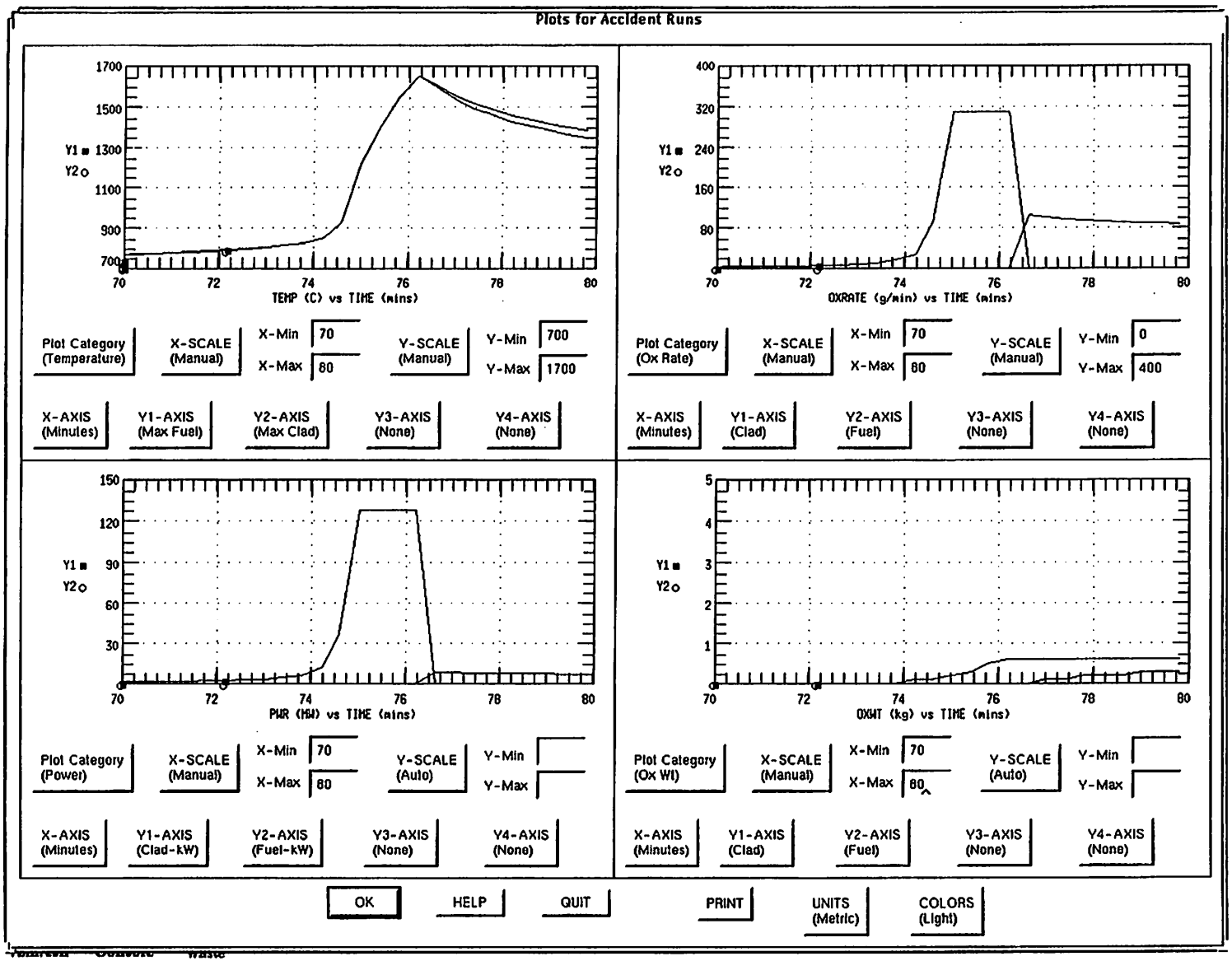

Fig. F.5. Results of French experiment simulation—one-node model, intermediate-flow case (15 g/s). Fuel oxidation allowed only if the cladding oxidation is >90% complete.

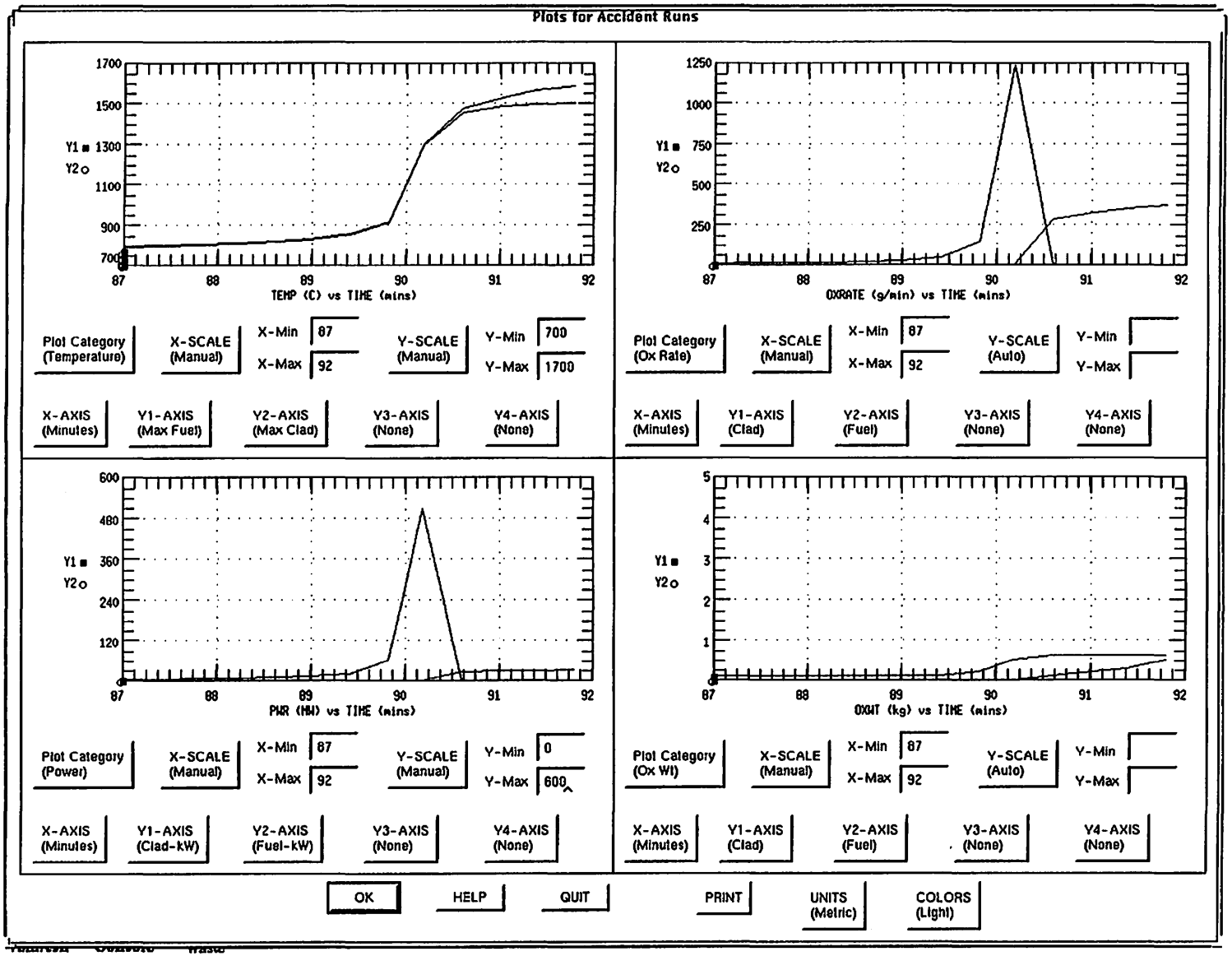

Fig. F.6. Results of French experiment simulation—one-node model, high-flow case (60 g/s). Fuel oxidation allowed only if the cladding oxidation is >90% complete.

F.6 REFERENCES

1. de Rouville, et al., " Partial Combustion of a Fuel Cartridge in Reactor G1," *Proc. 2nd U.N. Conf. on Peaceful Uses of Atomic Energy, Geneva,* **8**(1), 490–492 (1958).

2. Martin, D., et al., "The Combustion in Air of Fuel Elements," in *Proc. Symp. on Reactor Safety and Hazards Evaluation,* IAEA, Vienna (May 1962).

3. Darras, R., et al., "Inflammability of Magnesium and Uranium Heated in Various Gaseous Media," presented at Third Metallurgical Symposium, June 29–July 1, Saclay Center for Nuclear Studies (1959).

4. Fassel, W. M., et al., "Ignition Temperature of Magnesium and Magnesium Alloys," *J. Metals,* pp. 522–528 (July 1951).

5. Abbud-Madrid, A., et al., "Experimental Results on the Ignition and Combustion Behavior of Pure Bulk Metals," presented at Spring Meeting of the Western States Section of the Combustion Institute, March 1993, paper 93.007, pp. 1–10.

6. Blanchard, P., et al., "Metallurgical Studies at CEA of Gas-Graphite Fuel Element Behavior," pp. 352–364 in *Physical Metallurgy of Reactor Fuel Elements,* The Metals Society (1973).

APPENDIX G.
SEVERE ACCIDENT SIMULATIONS OF TYPICAL MAGNOX REACTORS

G.1 MAGNOX REACTOR CHARACTERISTICS

Although the earliest plutonium production reactors were air cooled (Windscale) and water cooled (Hanford), a more attractive next step upward is a moderately pressurized, carbon dioxide–cooled reactor, for the following reasons:

1. Although air-cooled, graphite-moderated reactors have the important advantage of simplicity, they are limited in temperature and pressure because of the potential for oxidizing (or burning) fuel and graphite. As a result, they cannot effectively produce electric power.
2. Because of the relatively high absorption cross-section of hydrogen, water-cooled reactors need some enriched uranium to run at full operating temperature.
3. Carbon dioxide cooling is a good compromise. A CO_2-cooled reactor can run on natural uranium at a reasonably high operating temperature, thereby enabling production of electric power, although at relatively low efficiency.

Two reactors that typify this category are the French G2 and the British Calder Hall reactors, often called Magnox reactors because of their magnesium alloy cladding. At one time about 40 such reactors were operating in England and France. Currently, about 20 are in operation in England and one in Japan. More detailed information on the G2 and Calder Hall designs may be found in Appendix H.

G.2 SELECTION OF SEVERE ACCIDENTS

The GRSAC code allows the analyst to implement and study a wide variety of severe accident scenarios, including anticipated transient without scram (ATWS) accidents, rapid (or slow) loss of forced circulation (LOFC) accidents, and depressurization accidents. Following depressurization, there is the option of assuming air ingress, which can lead to oxidation of the graphite, cladding, and (subsequently) the fuel. In this section of the report, two types of severe accident scenarios are presented as examples. It is emphasized that these examples present cases that are more severe than would normally be considered as design basis accidents. In the first, a typical Magnox design is used in investigating some of the factors that affect the chances of short-term cladding failure in combined ATWS-LOFC scenarios. In the second, a Magnox plant is used as the vehicle for investigating scenarios in which there is long-term clad and fuel failure from ATWS, LOFC, depressurization, and air ingress that results in considerable fuel element oxidation. Two variations of this second scenario are presented.

The first accident scenario is of particular interest because if there is significant short-term clad failure, damage to the fuel can occur which could lead to the buildup of a large circulating inventory of fission products in the primary circuit, so a subsequent depressurization (with a substantial driving force) could disperse the radioactivity over a wide area. Furthermore, in a subsequent core heatup following depressurization and air ingress, the localized heat generation from oxidation of the damaged fuel elements could cause the affected portion of the core to heat up much faster than the bulk of the core, thus reducing the time available to safely restart the core cooling function. Restart of air cooling with a portion of the core above a critical temperature can lead to "fanning the flames" rather than a cooldown.

Many variations on the longer-term transient are also possible, since the timing of the many postulated events can be crucial to the total amount of core damage and dispersion of radioactivity. Two variations are presented. With accident progressions that stretch out into days, there are many more possibilities for mitigating and/or well-meaning-but-detrimental actions by the operators. Unlike the older air-cooled designs, there needs to be a specific mechanism postulated for air ingress in the Magnox reactor types before clad and fuel oxidation can become a major problem. However, in these analyses it is shown that relatively small leakage rates can provide enough oxygen to damage substantial numbers of fuel elements over the long time period of the accident scenario.

G.3 GRSAC SIMULATION ASSUMPTIONS

The GRSAC simulation of the Magnox cores is similar to that noted in the Windscale analysis (Appendix E), and with the active core modeled by 163 radial × 10 axial nodes (1630 total), and with an additional 1240 nodes for the reflectors. The neutronics (point kinetics) model is used for the ATWS cases. Another difference in the modeling is that higher-grade nuclear graphite properties are assumed, with considerably more resistance to oxidation. The model for the magnesium cladding (vs aluminum) oxidation is also used (see Appendix B). In Windscale, the cladding was assumed to have a protective aluminum oxide film that made it resistant to oxidation up to its melting temperature, while for this analyses, the magnesium is assumed vulnerable to oxidation at lower temperatures. Also, because of its much lower (than aluminum) vapor pressure, a gas-phase burning model (Appendix B) is implemented. Validation studies using the French experiment data (Appendix F) indicated the need for implementation of this model.

The reference case radial and axial peaking factors (RPFs and APFs) used for both sets of analyses are shown in Figs. G.1 and G.2. While they can be altered as needed, these are the ones designated as "Magnox reference" curves in GRSAC.

G.4 GRSAC SIMULATION OF SHORT-TERM ATWS-LOFC SCENARIOS

The reference case simulation for a representative Magnox plant of the short-term ATWS-LOFC showed the design to have good inherent self-shutdown capabilities (via the negative temperature-reactivity feedback mechanisms). In the reference scenario, with a relatively fast flow coastdown (Fig. G.3), the maximum clad temperature peaked at 608°C (vs 640°C melting temperature) (Fig. G.4).

With the reference case flow coastdown sped up by a factor of 5, the inherent power response to the LOFC was faster, but the peak clad temperature was higher than in the reference case (623°C). Going further to a much faster coastdown (factor of 10), the peak clad temperature was somewhat higher (627°C) but clearly near an upper limit temperature for this scenario that would be less than the clad melting temperature. Conversely, slowing down the coastdown by a factor of 3.33 resulted in a lower clad peak temperature, 597°C. In the next variation, the flow coastdown is slowed considerably (factor of 10), resulting in a clad peak temperature of 589°C. Hence, for ATWS-LOFC cases, there do not appear to be multiple local optimums (for worst case) of flow coastdown rates, and the faster coastdowns are typically the worst cases.

Another significant factor in the response to the short-term ATWS-LOFC accident is the temperature-reactivity feedback. In the next variation it is assumed that the fuel feedback coefficient (nominally –2.0E-5 reactivity/°C) is halved, and the reference flow coastdown is sped up again by a factor of 5. The results are shown in Fig. G.5, where the peak clad temperature reaches 669°C, and 6.6% of the clad exceeds the melting temperature of 640°C. With a 25% reduction in fuel coefficient and a 75% reduction in moderator coefficient (nominally –4.0E-5 reactivity/°C) along with the sped up (by a factor of 5) coastdown, the peak clad temperature reaches 641°C, and 2.9% of the cladding exceeds the 640°C melting temperature (Fig. G.6). In this case, a 25% reduction in the fuel coefficient

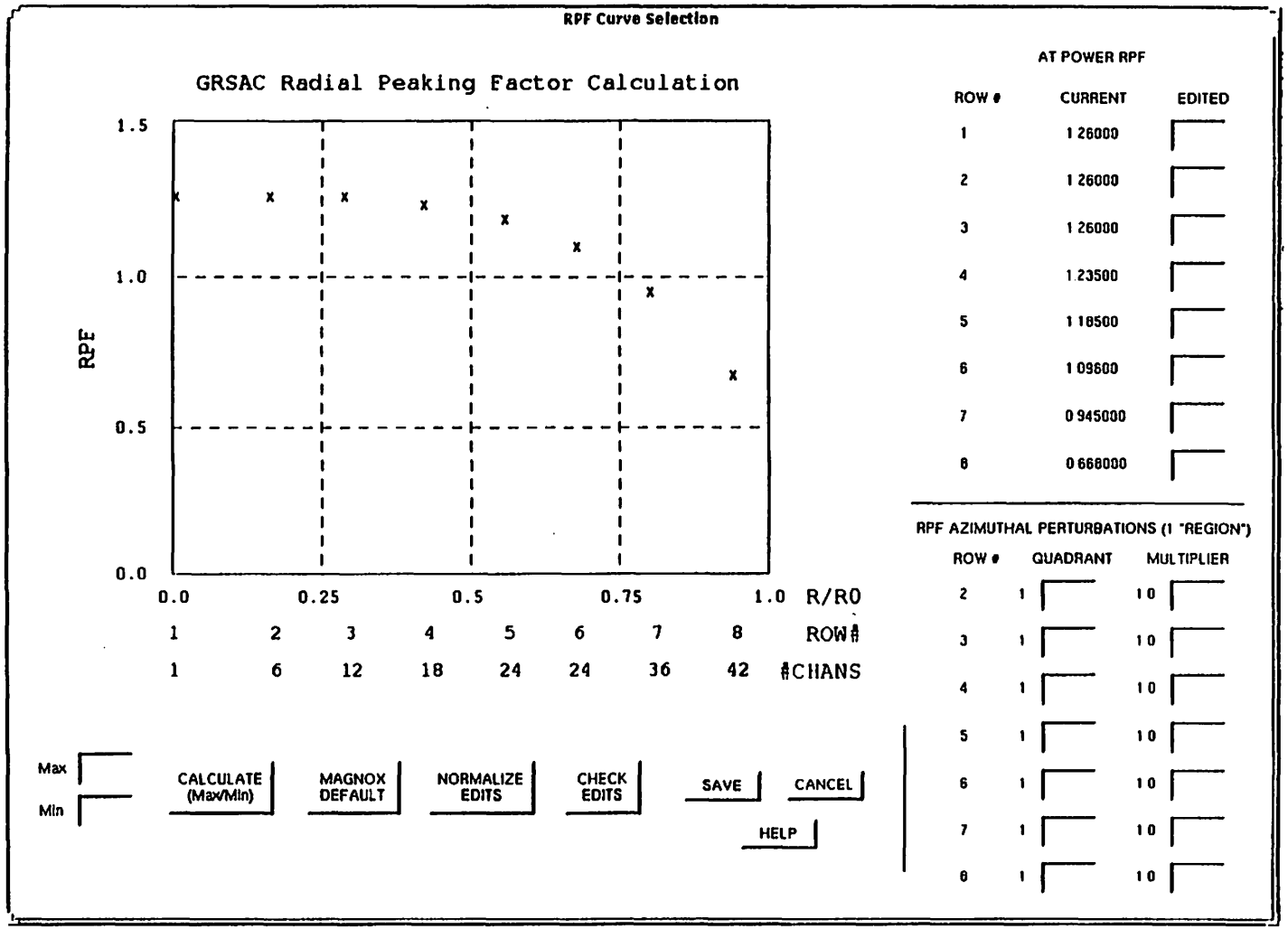

Fig. G.1. GRSAC radial peaking factors used for all reference case Magnox reactor accident studies.

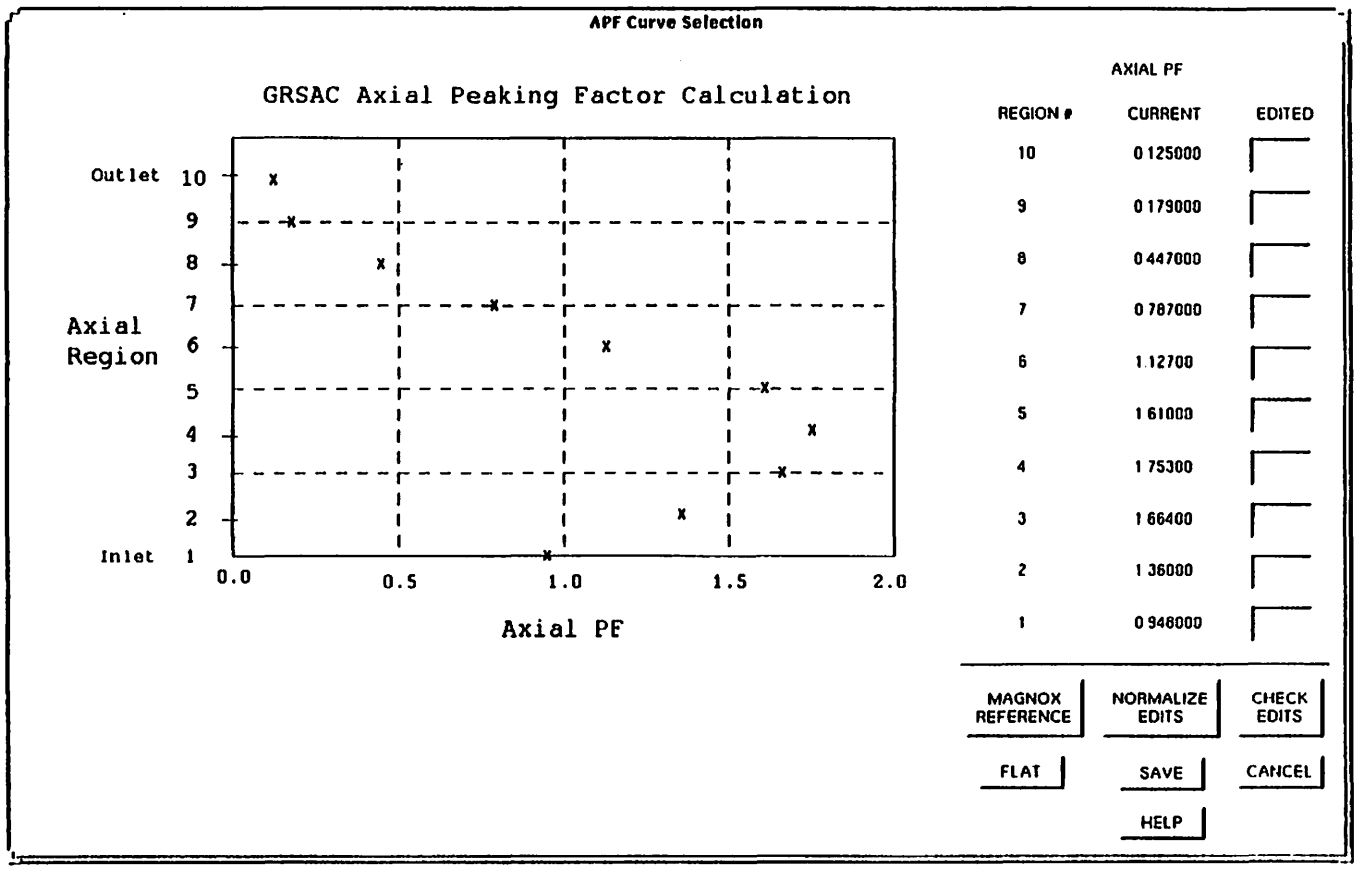

Fig. G.2. GRSAC axial peaking factors used for all reference case Magnox reactor accident studies.

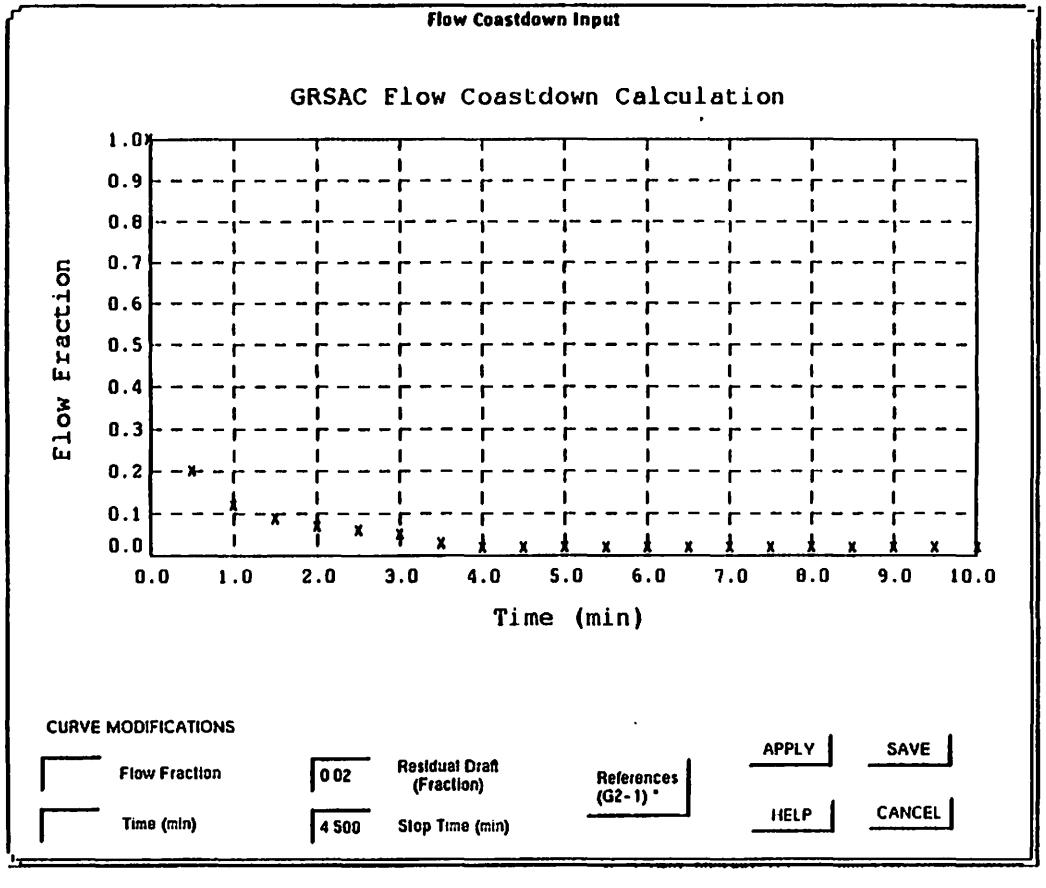

Fig. G.3. GRSAC reference case flow coastdown curve used for short-term ATWS-LOFC accident studies.

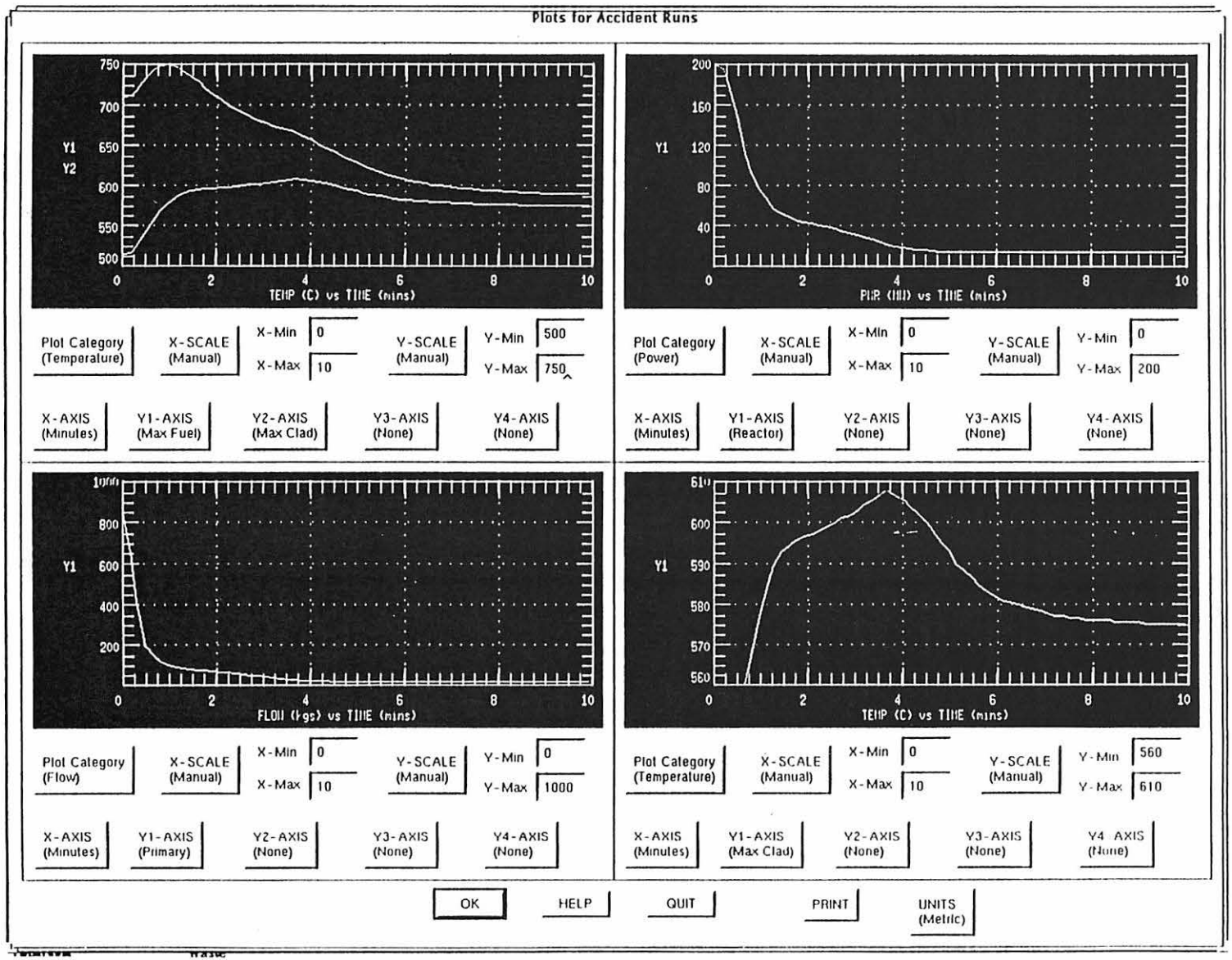

Fig. G.4. GRSAC reference case simulation of the short-term ATWS-LOFC accident.

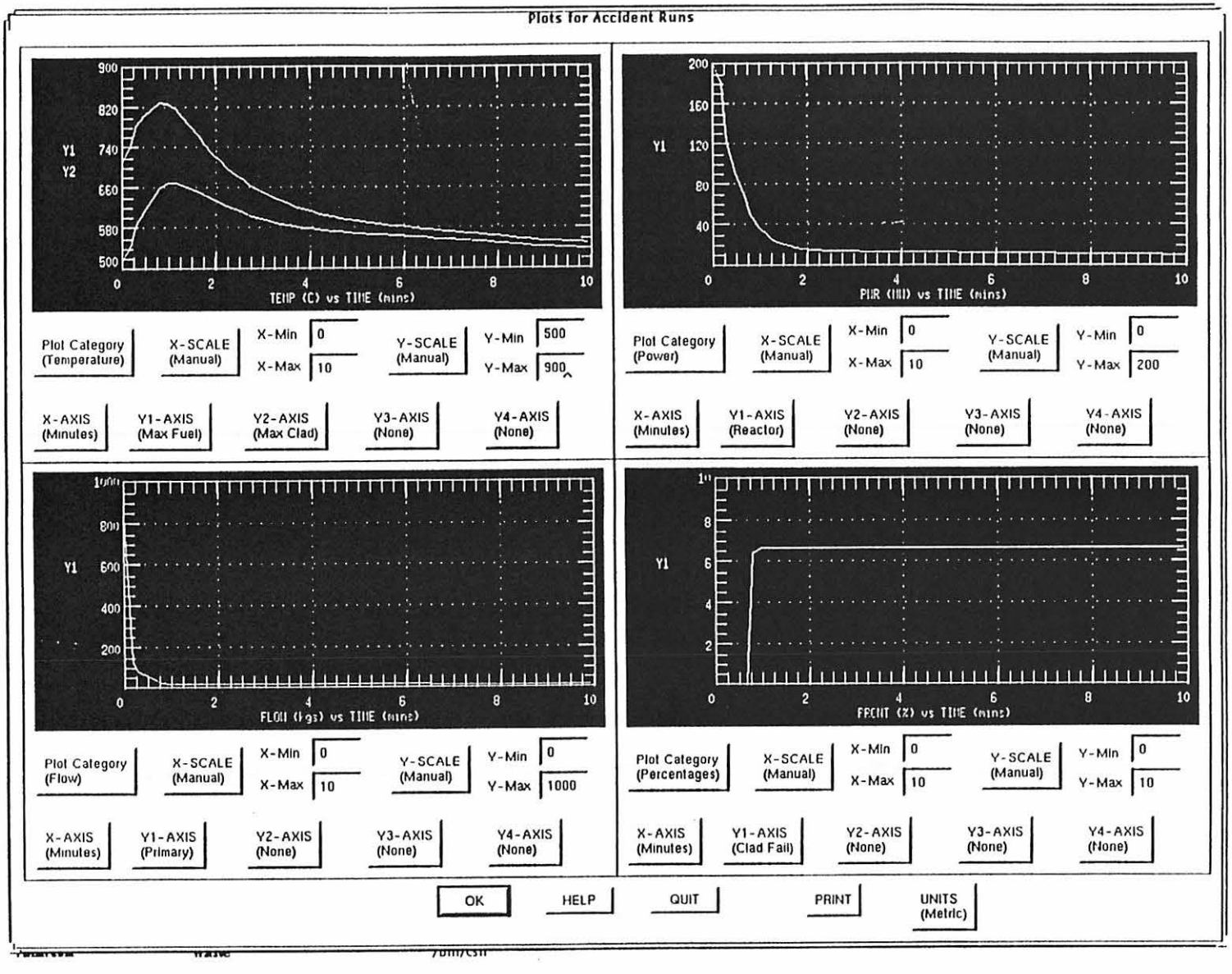

Fig. G.5. GRSAC simulation of the short-term ATWS-LOFC accident with a shorter-than-reference-case flow coastdown period (by a factor of 5) and the fuel temperature-reactivity feedback coefficient reduced by 50%.

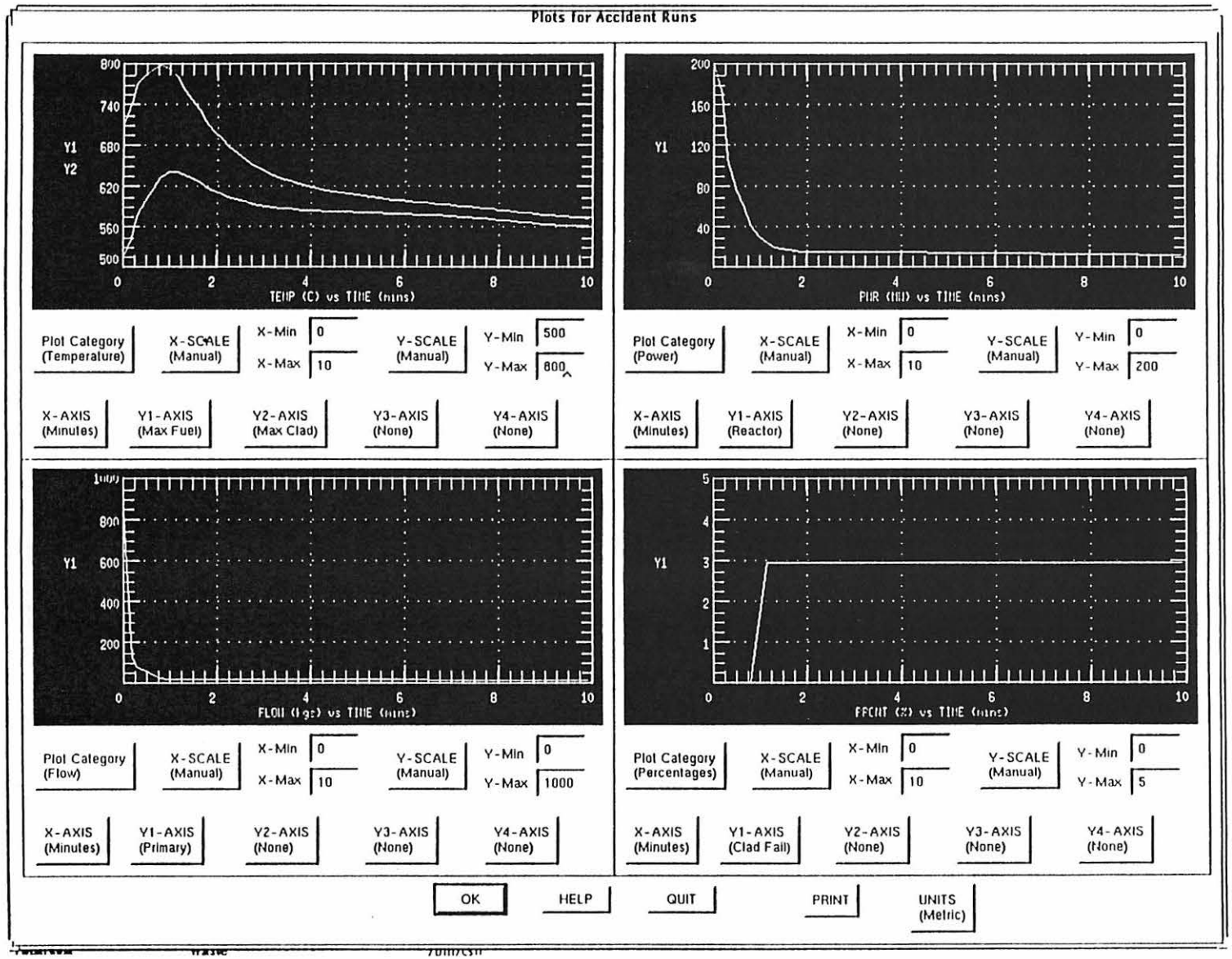

Fig. G.6. GRSAC simulation of the short-term ATWS-LOFC accident with a shorter-than-reference-case flow coastdown period (by a factor of 5), the fuel temperature-reactivity feedback coefficient reduced by 25%, and the moderator temperature-reactivity feedback coefficient reduced by 75%.

may be considered within the uncertainty range, and the 75% reduction in the moderator coefficient is typical of an expected change with core burnup for Magnox reactors. These results are summarized in Table G.1.

Table G.1. Summary of damage estimates from example GRSAC severe accident analyses of Magnox reactor: short-term ATWS-LOFC accident

	Maximum temperature (°C)		Percentage exceeding the melting temperature	
	Cladding	Fuel	Cladding	Fuel
1. Reference case	608	750	0	0
2. Flow coastdown faster (×5)	623	780	0	0
3. Flow coastdown faster (×10)	627	800	0	0
4. Flow coastdown slower (×3.33)	597	730	0	0
5. Flow coastdown slower (×10)	589	710	0	0
6. Faster coastdown (×5), fuel temperature-reactivity feedback reduced 50%	669	830	6.6	0
7. Faster coastdown (×5), fuel temperature-reactivity feedback reduced 25% and moderator feedback reduced 75%	641	800	2.9	0

Other runs were made to test various sensitivities to model and operational changes. It was found that for the short-term ATWS-LOFC cases, depressurization made little difference in the potential for clad damage. Also, changes in heat transfer mechanisms resulting in slowing the response of the fuel to transients made early clad failure more likely.

G.5 GRSAC SIMULATION OF MAGNOX LONG-TERM ATWS, LOFC, DEPRESSURIZATION, AND AIR-INGRESS SCENARIOS

In this Magnox reactor simulation, the effects of afterheat and of graphite, clad, and fuel oxidation provide the most significant contributions to the heatup scenarios. Using the Wigner energy release model described in Appendix D, the contribution of stored energy release to this accident scenario is insignificant. RPF and APF reference values are the same as for the first cases (Figs. G.1 and G.2).

The reference case flow coastdown for these analyses is much slower, as shown in Fig. G.7. Following the coastdown, the flow is assumed to go to ~5% of rated flow for the shutdown cooling system (SCS), or 0.54% of full-rated flow with the primary system at pressure. In this scenario, the residual flow is lower than is typical if there were natural circulation with intact primary piping and cooling system(s) with an upflow (vertical) core; hence some damage to the primary system may be implied.

The reference case scenario begins with an LOFC and ATWS, with the delayed scram occurring at time = 10 min. A 30-min depressurization (to 1 atm) begins at time = 60 min, and following the depressurization, air ingress to the core occurs at a rate equal to the primary flow rate. Due to the depressurization, the primary flow is reduced (assuming a constant volumetric flow) to 0.07% of

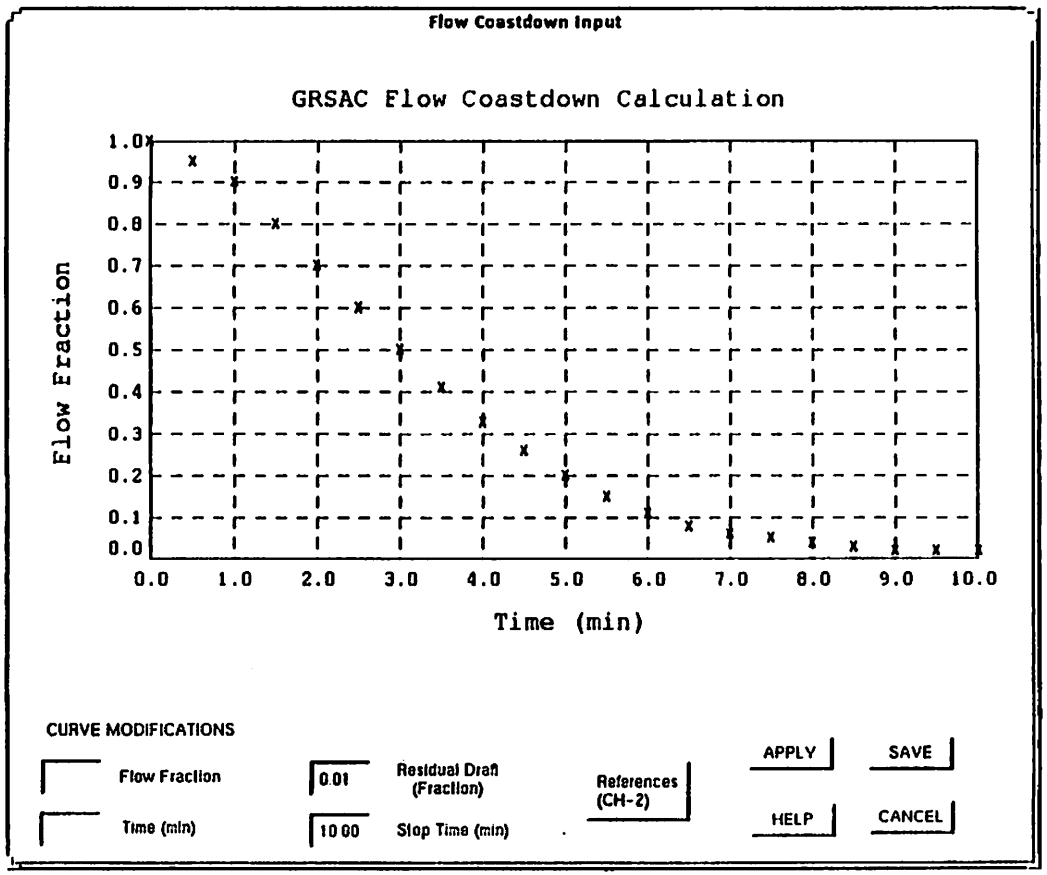

Fig. G.7. GRSAC reference case flow coastdown curve used for long-term accident studies.

full-rated flow. It is also assumed that the shield cooling system is degraded at time = 0, reducing the shield cooling flow to 10% of normal for the duration of the accident. The reference case model for fuel oxidation employs the option in which fuel is subject to oxidation whenever the clad (in that node) is either melted or 90% oxidized. Fuel and graphite oxidation model coefficient multipliers are assumed to be 0.6, and the magnesium cladding burn model hot spot factor is 100°C.

The example runs shown here illustrate a few of the significant aspects of core heatup air ingress accidents in which there is the potential for "fanning the flames" upon restart of forced circulation. In the first case there is a small but significant amount of fuel element cladding damage (~1.2%) that occurs in the initial (10-min) stage of the LOFC and ATWS, before the depressurization. This would result in significant circulating activity, primarily from the noble gases released, which would be driven out of the primary system by a subsequent depressurization. Hence any fuel element damage would be readily detectable.

Following the depressurization, a small amount of air ingress is assumed, which causes localized oxidation of the damaged fuel elements, and this heat of oxidation heats up these elements and their environs much faster than the bulk core heatup rate. In the reference scenario (Fig. G.8) with the early fuel damage, restart of the blowers (at 10% of full-rated flow) within 10.8 h results in an orderly core cooldown. With later blower restarts, however, the accident entails significant oxidation. For example, if the blower restart occurs only 30 min later (Fig. G.9), graphite, clad, and fuel oxidation occurs in a significant portion of the core. As seen in the figure, oxidation would also continue well past the 40 h shown. If the blower restart at 10.8 h provided only 8% of full flow (vs 10% reference), the cooling effect would not overcome the oxidation effect, and significant oxidation damage would occur (Fig. G.10). With lower flows, there is still significant oxidation occurring. In a slight variation on the reference case in which no early clad damage occurs (vs 1.2% reference), the same "point of no return" is not reached until 30.3 h (vs 10.8 h reference) into the accident, thus giving the operators much more leeway in a recovery operation. Figure G.11 shows the results of starting the blowers (at 10% of full-rated flow) 30 min later (at 30.8 h).

As in the case of the Windscale reactor accident, most of the significant clad, fuel, and graphite oxidation occurs with the blowers on; however, with only air available to cool the core internally, use of external (shield) cooling would be the only means of mitigating the accident consequences. Figure G.12 shows the results of the reference case with early clad failure with a 30-min delay in blower restart (as in Fig. G.9) and then shutting off the blowers and "sealing off" the core (inleakage 0.01% of full-rated flow) at time = 30 h. The total damage incurred is much reduced, and the core is gradually cooled by the degraded shield cooling system.

The GRSAC automated sensitivity study program was used to study effects of other parameter and operational changes on the accident sequence, using as a reference the case with early clad damage and a 30-min delay in blower restart (Fig. G.9). The sensitivity study display screen is shown in Fig. G.13, and the automatic report generator output in Table G.2. (Note that Table G.2 temperatures are in degrees Fahrenheit.) The sensitivity study results are interesting in that the reference case is "on the edge" of a situation between a non-accident and a serious one. As noted in the table, for a 10% higher value of core heat capacity or a 15°C higher clad melting temperature, further fuel element damage would have been avoided. Parameter changes resulting in significantly more damage are an additional 5-min delay in the scram (from 10 min reference). Other parameters shown to have noticeable effects are a 10% increase in afterheat and a 60 min additional delay in the time of depressurization (from 60 min reference). Had the changes seen as exacerbating the simulated accident been in the opposite direction, they would have resulted in avoiding the accident. For the case where the blowers are shut off and the core sealed off (Fig. G.12), an increase in shield cooling flow would have a significant effect on the ultimate cooldown rate.

Other sensitivity runs showed the fuel and moderator reactivity-temperature feedback coefficients (in inducing the initial clad failure, or not, during the ATWS), the fuel and graphite oxidation coefficient multipliers, and increases in core power density to also have significant effects on the accident outcome. Note that in the final sensitivity run (#7), all parameters are set to their worst-case

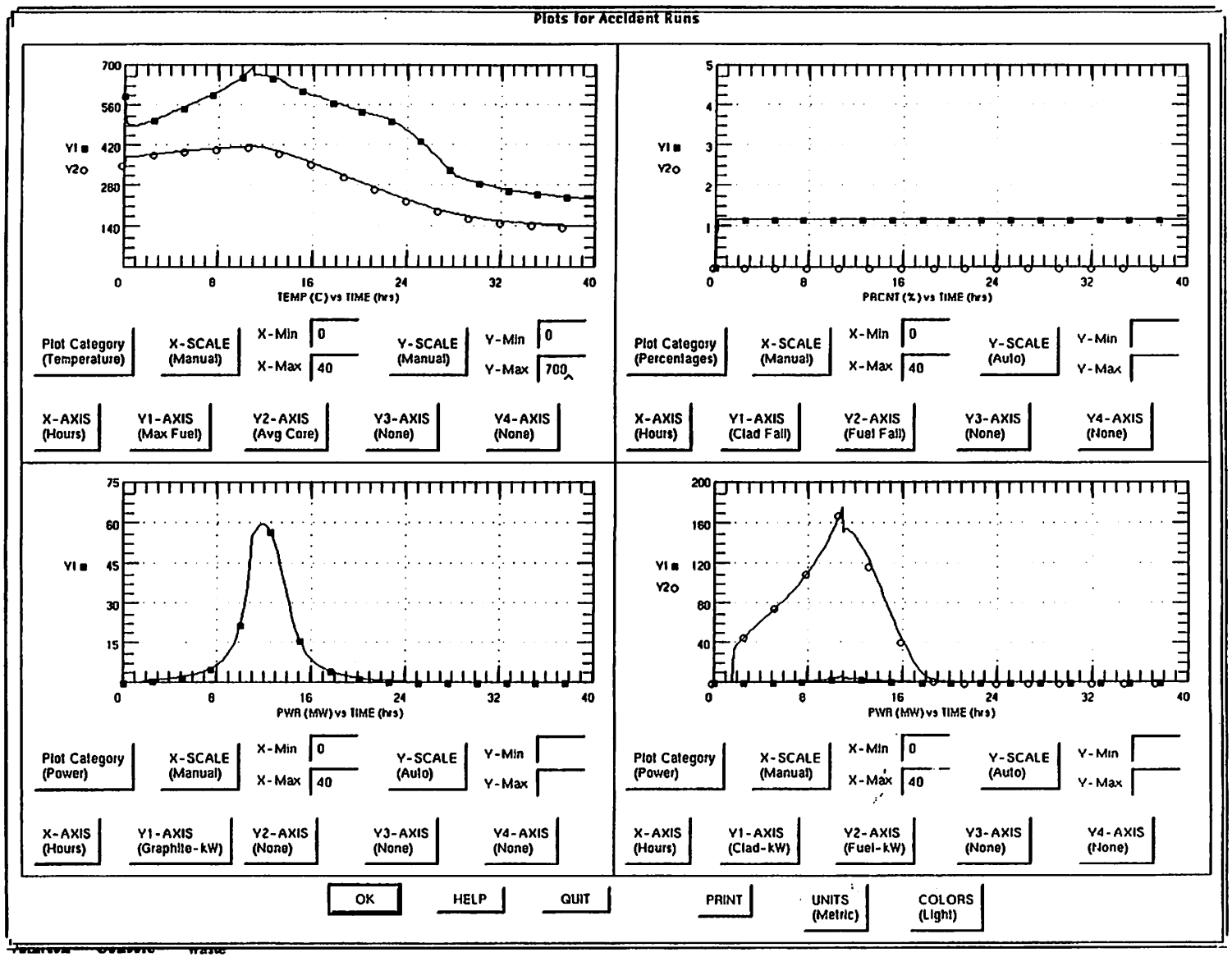

Fig. G.8. GRSAC reference case simulation of the long-term ATWS-LOFC accident with depressurization and air ingress and 1.2% early clad damage: Shutdown cooling (10% rated flow) begins at 10.8 h, in time to avoid an accident.

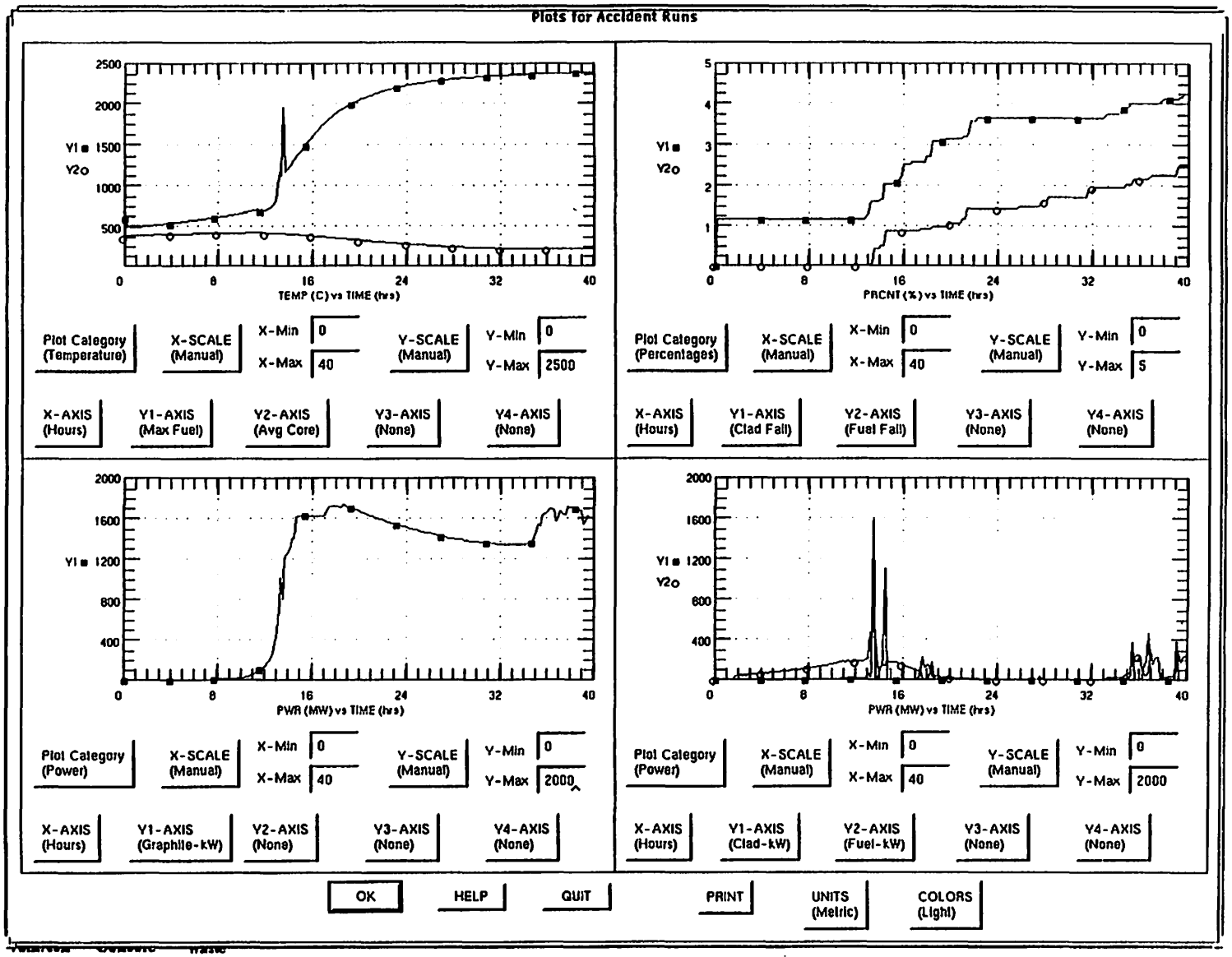

Fig. G.9. GRSAC reference case simulation of the long-term ATWS-LOFC accident with depressurization and air ingress and 1.2% early clad damage: Shutdown cooling (10% rated flow) begins at 11.3 h, not in time to avoid the accident.

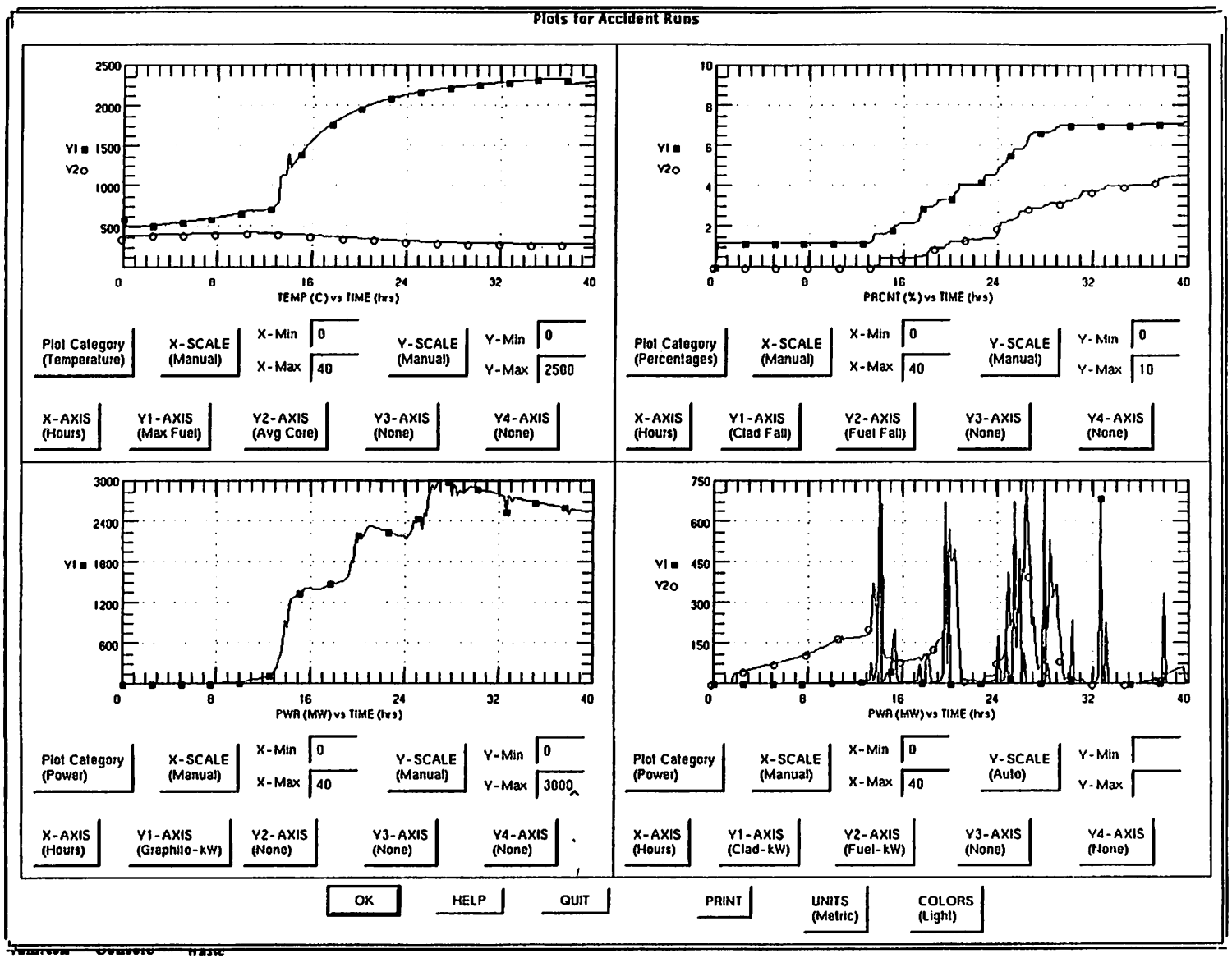

Fig. G.10. GRSAC reference case simulation of the long-term ATWS-LOFC accident with depressurization and air ingress and 1.2% early clad damage: Shutdown cooling (8% rated flow) begins at 10.8 h, with insufficient convection cooling to avoid the accident.

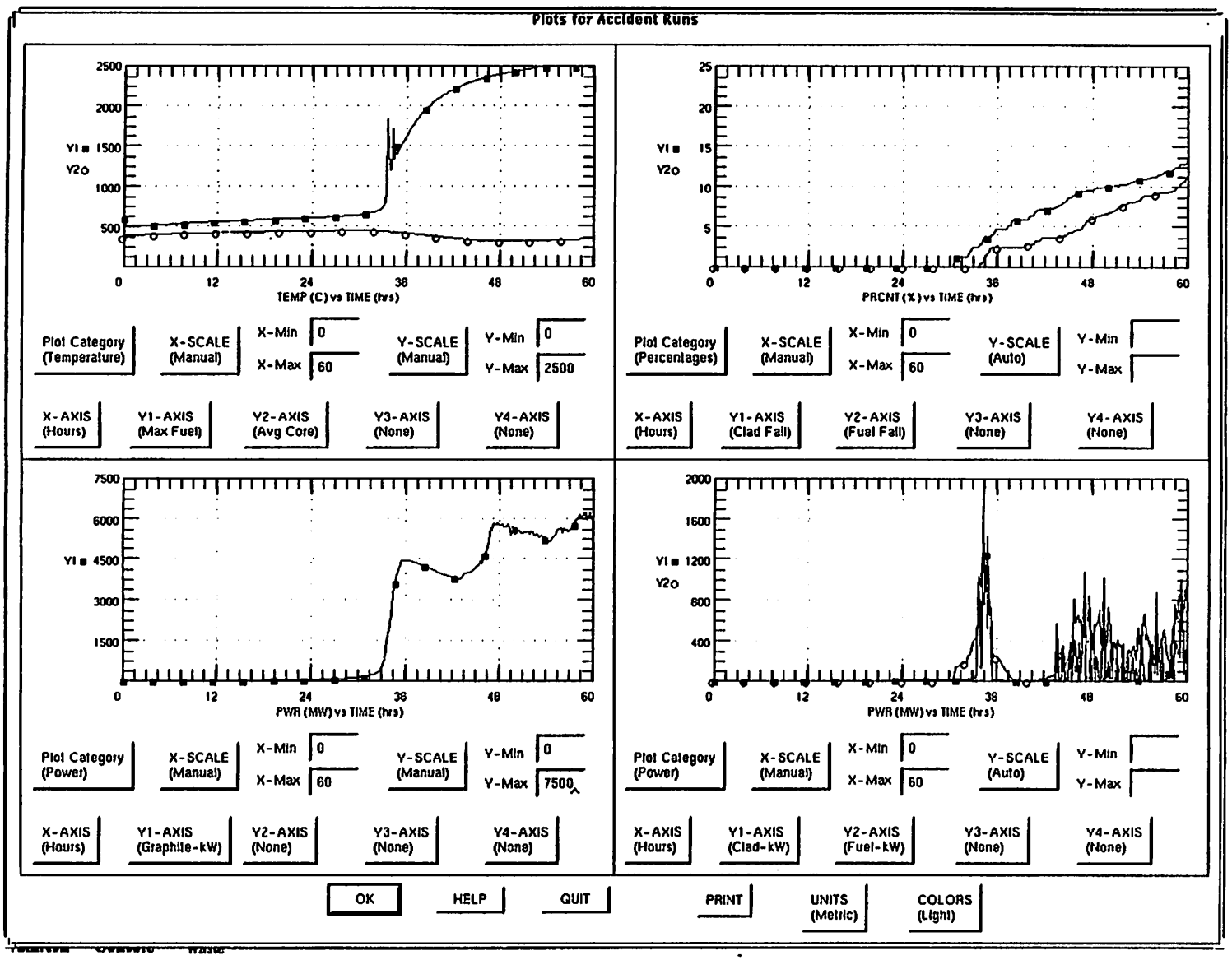

Fig. G.11. GRSAC reference case simulation of the long-term ATWS-LOFC accident with depressurization and air ingress and no early clad damage: Shutdown cooling (10% rated flow) begins at 30.8 h, not in time to avoid the accident.

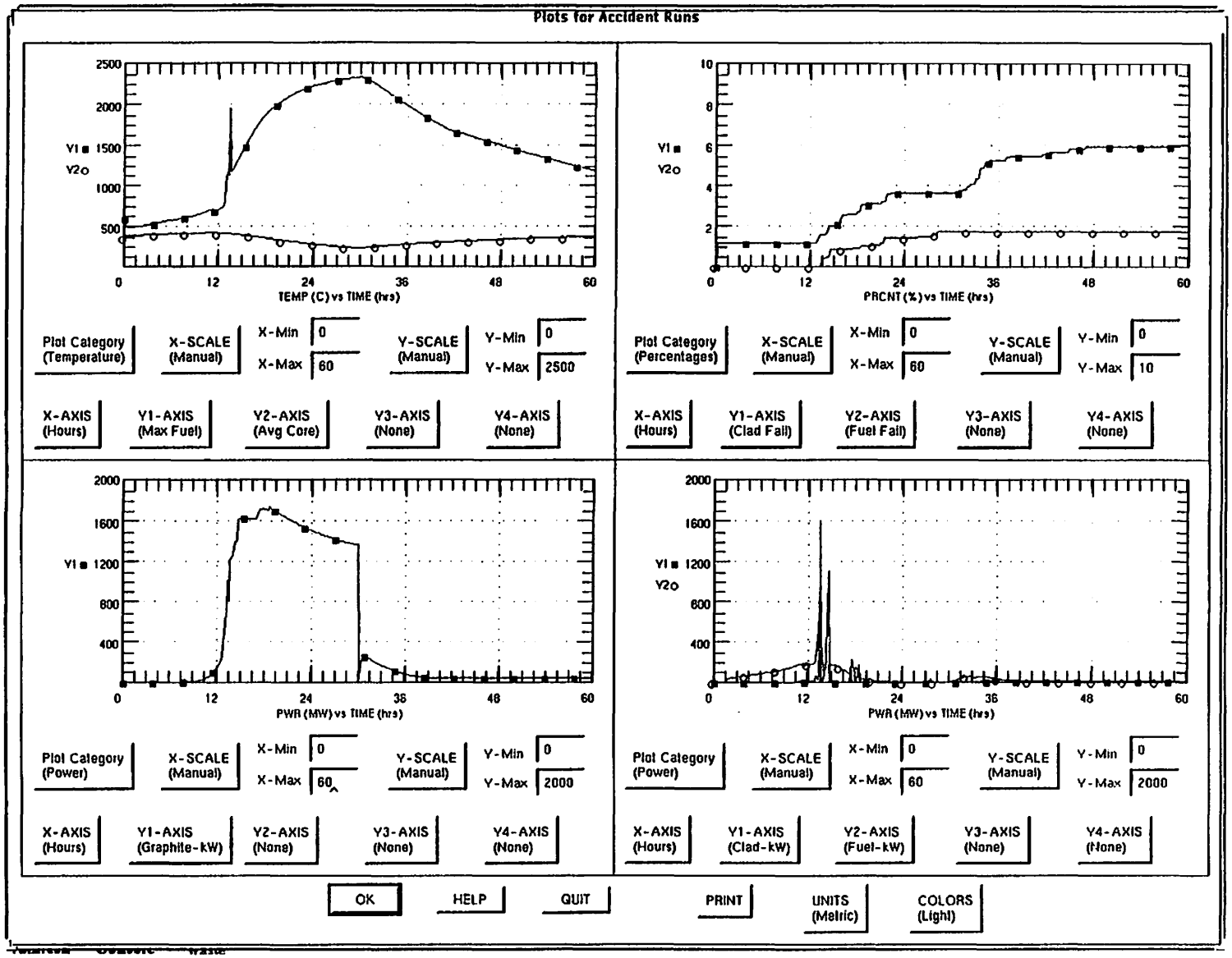

Fig. G.12. GRSAC reference case simulation of the long-term ATWS-LOFC accident with depressurization and air ingress and 1.2% early clad damage: Shutdown cooling (10%) rated flow) begins at 11.3 h, not in time to avoid the accident, and core is isolated at 30 h.

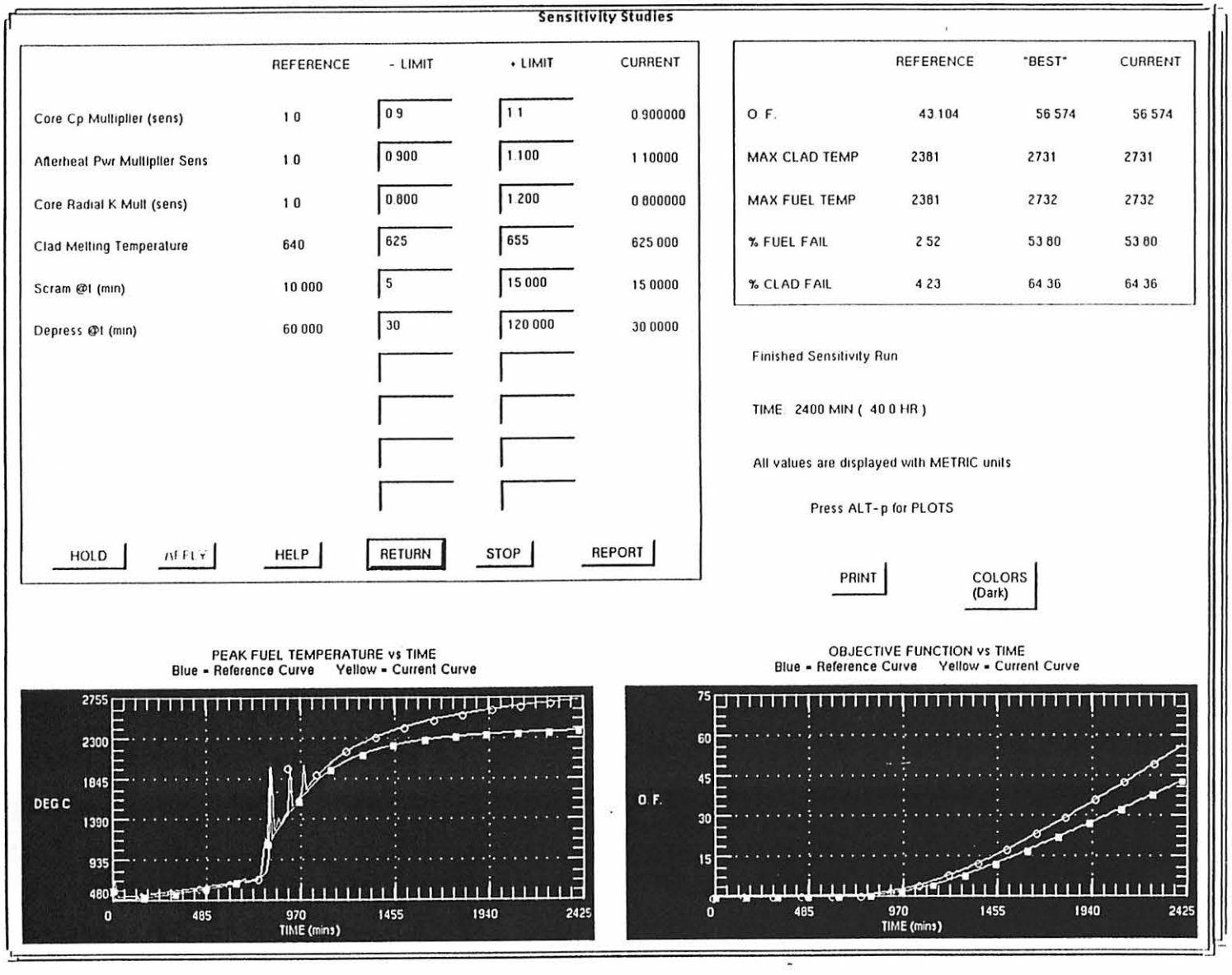

Fig. G.13. GRSAC automated sensitivity study case for the long-term ATWS-LOFC accident with depressurization and air ingress: Variations in core specific heat multiplier, afterheat multiplier, core radial conductivity multiplier, clad melting temperature, scram time, and depressurization time. (Plots with circles are for "best case" results.)

limited values, since in the setup of the study, the option to maximize the objective function (O.F.) was selected. A summary of the major results from the air ingress accident sensitivity study is given in Table G.3.

Table G.2. Report generated by GRSAC automated sensitivity study program for the severe accident study, showing results for variations in various model and operational parameters, including the changing of all selected parameters to "worst case" values

Reference Run: # Variables = 6		Reference O.F. = 43.104	
T-max clad = 4317	T-max fuel = 4318	% Clad fail = 4.23	% Fuel fail = 2.52
Param #3	Core specific heat multiplier		
Param #4	Afterheat multiplier		
Param #5	Core radial conductivity multiplier		
Param #7	Clad melting temperature		
Param #14	Delayed scram: @ time (min)		
Param #15	Depressurization @ time (min)		
Run #1 Param #3	Default Value = 1.000		
New Param = 1.100	New O.F. = 0.046	d(O.F.)/d(Param) = –0.43058E+03	
T-max clad = 1173	T-max fuel = 1256	% Clad fail = 0.00	% Fuel fail = 0.00
Run #2 Param #4	Default Value = 1.000		
New Param= 1.100	New O.F. = 49.578	d(O.F.)/d(Param)= 0.64740E+02	
T-max clad = 4542	T-max fuel = 4543	% Clad fail = 11.17	% Fuel fail = 8.90
Run #3 Param #5	Default Value = 1.000		
New Param = 1.200	New O.F.= 39.677	d(O.F.)/d(Param) = –0.17135E+02	
T-max clad = 4203	T-max fuel = 4204	% Clad fail = 3.62	% Fuel fail = 1.84
Run #4 Param #7	Default Value = 640.000		
New Param = 655.000	New O.F. = 0.037	d(O.F.)/d(Param) = –0.28711E+01	
T-max clad = 1186	T-max fuel = 1265	% Clad fail = 0.00	% Fuel fail = 0.00
Run #5 Param #14	Default Value = 10.000		
New Param = 15.000	New O.F. = 43.366	d(O.F.)/d(Param) = 0.52400E–01	
T-max clad = 4577	T-max fuel = 4578	% Clad fail = 38.77	% Fuel fail = 22.15
Run #6 Param #15	Default Value = 60.000		
New Param = 120.000	New O.F. = 20.103	d(O.F.)/d(Param) = –0.38335E+00	
T-max clad = 3310	T-max fuel = 3347	% Clad fail = 1.47	% Fuel fail = 0.12
Run #7	All params set to give best O.F.		
Param #3	Core specific heat multiplier	Param = 0.900	
Param #4	Afterheat multiplier	Param = 1.100	
Param #5	Core radial conductivity multiplier	Param = 0.800	
Param #7	Clad melting temperature	Param = 625.000	
Param #14	Delayed scram: @ time (min)	Param = 15.000	
Param #15	Depressurization @ time (min)	Param = 30.000	
	Final (Best) O.F. = 56.574		
T-max clad = 4948	T-max fuel = 4949	% Clad fail = 64.36	% Fuel fail = 53.80

Table G.3. Summary of damage estimates from example GRSAC severe accident analyses of long-term ATWS-LOFC accident with depressurization and air ingress

		Damage induced (at 40 hours)		
	Variation	Blower restart (h)	% Clad > T-melt	% Fuel > T-melt
R	Reference case[a]	11.3	4.2	2.5
V1	Blower flow 8% (vs 10%)[b]	10.8	7.1	4.5
V2	Scram delay 15 min (vs 10 min)	11.3	38.8	22.2
V3	T-clad melt 625°C (vs 640°C)	11.3	11.7	1.8
V4	Depressurize at t = 30 min (vs 60 min)	11.3	7.8	6.1
V5	Core specific heat (×0.9)	11.3	29.1	26.9
V6	Power density (×1.1)	11.3	31.4	22.9
V7	Afterheat (×1.1)	11.3	11.2	8.9
V8	Seal off core at t = 30 h	11.3	5.5	1.7
V9	No early clad damage[c]	30.8	13.2[d]	11.2[d]

a. Earlier restarts result in cooldown with no additional fuel element damage.
b. A flow of 10% at this restart time would have resulted in a cooldown.
c. Restarts earlier than this restart time would have resulted in a cooldown.
d. Damage after 60 h.

A second variation of the long-term heatup accident involving air ingress is presented specifically to demonstrate the characteristics of fission product release predicted from failed (and oxidized) uranium metal fuel. The sequence of this accident scenario for a representative Magnox reactor involves a long-term loss of forced convection cooling along with an immediate scram and primary system depressurization, followed by air ingress.

An important aspect of such a release of fission products into the primary cooling system is the extent of cladding failure at the time of depressurization. Although no fuel oxidation would occur until after the depressurization is complete and air ingress is initiated, the driving force from a rapid depressurization could contribute significantly to the rate of dispersal of noble gases into the reactor building structure (if applicable) and into the environment. If for example no cladding failures were to occur before the completion of the depressurization, and subsequent failures released fission product gases that leaked very slowly into a reactor building, the radioactive decay occurring during holdup in the building could significantly reduce the resulting radioactivity release to the environs.

For cases in which the natural circulation air ingress is driven by a tall chimney (equivalent) without a sealed confining building to restrict the circulation, the dispersal rate of fission products to the environment could be significant. For this reason, additional models under development for GRSAC, which are incorporating a tie-in with ORIGEN-PRO[1] and HASCAL,[2] will accommodate these scenarios and thus greatly aid the evaluation of the consequences for this class of accidents.

In the reference case for this scenario, a LOFC with scram and a 30-min depressurization rampdown occurs at time = 0, with air ingress beginning as soon as the depressurization is complete. Shield cooling flow is assumed to be degraded (10% of normal for the duration of the transient). The air ingress flow is held steady at a relatively low value of 0.6 kg/s (~0.05% of full rated mass flow).

The results are shown in Figs. G.14 (GRSAC on-line plot) and G.15 (post-run plot). In Fig. G.14 (upper left), the maximum fuel temperature is 1590°C at time = 120 h (5 days) and still rising; and (upper right) the axial profile of maximum fuel temperature shows that the peak (at 120 h) is at the inlet, due mainly to the heat generated by the graphite oxidation (lower left), which is leveling out at about 2 MW (the next most effective heat source is from fuel oxidation, with very little contributed by clad oxidation and Wigner energy); and (lower right) the major contributor to the fission product release percentage is the noble gases grouping, which begins to come into play at about t = 18 h, while the other chemical groupings (which rely more on fuel oxidation for the release of fission products) start off gradually after about 24 h.

In this scenario, the effect of the noble gas component release is mitigated somewhat by the 18-h period of radioactive decay, while if there had been early clad failure, the seriousness of the release would have been greater both due to the reduced time available to react and to the higher dose rates because of the shorter time for decay. Much more serious releases than the noble gases from a dosage standpoint, however, are the halogens. Note that after the first cladding failure (about t = 18 h), subsequent air cooling is counterproductive, generating more heat through oxidation than it removes by convection. The oxidation rate is limited by the available oxygen. More information about the transient is shown in Fig. G.15, including the cooling (air) flow (upper right) and the release percentages for all eight fission product groupings.

In a sensitivity study run, the shield cooling flow is maintained at 100% for the duration (vs cut back to 10%). In this "relatively short period" of five days, however, with several major heat sources contributing to the heatup in the central core, the extra shield cooling does not have a noticeable effect on peak fuel temperature or fission product release rate.In a second sensitivity study, the air flow following depressurization was assumed to be due to a chimney with an effective height of 10 m. The average flow in the 5-day period is about double that in the reference run, and it increases with core heatup. In this case (Fig. G.16), the maximum fuel temperature peaks at 1790°C after 97 h, due primarily to the increase in heat generated from the graphite oxidation. The process is still oxygen limited; however, noting the differences in shapes of the maximum fuel temperature profiles, the flatter profile in the second case implies that the oxygen is penetrating further into the core. While there is very little difference in the noble gas releases for the two cases, for the second case there is a ~20% increase in the halogen and noble metals releases and a ~30% greater release for the alkali metals, telluriums, and alkaline earths.

G.6 SUMMARY OF RESULTS

The two classes of severe accident cases presented indicate the sensitivity of the resulting damage estimates to relatively small changes in both model parameters (representing uncertainties in the representation of a given reactor configuration) and in the operational parameters (factors over which operators and/or circumstances of the accident have an influence. In the G2/3 short-term ATWS-LOFC case, the existence (or not) of substantial clad failure at the start of a transient could have a major influence on the subsequent course of the accident in terms of radioactivity release, since a depressurization occurring after the buildup of fission products in the primary system could be more of a problem (dispersal) than one occurring before the buildup.

In the long-term Calder Hall air ingress scenarios, examples were used to show how relatively minor changes in either model or operational parameters could make major differences in the total damage estimate—fuel failure, oxidation, and subsequent radioactivity release. Another aspect of the long-term Calder Hall scenario is similar to the Windscale aspect; that is, if forced circulation cooling were attempted past certain critical core heatup times, much more oxidation and fission product release would occur from "fanning the flames."

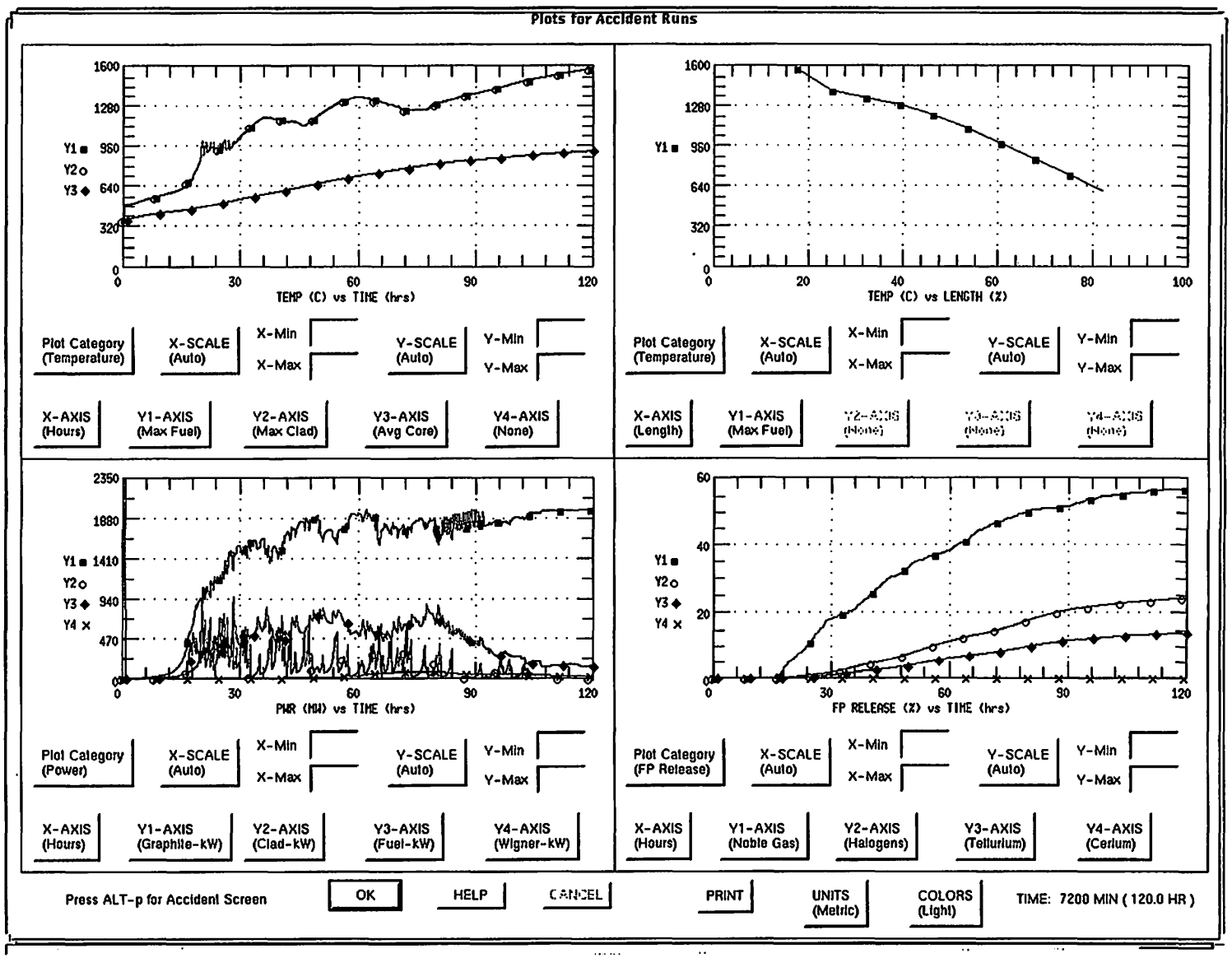

Fig. G.14. GRSAC reference case simulation of the variation on the long-term LOFC accident with depressurization and air ingress: on-line plot showing peak (vs time) and axial-profile fuel temperatures, heating due to oxidation, and fission product releases for several chemical groupings.

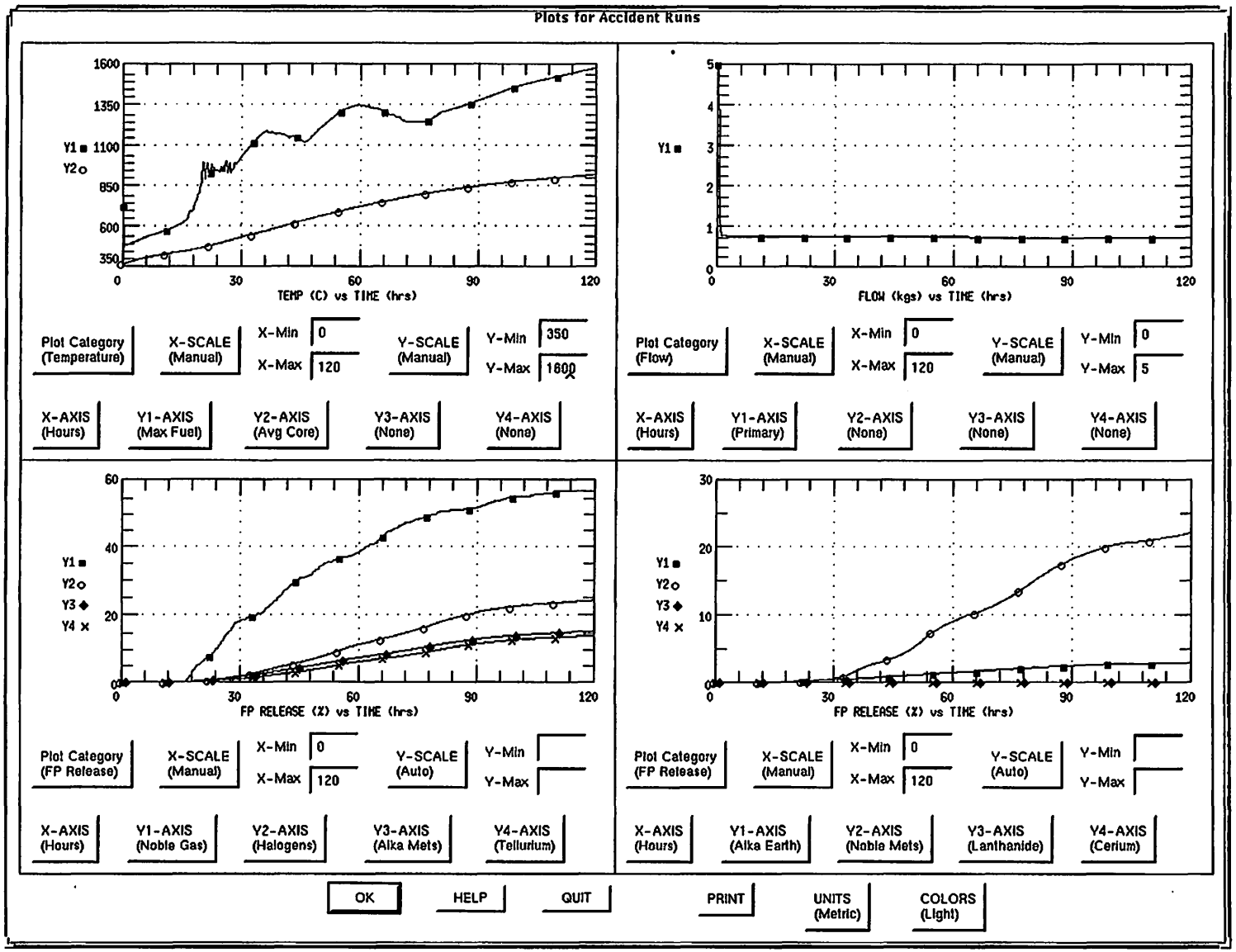

Fig. G.15. GRSAC reference case simulation of the variation on the long-term LOFC accident with depressurization and air ingress: Post-run plot showing assumed air ingress flow and fission product releases for all eight chemical groupings.

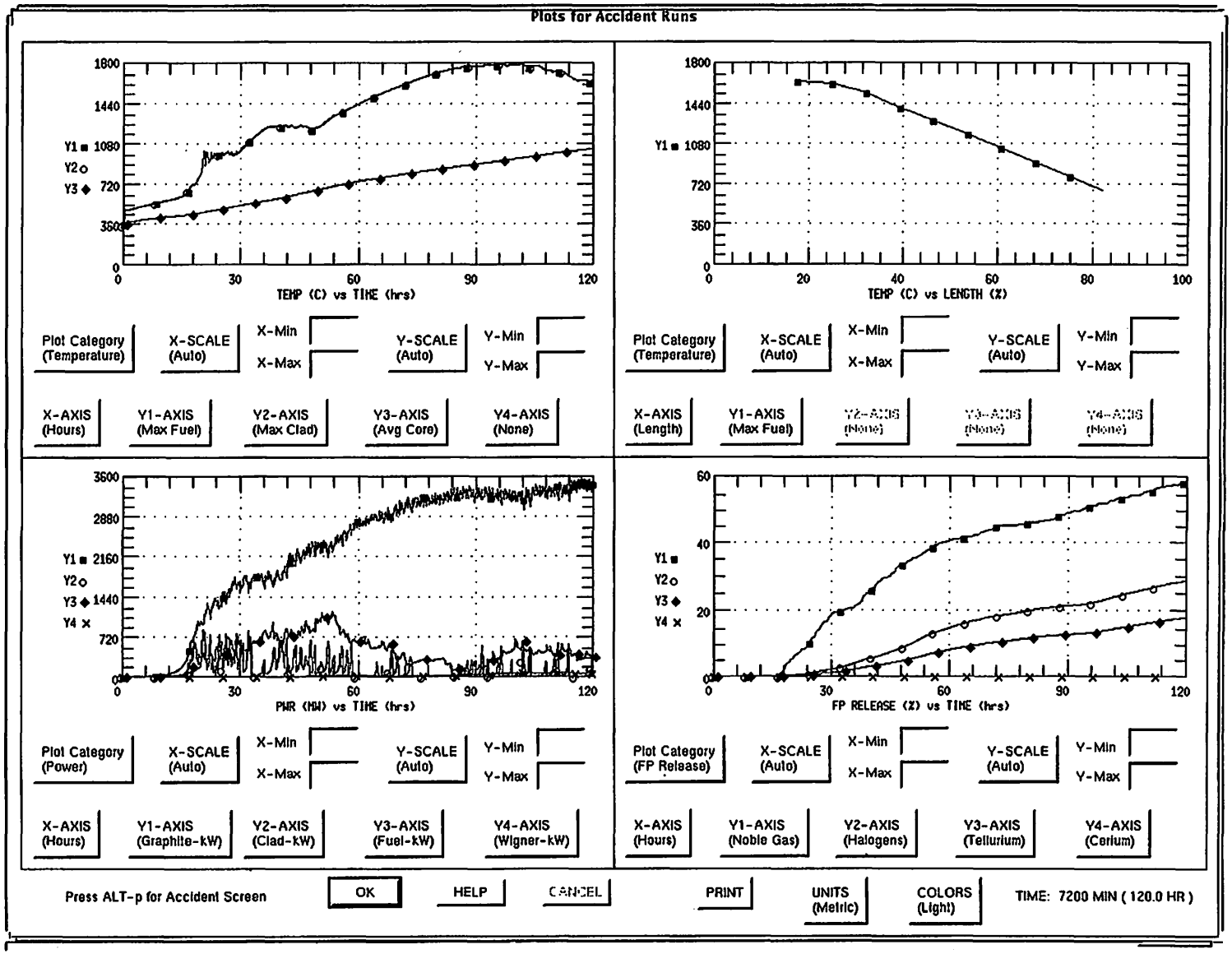

Fig. G.16. GRSAC simulation of the sensitivity study case for the variation on the long-term LOFC accident with depressurization and air ingress: On-line plot showing peak (vs time) and axial-profile fuel temperatures, heating due to oxidation, and fission product releases for several chemical groupings.

The second variation of the long-term LOFC accident emphasizes the fission product release characteristics. It was shown that there may be delays in the order of a day before any releases occur, and that the character of the more significant ones (from a dose standpoint) would be gradually increasing over a several-day period, as opposed to reactor accident scenarios characterized by an all-at-once release.

G.7 REFERENCES

1. Reiner, J-P., and D. J. Nypaver, *ORIGEN-PRO Users Manual* (in publication).

2. Defense Special Weapons Agency (DSWA), *HASCAL/SCIPUFF User's Guide* (March 1997).

APPENDIX H.
DESCRIPTIONS OF REPRESENTATIVE TYPES OF METAL-FUELED GAS-COOLED REACTORS

H.1 INTRODUCTION

The spectrum of natural uranium metal-fueled gas-cooled reactors of interest to this study is represented here by four different specific plant designs: (1) Windscale (air cooling at atmospheric pressure, horizontal-channels, aluminum cladding); (2) G1 (air cooling at atmospheric pressure, horizontal channels with the inlet flow entering at the mid-plane of the core and exiting at both ends, magnesium cladding); (3) G2/3 (CO_2 cooling at elevated pressure, horizontal channels, magnesium cladding); and (4) Calder Hall (CO_2 cooling at elevated pressure, vertical channels with upflow, magnesium cladding). The GRSAC code uses these four designs as basic models upon which other similar designs can be simulated. For example, the Brookhaven Graphite Research Reactor, with air cooling entering at the core mid-plane, is readily derived from the basic G1 model, and the Oak Ridge Graphite Reactor is of the same basic design as Windscale. Brief descriptions of each of these designs are given in Section 1.4. References (Sect. H.6) to more detailed design literature and operational histories are given for each reactor type.

H.2 WINDSCALE REACTORS

The Windscale Units 1 and 2 (UK) were completed in 1950 and 1951, and operated successfully until the accident and fire in unit 1 in October 1957, when both were shut down permanently. There is much information about the design and operating characteristics contained in the detailed descriptions of the 1957 accident (Sections 2.4 and 4.1, and Appendix E), which was used as a vehicle for benchmarking many of the GRSAC code models.

Table H.1 lists some of the important Windscale parameters. In the Windscale case, several parameters crucial to the simulation had to be inferred from various sources and references which had conflicting or incomplete data. Figure H.1 is a vertical section through the reactor showing the charge hoist (used for on-line refueling) at the coolant inlet side, and the discharge face from which the cooling air exits to the stack. Control rods and scram rods are inserted from the top, normal to the coolant/fuel channels.

The reference section for Appendix E (E.10) contains an extensive set of Windscale literature assembled for the benchmark study.

Table H.1. Windscale reactor parameters

Power		160 MW(t)
Reactor Core	Diameter	15.2 m
	Length of fuel channel	7.0 m
Fuel Channels	Number	3444
	Diameter	9.98 cm (2660); 9.02 cm (784)
	Pitch	21.0 cm, square
	Orientation	Horizontal
Fuel Element	Can length	31.3 cm
	Number per channel	21
	Total in core	72,240
	Cladding material	Aluminum
	Number of fins	13
	Cladding and fin thickness	0.112 cm
	Mass of aluminum/channel	6820 g
	Support in channel	Graphite tee-shaped inserts
Uranium	Chemical form	Metal
	Enrichment	Natural [c]
	Diameter	2.53 cm
	Mass per element	2700 g
	Mass in core	180 tonnes
Moderator	Mass of graphite	1966 tonnes [a]
	Surface area per fuel channel	21,950 cm^2
	Surface area per isotope channel	9790 cm^2
Isotope Channels	Number	1 per 4 fuel channels
	Channel diameter	4.45 cm
	Rod diameter	2.54 cm
	Cladding	Aluminum (unfinned)
	Cladding thickness	0.064 cm
	Number of AM channels in core	861 [b]
	Number of cartridges per channel	21 (max)
	AM alloy composition	11.5–13 wt % Li, balance Mg
	Mass of lithium per channel	518 g
	Mass of magnesium per channel	3465 g
	Other material in isotope channel (unspecified amounts)	Lead spacers, steel rods, graphite dowels
Coolant	Air at atmospheric pressure	
	Inlet temperature	20°C (ambient)
	Outlet temperature	170°C
	Flow	1072 kg/s

a. One reference states 1000 tonnes in the active core.

b. The majority opinion among sources indicates that most of the isotope cartridges at the time of the accident consisted of the AM cartridges of the latest design, the so-called Mark III, described in Appendix VI of Lorna Arnold's book (see references). The AM cartridges contained lithium/magnesium alloy and some lead to hold it in place.

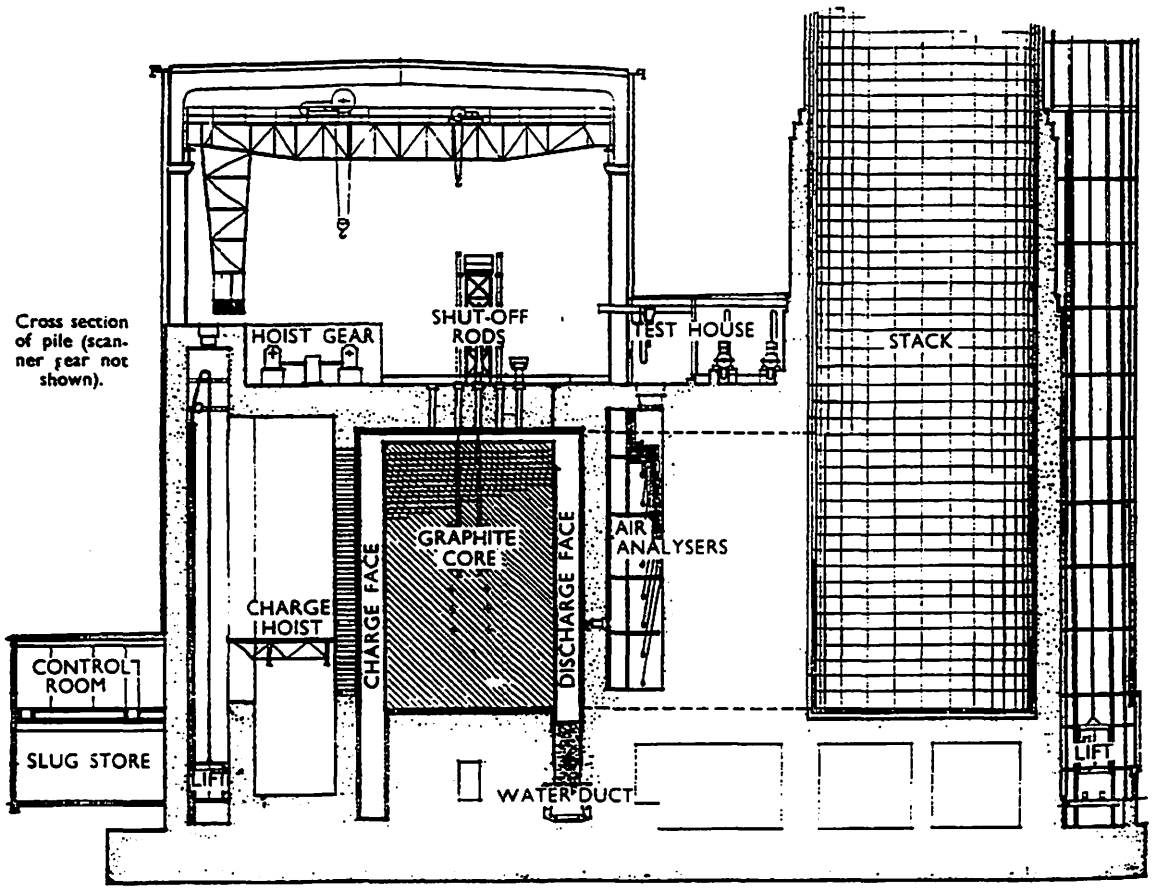

Fig. H.1. Vertical section through the Windscale reactor.

H.3 G1 REACTOR

The 38-MW(t) G1 reactor at Marcoule went critical in 1956, and was the first French reactor to produce electrical power, although it consumed (via the blowers, primarily) more electrical energy than it produced. The references reporting gross electrical output vary from 1.7 to 8.0 MW(e). Table H.2 lists many of the important G1 parameters, and Fig. H.2 is a flow diagram showing the reactor and the steam turbine plant.

Figure 4 in the main section of this report showing an isometric cutaway sketch of G1 gives a good idea of the layout and scale of the plant. More details of the core arrangement and cooling circuit are shown in the horizontal section (Fig. H.3) and a vertical section and typical fuel element and coolant channel (Fig. H.4).

References (in English) on G1 operating history[1,2] are given in Sect. H.6. Additional design data is available from an IAEA publication,[3] and from an early edition of Nuclear Engineering, in a description[4] of one of the world's reactors (G1, No. 18). Reference 5 is a report on the background and early operation of G1, as well as some descriptions of G2.

The reference section of Appendix F (F.6) also notes literature relating to the 1956 G1 accident by de Rouville et al. and Martin et al.

Table H.2. G1 reactor parameters

Overall	
Thermal power	38 MW
Gross electric power	1.7 MW
Core	
Core diameter	8.225 meters
Core length	8.40 meters
No. of fuel channels	1337
Diameter of channel	70 mm
Pitch	20 cm (square)
No. of fuel cartridges	2764 (one on each side of 80-mm slit)
Core loading	100,000 kg natural uranium
Amount of graphite	1.2 × 106 kg
Reflector thickness	0.8 m
Fuel element (cartridge)	
Material	Natural uranium metal
Uranium slugs	
Length	100.5 mm
Diameter	26 mm
Mass	1 kg
No./cartridge	37
Cladding	Magnesium, 1.6 mm thick
Fins	8, longitudinal
	Magnesium, 1.6 mm thick
Heat transfer	
Surface	
Fuel element	12,710 cm^2
Total core	3.26 × 107
Temperature	
Fuel	400°C (max)
Cladding	275°C (max)
Flow area	
Per channel	29.9 cm^2
Total core	76,600 cm^2
Air flow	
Total mass flow	222 kg/sec
Average velocity	30.5 m/sec
Max. velocity	58 m/sec
Pressure	Atmospheric
Inlet temperature	20°C (ambient)
Outlet temperature	200°C

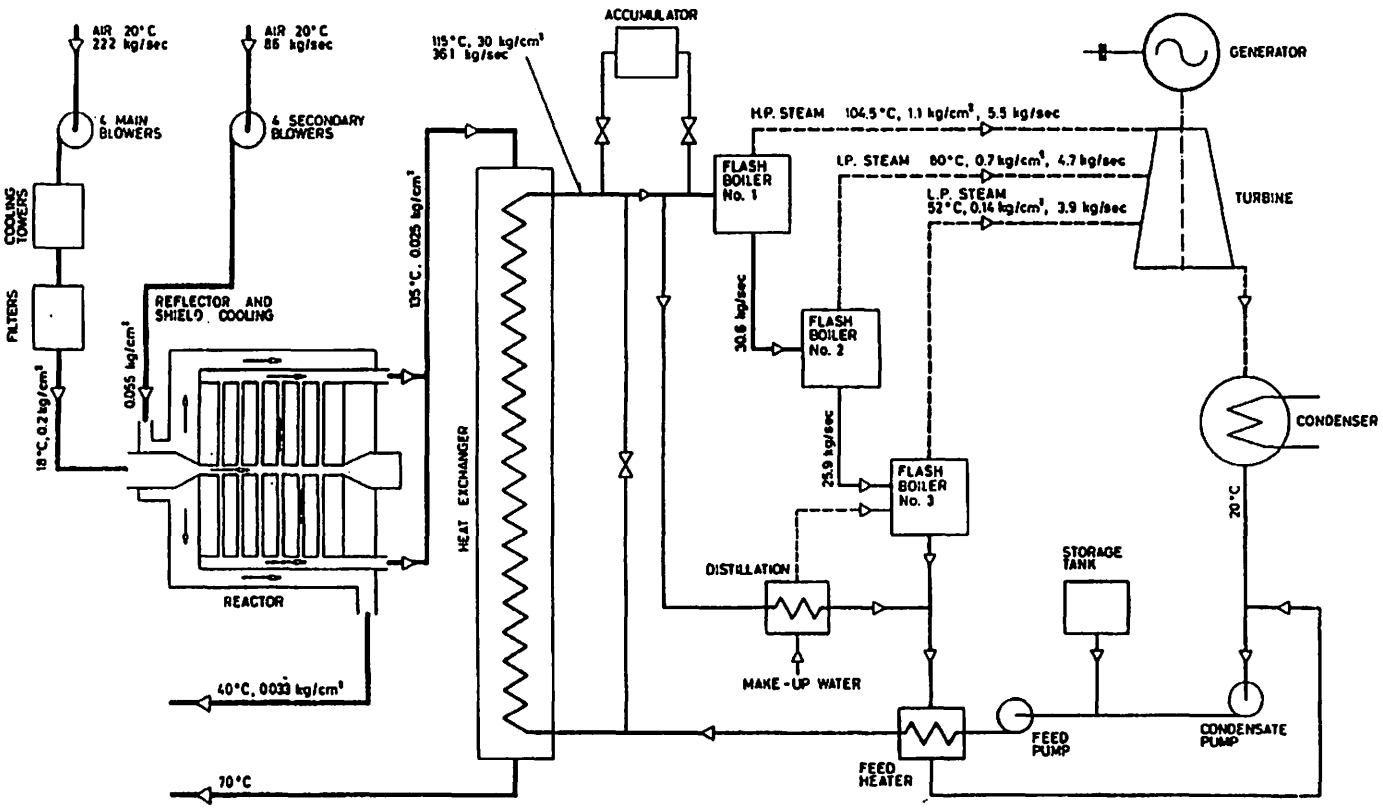

Fig. H.2. Flow diagram of the G1 reactor.

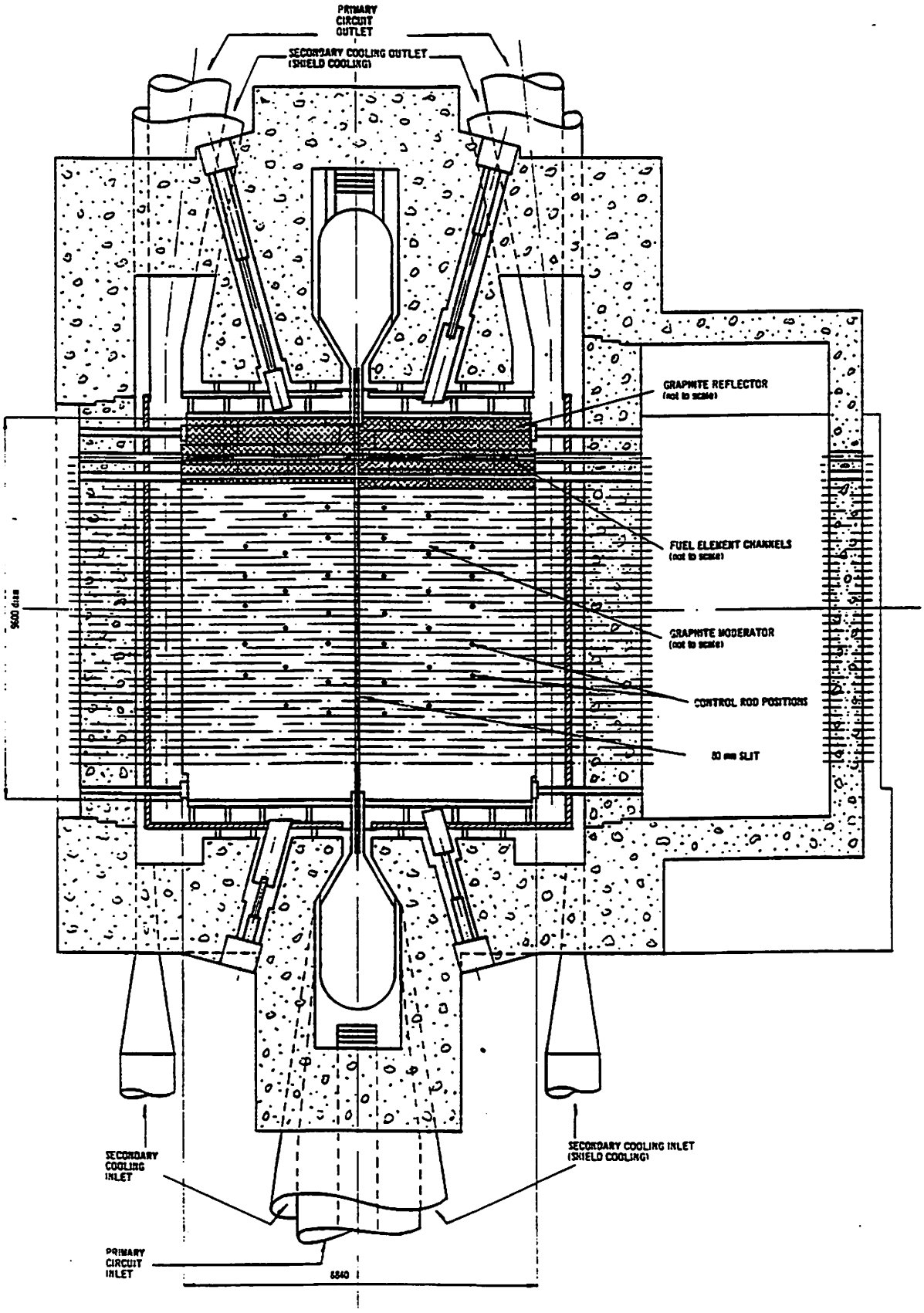

Fig. H.3. Horizontal section of the G1 reactor.

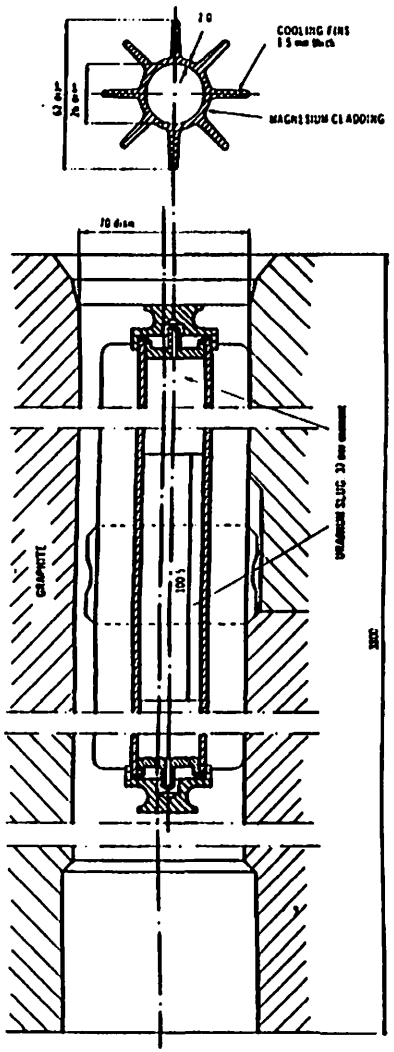

FUEL ELEMENT IN THE CHANNEL REACTOR G-1

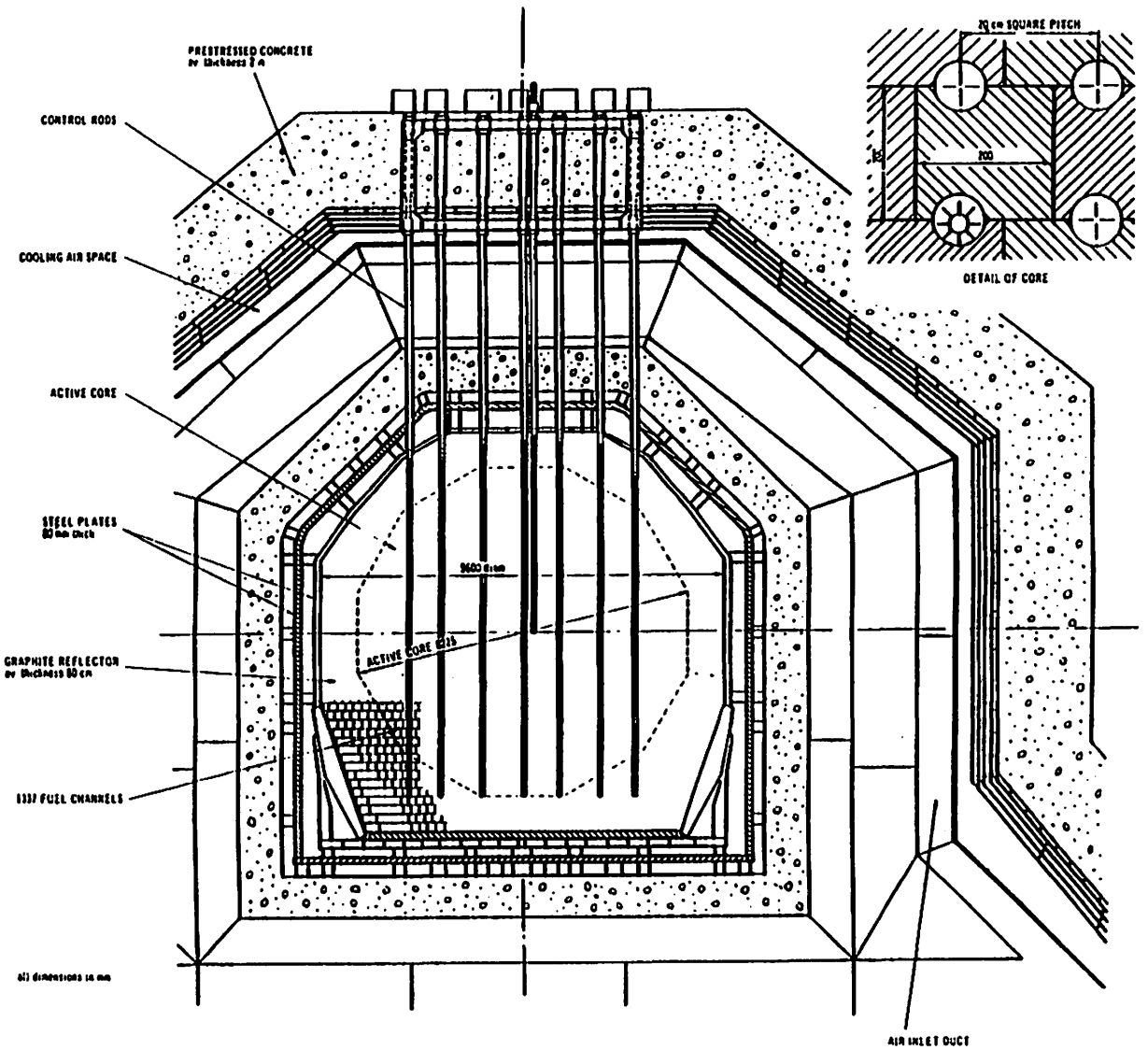

Fig. H.4. Vertical section and fuel element of the G1 reactor.

H.4 G2 REACTOR

The French G2 reactor and its sister plant G3 at Marcoule (1958 and 1959) were the first pressurized GCRs to allow on-line refueling and use prestressed concrete reactor vessels (PCRVs). They each had thermal outputs varying over their lifetimes between about 200 and 250 MW. Table H.3 lists many of the important G2 reactor parameters. A flow diagram of the reactor and secondary systems is shown in Fig. H.5. Note that the primary CO_2 inlet coolant flow path splits three ways, with one going to a set of central fuel channels, another to peripheral fuel channels, and a third to a pressurized reactor cavity cooling system. The flow split exiting the core differs from the entrance configuration, so special provisions for balancing the flows during operational changes would be necessary to achieve the desired reactor coolant temperature distributions.

Details of the core arrangement and cooling circuit are shown in the longitudinal section (Fig. H.6) and a vertical section with a typical fuel element and coolant channel (Fig. H.7).

A good description of the G2 reactor including an isometric drawing of the plant is in the Nuclear Engineering reference[6] on The World's Reactors (No. 24). A summary of the physics and engineering data is in the IAEA reference,[3] Ref. 7 provides a description of the fuel handling system design, and three other references[8-10] provide good design background information. Extensive coverage of many different features of the G2 design and operation was recorded at a 1959 ASME conference.[11]

Table H.3. G2 reactor parameters

General	
Thermal power	200 MW
Gross electric power	30 MW
Core	
Length	8.45 m
Diameter	7.85 m (octagonal)
Number of channels	1200 (each with 28 fuel elements)
Channel diameter	70 mm
Loading	110,000 kg natural uranium
Moderator	1200 tons of graphite
Fuel element	
Length	28.2 cm
Diameter	2.8 cm (central) 3.1 cm (periphery)
Pitch	20 cm (square)
Fuel	Natural uranium (4% of elements contain thorium)
Cladding	Magnesium (0.4-0.7% zirconium) Longitudinal cooling fins (see Fig H.7)
Core heat transfer	
Heat transfer area	1280 cm^2 per 2.8-cm element 1265 cm^2 per 3.1-cm element Total core—4.29×10^7 cm^2
Coolant flow	16.7 m/sec (average) 19.5 m/sec (maximum) 997 kg/sec CO_2
Coolant pressure	14.7 kg/cm^2 (average)
Inlet temperature	140°C
Outlet temperature	305°C
Flow area	27.24 cm^2 per 2.8-cm element 25.71 cm^2 per 3.1-cm element 32,100 cm^2 total core
Fuel temperatures	525°C (max. fuel) 400°C (max. cladding)

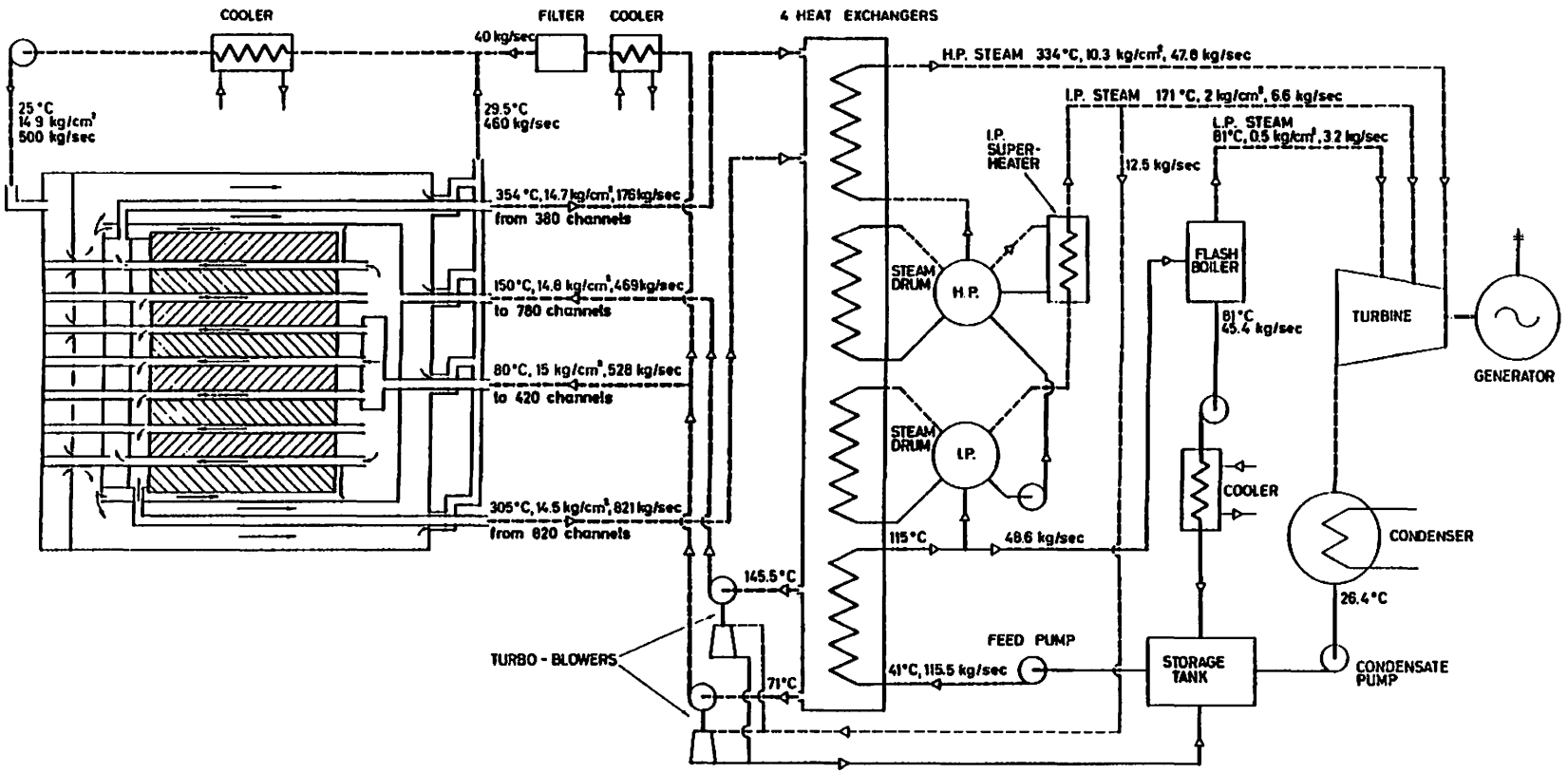

Fig. H.5. Flow diagram of the G2 reactor.

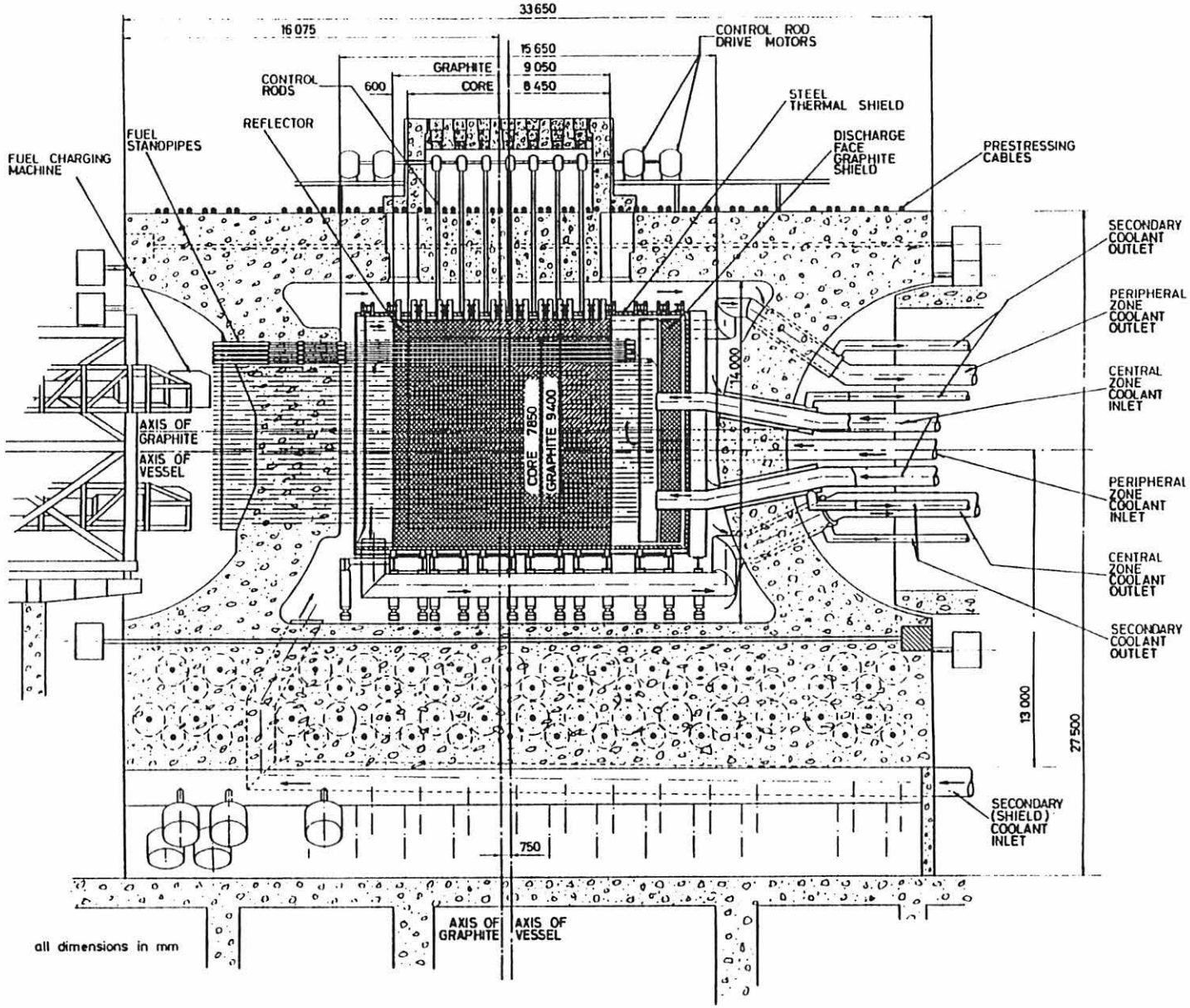

Fig. H.6. Longitudinal section of the G2 reactor.

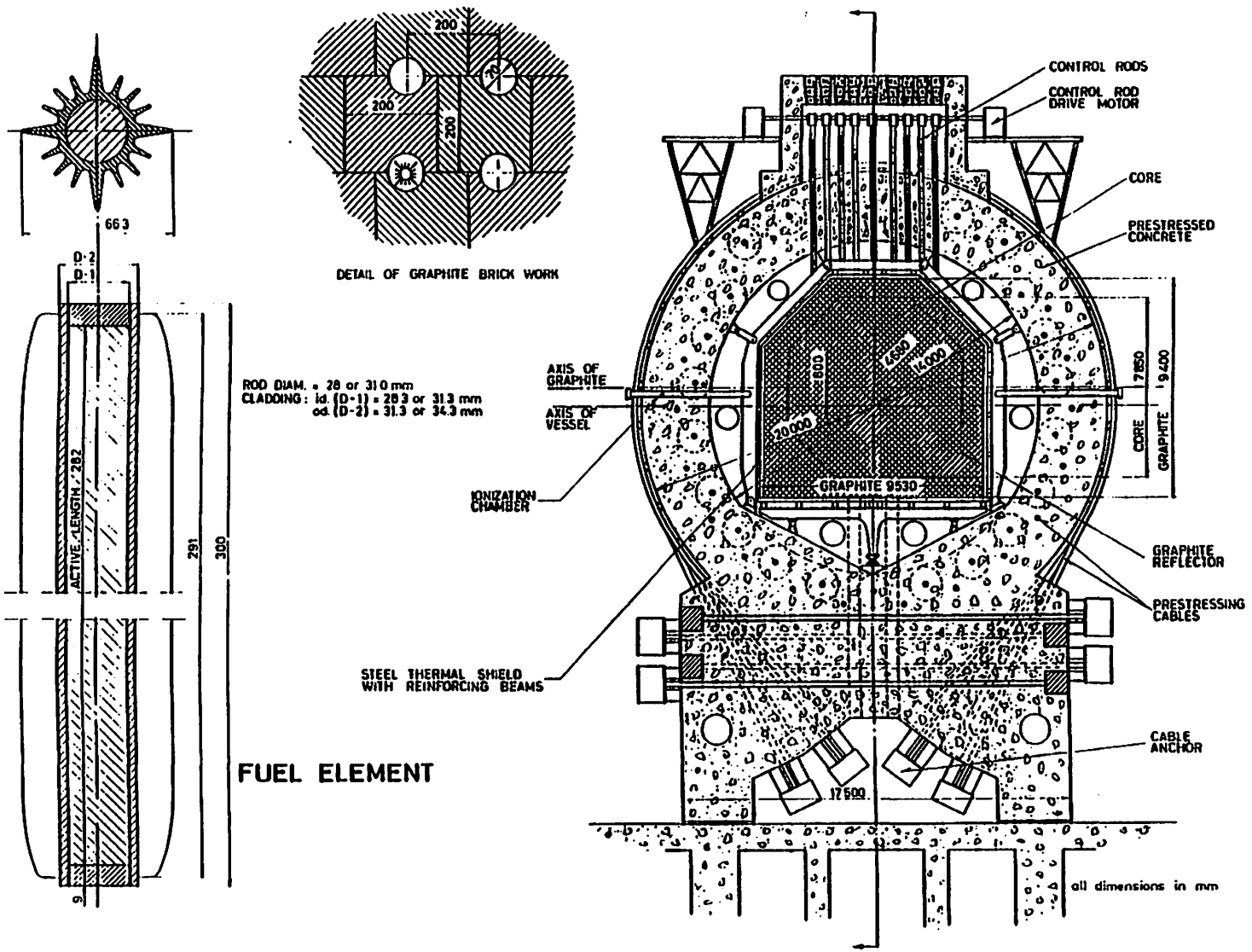

Fig. H.7. Vertical section of the G2 reactor.

H.5 CALDER HALL REACTOR

The first reactor of the four-unit Calder Hall plant at Sellafield (UK) began operation in 1956, the first nuclear generating station in the West. The last of the four units came on line in 1959. The initial unit power rating was 240 MW(t); however, the ratings were reduced to about 200 MW(t) to preclude CO_2 problems that surfaced in the late 1960s. Table H.4 lists some of the important Calder Hall parameters. All four units are still operational, producing approximately 200 MW(e) total, and the current plan is to relicense them, and the four identical reactors at Chapelcross, for longer service. The success of the Calder plant led to the spawning of many similar plants in the U.K. and elsewhere. The Tokai (Japan) reactor, very similar to the Calder design, is also still operating.

A flow diagram of the Calder reactor and its secondary systems is shown in Fig. H.8. Details of the core arrangement and cooling circuit are shown in the vertical section (Fig. H.9) and a horizontal section and typical fuel element (Fig. H.10).

Good background material on Calder Hall and other British Magnox plants is found in Refs. 12–15. More specific information about the Calder design and operation is in Refs. 16–19. Safety and licensing discussions are in Refs. 20–23, and information about Magnox plant dynamics and control characteristics is available in Refs. 24–26.

H.6 REFERENCES

1. Chambadal, P., and M. Pascal, "Recovery of the Energy Produced in Air-Cooled Graphite Reactor (G1)," *Proceedings of the International Conference on the Peaceful Uses of Atomic Energy,* Geneva 1955, P/333, Vol. 3, p. 81, United Nations, New York (1956).

2. de Rouville, M., M. Pascal, and M. Scalliet, "Experience Obtained During Two Years' Operation of the Reactor G1," *Proceedings of the 2nd International Conference on the Peaceful Uses of Atomic Energy,* Geneva 1958, P/1132, pp. 18–22, France.

3. IAEA (International Atomic Energy Agency), *Directory of Nuclear Reactors, Vol. 1: Power Reactors*, IAEA, Vienna (1959).

4. "The World's Reactors: No. 18 G1," *Nuclear Engineering,* Vol. 3 (June 1958).

5. "Report from Marcoule," *Nuclear Power* (September 1957).

6. "The Marcoule Reactor G2," *Nuclear Engineering* (December 1959).

7. Derome, G., and A. Ertaud, "Fuel Handling on the Plutonium Reactors," *Nuclear Power,* pp. 127–129 (April 1960).

8. Rastoin, J., and J. Brisbois, "Gas Cooled Reactor Experience and Programs in France," *Nuclear Energy,* Vol. 5, pp. 455–488, Pergamon Press (1978).

9. Pascal, M., J. Horowitz, J. Bussac, M. Joatton, F. de Lagge, M. de Meux, and R. Martin, "General Characteristics and Original Aspects of Reactors G2 and G3," *Proceeding of the 2nd International Conference on the Peaceful Uses of Atomic Energy, Geneva 1958,* P/1133, pp. 329–333, France.

Table H.4. Calder Hall reactor parameters

General	
Thermal power	225 MW
Gross electric power	51 MW
Core	
Height	6.40 m
Diameter	9.45 m (polygonal)
Number of channels	1696 (each with 28 fuel elements)
Loading 1	27,000 kg natural uranium
Moderator	650 tons of graphite
Fuel element	
Length	101.5 cm
Diameter	2.92 cm
Pitch	20 cm (square)
Fuel	Natural uranium (4% of elements contain thorium)
Cladding	Magnox alloy A12 1.5 mm thickness
Fins	Helical (see Fig. H.10) 0.8 mm thickness 13 mm height 3.16 mm pitch
Core heat transfer	
Heat transfer area	10,400 cm^2 per element Total core—1.05 × 108 cm^2
Coolant flow	13 m/sec (average) 20.2 m/sec (max.) 1150 kg/sec CO_2
Coolant pressure	7.03 kg/cm^2 (inlet, 100 psig) 6.7 kg/cm^2 (outlet, 95 psig)
Inlet temperature	145°C
Outlet temperature	340°C
Flow area	64.8 cm^2 per inner element 43.2 cm^2 per outer element 86,300 cm^2 total core
Fuel temperatures	418°C (nominal cladding surface)

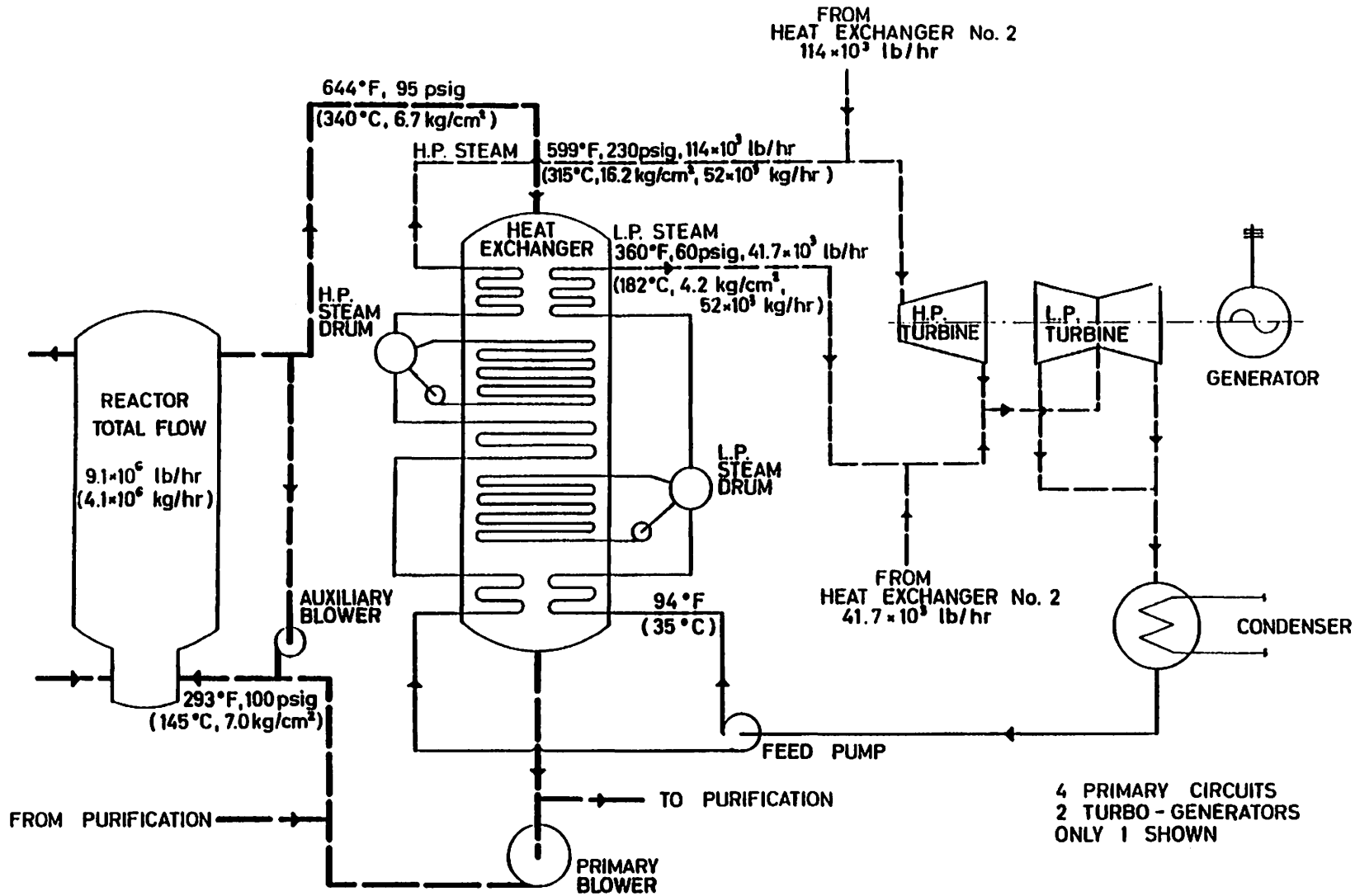

Fig. H.8. Flow diagram of the Calder Hall reactor.

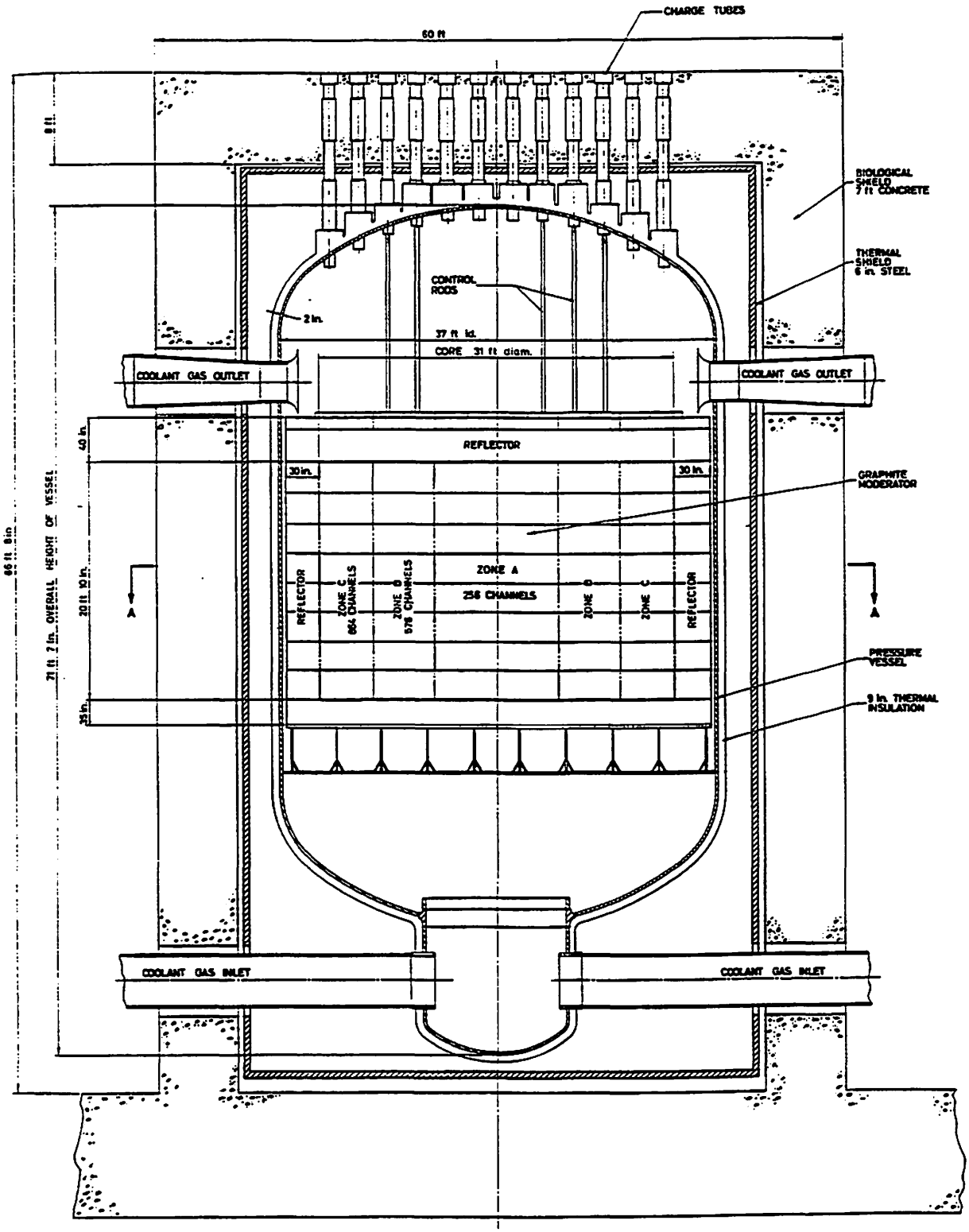

Fig. H.9. Vertical section of the Calder Hall reactor.

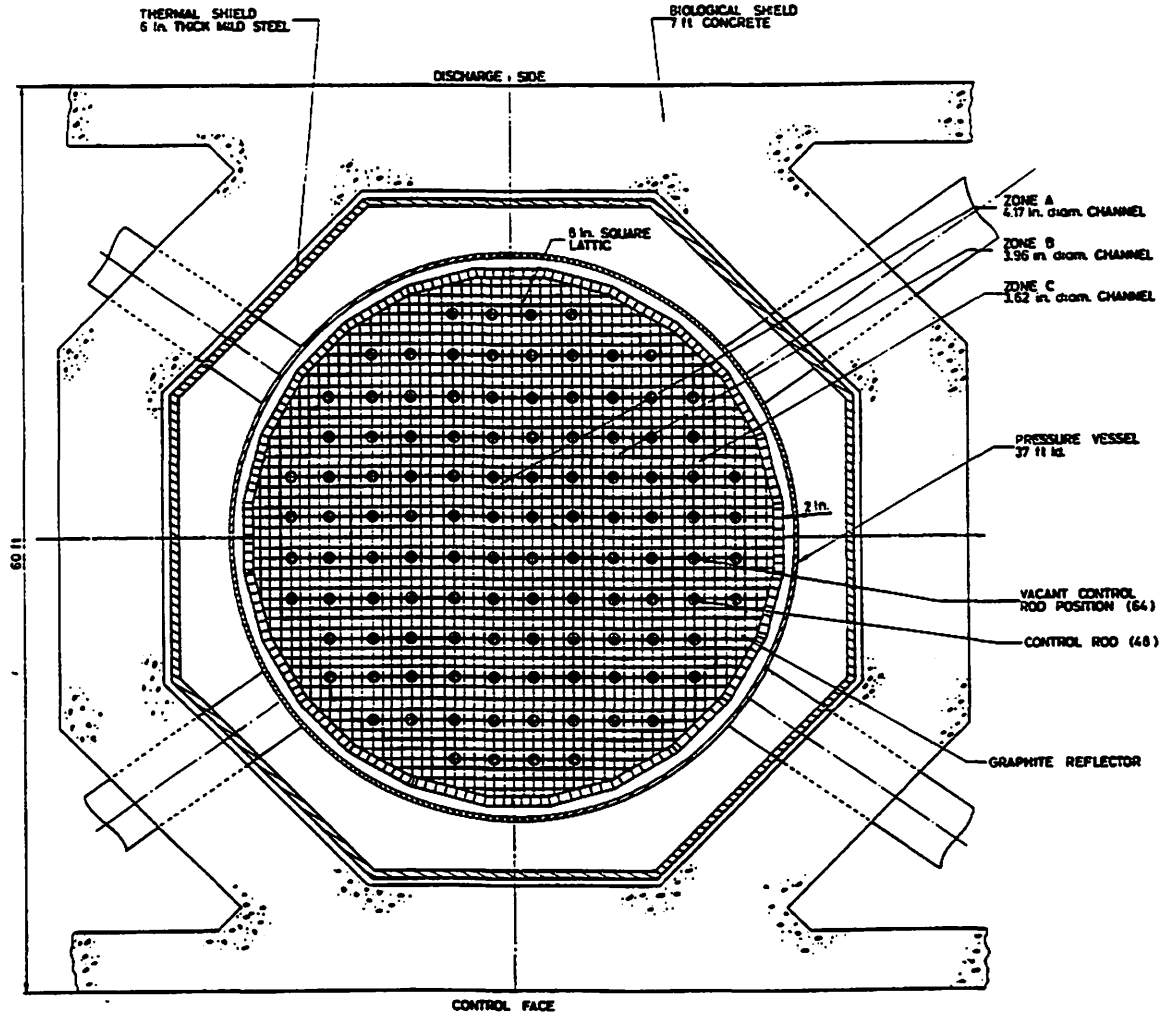

Fig. H.10. Calder Hall reactor, showing (a) horizontal section through the core and (b) longitudinal section through a fuel element.

10. Bacher, P., J.-C. Koechlin, R. de Mazancourt, A. Teste du Bailler, and C.-P. Zaleski, "Natural Uranium-Graphite Lattices," *Proceeding of the 2nd International Conference on the Peaceful Uses of Atomic Energy, Geneva 1958,* P/1191, pp. 666–684, France.

11. Deleuze, G., and M. Tourasse, "Reactors G2 and G3," Nuclear Engineering and Science Conference, Cleveland, Ohio, April 6–9, 1959, published by Engineers Joint Council.

12. Jay, K. E. B., *Calder Hall: The Story of Britain's First Atomic Power Station,* Harcourt, Brace and Co., New York (1956).

13. Poulter, D. R. (Ed.), *The Design of Gas-Cooled Graphite-Moderated Reactors,* Oxford University Press, London (1963).

14. Cameron, P. J., "The Background and Status of the Gas Cooled Reactor in the United Kingdom," *Annals of Nuclear Energy,* **5**, 489–505 (1978).

15. Dent, K. H, "The Standing of Gas-Cooled Reactors," *Nuclear Energy (British Nuclear Energy Society),* **19**(4), 257–271 (1980).

16. "Calder Hall," *Nuclear Engineering, London,* **1**(7), 266–303 (October 1956).

17. "Calder Hall: The British Nuclear Energy Conference Symposium Papers," *Nuclear Engineering, London,* **1**(9), 383–390 (November 1956).

18. "Symposium: Calder Works Nuclear Power Plant," *Journal of the British Nuclear Energy Conference,* **2**, 41–232 (technical papers, April 1957) and 233–305 (general reports and discussions, July 1957).

19. Cunningham, J. B. W., "Current Re-designs of Calder Hall," *Second International Conference on the Peaceful Uses of Atomic Energy,* A/CONF.15/P/73, Vol. 8, 416–423, United Nations, Geneva (1958).

20. Brown, G., et al., "Safety Aspects of the Calder Hall Reactor in Theory and Experiment," *Second International Conference on the Peaceful Uses of Atomic Energy,* A/CONF.15/P/267, 202–216, United Nations, Geneva (1958).

21. Farmer, F. R., P. T. Fletcher, and T. M. Fry, "Safety Considerations for Gas Cooled Thermal Reactors of the Calder Hall Type," *Second International Conference on the Peaceful Uses of Atomic Energy,* A/CONF.15/P/233, 197–201, United Nations, Geneva (1958).

22. Magnox Nuclear Power Reactor Programme," *Health & Safety Executive,* The British Library Document Supply Centre (July 1994).

23. Hughes, H. A., and R. M. Horsley, "Application of the Safety Limitation Against Depressurization to the Calder and Chapelcross Reactors," *J. Brit. Nucl. Energy Soc.,* pp. 198–203 (July 1964).

24. Brown, J., A. B. Whiteley, and M. J. Whitmarsh-Everiss, "Control, Stability and Protection of a Gas-Cooled Graphite-Moderated Reactor," *Second International Conference on the Peaceful Uses of Atomic Energy,* P/179, pp. 255–266, United Kingdom.

25. Branson, P. B., R. L. Carstairs, and A. J. Spurgin, "Design of Control Rod Systems for Gas-Cooled Reactors,"*Second International Conference on the Peaceful Uses of Atomic Energy,* P/180, pp. 267–276, United Kingdom.

26. Smith, R. J., "The Overall Control of Nuclear Power Stations of the Gas-Cooled Thermal Reactor Type," *Second International Conference on the Peaceful Uses of Atomic Energy,* P/85, pp. 360–369, United Kingdom.

DISTRIBUTION

1. General M. Byers, DOE-DP-22, 19901 Germantown Road, Germantown, MD 20874
2. C. F. Carson, MS L387, Lawrence Livermore National Laboratory, 700 East Avenue, Livermore, CA 94550
3. H. E. Clark, DOE Field Office, Oak Ridge, TN 37831-6269
4–5. J. C. Cleveland, Division of Nuclear Power, IAEA, Wagramerstrasse 5, Postfach 100, A 1400, Vienna, Austria
6. E. G. Cumesty, ORNL Site Manager, DOE-ORO, Oak Ridge, TN 37831-6269
7. Dr. R. E. Dahl, 1815 S. Rocky Ridge Drive, Spokane, WA 99212
8–22. J. M. Davidson, Los Alamos National Laboratory, P.O. Box 1663, Los Alamos, NM 87545
23. Jeff Emde, P.O. Box 567254, Atlanta, GA 31156
24. D. Erb, Office of Nuclear Energy, DOE, NE-42, Washington, DC 20585
25. M. Forehand, NIS-8, MS-B230, Los Alamos National Laboratory, P.O. Box 1663, Los Alamos, NM 87545
26. Dr. C. P. Greef, Magnox Electric, Berkeley Centre, Gloucestershire, GL13 9PB, United Kingdom
27. K. Horton, International Programs, NE-14, DOE, 19901Germantown Road, Germantown, MD 20874
28. Dr. K. Kunitomi, Japan Atomic Energy Research Institute, Oarai-Machi, Ibaraki-Ken, 311-1394, Japan
29. Dr. Barry J. Marsden, AEA Technology, Risley, Warrington, Cheshire WA3 6AT, United Kingdom
30. Major David Myers, Defense Threat Reduction Agency, 6801 Telegraph Road, Alexandria, VA 22310-3398
31. Dr. Richard E. Nightingale, 2711 W. Canal Drive, Kennewick, WA 99336
32. Mr. John M. Rooney, PM/NE, Room 7828, U.S. Department of State, Washington, DC 20520
33. D. G. Schweitzer, Brookhaven National Laboratory, Building 701, Upton, NY 11973
34. A. Shenoy, General Atomics, P.O. Box 85608, San Diego, CA 92186-9784
35. J. H. Ware, Safeguards and Security Division, DP-82, DOE-ORO, P.O. Box 2001, Oak Ridge, TN 37831-8570
36. Dr. A. J. Wickham, Cwnchwefru Farm, Lianafan Fawr, Builth Wells, Powys LD2 3PW, United Kingdom
37. Dr. Peter M. Williams, 9418 Thrush Lane, Potomac, MD 20854
38–40. Dr. Colin H. Zimmerman, Nuclear Data and Computational Physics, British Nuclear Fuels, Sellafield, Seascale, Cumbria CA20 1PG, United Kingdom
41. F. H. Akers
42. S. T. Baker
43–72. S. J. Ball
73. E. R. Bowers
74–83. T. D. Burchell
84. N. E. Clapp
85. J. C. Conklin
86. C. W. Forsberg
87. D. N. Fry
88. R. G. Gilliland

89. S. R. Greene
90. R. B. Honea
91. E. P. Howard
92. E. K. Johnson
93. H. T. Kerr
94. S. R. Martin, DOE-ORO
95. D. W. McDonald
96. G. E. Michaels
97. D. G. Morris
98. R. H. Morris
99–100. D. L. Moses
101. J. P. Nichols
102. D. J. Nypaver
103. J. P. Renier
104. A. W. Riedy
105. J. Sheffield
106. J. D. White
107–116. R. P. Wichner
117. T. L. Wilson
118–137. B. A. Worley
138–139. Laboratory Records Department–RC
140. ORNL Patent Section
141. ORNL Public Relations Office
142–144. NSPO Central Files